Universidad Autónoma de Madrid
Departamento de Física de la Materia Condensada

TRANSPORT PROPERTIES IN NANOPARTICLE ARRAYS

Tesis doctoral presentada por
Virginia Estévez Nuño

Programa de doctorado de Física de la Materia Condensada

Directora:
Elena Bascones

Madrid, Febrero de 2011

Contents

Acknowledgements

First of all, I would like to express my deepest gratitude to my advisor Elena Bascones. Thanks to her intuition and better knowledge of the condensed matter physics, I have been able to learn this subject in depth. She always found time to discuss my work and helped me with everything. Moreover, she gave me the possibility to go to several schools and attent congresses, where I could learn a lot of things related with my thesis.

I would also like to thank Guillermo Gómez Santos my tutor at the Universidad Autonoma de Madrid, for his help and interest in my work.

I would like to express my gratitude to my hosts during my short stays in other universities abroad and their hospitality. Heinrich M. Jaeger at the University of Chicago and his group made me feel one more. This stay gave me the opportunity to colaborate with an experimental group which has been very useful to understand the systems studied in my thesis. During my stay in this group I also worked with Igor Beloborodov, who always had time to discuss physics and showed me a different way to do theory. Also, I am very grateful to Jürgen König at University of Duisburg-Essen. He proposed me the study of the interplay between ferromagnetism and charging effects, one important topic in this thesis. I also want to thank the rest of nice people that I met in my two stays.

I appreciate the efforts made by Arne Brataas and Rodolfo Jalabert in writting the reports for the European Doctorate.

I have done most of my work in the deparment of Theory and simulations of materials at Instituto de Ciencia de Materiales de Madrid. During all the years in this institute I have had the opportunity to meet a lot of people who have accompanied me in this experience, I would like to thank all of them: Ramón, Geli, María José, Pilar, Debora, Belén, Rocio, Unai, Juan Luis, Alberto, Fernando, David, Juan, César, Rafas, María, Javi, José María,Felipe. I am grateful to my office mates by the great environment and for the good moments, in the present Carlos, Chicho y Mariano. And in the past Luis, José Luis, Teresa, David y Elisabet.

I would like to thank to Fernando for his help with the computers, to Santiago, Ramiro and José Luis for their help with the Cluster.

I want to thank to my friends during my stays in Chicago and Duisburg for the good moments: Thu, Carlos, Nataliya and my close friends at the International house in Chicago and Saad in Duisburg.

Last but not least, I am very grateful to my family, this thesis has been possible thanks to their support. I would also like to thank to my friends.

1 Introduction

In this introductory chapter, I will first review the main features of the nanostructure arrays. After that I will introduce the Coulomb Blockade. The Coulomb blockade is the physics that governs the transport in these systems. Next, I will see the specific nanostructures studied in this thesis: the nanoparticle arrays. Besides, I will introduce the most important types of disorder which affect these systems. Finally, I will resume what is already known about the transport in nanoparticles arrays.

1.1 Nanostructure Arrays

During the last two decades there has been an intense scientific research in nanoscience and nanotechnology in general, due to the wide variety of applications in the fields of electronics, magnetism, biomedical, pharmaceutics, cosmetics, energetics, catalytics and in material science. Among the systems used in these fields are the nanostructure arrays, being the size of the nanostructure of the order of nanometers, from 1 nm to 100 nm. These systems are situated between the bulk materials and the atoms or molecules. Thanks to their small size, electronic and magnetic devices can be built.

One of the reasons why the nanostructures are so interesting, is because the physical properties at the nano-scale are different to the properties in the macroscopic materials. When the size of the material is small enough the discrete nature of the charge becomes important, and the system starts to show quantum behavior. Specially, the electronic transport is affected by the charge confinement. To add a charge to a confined region costs energy. This energy is the charging energy E_c, that will be larger when the place is smaller. Thus, for energies smaller than the charging energy, the system is in the Coulomb blockade regime, that I will explain in detail in the following section.

The physical properties of nanostructures depend on their size, shape, and material. In this thesis I will focus on the properties of nanostructures arrays, mostly in nanoparticle arrays. Nowadays there is a wide variety of materials which are used to prepare nanoparticle arrays in one, two and three-dimensions. Arrays made of metallic [1–13], semiconducting [13–22], magnetic [23–25] or mixed property [26, 27] nanoparticles with a radii of $\sim 2-7$ nm have been synthesized by several techniques such as the nanolithography, molecular epitaxy, vapor deposition, electron-bean lithography or self-assembly techniques.

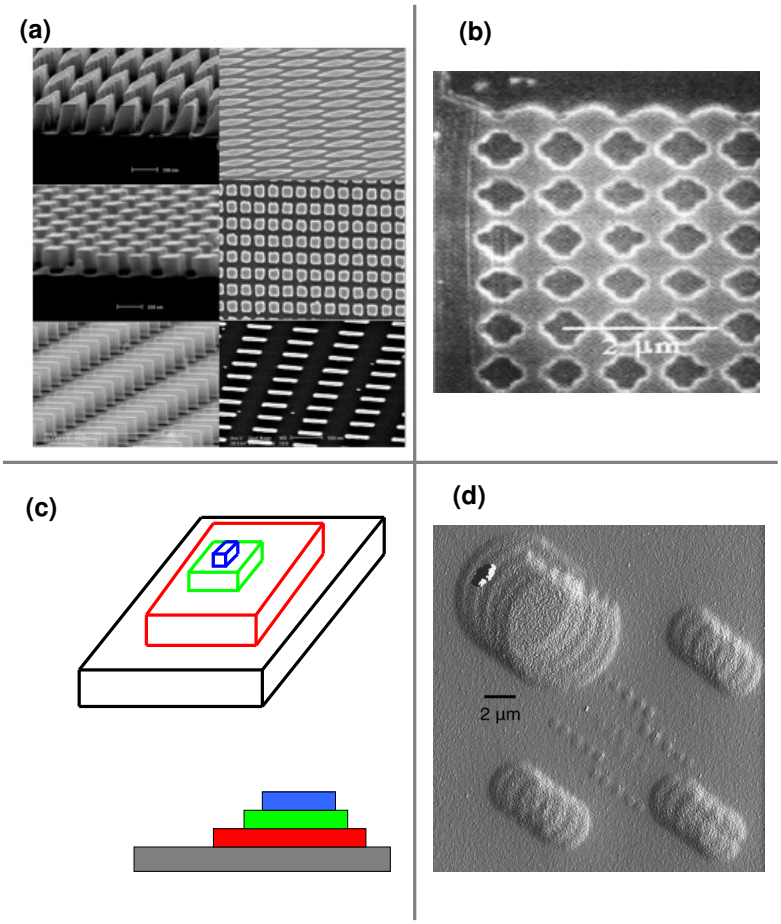

Figure 1.1: (a) Ag and Au nanoparticle arrays with different size and shape fabricated with nanoimprint lithography from Chin [6]. (b) Array of GaAs quantum dots created by electron-beam lithography from Duruöz et al [21]. (c) Schematic diagram of a nanostructure created by epitaxy, frontal and lateral views. (d) Overlapping gold circles of various size created with shadow mask deposition from Wasserman et al [28].

Some examples of these systems can be observed in figures 1.1 and 1.2. Fig. 1.1 (a) shows metallic nanoparticle arrays with different size and shape fabricated with nanoimprint lithography. Fig. 1.1 (b) shows an array of semiconducting quantum dots that was created by electron-beam lithography [21]. The nanostructures can be also grown layer to layer onto a substrate by epitaxy as we can see in the squematic diagram in Fig. 1.1 (c). The nanostructures with overlapping layers can be created by shadow mask deposition, see Fig. 1.1

(d). Other example that I show here is a three-dimensional superlattice fabricated with self-assembly techniques, where there are two kind of materials, *PbSe* semiconductor quantum dots and Fe_2O_3 magnetic nanocrystals [26] see top in Fig. 1.2. There are also nanostructures with a very amorphous shape such as the branched carbon nanostructure arrays [29], see bottom in Fig. 1.2.

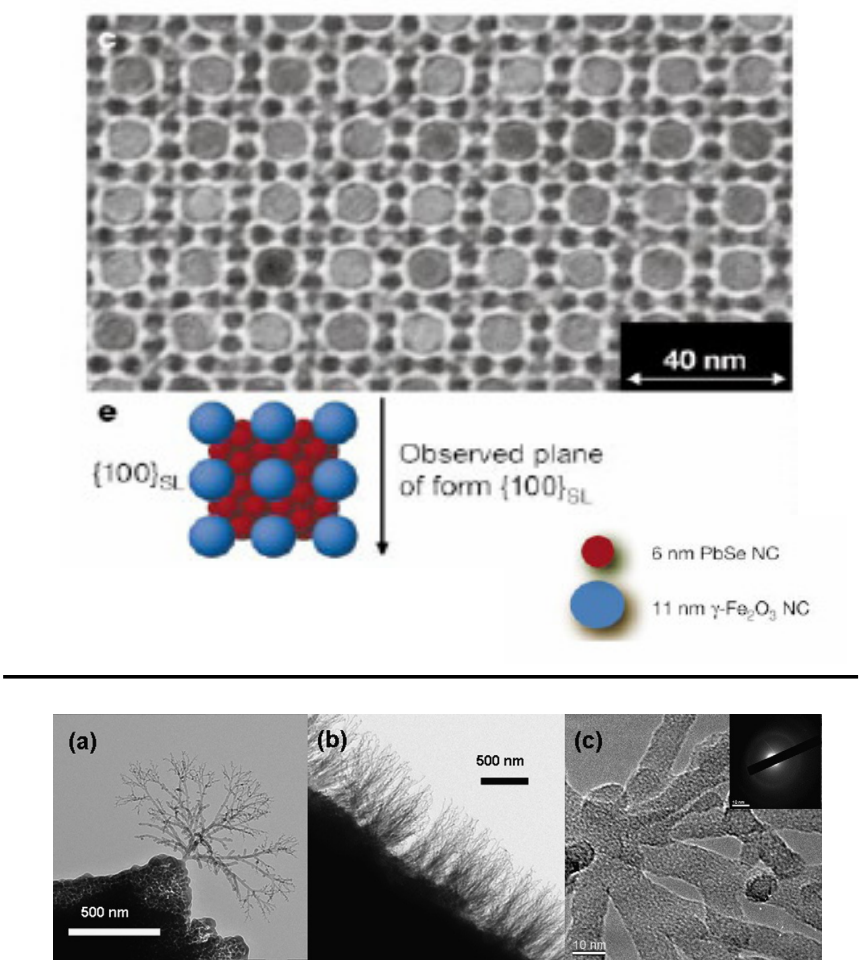

Figure 1.2: Top: Three-dimensional supperlattice composed of magnetic nanocrystals and semiconductor quantum dots from Redl et al [26]. Bottom: branched carbon nanostructures from Solá et al [29].

Despite the large number of experimental and theoretical works done throughout these years, so far there are many questions in the electronic transport through nanostructure arrays that have not been answered. Some of them have not been studied, while others are not completely understood or there is controversy. In this thesis I analyze from a theoretical point of view some of these unanswered questions.

1.2 Coulomb Blockade

As mentioned in the previous section, nanostructure arrays are systems in which the charging effects are relevant. Let us consider the case where there is a metallic island placed between two metallic electrodes (source and drain), see Fig. 1.3. The island is separated by insulating barriers from the leads. To go from the source to the drain the electron must pass through the island. The transport between the different conductors occurs by tunneling events. During these processes the charge of the island varies by e. However, adding one charge to the island costs a finite energy, because when two electrons are close enough to each other there is an electrostatic repulsion between them. Thus, in order to add one charge onto the island, a finite energy is necessary to overcome this Coulomb repulsion. The energy required is the charging energy, that is given by $E_c = e^2/2C$, where C is the capacitance of the nanoparticle.

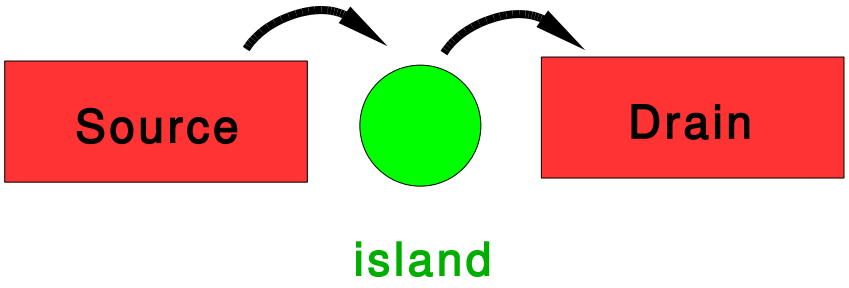

Figure 1.3: Schematic diagram of a system consisting of an island separated from the two metallic electrodes by insulating barriers. Tunneling processes are represented by arrows. Due to the electrostatic repulsion between the electrons in the island, the transport is blocked when this energy is larger than the thermal energy or the voltage drop.

Single charge tunneling phenomena occurs if the two following conditions are met:

- First: The resistance of the tunneling barriers R_T is much larger than the quantum of resistance $R_K = h/e^2 \simeq 25.8K\Omega$, i.e.

$$R_T >> R_K \tag{1.1}$$

  This condition ensures that the charge is localized at the island.

- Second: The island has to be small enough and the temperature low enough, so that the energy necessary to add one charge into the island exceeds the mean thermal energy of the charges, i.e,

$$E_c >> K_B T \tag{1.2}$$

  It ensures that the transport of charge is governed by the Coulomb charging energy.

Then at zero temperature the tunneling of an electron can only occur when the gain in energy from the applied voltage is larger than the repulsion energy, otherwise the transport is blocked. This means that for voltage drops smaller than E_c the current is suppressed, yielding the Coulomb blockade [30], which governs the electronic transport through nanostructure arrays described in this thesis. Here and through all the thesis I consider the tunneling processes only between nearest neighbors, and the transport is treated at the sequential tunneling level, where only one charge is involved in each tunneling process. Coulomb blockade can be in the classical or in a quantum regime depending on the ratio between the level spacing, δ, and the thermal energy, $K_B T$. For $\delta << K_B T$ the regime is classical, whereas in the case of $K_B T << \delta$ we are in the quantum regime. The systems studied in this thesis are all in the classical regime.

The suppression of current for voltages smaller than the charging energy can be observed in Fig. 1.4, where the I-V curve characteristic for a single nanoparticle at zero temperature is represented. Once the charge can enter into the island from one electrode, it can flow to the other electrode because it is energetically favorable, and as a result, current flows through the array. The minimun voltage at which the current starts to flow is the threshold voltage V_T, that for one island with a voltage drop as the represented in the top inset of Fig. 1.4 is given by $V_T = 2E_c^{isl}$. The current is a strongly non-linear function of the voltage due to the discrete charging effects. At high voltages the charging effects are less important and in the current there is a linear dependence on the voltage.

On the other hand, in the case of a single nanoparticle, when one of the resistance junc-

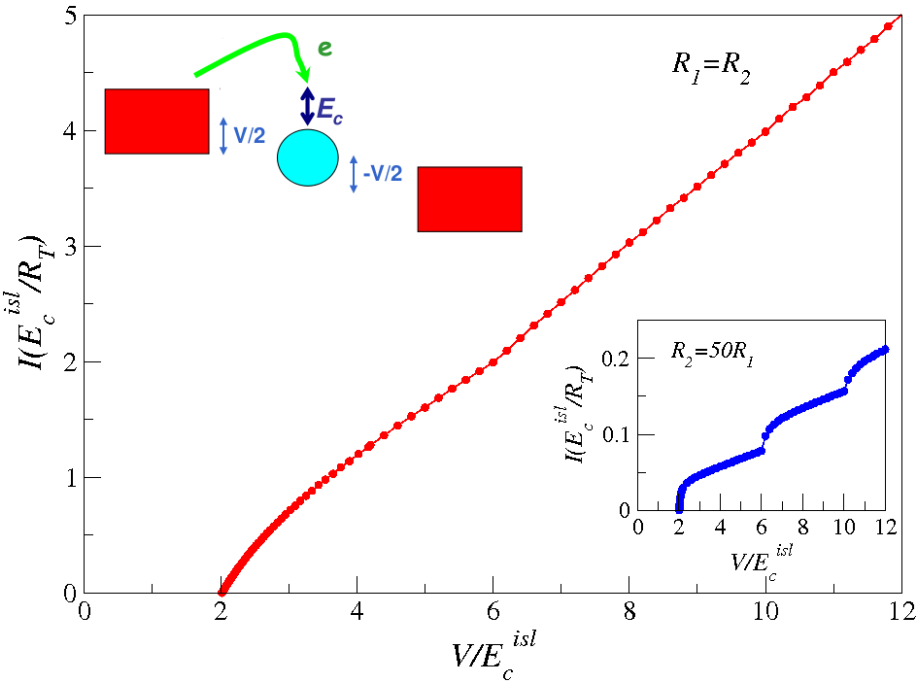

Figure 1.4: I-V curve at zero temperature for a single nanoparticle placed between two metallic leads, source and drain which are at a voltage $V/2$ and $-V/2$ respectively. Main figure: $R_1 = R_2$. Bottom inset: $R_2 = 50R_1$. The current is suppressed for voltages smaller than the E_c

tions is much larger than the other one, the current can show a marked step-like structure. This regime is the Coulomb staircase, see Fig. 1.5 where the I-V curve characteristic is represented for a single nanoparticle when the second junction resistance is 50 times larger than the resistance of the first junction. The Coulomb staircase has been well known for a long time [30–36]. If the voltage drop is only at the first junction and $R_1 << R_2$, the charge will enter into the nanoparticle through the first junction. Whenever a charge will exit the island through the second junction, the current will show a step.

It is relevant to highlight that the threshold voltage is different in the cases plotted in figures 1.4 and 1.5. This is not a consequence of the fact that in one of the cases one junction resistance is much larger than the other, because as it can be observed in Fig. 1.4, the two $I-V$ curves represented in the main and bottom inset start to flow at the same threshold voltage, and however in one of the systems $R_1 = R_2$ while in the other $R_2 = 50R_1$. The threshold voltage is controlled by the change in energy in the tunneling process, and it is independent of the resistance of the junctions. In the cases analyzed in Figs. 1.4 and 1.5, the system consists of a metallic nanoparticle placed between two metallic electrodes, however, the arrays are biased in a different way. Then, the transport depends on how the array is biased. The bias voltage through the array is $V = V_0 - V_{N+1}$, where V_0 and V_{N+1} are the

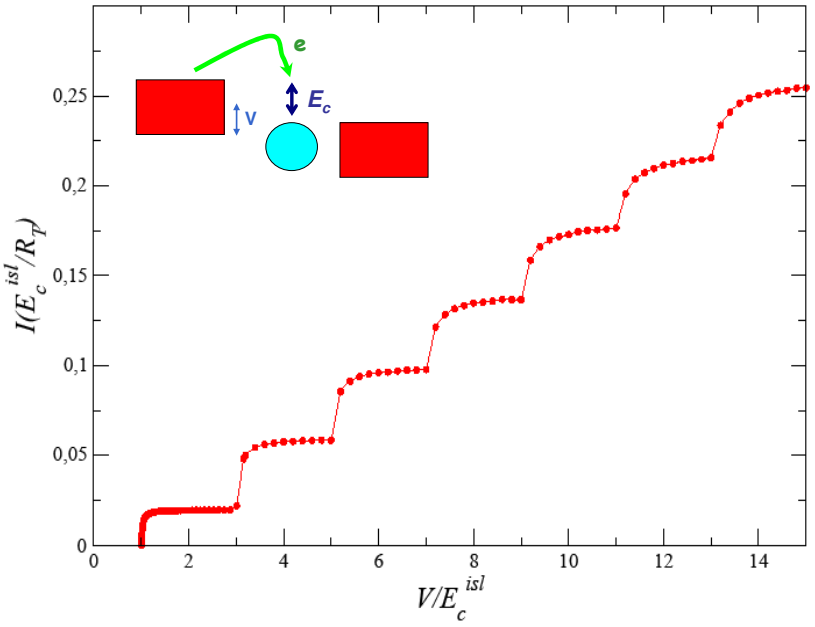

Figure 1.5: I-V curve for a single nanoparticle placed between two metallic leads at zero temperature with $R_1 = R_T$ and $R_2 = 50R_T$. Source and drian leads are at V and 0 respectively . The current shows clear steps, this regime is the Coulomb staircase.

voltages at source and drain electrodes respectively. But as I will discuss in this thesis the transport depends not only on V but also on the specific values of V_0 and V_{N+1}. So far, this dependence has been barely discussed in previous works.

In this thesis I study this dependence by means of an asymmetric external parameter α which controls how the bias voltage is partitioned between source and drain chemical potential shifts. The potential at the electrodes depends on α as $V_0 = \alpha V$ and $V_{N+1} = (\alpha - 1)V$. The total potential drop through the array is $V_0 - V_{N+1} = V$. There are limiting cases: when $\alpha = 1/2$ or $\alpha = 0, (1)$. For $\alpha = 1/2$ the array is symmetrically biased, and the potential drop at both contact junctions is equally modified by the bias voltage, see left-top in Fig. 1.4. While in the case of $\alpha = 0, (1)$ only one of the contact junctions, drain (source) is affected by the bias, see left-top in Fig. 1.5. This last case correspond to completely asymmetric biased array. $\alpha = 1$ has been also called the forward bias condition [37]. Both values, $\alpha = 1/2$ and $\alpha = 1$ have been used in the literature, but as I said before, mostly without discussion.

The dependence on α can be seen clearly if we study the case of a single nanoparticle. We know that when there is an island situated between two electrodes, adding one charge to the island costs the charging energy E_c. If the total voltage applied to the leads is V, in the case

of total asymmetry ($\alpha = 1$) the potential drop at the source junction is large, just the double, than in the case of $\alpha = 1/2$. As a consequence, the charge can enter for lower voltages in the case of completely asymmetric biased arrays than for symmetrycally biased ones. Then the transport properties through a single nanoparticle depend on α. In the nanoparticle arrays there is a similar situation.

1.2.1 Systems where Coulomb Blockade appears

Several decades ago when the first evidences of the Coulomb charging effect in small systems appeared, the Coulomb blockade phenomena could only be observed in granular metallic materials [38–41]. However, in the last two decades, thanks to the use of the nanolithography techniques the charging effects have been observed in other systems.

Metallic islands or nanoparticles

This is one of the main systems where the charge tunneling effects have been studied. Principally they are fabricated by litography and self-assembly techniques in the case of several nanoparticles. The islands are separated by oxide layer tunnel barriers. This system is a three-dimensional electron gas confined to small regions. Very often it is in classical Coulomb blockade regime. However, when the islands are very small ($\sim 5 - 10A^o$) and they are situated in a quantum point contact, they can have a discrete energy spectrum and show a similar behavior to that of the quntum dots. This situation has been studied by several groups [42–48].

Quantum dots

These systems are two dimensional electron gas heterostructures, that are usually in the quantum regime. There are two different types, lateral and vertical. Lateral quantum dots are generally made of GaAs/AlGaAs and are confined to small islands by means of Schottky gates. The transport is in the plane of the two dimensional electron gas. On the other hand, in the vertical quantum dots the transport is perpendicular to the plane of the 2DEG [49].

Apart from these cases, there are other systems where the Coulomb blockade phenomena can be observed. For example in disordered quantum wires [50] or carbon nanotubes [51].

1.2.2 Tunnel junction circuits

Coulomb blockade can be studied in several devices. Two basic devices are Single Electron Box (SEB) and Single Electron Tunneling (SET) Transistor. More complex devices such as multijunctions circuits can be built using SEB and SET as basic units. A gate electrode is coupled to the island. This gate electrode is used to control the number of electrons in the island.

Single Electron Box [52] is the simplest device, which is composed of a small island and source and gate electrodes. In this system there is no net current because there is only one electrode and the charge only can tunnel from the electrode to the island, and from it to the electrode. However, in the case of a Single electron transistor there is current through the system because there are two tunneling junctions which couple the island with the electrodes and there is a bias voltage $V = V_L - V_R$ in the system. Now the electron can enter into the nanoparticle by one tunnel junction and leave it across the other, as a result current flows through the device. An important part of the studies of Coulomb blockade have used this type of system[53–55]

1.3 Nanoparticle Arrays

Although the physics studied in this thesis is valid for a lot of systems, I focus in the study of the metallic nanoparticle arrays. Metallic nanoparticles have interesting structural, electronic or magnetic properties. The transport properties of these systems are influenced by the ratios between the energy level spacing, the charging energy of the nanoparticles, and the temperature. The first two quantities depend on the material and the size of the nanoparticle. Strong interactions between the electric charges and the possibility of tuning interparticle coupling make nanoparticle arrays an ideal system to study correlated motion [56–77]. The size and the shape of the nanoparticles are determined by the techniques of fabrication. Although, these nanostructures can be fabricated by lithography with high resolution and a good ordering between the nanoparticles, as Fig. 1.1 (a) shows, this method is very expensive, the processes of fabrication are slow and the arrays created do not have a good ordering between the nanoparticles for large distances. However, using self-assembly techniques the nanoparticle arrays obtained are well characterized and have an excellent long-range ordering, that can reach areas with 10^8 particles. Moreover, this mechanism is less expensive than the lithography. Self-assembly is one of the most important techniques to prepare nanoparticle arrays. Two examples of nanoparticle arrays made with this method are shown in Fig. 1.6, for a two-dimensional array [1] (left), and quasi-one dimensional arrays [78] on the right. In both cases the electrodes have been fabricated on the substrate by electron-beam lithography.

One of the self-assembly techniques is by means of thiols as the used in [1], and this consists in several steps. First, the nanocrystals, which can be of different materials, are ligated to thiols, or organic molecules by chemical techniques. The reason to ligate the nanocrystal with thiols is because the thiols strongly ligate to metal producing monodisperse metal-thiol nanocrystals in dissolution, that allow a more regular organization of the nanocrystals once they are deposited onto the substrate. Not all the substrates can be used for creating self-

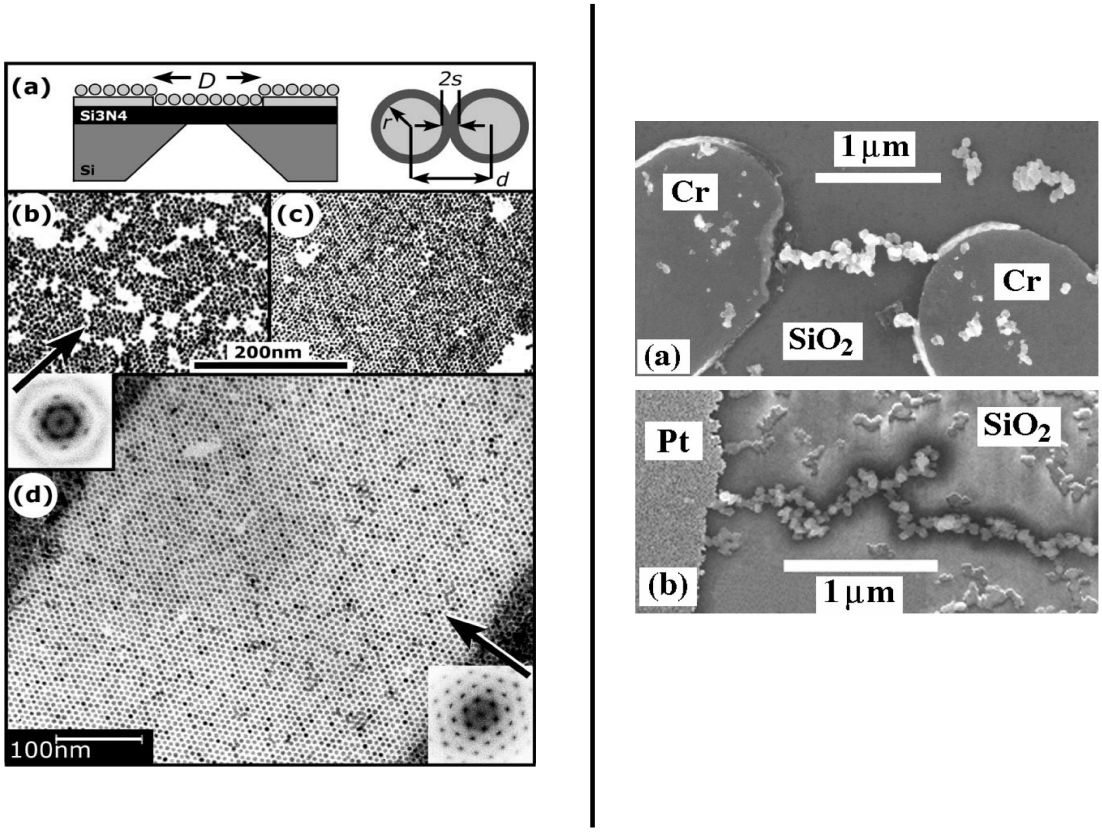

Figure 1.6: Left: (a) Sketchs of a nanocrystal monolayer and of the interparticle geometry. (b) 2D nanoparticle arrays formed without excess dodecanethiol. (c) 2D nanoparticle arrays formed with excess dodecanethiol, showing $< 5\%$ voids and long-range ordering. (d) Highly ordered superlattice. Images from Parthasarathy et al. [1]. Right: Top: Chain of graphitized carbon nanoparticles self-assembled between two Cr electrodes. Bottom: Same that in top with one Pt electrode. Images of quasi-one dimensional nanoparticle arrays from Bezryadin et al. [78].

assembly nanoparticle arrays, the substrates used are insulating and the typical materials are SiO_2 or carbon. Generally the self-assembled arrays do not have a gate electrode.

Depending on the way of preparation, the nanoparticles can be well ordered for long or short distances. When there is a simple deposition of the solution onto the substrate, after the drying, the nanoparticle arrays created have well-ordering only for short-range, because there are a lot of voids, see Fig. 1.6 left (b). The voids will appear in the array although the quantity of solution deposited onto the substrate will be larger or the concentration of nanocrystals in the solution will increase. However, if the quantity of thiols is increased in the nanocrystal solution, and there is a slow evaporation in the process of fabrication,

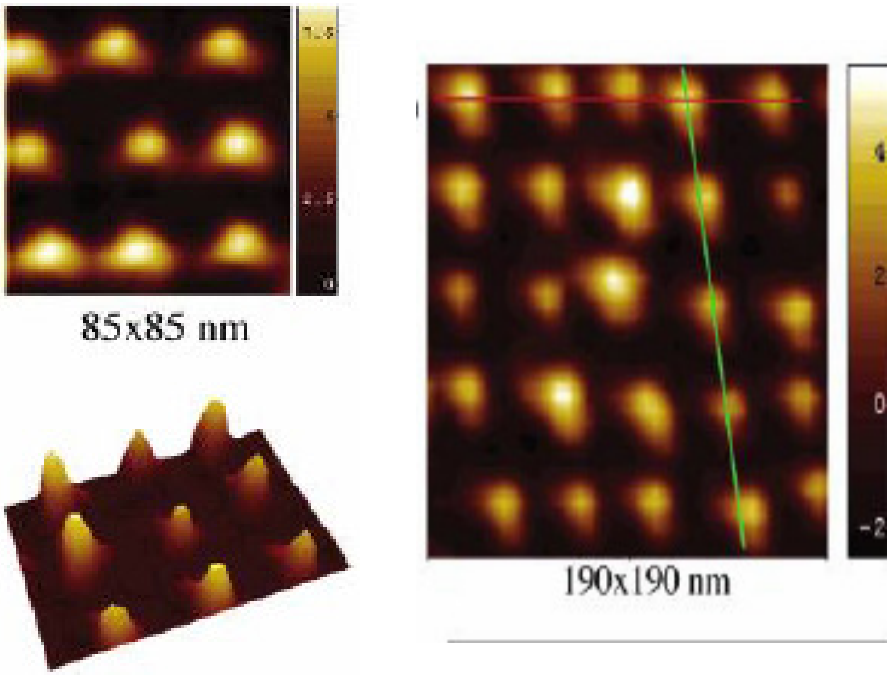

Figure 1.7: Images of two dimensional nanoparticle arrays with square lattice from Zhang et al. [10].

the array formed has a long-range ordering, as we can see in Fig. 1.6 left (c) and (d) from Parthasarathy et al [1], where the nanoparticle arrays have triangular lattice. Self assembly arrays with square lattice can also be synthesized, see Fig. 1.7, where DNA nanogrids have been used as a template for creating the metallic square array [10].

1.3.1 Types of arrays

In this thesis I study the transport properties through metallic nanoparticle arrays in one and two-dimensional arrays, see Fig. 1.8 which shows schematic diagrams of one-dimensional nanoparticle array in (a), and two dimensional arrays in (b), (c) and (d). For two-dimensional arrays I study two different lattice geometries, square and triangular, see Fig. 1.8 (b) and (c) respectively. In this work the size of the two-dimensional arrays is given by m x k, where m is the number of rows and k of columns.

1.3.2 Types of Disorder

Nanoparticle arrays are strongly influenced by disorder in the experiments [79–87]. There are several types of disorder in these systems. Until now the theoretical studies have mostly

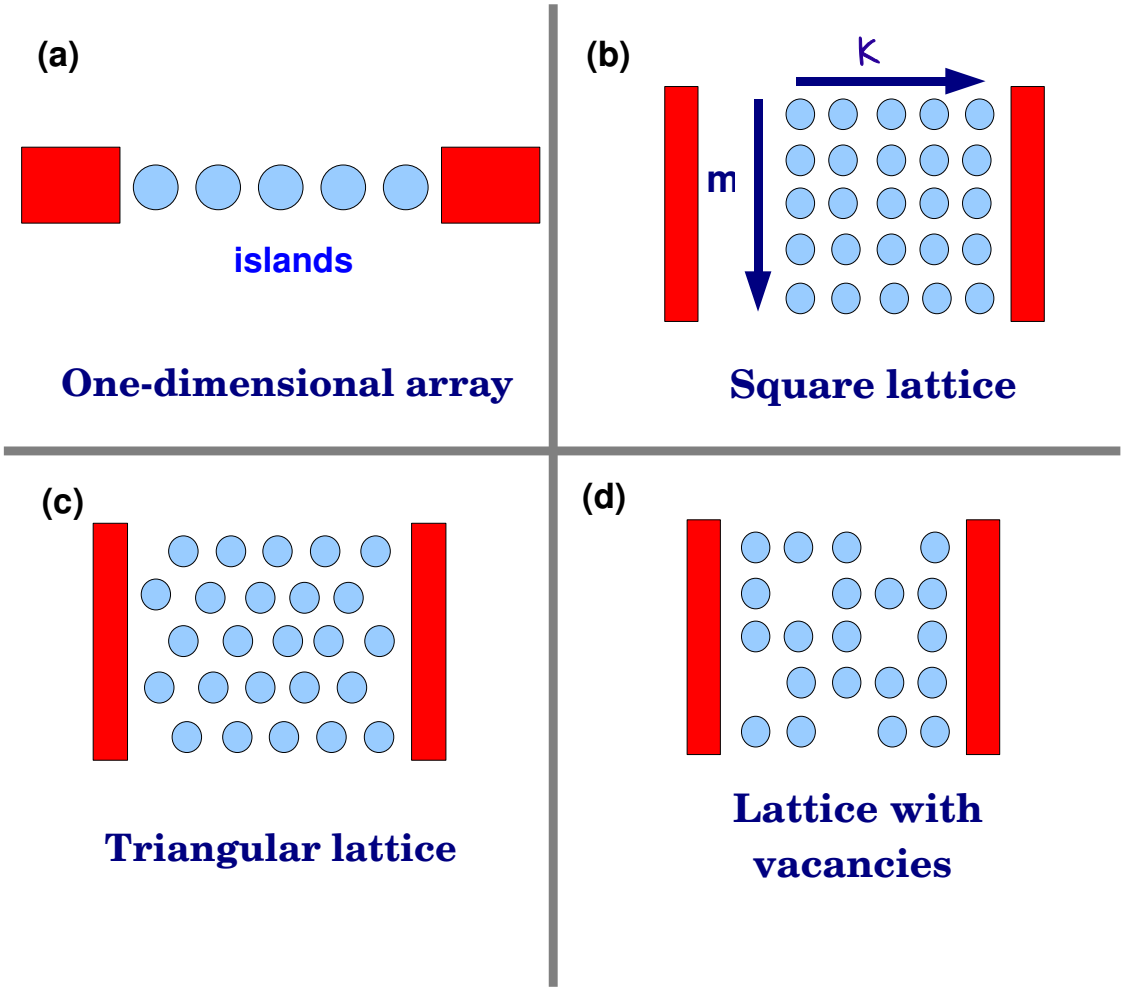

Figure 1.8: Schematic diagrams of the different types of nanoparticle arrays.(a) One-dimensional array. (b) Array with square lattice, where m is the number of rows and k the number of columns. (c) Triangular lattice. (d) Lattice with vacancies.

focused on the local charging disorder [64, 88–91], although there is also a study in vacancies [92]. I have analyzed three different types of disorder: charging disorder, disorder in resistances and structural disorder or vacancies. The disorder in capacitances is not considered because the nanoparticles synthetized nowadays in the experiments are 5% monodisperse in size, i.e, the nanoparticles have almost the same size.

Charge Disorder

Local charging disorder appears in the self-assembled arrays due to the fact that the randomly dispersed charged impurities lodged in the substrate or in the materials that separate and surround the nanoparticles [93] create random potentials in the nanoparticles. Sometimes these random potential are described as effective charges. This type of disorder is very

important in the transport properties at not very high voltages. In the next chapter I will explain how the charge disorder is included in our model.

Disorder in Resistances

There is disorder in resistances in a nanoparticle array when the junction resistances are not all of them equal. This type of disorder can be present in the self-assembled array when the distances between the nanoparticles are not the same. In this thesis the effect of non homogeneous resistances has been studied in two ways. The first case (mostly of academic interest) is when one of the junction resistances at a given position is larger than the other ones, which are given by R_T. While in the second way, all the junction resistances are different and vary between two values that are randomly assigned to the junctions. The disorder in resistances originates in the variations in distances between the islands in the array, and exponentially depends on these distances. Then the junction resistance is given by

$$R = R_0 exp(\gamma dist) \tag{1.3}$$

where R_0 and γ are input parameters and $dist = 1 + random/2$. Here $random$ is a random number between 0 and 1.

Vacancies

When the nanoparticle arrays are synthesized experimentally, despite the well-ordering of the nanoparticles, vacancies always appear in the samples, as we can see in Fig. 1.9. Until now the effect of these vacancies or voids also called structural disorder in the transport has barely been studied theoretically [92]. However the vacancies affect the transport properties. I have analyzed the effect of the vacancies in two dimensional arrays. While in the case of one-dimensional array I have not considered this type of disorder, because the tunneling processes are only between nearest neighbors, and if there is one void in the array, this will completely prevent current flow.

1.4 Solved and Unsolved questions in transport through nanoparticle arrays

Before beginning with the work done in this thesis, we will see what was already known about the transport in nanoparticles arrays.

As we already know, the transport through nanostructure arrays is governed by the Coulomb blockade physics, and some of its effects had been predicted and observed. One of them is the existence of a threshold voltage below which there is no current in the system. The suppresion of the current has been theoretically studied [30, 31, 64, 89, 94, 95] and experimentally

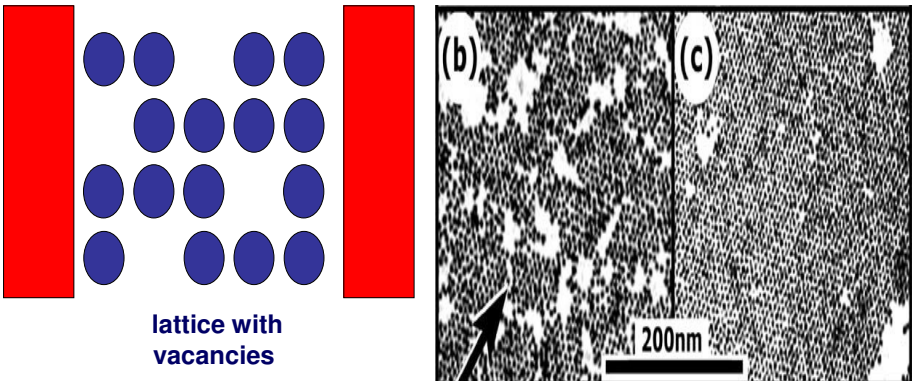

Figure 1.9: Left: Schematic plot of a two dimensional array with vacancies. Right: Images of nanoparticle arrays with vacancies from Parthasarathy et al. [1] .

observed [1, 21, 24, 86, 78, 96–101].

Another characteristic known of the Coulomb blockade in these systems is the nonlinearity in the current. As we mentioned above, Coulomb staircase regime has been studied for a long time [30–36, 99, 101]. At high voltages the current depends linearly on voltages. This linear dependence was known, but has been in this thesis where it has been studied more carefully extending analytical calculations.

However, the current in these systems was not completely understood. So far, it has been considered that the transport already close to threshold was controlled by the array. However, when the arrays are finite and are placed between electrodes, the entrance of charge into the array will be decisive for transport. One important point in the transport that until now was not well understood is how the voltage drops through the array. This is affected by the way in which the array is biased and by the range of interactions between the electrons. So far, there were hardly studies of the way in which the array is biased. Moreover, the several types of disorder that appears in the synthesized arrays, and different array parameters also affect the transport, as we will see throughout this thesis.

One of the unsolved questions is the behavior of the current for voltages close to threshold. Most studies have focused on the power-law behavior of the current in this regime. It was predicted that $I \propto (V - V_T)^{\zeta}$, where the exponent depends on the dimensionality of the array. There is controversy between different theoretical approaches in one-dimensional case with both linear [64, 89, 102] and square-root [90] predictions. On the other hand, much experimental work has been concentrated in two-dimensional arrays. In 1993 Middleton and Wingreen predicted theoretically that in two-dimensional arrays the current shows a power-law behavior with $\zeta = 5/3$ [64]. Since this pioner work, all experimental work have sistematically disscused the $I - V$ curves in terms of this power-law. However, the exponent observed varies in a wide range of values, depending on the experiment and sample. Desviations of the exponent observed from the predicted value have been interpreted as a consequence of the dimensionality or the different types of disorder present in the array. Moreover, the results found numerically do not reproduce the theoretical prediction. Despite this, during the last two decades this theoretical prediction has been considered valid. In this thesis we demostrate that this theoretical prediction is wrong, and that so far the transport in these systems for voltages close to threshold was not understood.

Most theoretical works have considered arrays in which each nanoparticle is capacitively coupled only to its nearest neighbors [64, 89, 102–106], especially the case in which this coupling is small. This limit is relevant for those arrays coupled to a gate electrode [97], as the mobile charges in the gate electrodes effectively screen Coulomb interactions. However, self-assembled arrays fabricated nowadays are deposited onto insulating substrates and generally these arrays do not have a gate voltage. On the other hand, there are very few theoretical works in which the effect of the long-range interactions have been included [89, 90, 107].

So far, the potential drop through the array has not been analyzed theoretically, although it can be measured nowadays. In this work I study the potential drop through the nanoparticle arrays.

In the first part of this thesis, I provide a complete description of the zero-temperature transport properties of one and two-dimensional metallic nanoparticle arrays when they are placed between non-magnetic electrodes. I analyze arrays with and without disorder. Although clean arrays are mainly of academic interest, their analysis will help us to understand the main features of the experimentally more relevant, disordered arrays. Later, I study disordered systems. We consider two different ranges of interaction, when they are restricted to charges in the same nanoparticle (onsite limit) and the case where the charge in one conductor can interact with the charges in other conductors, long-range limit. In the last case, we take into account the effect of screening.

In the second part of the thesis, I study the tranport properties through the metallic nanoparticle arrays when they are placed between two ferromagnetic electrodes. Until now all the studies done have restricted to the cases of one and two nanoparticles. In this thesis I study the influence of the interplay between the ferromagnetism of the electrodes and the charging effect of the nanoparticles in the transport through arrays with $N \geq 3$ nanoparticles. I analyze the system in one and two-dimensional arrays, for short and long-range interactions, and how the transport is affected by the different types of disorder or the temperature. The results of this thesis are unexpected.

Part I

Non-magnetic Electrodes

2 Model and Numerical Simulation

In this chapter I will explain the model and the numerical simulations that I have used to study the systems analyzed in the first part of this thesis. In the long-range case the model has some differences with respect to the works done by other groups. For the case of ferromagnetic electrodes studied in the second part of this thesis the model has little changes that I will explain in detail in chapter 6.

2.1 System under study

In the first part of the thesis, I have analyzed the transport properties through one and two dimensional metallic nanoparticle arrays when they are placed between two metallic electrodes. The dimension of the array does not affect much the model. Therefore, I am going to explain the model for one-dimensional arrays. After that, I will see the small differences that appear in the two dimensional case.

We consider a one-dimensional array composed of N metallic spheres of radius r^{isl} and with a center to center distance of $2r^{isl} + d$. In our model, the lengths are measured in units of r^{isl} and energies in units of $E_c^{isl} = e^2/(2C^{isl})$ the charging energy of an isolated nanoparticle with capacitance C^{isl}. Here and in the following, the electronic charge $e = 1$. In order to analyze the transport, the array is sandwiched between two large electrodes, see Fig. 2.1. As we saw in Section 1.2, due to the small size of the nanoparticles, the transport is governed by the Coulomb blockade physics. We consider the classical Coulomb blockade regime where $\delta \ll K_B T < E_c^{isl}$. δ is the level spacing and T the temperature. We assume that each nanoparticle has a continuum level spectrum ($\delta = 0$) and a constant density of states at the Fermi level, but a gap E_c^{isl} for adding charge.

The nanoparticles are separated by high tunneling barriers with a resistance much larger than the quantum of resistance. In these conditions the charge in the islands can be assumed fixed and quantized. The transport of charge is via tunneling processes between nearest neighbors, and we treat the transport at the sequential tunneling level, where only a single charge is involved in the tunneling process. We assume that when a charge hops, the charge density in the final state of the array immediately relaxes to the electrostatic equilibrium

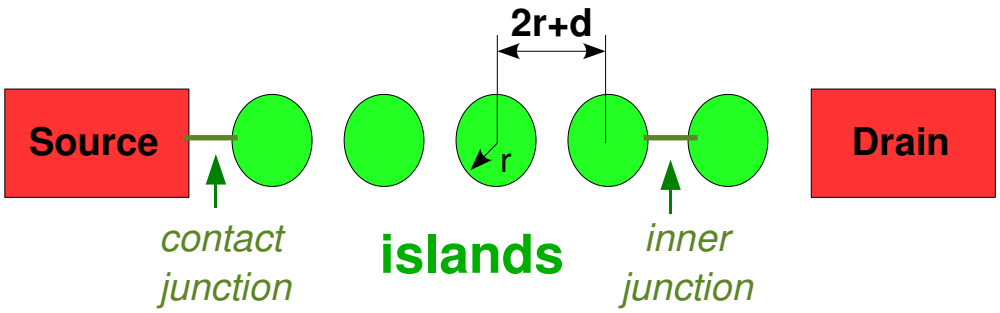

Figure 2.1: Schematic diagram of a one-dimensional nanoparticle array between two metallic electrodes.

configuration. The probability of a tunneling process [30] is given by

$$\Gamma(\Delta E) = \frac{1}{R}\frac{\Delta E}{exp(\Delta E/K_BT) - 1} \tag{2.1}$$

with R the tunneling resistance of the junction. If there is no disorder in resistances (subsection. 1.3.2), all the junction resistances R_i are equal and given by R_T. Unless specified, we assume this situation. ΔE is the difference between the energy of the system before and after the tunneling event. At zero temperature the probability of a tunneling process is $\Gamma(\Delta E) = -\Delta E/R\Theta(-\Delta E)$, with the sign convention that ΔE is negative if the energy decreases. The energy gained by tunneling is assumed to be dissipated.

2.1.1 Electrostatic interactions

In our model we only consider the electrostatic interactions, which are defined through an inverse capacitance matrix C^{-1}. The interaction between the charges in conductors γ and β is given by $C^{-1}_{\gamma\beta}$. All the elements $C^{-1}_{\gamma\beta}$ are positive. The inverse capacitance matrix is symmetric, $C^{-1}_{\gamma\beta} = C^{-1}_{\beta\gamma}$, and has dimension $(N+2)\times(N+2)$, i.e. it includes both islands and electrodes. Although the interaction between the electrodes in fact does not influence the transport because their self-capacitance is large, it will help us to introduce some terms in the model as the polarization potential that we will explain later. In previous works the interaction between electrodes has been neglected. In our system the interactions between islands and electrodes, islands and islands and between electrodes and electrodes are all calculated on the same ground.

We consider two different types of interactions:

- *short-range or onsite limit:* the electrostatic interactions are restricted to those charges in the same conductor, then $C^{-1}_{\gamma\beta} = 0$ if $\gamma \neq \beta$.

- *long-range interaction:* the charges in different conductors can interact. We will explain the long-range interaction in more detail in chapter 4.

The energy of a system of conductors is given by

$$Energy = \frac{1}{2}\sum_{i=1}^{N} Q_i V_i \tag{2.2}$$

and as the charge of a conductor is $Q_i = \sum_j C_{ij} V_j$, then $V_i = \sum_j Cij^{-1} Q_j$. Thus, the energy of our system for short and long-range interaction is given by

$$F = \frac{1}{2}\sum_{\gamma,\beta=0}^{N+1} Q_\gamma C^{-1}_{\gamma\beta} Q_\beta \tag{2.3}$$

Labels 0 and $N+1$ refer to source and drain electrodes and $1,\ldots,N$ to the islands. Latin capital and lower case letters are used to denote electrodes and islands respectively. Greek indexes will be used when the labels refer to both islands and electrodes. Q_γ is the charge present in the conductor. Charges Q_0 and Q_{N+1} maintain source and drain electrodes at potentials V_0 and V_{N+1}, respectively.

The electrodes are not ideal voltage sources, but have a finite self-capacitance. In equilibrium, and before the tunneling event the electrodes are held at a given potential due to the charge provided by a battery. We assume that the tunneling time, i.e. the time needed by the electron to cross the tunnel barrier, is smaller than the circuit characteristic time that determines how quickly the battery can transfer charge to the leads in order to restore the voltage at the electrodes. As a consequence, just after the tunneling process the electrodes will not necessarily be at the same potential at which they were before the tunneling event because the charge, provided by the battery, necessary to restore their initial potentials has not arrived yet. The voltage is restored to the nominal value before the next tunneling event. Then the voltage is the same before each tunneling process. We also assume that the tunneling time is larger than the time necessary for the islands to reach the equilibrium.

2.2 Potential at the islands and junctions

In order to understand the electronic transport in these systems, it is very important to understand the potential drop through the array. The relevant quantity for the transport is the change in energy due to a tunneling event, see Eq. (2.1). A tunneling process can be seen as the creation of a hole in the conductor γ from which the charge leaves, $Q_\gamma \rightarrow Q_\gamma - 1$, and the addition of an electron in β at which the charge arrives, $Q_\beta \rightarrow Q_\beta + 1$. Here and

thereafter, we let $+1(-1)$ denote the charge of an electron (hole). The change in energy can be written as

$$\Delta E = E^{e-h}_{\gamma,\beta} + (\phi_\beta - \phi_\gamma) \tag{2.4}$$

where the first term gives the energy to create an electron-hole pair in conductors α and β in an uncharged clean array. We call this term excitonic energy and is given by

$$E^{e-h}_{\gamma,\beta} = \frac{1}{2}C^{-1}_{\gamma\gamma} + \frac{1}{2}C^{-1}_{\beta\beta} - C^{-1}_{\gamma\beta} \tag{2.5}$$

This energy is independent of the direction of tunneling (from γ to β or from β to γ). For the short-range interaction, this energy is reduced to

$$E^{e-h}_{\gamma,\beta} = \frac{1}{2}C^{-1}_{\gamma\gamma} + \frac{1}{2}C^{-1}_{\beta\beta} \tag{2.6}$$

and is always a positive quantity.

Between one electrode and one island there is a contact junction, whereas the inner junctions are between two islands, see Fig. 2.1. For the contact junctions $E^{e-h}_1 = E^{e-h}_{N+1} \sim E^{isl}_c$ because of $E^{source,drain}_c << E^{isl}_c$ while for the bulk or inner junctions $E^{e-h}_i = 2E^{isl}_c$.

The second term in Eq. (2.4) can be seen as the change in potential between the conductors involved in the tunneling process. The potential at each site depends on the charge state of the array prior to the tunneling event, which at the electrodes is $\phi_0 = V_0 = \alpha V$, $\phi_{N+1} = V_{N+1} = (\alpha - 1)V$. The parameter α characterizes how the bias voltage is partitioned between the source and drain electrodes. The total potential drop through the array is $V_0 - V_{N+1} = V$. However, at the islands when the electrodes are non-magnetic, the potential can be decomposed into three terms $\phi_i = \phi^{dis}_i + \phi^{pol}_i + \phi^{ch}_i$, the disorder potential ϕ^{dis}_i, the polarization potential ϕ^{pol}_i and the charge potential ϕ^{ch}_i. The first two ϕ^{dis}_i and ϕ^{pol}_i are static potentials, that do not change during the simulation because these only depends on the initial parameteres. However, ϕ^{ch}_i depends on the charge state of the array, and this changes during the simulation, for this reason we say that it is a dynamic potential.

2.2.1 Polarization Potential

One of the main differences of our model with respect to the models of other groups is that we introduce the polarization potential drop within the array directly by the interaction with the electrodes. The polarization potential ϕ^{pol} is a consequence of the interaction between islands and electrodes, and it is proportional to the applied voltage. A priori one might expect that the potential drops linearly within the array, and indeed some previous works

[90, 78] have assumed that an equivalent potential to which we call polarization potential is linear. However, if we assume it at the same time we are considering a particular form of interaction. In this system the potential drop due to the interaction with the electrodes is not linear, and at the islands is given by

$$\phi_i^{pol} = \lambda_i^{\alpha} V \tag{2.7}$$

with

$$\begin{aligned}\lambda_i^{\alpha} = C_{gen}^2 \Big[& \alpha \left(C_{i0}^{-1} C_{N+1,N+1}^{-1} - C_{i,N+1}^{-1} C_{N+1,0}^{-1} \right) \\ & + (\alpha - 1) \left(C_{iN+1}^{-1} C_{00}^{-1} - C_{i0}^{-1} C_{N+1,0}^{-1} \right) \Big]\end{aligned} \tag{2.8}$$

and

$$C_{gen}^2 = \frac{1}{C_{00}^{-1} C_{N+1,N+1}^{-1} - (C_{N+1,0}^{-1})^2} \tag{2.9}$$

These equations are obtained from Eq. (2.3), and are valid for short and long-range interactions. We can define the polarization potential at the junctions as

$$\Phi_i^{pol} = \Lambda_i^{\alpha} V = (\lambda_i^{\alpha} - \lambda_{i-1}^{\alpha}) V \tag{2.10}$$

Note that capital letters (Φ, Λ) are used for the junctions, and lowercase (ϕ, λ) for the islands.

From these equations we can see that ϕ^{pol} is not linear and depends on how the array is biased. Let us consider one array in which there is short-range interaction, i.e. only the charges in a same conductor can interact between them, $C_{\gamma\beta}^{-1} = 0$ for $\gamma \neq \beta$. As a result, the polarization potential ϕ_i^{pol} vanishes at the islands and there is only polarization potential at the electrodes $V_0 = \alpha V$ and $V_{N+1} = (\alpha - 1)V$. Therefore, the polarization potential drop through the array is not only not linear, as had been considered by other groups, but it also vanishes at the inner junctions, while at the contact junctions depends on α. This can clearly seen in Fig. 2.2 where the schematic diagrams are represented one-dimensional nanoparticle arrays biased in a different way. Previous studies have not considered the effect of how the array is biased on the transport. However, this is very important in the flow of current as we already saw in section 1.2. As we will see throughout all this thesis, ***the polarization potential drop through the array will be very important in the electronic transport, including when the electrodes are ferromagnetic***.

2.2.2 Charge Potential

The charge potential ϕ_i^{ch} depends on the number of charges in the nanoparticle, and it changes during the simulation. In the short-range limit, the charge potential at one island is

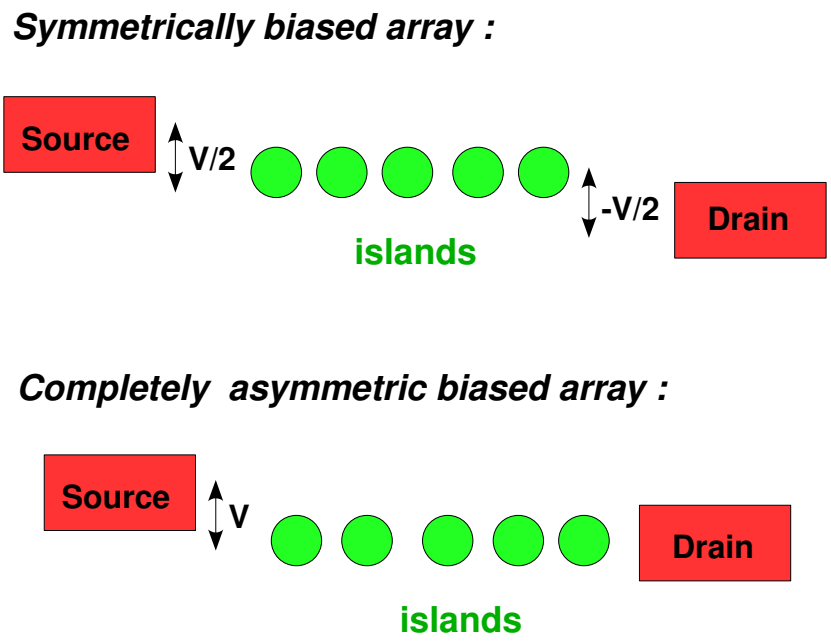

Figure 2.2: Schematic diagram of a one-dimensional nanoparticle array between two metallic electrodes with different partion of bias voltage for short-range interaction. Top: Symetrically biased array, where $\alpha = 1/2$. Bottom: Completely asymmetric biasing array with $\alpha = 1$. The total potential drop through the array in both cases is V.

given by the charges in this island, and equals

$$\phi_i^{ch} = \frac{Q_i}{C_i} \tag{2.11}$$

while for long-range interactions the charge potential depends not only on its charges, but also the interaction with the charges of all conductors, and it is given by

$$\phi_i^{ch} = \sum_{j=1}^{N} Q_j \tilde{C}_{ij}^{-1} \tag{2.12}$$

with

$$\begin{aligned} \tilde{C}_{ij}^{-1} = C_{ij}^{-1} + C_{gen}^2 \Big[& C_{0,N+1}^{-1} \left(C_{iN+1}^{-1} C_{j0}^{-1} + C_{i0}^{-1} C_{j,N+1}^{-1} \right) \\ & - C_{00}^{-1} C_{N+1,i}^{-1} C_{j,N+1}^{-1} - C_{N+1,N+1}^{-1} C_{i0}^{-1} C_{j0}^{-1} \Big] \end{aligned} \tag{2.13}$$

where C_{gen}^2 is given by Eq. (2.9). $\tilde{C}^{-1}$ can be interpreted as a modification of the interaction between the charges in the islands due to the proximity of the electrodes at a fixed potential.

For the case $i = j$ in which both charges are on the same island this modification was already discussed in [103]. Expression (2.13) shows that not only when the charges are in the same island, but also when they occupy different islands, their effective interactions are modified by the presence of the voltage-biased leads.

2.2.3 Disorder Potential

As we said before, charges trapped in the substrate underlying the nanoparticle array create random potentials at the islands, the disorder potential ϕ^{dis}. This potential only exists at the islands because a similar term at each electrode is compensated by the battery and thus has no effect on transport. In clean arrays there is no disorder potential, then $\phi_i^{dis} = 0$ for all the conductors. For charge disordered arrays the energy of the system is given by

$$F = \frac{1}{2} \sum_{\gamma,\beta=0}^{N+1} Q_\gamma C_{\gamma\beta}^{-1} Q_\beta + \sum_{i=1}^{N} Q_i \phi_i^{dis} \tag{2.14}$$

In the case of charge disordered arrays, the disorder potentials can, in principle, take values larger than the charging energy E_c^{isl}. However, for large values of the disorder potential, charges flow to compensate for these large fluctuations. The way to introduce the disorder potential in the model is different depending on the range of interaction.

In the case of short-range interactions, except if the original disorder potential is very weak, once the screening of the potential due to the mobile charges is taken into account, the set of disorder potentials is uniformly distributed in the interval $-E_c^{isl} \leq \phi_i^{dis} \leq E_c^{isl}$ [79, 80].

Whereas in the presence of long-range interactions, the charges which flow to compensate the large fluctuations of the disorder potential, modify the potential at neighboring islands and the screened disorder is correlated [79, 80]. In order to analyze these correlations and obtain the proper disorder potential distribution we assign the potentials by first randomly assigning potentials to the islands $\phi_i^{dis-bare}$, in the interval $-W \leq \phi_i^{dis-bare} \leq W$ with W larger than the charging energy. We then find the equilibrium configuration of charges $\{Q_j^{sc}\}$ that occupy the array with island disorder potentials $\{\phi_i^{dis-bare}\}$ and grounded leads ($V_0 = V_{N+1} = 0$) and redefine the potentials at each site using the expression

$$\phi_i^{dis} = \sum_{j=1}^{N} \tilde{C}_{ij}^{-1} Q_j^{sc} + \phi_i^{dis-bare} \tag{2.15}$$

The effect of the screening charges $\{Q_j^{sc}\}$ is included in the redefined potentials $\{\phi_i^{dis}\}$ so we then reset the number of charges at each site to zero to avoid doublecounting the charge when we calculate the total electrostatic energy of our system. Following the redefinition of

the disorder potentials, we find that on average the distribution of the disorder potentials and the disorder potential drops $\{\Phi_i^{dis}\}$ between adjacent islands are independent of W.

2.3 Non-equilibrium Monte-Carlo Simulation

Numerical simulations allow us to solve problems that are too complicated to solve analytically. One of the most important numerical simulations is the Monte Carlo method [108, 109], which is used in different areas of the physics, such as disordered materials, strongly coupled solids, fluids or in the study of different structures. In this thesis we use Monte Carlo simulations to study the transport through nanoparticle arrays.

The current in our system is calculated numerically by means of a non-equilibrium Monte Carlo simulation [103], which depends on the tunneling rates. We iteratively determine the time evolution of the state of an array of nanoparticles sandwiched between two large metallic leads symmetrically biased at potentials V_0 and V_{N+1}, with $V_0 - V_{N+1}$.

The state of the array consists of the set of charges $\{Q_\beta\}$ that occupy the array islands and the leads. The island charges take on integer values. The charge of the nanoparticles is modified when an electron tunnels between two adjacent sites. On the other hand, the charges in the leads keep them at voltages V_0 and V_{N+1}. The charges of the source and drain can take on any real value because they can be modified discretely via the tunneling of charges or continuously via the charging of the leads by a battery.

At each iteration a single tunneling event takes place. The time involved in this event τ depends on the tunneling rates of all the possible tunneling processes. First, the change in energy and the tunneling rate of the all possible hopping events are computed. For one-dimensional array there are $2(N+1)$ possible hopping events, corresponding to the tunneling of a single electron, to the left or to the right, through any of the $(N+1)$ junctions. However, for two-dimensional arrays the number of possible processes is larger. For arrays with square lattice the number of nearest neighbors is four, then the electron can tunnel to the left, to the right, up or down. Whereas for arrays with triangular lattice, the number of nearest neighbors is six. Then the number of possible hopping events increases in two dimensional arrays and it is larger in the case of a triangular lattice than in the square case. Γ_i^+ and Γ_i^- are the tunneling rates through the i junction to the left or to the right, respectively, and are calculated from Eq. (2.1). Thus, $\Gamma^{tot} = \sum_{i=1}^{N+1}(\Gamma_i^+ + \Gamma_i^-)$ for one-dimensional arrays. Similarly in the case of two-dimensional arrays Γ^{tot} is given by the addition of all the possible tunneling rates. The probability of changing the initial configuration varies with time like

$$P^{change}(t) = 1 - P^{stay}(t) = 1 - e^{-\Gamma^{tot}(t-t_0)} \tag{2.16}$$

with t_0 the time at which the preceding tunneling process took place. In order to sample the time interval between two hopping events we generate random numbers between $[0,1]$ to mimic P^{change} and obtain $\tau = t - t_0$ from Eq. (2.16). As the average of $-lnP^{stay}$ is the unity, if one is interested only in the average values of the charge or the current, and not on its fluctuations, the time step τ could be fixed to $1/\Gamma^{tot}$ [110].

The relative probability of each tunneling event is $\Gamma_i^{\pm}/\Gamma^{tot}$. To determine the hopping process which changes the charge state, the relative probabilities are consecutively arranged in the interval $[0,1]$. A second random number in this interval is generated to select the tunneling process.

Then, the charge configuration is updated. Just after the tunneling process, it is possible that the electrodes are not at the same potential at which they were before the tunneling event, due to the fact that the charge, provided by the battery, necessary to restore the initial potential at the electrodes has not arrived yet. Thus, we allow the external circuit to return the leads to their applied bias values prior to the selection of the next hop. This effect is simulated by resetting the charges on the source and the drain to the values that restore the nominal applied bias.

In order to remove all sensitivity to initial conditions, before we track the evolution of $\{Q_i\}$ as a function of time at any voltage, we perform $N_{eq} \geq 10^4$ iterations to equilibrate the system. Following these iterations, we track the evolution of the charge state until the total number of electrons that has arrived at the drain, Q_{drain}, equals a very large number ($\geq 10^5$). The average calculated current is given by

$$I = \frac{Q_{drain}}{t_{tot}} \tag{2.17}$$

where t_{tot} is the sum of all time intervals between hopping processes when the evolution is running. If a tunneling event involving the drain is selected, an amount $\delta q = \pm 1$ is added to Q_{drain} depending on whether an electron hopped to or from the drain. Current conservation ensures that the average current is the same through any junction. The minimum numbers of equilibration cycles, N_{eq}, and evolution cycles (set by Q_{drain}) depend on the voltage.

Besides, we analyze the average potential drop through the array, that is the average of the addition of all the potential drops in the array, $\phi^{tot} = \phi^{pol} + \phi^{ch} + \phi^{dis}$. In order to calculate this average potential drop, we assume that the system is in a given state a time equal to the interval τ until the next tunneling event takes place.

3 Transport through one-dimensional nanoparticle array. Short-range interactions

In this chapter I will give a complete description of the transport properties through one-dimensional metallic nanoparticle arrays when they are placed between metallic electrodes, considering short-range interaction and zero-temperature. I will also see how they are affected by different types of disorder. I will first study the threshold voltage, at which the current starts to flow in these systems. After that, I will see the characteristics of current flow. And finally, I will analyze the potential drop through the array.

3.1 Threshold Voltage

The threshold voltage is the minimun bias voltage at which the current can flow through the array. It is controlled by changes in the energy for tunneling. There is current through the array when the charges are able to be transferred from one electrode to the other one through the whole array. At zero temperature, the probability of a tunneling process is given by $\Gamma(\Delta E) = \frac{-1}{R_T}\Delta E\Theta(-\Delta E)$ and vanishes when ΔE is positive or zero. It means that only the processes with gain in energy will be possible.

3.1.1 Clean Arrays

The clean case of a related system was studied by Hu and O'Connell [104]. They analyzed an one-dimensional array of N gated junctions with equal junction capacitances C_J and equal gate capacitances C_g. Due to the finite value of C_J charges in a given island interact with charges in other islands and with charges in the electrodes. With an applied bias voltage the interaction between charges in the electrodes and in the islands results in a bias induced potential drop at the bulk junctions. Once a charge is injected unto the array, it will have no difficulty in traveling through it, and the threshold voltage equals the voltage required for injection of a charge from the electrodes. As the ratio C_g/C_J increases the threshold voltage of a long array tends to an N-independent value of the order of the charging energy. The on-site case discussed here corresponds to $C_J = 0$. If one extrapolates the case discussed by Hu and O'Connell [104] to $C_g/C_J \to 0$ an N-independent threshold voltage would be expected for onsite interactions. For the case studied in this thesis this prediction is not satisfied. This

is because unlike the case of [104] in which once the charge enters into the array it can flow freely, for a clean array with $C_J = 0$ at zero temperature the charges cannot travel through the array if there is not gain in energy. As a result, the threshold voltage depends on the size of the array, increasing with the number of islands.

In a clean array the difference between the energy of the system before and after the tunneling event is given by

$$\Delta E = E^{e-h}_{\gamma,\beta} + (\phi_\beta - \phi_\gamma) \tag{3.1}$$

Therefore, in order to allow charge tunneling it is necessary that the potential drop in the junction overcomes the excitonic energy $E^{e-h}_{\gamma,\beta}$, which is always positive. In clean arrays $\phi^{dis} = 0$ and for short-range interaction ϕ^{pol} is only finite at the contact junctions (section 2.2). In this situation the charge can enter into the array through the contact junctions, but once it is in the first or last island it cannot pass to the next one because there is no potential drop which allows the flow. As at the inner junctions there is no potential drop, these $N-1$ junctions prevent the flow of charge. A charge gradient at each bulk junction has to be created to allow the charge transfer from one electrode to the other one. The charge gradient is created by the accumulation of the charges that enter into the array, see Fig. 3.1 where a charge gradient is represented for a symmetrically biased array. In this case the charge gradient consists in the accumulation of charges positive and negatives. The positive charge enters into the array from the source electrode and the holes or negative charges appear when the charges exit the array from the drain.

The threshold voltage depends on the way the array is biased, as we can see in Fig. 3.2(a) where the threshold corresponding to the clean case is plotted for the case of symmetrically biased arrays ($\alpha = 1/2$), asymmetrically biased arrays ($\alpha = 1$), and an intermediate biasing ($\alpha = 3/4$). This dependence appears because at the contact junctions the polarization potential depends on α. Then for a given voltage, for some values of α the polarization potential can overcome the charging energy at one of the contact junction but not at the other one. As a result, the charges enter into the array at different voltages.

In the symmetrically biased case, the threshold voltage V_T shows a step-like dependence on N. There is an even-odd effect. This even-odd effect is absent for completely asymmetric biased arrays ($\alpha = 1$ and $\alpha = 0$). For the case of symmetrycally biased arrays $\alpha = 1/2$, increasing the potential at the electrodes allows positive and negative charges to enter from the source and the drain respectively. These charges accumulate on the array and create potential drops across the bulk junctions. At voltages just below the threshold, the charges accumulated at the first and last islands are equal in number and opposite in sign, Fig. 3.1. Current starts to flow at voltages larger than $V_T = 2NE^{isl}_c$ when N is odd and $V_T = 2(N-1)E^{isl}_c$

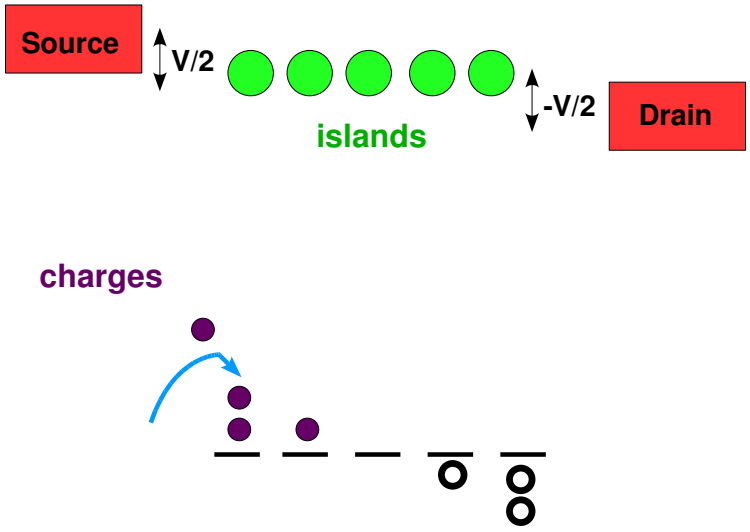

Figure 3.1: Schematic diagram of a clean symmetrically biased array and the charge gradient that has to be created in this array to allow the flow of charge in the onsite limit.

when N is even. These values allow for the build up of $\pm(N-1)/2$ and $\pm(N-2)/2$ charges at the first and last islands for odd and even N respectively, creating a charge gradient $dQ_i = Q_i - Q_{i-1} = -1$, across all bulk junctions for odd N and across all bulk junctions except one for even N. In the case of even N one junction can be uncharged, because the contact junctions are equivalent and charge can enter from both leads so it is possible in some cases for the energy barrier across one of the bulk junctions to be overcome by the potential drop due to two injected charges of opposite sign from the two leads, i.e. by the aniquilation of these two charges. Then V_T for even N is equal to the V_T for a clean array with $N-1$. However, for $\alpha = 0, 1$, charge can only enter into the array from one lead and the energy barriers across all $N-1$ bulk junctions must be overcome by accumulated charges. As a result, the even-odd effect dissapears for completely asymmetrically biased arrays, which threshold voltage is given by $V_T = E_c^{isl}(2N-1)$. There are also intermediate situations such as $\alpha = 3/4$, see Fig. 3.2 (a).

Futhermore, the threshold voltage changes in a periodic way with α for a given N, see Fig. 3.2(b). The period depends on the number of barriers in the array. The number of charges that have to be accumulated in the first and last island to allow the flow of current is reflected by the dependence of V_T on N and periodic characteristics in V_T with respect to α.

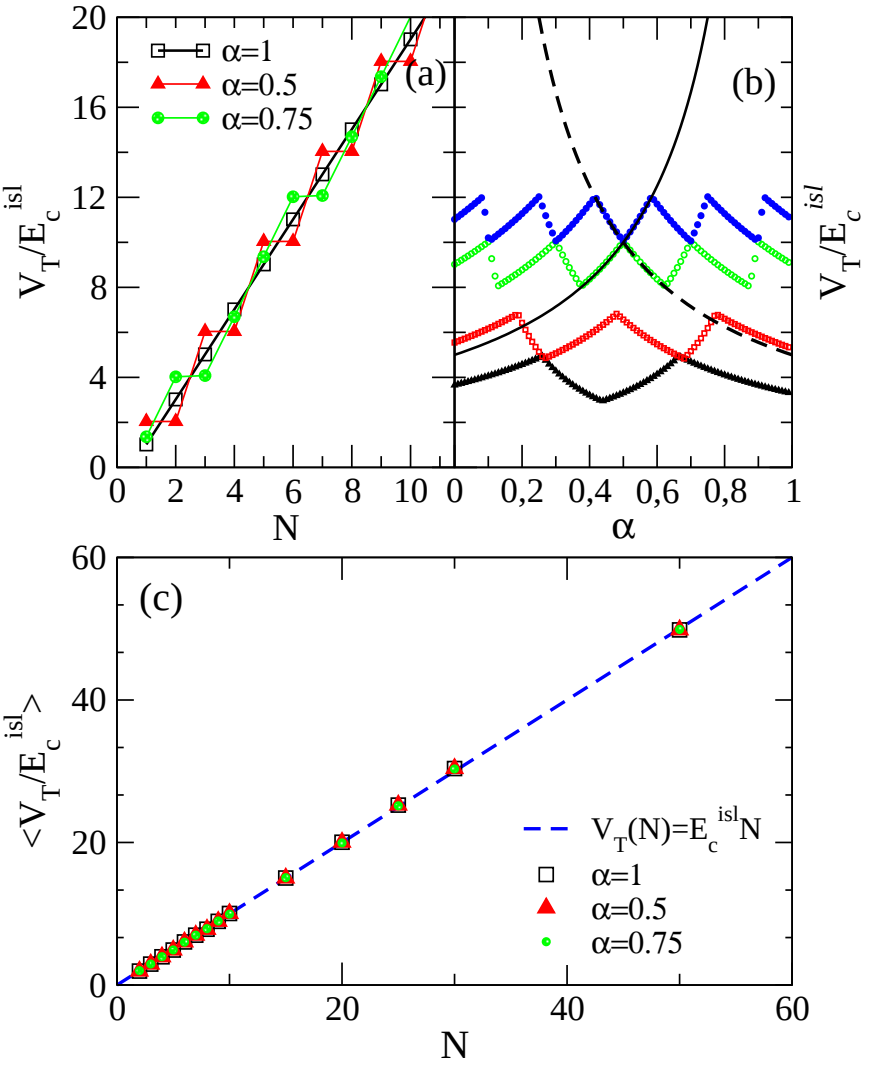

Figure 3.2: (a) Threshold voltage of clean arrays as a function of the number of islands N for different values of the asymmetry bias parameter α. (b) Threshold voltage as a function of α. From top to bottom lines with symbols correspond to clean arrays with 6 and 5 islands and to disordered arrays with 6 and 5 islands. For comparison thin solid and dashed lines give, for clean arrays, the bias voltage at which 2 and -2 charges can be placed at the first and last islands. (c) Average threshold voltage for disordered arrays as a function of the number of islands.

3.1.2 Disordered Arrays

Once we have seen the threshold voltage in the clean case, we study now how it is affected by the disorder. Specifically by charge disorder. Here we do not analyze the disorder in resistances because it does not have any influence in V_T, due to the fact that the threshold voltage is controlled by changes in energy in tunneling, which are independent of the resistance of the junctions.

In charge disordered arrays $\phi_i^{dis} \neq 0$, then at the bulk junctions there is a finite potential drop. This disorder potential ϕ_i^{dis} at the islands can be either positive or negative ($-E_c^{isl} \leq \phi_i^{dis} \leq E_c^{isl}$). The potential drop at the junctions ($\Phi_i^{dis} = \phi_i^{dis} - \phi_{i-1}^{dis}$) can also be positive or negative. Only junctions with upward steps in the disorder potential $\Phi_i^{dis} > 0$ prevent the flow of charge, while the downward steps $\Phi_i^{dis} < 0$ facilitate it. In average there are $N/2$ upward steps. To allow the flow of current a charge gradient has to be created only in step-up junctions. The threshold voltage is reduced with respect to the clean case. For short-range interactions in average it results $< V_T >= E_c^{isl} N$ and the dependence with α disappears, see Fig. 3.2 (c). The linear dependence of the average threshold voltage on the array length was already known, in this thesis we only recover this prediction [64].

3.2 Flow of Current

For bias voltages larger than the threshold voltage the current I can flow through the array. The current is a strongly non-linear function of voltage. Although the dependence of the current with the voltage has been studied by several groups for years, there are some behaviors of the current that are not well understood. In this thesis we analyze the three different regimes which can be distinguised in the $I - V$ curve, see Fig. 3.3. There are two linear regimes and a step-like behavior between them, called Coulomb staircase. Specially this last has been known for a long time [30, 35, 36], in this work we clarify the dependence of the Coulomb staircase profile on the bias parameter α. At very low voltages there is a power-law dependence, we resolve analytically and numerically the controversy on the exponent of this power-law. We also estimate the asymptotic current at high voltages. The current depends on the charging energy, the number of islands, the presence or not of charge disorder in the array, the resistances of the junctions and on the asymmetry of the applied bias voltages. In the following subsections we disscuss all these dependences in each regime of voltage.

3.2.1 Linear dependence close to the threshold

Until now in nanoparticle arrays, most studies have focused on the power-law behavior of the current close to the threshold, with main emphasis in the case of disordered arrays. There has been some controversy regarding this power-law of the current with $(V - V_T)$ through one dimensional disordered arrays for voltages close to V_T, $I \sim (V - V_T)^{\zeta}$. Middleton and Wingreen [64] predicted linear behavior for both the long and short range interaction. Reichardt and Reichardt [90] found a square root behavior using a model with a $1/r$ interaction between the charges in the islands. $\zeta = 1/2$ is the exponent corresponding to an sliding

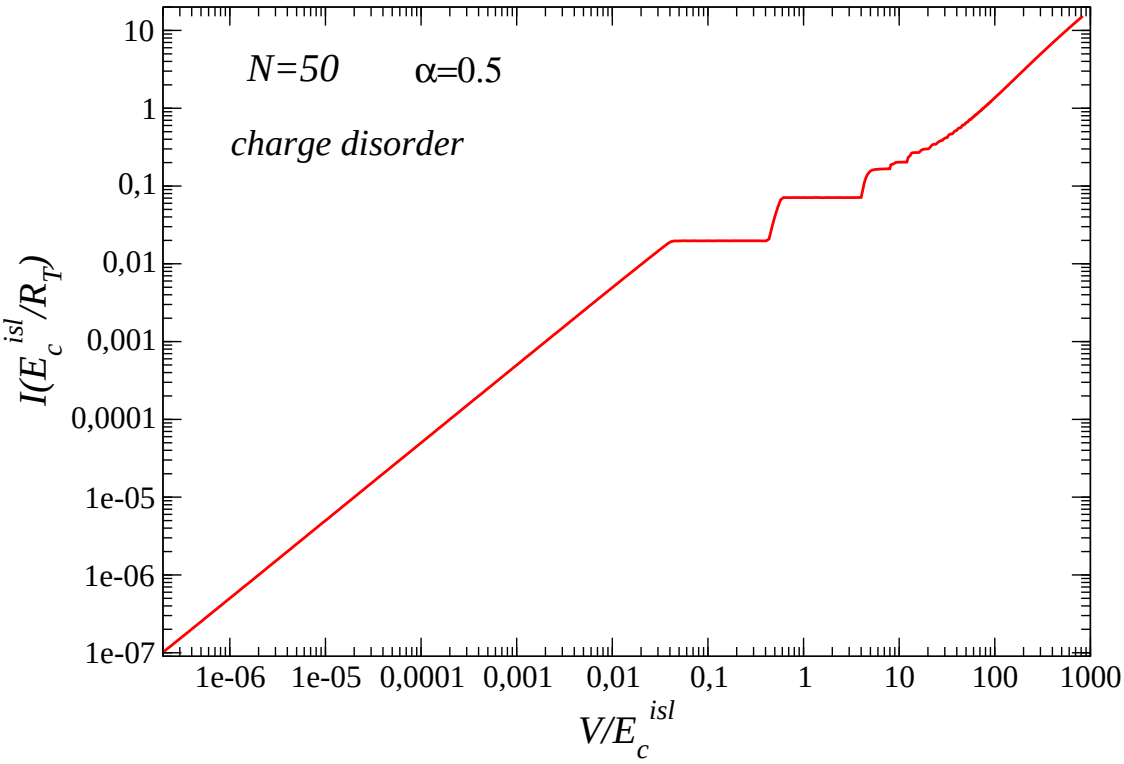

Figure 3.3: I-V curve for a charge disordered symmetrically biased array with $N = 50$ islands at zero temperature. The current is a non-linear function of the voltage. The $I - V$ shows three different regimes, two linear and the Coulomb staircase.

charge-density wave. They argued that the value $\zeta = 1$ obtained by Middleton and Wingreen [64] is a consequence of using voltages which are not small enough. Kaplan *et al* [89] found $\zeta = 1$ in the long-range limit of an array of dots capacitively coupled to their nearest neighbors. Jha and Middleton [102] argued that the dependence of the current of disordered arrays in the onsite limit on $(V - V_T)$ for voltages marginally greater than V_T is linear with a slope inversely proportional to the length of the array. As $V_T \sim N$ this would result in a scaling law $(V/V_T - 1)$. So far, in one-dimensional arrays practically there are not experiments [22], and in the case of quasi-one dimensional systems there are few experiments. The approximate power-law measured in quasi-one dimensional systems [9, 78] at voltages in the region $(V/V_T - 1) \sim 0.02 - 10$ is larger than unity, which has been attributed to the fact that the system is not strictly one-dimensional.

The prediction of Middleton and Wingreen is based in the fact that for voltages close to threshold the current flows through different channels in which the current depends linearly on $(V - V_T)$. The number of channels depends on the dimensionality of the array. For the case of one-dimensional arrays they predicted that there is only a conducting channel, and

as a result, the current depends linearly on $(V - V_T)$.

In this thesis, we show that the current varies linearly with respect to $(V - V_T)$ for very small $(V - V_T)$ and a single channel contributes to it. However the slope is not inversely proportional to N, as until now has been predicted by previous groups. The dependence of the slope on the length of array could be possible if the value of the current was controlled by the whole lattice, and was predicted assuming a linear drop of the polarization potential. But as we will see in this thesis at low voltages it does not occur. The linear behavior appears for several orders in magnitude, see Fig. 3.4 what confirms that it is a real close to threshold power-law.

The linear dependence for voltages close to threshold can be easily understood. The current through the array is given by the average charge transferred per unit time. The average time necessary to transfer a charge through the array is the sum of the time involved in all the processes in the sequence of tunneling events from the moment in which the charge enters into the array from one electrode until it leaves the array from the other one. If the time for tunneling through one junction is much larger than the time associated to the other ones, this junction acts as a bottleneck. The time necessary to tranverse the array is approximately equal to the time associated to tunnel through this junction. On average this time is equal to the inverse of the tunneling rate given by Eq. (2.1). Therefore, the current can be approximated by the tunneling rate across the bottleneck junction:

$$\Gamma(\Delta E) = \frac{1}{R_{bn}} \frac{\Delta E}{exp(\Delta E / K_B T) - 1} \tag{3.2}$$

The charges can enter into the array only through the contact junctions from the electrodes. For voltages smaller than the threshold, a tunneling process at the contact junctions costs finite energy, and as a consequence the transport is suppresed. When $V > V_T$ but very close to V_T the charge can enter into the array through a contact junction, and once inside, it can flow freely through the array thanks to the charge gradient created at the inner junctions. Then the entrance junction acts as a bottleneck for the transport. We remember that at zero temperature the probability of a tunneling process is $\Gamma_T = -\Delta E/R$, and the change in energy in a tunneling process at the contact junctions depends linearly on voltage due to the polarization potential. $\Delta E = \alpha(V - V_T)$ and $\Delta E = (\alpha - 1)(V - V_T)$ for the source and the drain junctions respectively. Then, if the charge enters to the array by the source junction, the current is approximately

$$I = \frac{1}{R_1} \alpha (V - V_T) \tag{3.3}$$

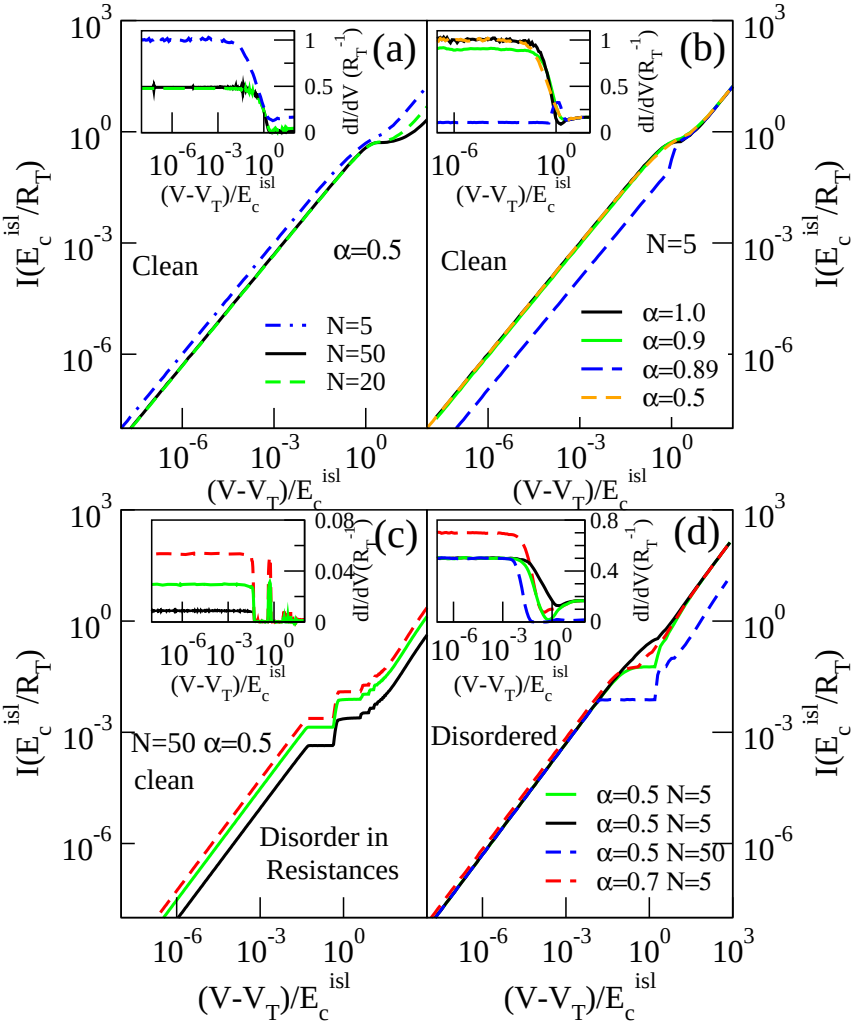

Figure 3.4: Main figures: I-V curve in logarithmic scales for different array parameters. Insets show the derivaties (in units of $1/R_T$) of the curves plotted in the main figure. (a) to (c) show I-V curves corresponding to clean arrays, it means without charge disorder. All junction resistances are equal in (a) and (b). In (c) I-V curves for arrays with junction resistances randomly assigned varying between $(5-11)R_T$ (upper curve), $(8-21)R_T$ (middle curve) and $(23-83)R_T$ (bottom curve). (d) I-V curves of charge disordered arrays with homogeneous contact resistance. The $\alpha = 0.5, N = 5$ curves correspond to different realizations of disorder.

while if the threshold is controlled by the drain junction the current resulting is

$$I = \frac{1}{R_{N+1}}(1-\alpha)(V-V_T) \tag{3.4}$$

In particular, in the case of symmetrically biased arrays $\alpha = 1/2$, the current depends on whether the number of islands in the array is even or odd. When N is odd the charge can

enter through both source and drain junctions, then both have to be taken into account.

$$I = \left(\frac{1}{R_1} + \frac{1}{R_{N+1}}\right)\frac{1}{2}(V - V_T) \tag{3.5}$$

For N even, the flow of current requires that charge enters through both junctions and the current is approximately equal to

$$I = \frac{2}{R_1 + R_{N+1}}\frac{1}{2}(V - V_T) \tag{3.6}$$

This even-odd effect of the slope in current has the same origin as the one in the threshold voltage. When N is odd to transfer one charge across the array from one electrode to the other one, there is only one bottleneck process, while in arrays with N even there are two. It can be better seen with schematic diagrams, see Fig. 3.5 in which the charge gradients and the schematic diagrams for the flow of a charge through the array are represented for two arrays with an odd and even number of islands in (a) and (b) respectively. In the case of a clean array with $N = 5$ islands, if a charge enters into the array it can arrive at the central island thanks to the charge gradients. In this case, the charge has been transferred through the array see Fig. 3.5 (a). However, for an array with $N = 6$ islands, if through the source junction one charge enters into the array, it can only reach the third island, see (2) in Fig. 3.5 (b) in which it can be observed that the tunneling processes from third or fifth islands to the fourth one are not energetically favorable. As a result, there is no current through the system. Therefore, one charge more has to enter through the other contact junction to allow the current flow through the array, see (3) in Fig. 3.5 (b).

This even-odd effect in the slope in current and the linear dependence close to the threshold are clearly observed in Fig. 3.4, where in the main figures the I-V curves are represented in logarithmic scale for different arrays parameters, and their derivatives dI/dV in the insets. For clean arrays the slope of the linear dependence is independent of the number of islands Eqs. (3.3) and (3.4), except for $\alpha = 1/2$. For symmetrically biased array the slope shows the even-odd effect explained above which is predicted by Eqs. (3.5) and (3.6), and that is equal to 0.5 for odd arrays with any odd number of islands, and double (unity) for even arrays, see inset of Fig. 3.4 (a). The slope of the current depends on α. The change in slope with α is smooth and given by α/R_1, as predicted by Eq. (3.3), but turns nonmonotonously if currents starts to be controlled by the other contact junction, Eq. (3.4) with slope $(1-\alpha)/R_{N+1}$.

The disorder in resistances affects the slope in the current. The slopes are different because there are different resistances at the bottleneck junction, see Fig. 3.4 (c), where $I - V$ curves are represented for several resistance disorder configurations.

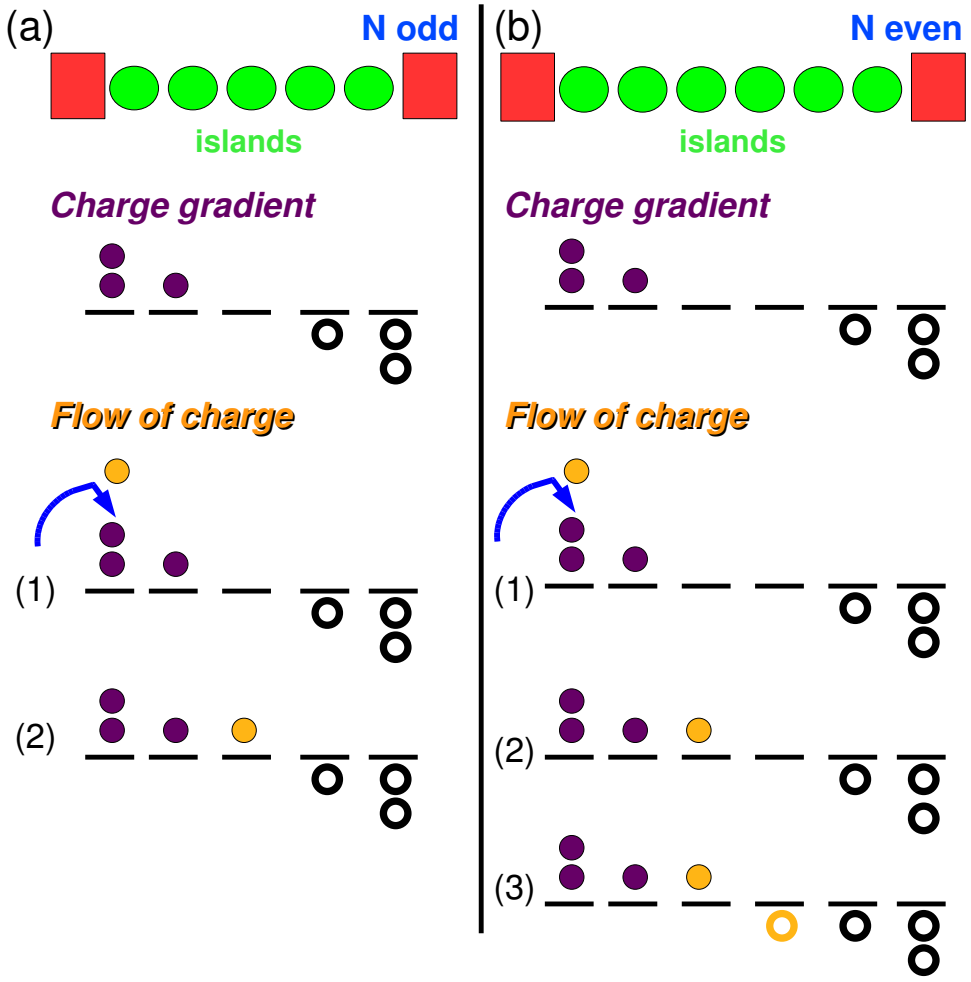

Figure 3.5: Schematic diagrams of the charges at sites in two symmetrically biased arrays with different length, $N = 5$ (a) and $N = 6$ (b) at voltages just above the threshold. The charge which flows is represented in different color to the charges accumulated that form the charge gradient. For odd N the charge can enter from both electrodes, however in the case of even N to allow the flow of current the charge has to enter through both contact junctions.

The even-odd effect dissapears when there is charge disorder in the array, see Fig. 3.4 (d). This is due to the fact that the charge disorder modifies the potential drop and ΔE of all tunnel barriers with respect to the clean case, and now in the array only one contact junction acts as a bottleneck, regardless of whether N is odd or even. The slope in current depends on α although there is charge disorder in the array, see inset of Fig. 3.4 (d).

Although the linear dependence appears for several orders in magnitude, it disappears for $V - V_T \approx 10^{-2}$ or $(V - V_T)/V_T \sim 10^{-4}$. The magnitude of the current is probably too small for this linearity to be detected experimentally.

3.2.2 Intermediate voltages and Coulomb staircase

At intermediate voltages there is a loss of linearity. It occurs when the junction that acts as a bottleneck stops controlling the current. We have found that linearity gives rise to sublinear behavior when the time of the other tunneling processes become relevant compared to the time spent at the bottleneck. Upon increasing V the tunneling rates of the different processes involved in the transport become more homogeneous. To obtain sublinear behavior, it is just necessary that the two slowest processes in a sequence have comparable rates. Then the loss of linearity can depend on different factors. For example, when a non bottleneck junction has a resistance much larger than the resistance of the bottleneck's, the time required to tunnel through these junctions can be comparably long for smaller voltages than in the case of homogeneous resistances. In the case of longer arrays, we can expect that the loss of linearity happens at smaller voltages, because there are more tunneling processes which contribute to the total time. On the other hand, in charge disordered arrays, the energy gain of some of the tunneling processes is smaller than in the clean case and the contact junctions could stop being the bottleneck earlier, i.e. for smaller $V - V_T$. But, in general we have not found very significative differences for different array parameters in the value of the bias voltage at which the linearity disappears.

At intermediate voltages the current shows steps, as can be observed in Fig. 3.6. This regime is called Coulomb staircase. As we mentioned before, the existence of the Coulomb staircase regime has been known for a long time [30–36, 99, 101]. Early claims reported a Coulomb staircase only in the asymmetrically biased case [30]. More recent results in clean capacitively coupled nanoparticle arrays, show that a staircase also emerges in a symmetric array under symmetric bias [37], but claim that the I-V characteristic for an N-dot array under forward bias is identical to that for a 2N-dot one under symmetric bias. We show here that while the appearance of the staircase is generic, the last statement is not correct.

Clen arrays

The Coulomb staircase in the current is a consequence of the fact that the junction that controls the transport is a bulk junction. Specifically, the tunneling process at this junction has a small gain in energy and a long time associated to the tunnel. The energy of a tunneling process through an inner junction in the pure short-range does not depend on the applied voltage. Thus, increasing the voltage does not change the value of the current. In case of clean arrays, the staircase profile showed by the current is very soft due to the charge gradient created through the array, see insets in Figs. 3.6 (a) and (b).

Although the current is weakly dependent of the voltage within the steps, at some voltages the current changes. These changes are produced because new transport processes are

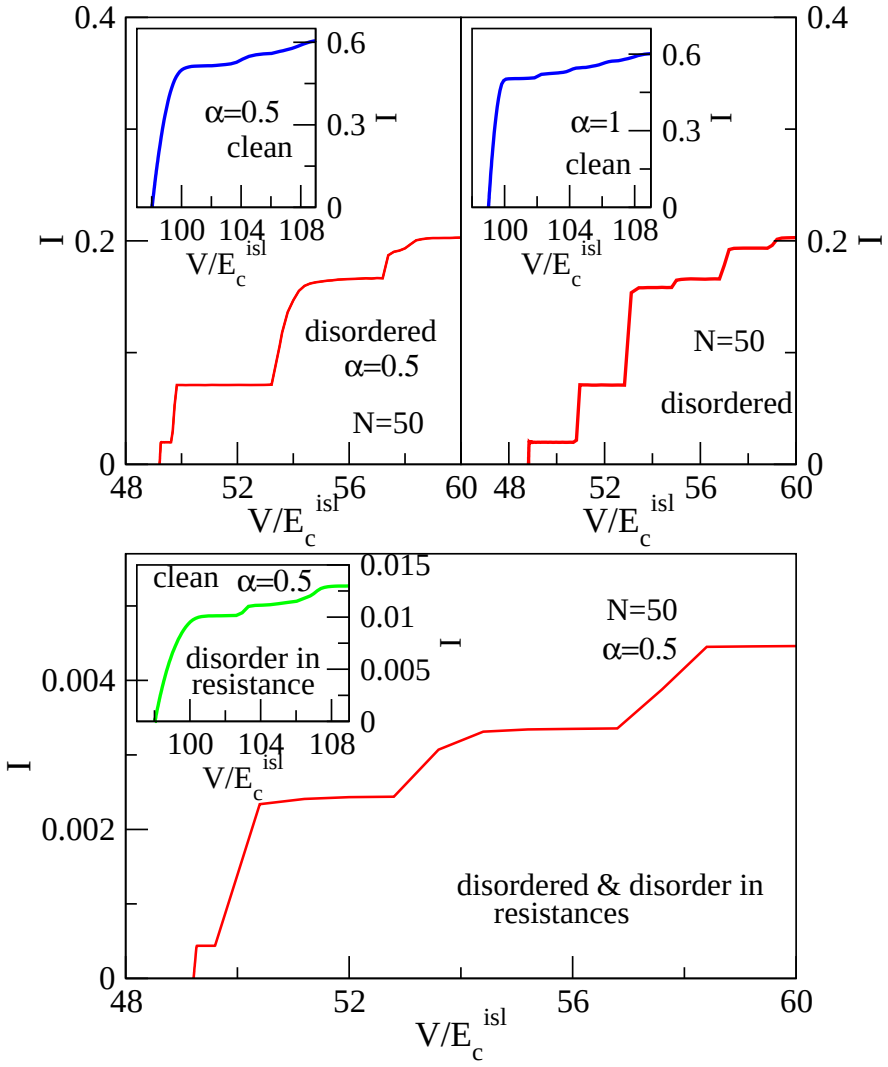

Figure 3.6: I-V curves for N=50 and different array parameters at intermediate bias voltages showing the Coulomb staircase. Insets in (a) and (b) correspond to an array without charge or resistance disorder and $\alpha = 0.5$ and $\alpha = 1$ respectively. Main figures in (a) and (b) show I-V curves for arrays with charge disorder but homogeneous resistances. $\alpha = 0.5$ in (a) and $\alpha = 1$ in (b). (c) The I-V curves correspond to arrays with resistance disorder and $\alpha = 0.5$ without charge disorder in the inset, and with charge disorder in the main figure.

allowed, thanks to the accumulation of charges at the first or last island. It means that when the maximun number of charges that can be accumulated at the first or last island changes because of a change in voltage, a new tunnel process can occurs. For adding one charge more to the first or last island it is required that the potential drop at the contact junctions increases a quantity equal to $2E_c^{isl}$. Thus, the voltages at which the new processes occur depend on α. For example, in a clean completely biased array ($\alpha = 1, 0$), the polarization potential only varies in one electrode, then the width of the steps in bias voltage is $2E_c^{isl}$. Whereas, in

a symmetrically biased array ($\alpha = 1/2$) the charge can enter through both contact junctions, then the change in potential of a given electrode is just half the change in bias voltage and steps appear in intervals of $4E_c^{isl}$, see Fig. 3.6 (a) and (b) insets. As we can see, in the current there is a big jump at the threshold, associated with requirement of creating a charge gradient through all the array to allow the flow of current. Once the charge gradient is created, the charge can be easily transferred across the array. The steps at higher voltages are much smaller in height, and they have the width predicted.

Charge disorderded arrays

For charge disordered arrays, the steps are more clearly observed than in the clean case because tunneling processes in the bulk can have small energy gain and become the bottleneck more easily in the disordered case than in the clean one. As can be observed in main Figs. 3.6 (a) and (b) in which the $I - V$ curves are represented for disordered arrays with different α, there are clear plateaux in the current.

The position of the voltages at which the current has kinks, also depends on the charge disorder. For charge disordered arrays with $\alpha = 0,1$ the width of the voltage intervals is equal to the one found in the clean case, $2E_c^{isl}$, see main figure and inset in Fig. 3.6 (b). This is because the new charges are added through a single junction. When $\alpha = 1/2$, charges enter the array from both contact junctions but the corresponding kinks in the current do not appear at the same voltage. While the width of a kink corresponding to a given contact junction remains equal to $4E_c^{isl}$, in a general case in the I-V characteristic there will be two kinks in each $4E_c^{isl}$ interval in bias voltage due to the alternative position of the kinks of both contact junctions, see main Fig. 3.6 (a). On the other hand, if we compare the main figures with the insets in Figs. 3.6 (a) and (b), can be seen that in the $I - V$ curves for charge disordered arrays, the big jump that appears in the clean case is reduced. It is a consequence of the fact that in the disordered case the charge gradient is created only in the step-up junctions, which prevent the flow of charge. However in the clean case as all the inner junctions prevent the current flow, the charge gradient has to be created through all the array.

Disorder in resistances

Disorder in resistances affects the Coulomb staircase regime. Specially, it affects the staircase profile of the current, whereas the voltages at which the kinks in the current appear are not modified by this type of disorder. The change in the staircase profile due to the disorder in resistance with respect to the clean or charge disordered cases with all the resistances equal can be observed in Figs. 3.6 (c) and (a). When there is a very large resistance in a bulk junction it can sharpen the steps, because of the energy for the tunneling through this junction, that acts as a bottleneck, it is independent of the bias voltage. However, the opposite case with a

very large resistance at a contact junction can be possible too. In Fig. 3.6 (c) we can see the characteristic profile for an array with charge disorder and disorder in resistances.

3.2.3 Linear behavior at high voltages

At high voltages a linear dependence is recovered. Although this linear behavior was already known, in this thesis it has been calculated analytically.

Clean and Charge disordered arrays

At very high voltages, all the tunneling processes required to transfer one charge from source electrode to drain one through the array decrease the energy because of the large charge gradient. As a result, all of them are possible. The corresponding tunneling rates are $\Gamma_i = R_i^{-1}(\Phi_i - E_i^{e-h})$ and the total tunneling rate Γ^{tot} is $\sum_{i=1}^{N+1}\Gamma_i$. Besides, the total potential drop through the array is equal to bias voltage applied, $\sum_{i=1}^{N+1}\Phi_i = V$, then for no resistance disorder $\Gamma^{tot} = R_T^{-1}\left(V - \sum_{i=1}^{N+1} E_i^{e-h}\right)$. This rate is independent of the selected tunneling process. To transfer a charge from the source to the drain requires in average $(N+1)$ tunneling events. Thus, the average current is

$$I_{asympt} \sim \frac{1}{(N+1)R_T}\left(V - \sum_{i=1}^{N+1} E_i^{e-h}\right) \tag{3.7}$$

This prediction is valid for clean and charge disordered arrays with homogeneus junction resistances, see Fig. 3.7 (a) where $I-V$ curves numerically obtained for clean and charge disordered arrays are compared with the theoretical prediction given by Eq. (3.7). Both curves approach the same asymptotic curve, even if the threshold voltage is different. In this regime of voltages the charge does not feel the presence of charge disorder.

The slope of current only depends on the number of junctions in the array, $(N+1)$. The slope is equal to the inverse of the addition in serie of all the junctions resistances. At high voltages, the slope of current does not depend on α or charge disorder. See Fig. 3.7 (c) where the theoretical prediction is compared with the numerical results.

On the other hand, the asymptotic current does not extrapolate to zero current at zero voltage, but it cuts the zero current axis at a finite offset voltage. This offset voltage is a charging effect, which is observed in single junctions systems. The offset voltage is proportional to the number of islands in the array and is given by the sum of the excitonic energies of all the junctions, $V_{offset} = \sum_{i=1}^{N+1} E_i^{e-h}$, see inset in Fig. 3.7 (c). Futhermore, it is independent of the resistance of the junction and α. In general, V_{offset} is different from the value of the threshold voltage.

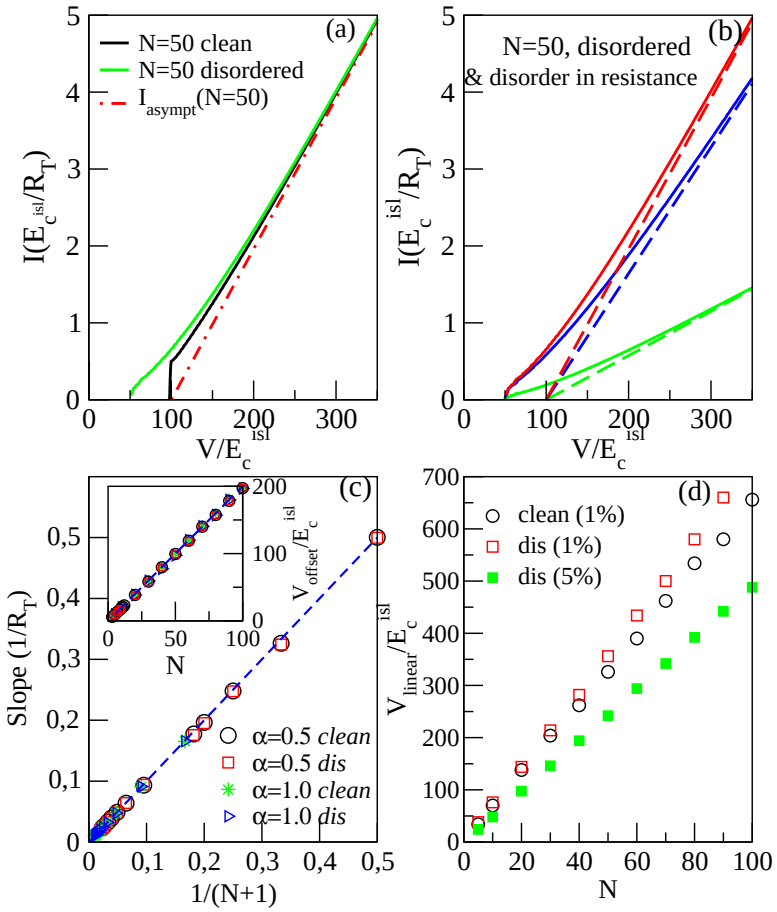

Figure 3.7: I-V curves calculated up to high-voltages for $N = 50$, $\alpha = 0.5$ for clean and charge-disordered arrays. Theoretical prediction is included for comparison. (b) Computed I-V curves for charge-disordered arrays with different junction resistances (solid lines) with their theoretical asymptotic predictions (dashed lines). From top to bottom a curve corresponding to an array with all-equal junction resistances, an array with randomly assigned resistances and an array with all-equal random resistances, except the first one which is ten times R_T. (c) Slope (main figure) and offset voltage (inset) which give better fitting to the numerically computed current at high-voltages as a function of the number of islands in the array, for several array parameters, all of them with homogeneous junction resistances. For comparison the theoretical prediction (dashed-line) is included. (d) Voltage at which the high-voltage asymptotic behavior is reached.

Resistance disorder

For arrays with disorder in resistances the asymptotic prediction Eq. (3.7) is not valid. In this last case the total tunneling rate of each step in a sequence is $\Gamma^{tot} = \sum_{i=1}^{N+1} R_i^{-1}(\Phi_i - E_i^{e-h})$. We assume that on average, the charge gradient would be such that it ensures a uniform tunneling rate Γ^{uni} through all the junctions. The potential drop which gives such a tunneling rate is $\Phi_i = R_i\Gamma^{uni} + E_i^{e-h}$ and $\Gamma^{uni} = \left(V - \sum_{i=1}^{N+1} E_i^{e-h}\right)/R_{sum}$ with $R_{sum} = \sum_{i=1}^{N+1} R_i$. There

are $(N+1)$ possible tunneling events at each step in a sequence and $(N+1)$ steps. Both $(N+1)$ factors cancel out. The resulting average current is

$$I_{asympt} \sim \frac{1}{R_{sum}} \left(V - \sum_{i=1}^{N+1} E_i^{e-h} \right) \tag{3.8}$$

Again the slope in the current corresponds to the addition in series of all the junction resistances. When all resistences are equal this equation reduces to Eq. (3.7). The predicted asymptotic high-voltage behavior is observed in Fig. 3.7 (b) for arrays with different parameters. Good agreement with Eq. (3.8) justifies the uniform tunneling rate assumption. Arrays with the same threshold voltages have different slope depending on the junction resistances.

In order to know if the linear regime at high voltages can be seen experimentally, we compute the voltage at which the linear behavior is reached, V_{linear}. It is estimated as the value at which $(I - I_{asympt})/I$ is smaller than a given value, 1% and 5% in Fig. 3.7 (d). It is slightly larger for disordered arrays, increases linearly with the number of islands and it is approximately three and 2.5 times the offset voltage. The longer the array the larger the voltage required to reach the linear behavior. As a consequence, in very long arrays it is possible that V_{linear} will be very large and the linear behavior will not be easily reached experimentally.

3.3 Potential drop through the array

Although nowadays the potential drop through the array can be measured [111], it has not been studied theoretically. In conventional ohmic systems with a linear current-voltage relation $V = IR$ the potential drops homogeneously through the array if the resistivity of the system is homogeneous. When the proportionality constant between voltage and current is given by the sum of the resistances in series, but these resistances are not all equal, the voltage drop at each point is proportional to the local resistance. However, the nanoparticle array I-V characteristics are highly non-linear and in general it is not obvious how the potential drops through it. In this thesis we study the potential drop through the array at different regimes of voltages. These regimes are the same in which we have analyzed the flow of current, at low, intermediate and high voltages.

We remember from section 2.2 that in the onsite limit the total potential at the islands is the sum of disorder and charge potentials $\phi_i = \phi_i^{dis} + \phi_i^{ch}$, due to the fact that the polarization potential vanishes at the islands. At the electrodes, the potential is controlled by the applied bias voltage. But a crucial quantity for the transport is the potential drop at the junctions, because depending on it the charge flow will be allowed or forbidden. At the junctions

the potential drop is given by

$$\Phi_i = \phi_i - \phi_{i-1} \tag{3.9}$$

The potential drop varies with the time, for this reason we study the average potential drop, which in the junction is $\bar{\Phi}_i$.

3.3.1 Low Voltages

The current depends linearly on $V - V_T$ for voltages close to the threshold. In this regime, the average potential drop mainly reflects the charge state of the array at threshold. This is because the transport is controlled by a bottleneck junction, and the time required to tunnel through this junction is much larger than the one associated to the tunneling processes through the rest of the junctions. Then most of the time the charge state is equal to the one at threshold, and only changes with the fast passage of charges.

This charge state depends on charge, on the asymmetry of the voltage drop α, and on the presence or ausence of disorder in the array. Moreover, in the case of symmetrically biased clean array it depends on the even or odd number of islands.

Clean arrays

In the case of a completely asymmetric biased clean array with $\alpha = 1$, at the drain contact junction there is no potential drop, then the charges can only enter into the array from the source and $(N-1)$ bulk junctions prevent the flow of charge. If an electron reaches the last nanoparticle, it can freely jump onto the drain at zero potential. There is no charge gradient at the drain junction. Consequently, the potential drop at this junction vanishes at threshold, see Fig. 3.8 (a). On the contrary, at the $(N-1)$ bulk junctions there is a charge gradient equal to one, which corresponds to a potential drop $2E_c^{isl}$. At the source junction it is equal to the excitonic energy, that approximately equals E_c^{isl}. The average potential drop, plotted in Fig. 3.8 (a) for a clean array with all junction resistances equal is almost the same as the static potential drop at threshold.

For symmetrically biased arrays $\alpha = 1/2$, as for $\alpha = 1$ the average potential drop is very similar to the one at threshold. In this case it is equal to the excitonic energy at each junction. $2E_c^{isl}$ for bulk junctions and $\sim E_c^{isl}$ at the contact ones. Then if we substract to the potential the excitonic energy, it is approximately zero, $\bar{\Phi}_i - E_i^{e-h} \sim 0$, as we can see in the main figure in Fig. 3.8 (b). But this only occurs when a charge gradient is created in all junctions, i.e. when the number of islands is odd. However, in the case of even N, there is one junction which does not have charge gradient, then $\bar{\Phi}_i - E_i^{e-h}$ is finite. Inset in Fig. 3.8 (b) shows that

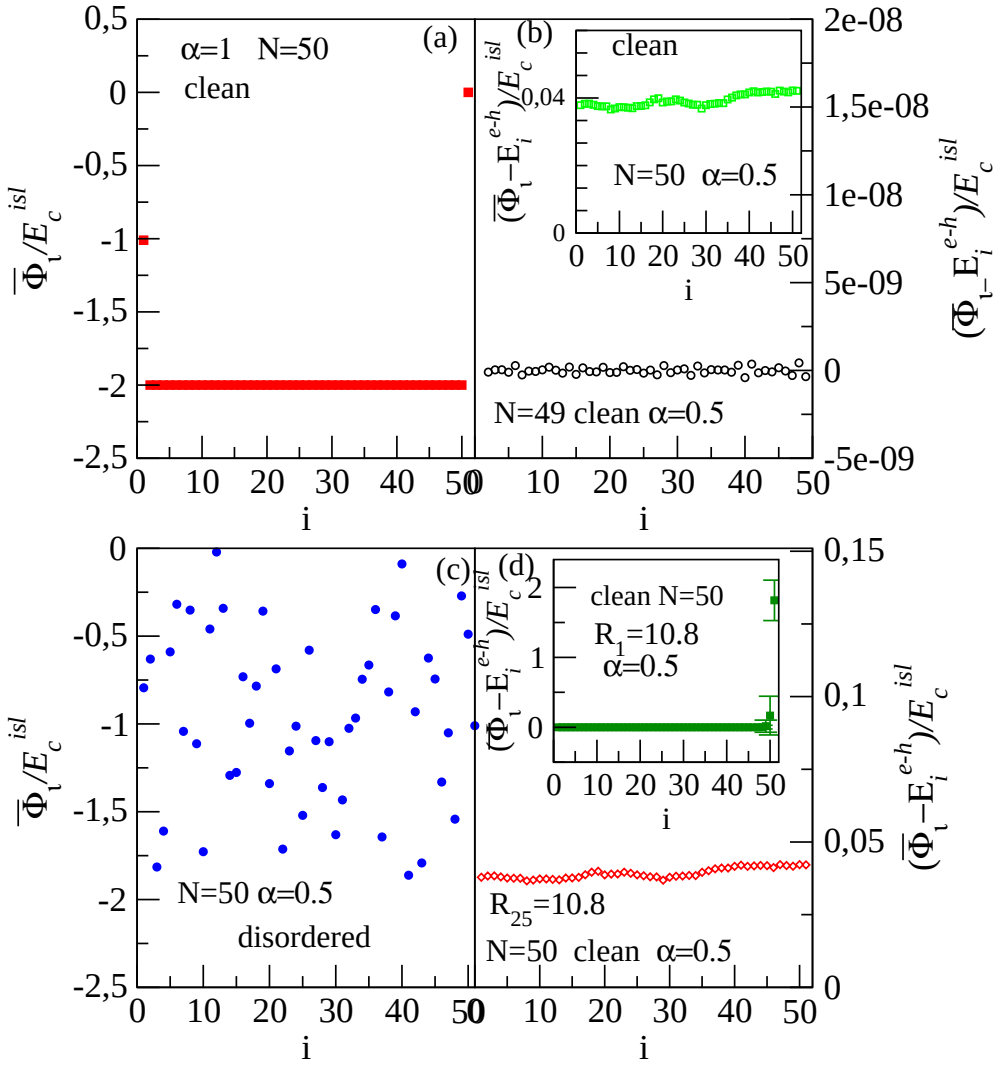

Figure 3.8: Average potential drop through the array at bias voltages very close to threshold. Fluctuations are smaller than the symbols. (a) Clean N=50 array with $\alpha = 1$. (b) Average potential drop for a symmetrically biased N=49 array in main figure (N=50 in the inset) with the excitonic energy substracted. (c)Average potential drop at the junctions $\bar{\Phi}_i$ corresponding to a disordered array with $N = 50$ islands and $\alpha = 1/2$. (d) Main figure (inset) $\bar{\Phi} - E^{e-h}$ corresponding to a $N = 50$ clean array with the middle (first) junction resistance 10.8 larger than the other ones.

$\bar{\Phi}_i - E_i^{e-h}$ is finite and equal for all the junctions. This indicates that the uncharged junction can be any of them, and all of them have the same probability to be uncharged.

Charge disordered arrays

For arrays with charge disorder, the charge gradient is only created at the junctions which prevent the flow of charge, i.e. those that have upward steps in the disorder potential. And this is reflected in the average potential drop, see Fig. 3.8 (c).

Disorder in resistances

The disorder in resistance does not have any influence in the threshold voltage, however at this bottleneck regime the flow of charge is affected by it. When in an array with even number of islands the resistance of a junction is much larger than the other ones, depending on where this junction is placed, different behaviors are observed. If the large resistance is in the middle of the array, it barely affects the average potential drop, see main figure in Fig. 3.8 (d) . And the potential drop is practically equal to the case with homogeneous resistances, represented in the inset in Fig. 3.8 (b). As we will see later, this is very different from what happens at high voltages. On the contrary, when the large resistance is at a contact junction, the behavior is completely different. The presence of the larger resistance at a contact junction modifies the average charging of the array and selects the opposite contact junction as the one which lacks charge gradient.

3.3.2 Intermediate voltages

Clean arrays

At intermediate voltages where the $I-V$ curve shows the Coulomb staircase, a very interesting regime in the potential drop appears. The potential drop shows almost regular oscillations when it is represented at the junctions as a function of the position, as we can see in Fig. 3.9 for different voltages in the case of a symmetrically biased array. The number of oscillations depends on α and on the voltage. This number of oscillations or maxima/minima does not change in a given step in the Coulomb staircase. However they increase from a step to the next one. First, we focus in the case of $\alpha = 1/2$, where the number of oscillations increases in pairs. Besides, there is an even-odd effect. For arrays with odd number of islands, there is always a minimun at the center of the array, while for even N there is a maximun, see Fig. 3.9. The rest of maxima and minima tend to be as equally spaced as possible. Inconmensurability beween the period of the oscillations and the lattice can distort equal spacement. When two new maxima or minima appear, at the beginning they are closer to the electrodes, but at increasing voltage they move inwards, yielding a general movement of the other maxima or minima.

These oscillations in the potential drop indicate that the charges are distributed in a particular way within the array. The change in the number of maxima and minima is associated with the entrance of new charges into the array. Moreover, the position of maxima is slightly adjusted within a step. The number of charges in the array increases when increasing the bias voltage, and the amplitude and the period of the oscillations decrease. For the case of

a clean array with capacitively coupled nanoparticles Stopa [37] argued that the steps in the I-V characteristic correspond to alternation of the charge density between distinct Wigner crystalline phases. In our system there is not a Wigner crystal, because this consists in the localization of the charges in order to minimize the repulsion between them in the case of long-range interaction, and we have short-range interaction. However, the possibility of a state with charges periodically ordered to minimize their repulsion, if present, should lead to oscillations in the potential drop along the array. Thus, in our system these oscillations are a clear evidence of correlated motion of the charges.

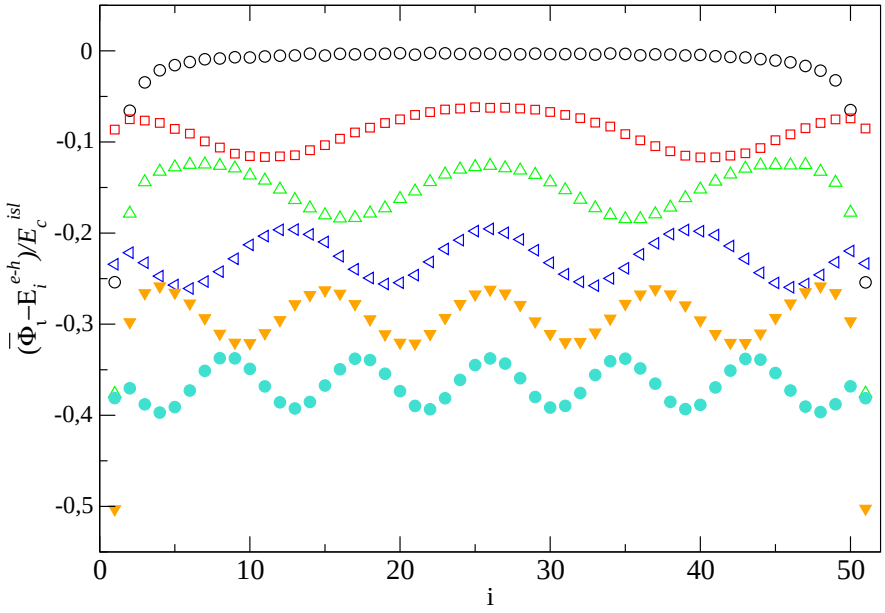

Figure 3.9: Average potential drop, with the excitonic energy substracted, $\bar{\Phi}_i - E_i^{e-h}$ at the junctions as a function of position at several values of the bias voltage, for which the current is in the Coulomb staircase regime, corresponding to a clean $N = 50$ array and $\alpha = 1/2$, see inset in Fig. 3.6 (a). This current starts to flow at $V_T = 98E_c^{isl}$. From top to bottom $V = 102, 104, 106, 108, 110, 112E_c^{isl}$. Curves have been vertically displaced to avoid overlap.

For completely asymmetric biased arrays, $\alpha = 0, 1$, the charges only enter into the array through one of the contact junctions, then the number of maxima or minima only increases in one by one between two consecutive steps. And at the center of the array the potential drop alternates between being a maximun and a minimun. As a result, the even-odd effect dissapears.

On the other hand, if we study the potential drop at a given junction as a function of the bias voltage, we can see that the behavior is different depending on the position of the junction.

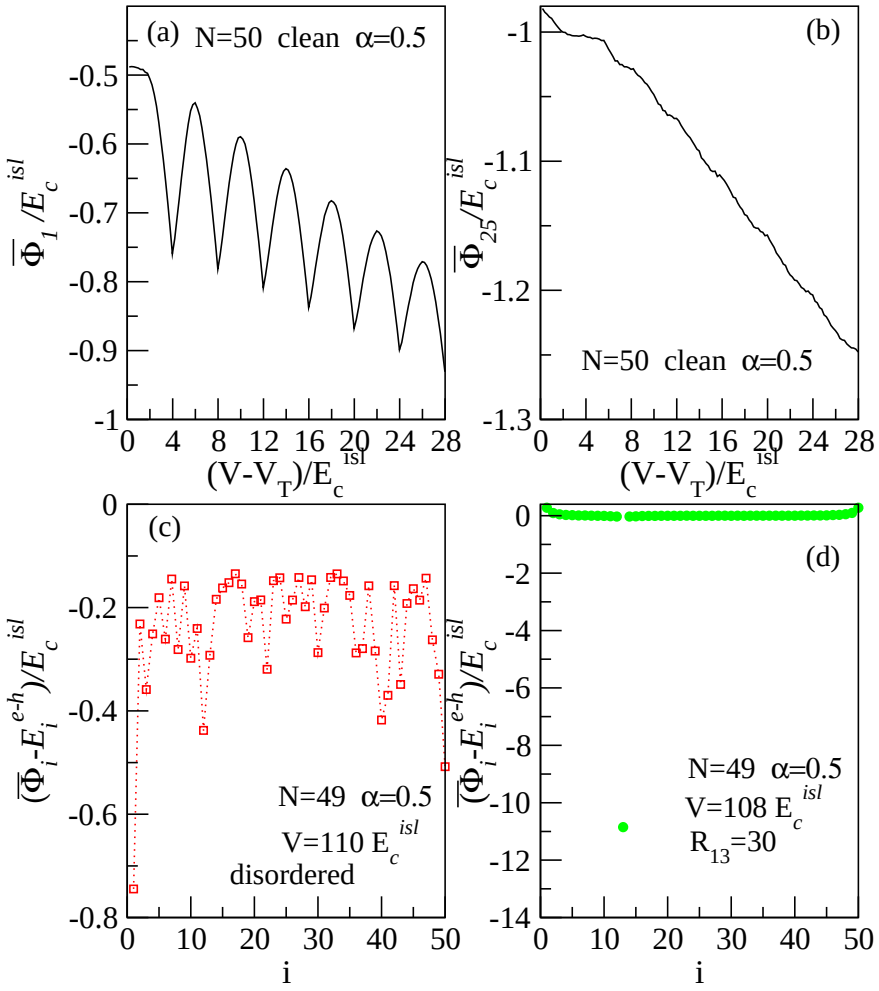

Figure 3.10: (a) and (b) show the average potential drop at the first and 25th junctions as a function of bias voltage for a clean array with $N = 50$ islands, $\alpha = 1/2$ and no resistance disorder at intermediate voltages. (c) and (d) show $\Phi_i - E_i^{e-h}$ for charge and resistance disordered 49-islands arrays respectively and $\alpha = 1/2$.

See Figs. 3.10 (a) and (b) where the potential drop is represented for the first junction and at junction number 25, that is the junction at the center of an array with $N = 50$ islands. The average potential drop at the contact junction oscillates as a function of the bias, whereas at the center of the array it depends monotonously on V. The oscillations at the first junction indicate that new charge states at the first island are allowed. The potential drop increases until an extra charge can be accumulated at the first nanoparticle, for larger voltages the average occupation of the first island increases and the potential drop decreases smoothly until a new value at which it increases again as the increase in occupation of first island cannot compensate the increase in the electrode potential. In the case of the central junction there are oscillations but they are very small and less pronunced. These oscillations are a conse-

quence of the movement of the maxima and minima within the array. The potential drop is much more homogeneous in the middle of the array, this is because the array analyzed is symmetrically biased and at the center of the array there is always a maximun or a minimun in the potential drop, see Fig. 3.9.

Charge and Resistance disorder

The charge and resistance disorder affect the potential drop. As these types of disorder alter the charge motion, the charges cannot be periodically ordered and the oscillations dissapear, see Fig. 3.10 (c) and (d). This is the opposite behavior that would be naively expected if one just associates the appearance of plateaux with the oscillations in voltage drop as done by Stopa, and emphasizes that the step profile is just a consequence of the dependence on the bias voltage of the tunneling rate of the processes which control the current.

3.3.3 High voltages

In the linear regime at high voltage, we could have expected that the potential drop at each junction was equal to the current divided by the junction resistance as it occurs in the conventional ohmic systems. However, in this thesis we show that this is not exactly correct.

The average potential drop is equal for the clean and charge disordered case. Main figure in top Fig. 3.11, shows the average potential drop at the islands ϕ_i as a function of the position for a disordered array with all the junction resistances equal. Although this potential seems linear, it is not exact. If this potential drop was linear through the array, the potential drop at all the junctions Φ_i would be equal. However, at the contact junctions $\bar{\Phi}_i$ is approximately E_c^{isl} times smaller than at the bulk junctions. Then the average potential drop at the junctions is homogeneous only once the excitonic energy is substracted, see inset in top Fig. 3.11. The origin of this effect is the different value of the excitonic energy, see Eq. (2.4).

The average potential drop can be calculated analytically. At high voltages the I-V curve is linear but the total voltage drop through the array does not equal $R_{sum}I$ due to the offset voltage $V_{offset} = \sum_{i=1}^{N+1} E_i^{e-h}$. The excitonic energy E_i^{e-h} is equal to $2E_c^{isl}$ at the bulk junctions and approximately E_c^{isl} at the contact ones. Remember that at high voltages the charge gradient ensures a uniform tunneling rate Γ^{uni} through all the junctions. The potential drop is $\Phi_i = R_i\Gamma^{uni} + E_i^{e-h}$ and $\Gamma^{uni} = \left(V - \sum_{i=1}^{N+1} E_i^{e-h}\right)/R_{sum}$ with $R_{sum} = \sum_{i=1}^{N+1} R_i$. Substituting the second equation in the first one, we obtain that at high voltages the average potential drop through the array is given by

$$\bar{\Phi}_i = E_i^{e-h} + \frac{R_i}{R_{sum}}\left(V - V_{offset}\right) \tag{3.10}$$

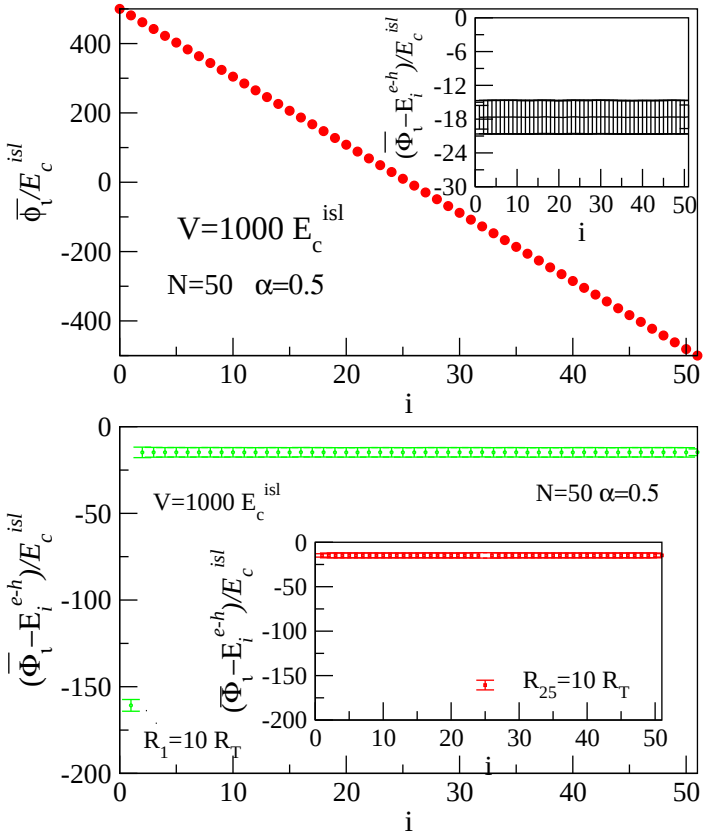

Figure 3.11: Top: main figure shows the average potential at the islands $\bar{\phi}_i$ as a function of position for a disordered array with $N = 50$, $\alpha = 0.5$ and all junction resistances equal. Inset shows the average potential drop with the excitonic energy susbtrated at the junctions Error bars give an estimation of the fluctuations of the potential drop. Bottom: main figure (inset) shows the average potential drop, with error bars giving its root mean square, at the junctions with the excitonic energy substracted corresponding to a clean array with the first (middle) junction ten times larger than the rest.

The average potential drop is independent of the asymmetry α of the applied voltage and it is not affected by the presence of charge disorder in the array (although it would change if capacitances are not homogeneous, via E_i^{e-h}), see top in Fig. 3.11. It is proportional to the resistance of the junction and equal at every junction if all resistances are the same. Unlike in low voltage regime, this statement is valid independently of the position of the resistance, as shown in the bottom figure of Fig. 3.11 and its inset. The dependence of the potential drop on the resistance is a consequence of the fact that the tunneling probability through a junction is inversely proportional to its resistance. When the resistance is very large, the charge has a lesser tendency to jump from an island to its neighbor and it will spend more time in the island producing a dependence of the time-averaged potential drop

on the junction resistance distribution.

3.4 Summary

In this chapter we have studied the transport properties through one-dimensional nanoparticle arrays placed between two metallic electrodes when the interactions are restricted to the charges in the same conductor, limit which we have called short-range interaction. The transport has been treated at the sequential tunneling level. We have analyzed how the transport properties are affected by the charge or resistance disorder, and how they depend on the number of nanoparticles or on how the array is biased. To quantify this symmetry we have introduced a parameter α as $V_0 = \alpha V$ and $V_{N+1} = (\alpha - 1)V$. The current not only depends on the total voltage drop $V_0 - V_{N+1}$, but also on the values of V_0 and V_{N+1}.

We have seen that there is a minimun bias voltage, the threshold voltage V_T, which has to be applied to have current flow through the array. It depends on the number of nanoparticles, the charging energy and the asymmetry of the array. In clean systems, for symmetrically biased arrays $\alpha = 1/2$ ($V_0 = V/2$, $V_{N+1} = -V/2$) there is an even-odd effect as a function of the number of nanoparticles, and the threshold is given by $V_T = 2E_c^{isl}N$ for odd N and $V_T = 2E_c^{isl}(N-1)$ for even N. In the case of completely asymmetric biased arrays ($\alpha = 0, 1$) the even-odd effect disappears and $V_T = E_c^{isl}(2N-1)$ regardless if N is even or odd. The dependence on the number of nanoparticles is qualitatively different to the dependence predicted for systems where the islands are weakly coupled [104], because in our system in the short-range limit at zero temperature the charge cannot flow freely through an uncharged and clean array. To allow the flow of charge a charge gradient has to be created in the array. In the system in [104] for $0 < C/C_g << 1$ the theoretical threshold is smaller than our threshold, but this current extrapolates to zero with $C/C_g \to 0$, and when it starts to be relevant is for a value of voltage similar than our V_T. The presence of charge disorder modifies the threshold with respect to the clean case. And it depends on the charge disorder configuration. For the case of charge disordered arrays, on average, threshold voltage is independent of α, and the previous prediction [64] $V_T = E_c^{isl}N$ is recovered. The disorder in resistances does not affect the threshold voltage.

For $V > V_T$ the current can flow through the array. We can observe three different regimes in the $I - V$ curve. Two of them have linear dependence on the voltage at low and high voltages and an intermediate regime called the Coulomb staircase. At voltages very close to threshold, current depends linearly on $(V - V_T)$. This is because the junction that controls the entrance of charge into the array acts as a bottleneck. We have obtained this linear dependence both numerically and analytically, and we have resolved the previous controvesy

on the power-law for voltages close to threshold. There is a linear dependence for clean, charge and resistance disordered arrays. The loss of linearity occurs when the probability of a tunneling process through a contact junctions is comparable to the probability of other processes at the inner junctions. The slope of current depends on the resistance of the contact junctions and the bias parameter α. Moreover, in symmetrically biased arrays the slope of current shows an even-odd effect depending on whether the number of nanoparticles is even or odd.

At intermediate voltages we find the Coulomb staircase, where the current shows a step-like behavior as a consequence of the fact that the transport is controlled by a bulk junction, which tunneling rate is independent of the applied voltage. The width of the step depends on the value of α and the charge disorder. In the case of a clean array symmetrically biased, the width of the step is equal to $4E_c^{isl}$, whereas for completely asymmetric bias it is $2E_c^{isl}$. This is because for adding one charge to the array it is necessary a potential drop at the contact junctions equal to $2E_c^{isl}$. Thus, for completely asymmetric arrays as the potential drop only occurs at a contact junction the width of the step is $2E_c^{isl}$. However, for arrays with $\alpha = 1/2$ the potential drop at the contact junctions is the half, then to introduce one charge the potential drop must be the double, and as a result the width of the steps is $4E_c^{isl}$. The disorder in resistances affects the staircase profile of the current.

At high voltages the current depends linearly on voltage. We have derived the asymptotic $I - V$ characteristic. This asymptotic $I - V$ cuts the zero current at a finite offset voltage which is given by the sum of the excitonic energies of all the junctions. The slope of current is equal to the inverse of the sum of the junction resistances in serie. In this regime the charge does not feel the presence of charge disorder, and the current for a clean and charge disordered array is the same. This is because at high voltages the charging effects are not very important. In this regime the current is independent of α. However, the current depends on the disorder in resistances. Besides, we have calculated V_{linear} the voltage at which the linear behavior is reached. It is approximately three times larger than the offset voltage, and can be very large in long arrays. This may hinder their experimental observation.

So far, the potential drop had not been studied theoretically. As in nanoparticle arrays the $I - V$ curves are strongly non-linear function of the voltage, it is not obvious a priory how the potential drops through these systems. In this chapter we have theoretically analyzed the potential drop through the array. In the low voltages linear regime, the potential drop reflects the charge gradient created to allow the flow of current through the array. Besides, the potential drop depends on α and charge disorder. The effect of disorder in resistances is extremely weak, except for the case of symmetrically biased arrays with even number of particles.

In the Coulomb staircase regime, for clean arrays the potential drop at the junctions shows almost periodic oscillations which reflects the correlation of charges. These oscillations dissapear when there is charge or resistance disorder in the array.

At high voltages, in this linear regime the potential drop at the junctions is only proportional to the resistance junctions once the excitonic energy is substracted. The charge disorder does not have any influence in the potential drop, however it is affected by the disorder in resistances.

4 Effects of the long-range interaction in one-dimensional nanoparticle array

In this chapter I will study the transport properties through one-dimensional nanoparticle arrays when interactions are long-range. I will highlight the main differences with the case of short-range interactions. As in the previous chapter, I will analyze the threshold voltage, the flow of current and the potential drop through the array. The influence of the different types of disorder will be also studied.

4.1 Introduction

In the case of long-range interaction all the charges in different conductors can interact between them. So far, the theoretical analysis of long-range interactions have mainly considered arrays in which each nanoparticle is capacitively coupled only to its nearest neighbors [64, 66, 103–106, 102], specially the case in which the coupling goes to zero. The interaction between the charges in different conductors decays exponentially with the distance between them [64, 103]. This limit is relevant for arrays coupled to a gate voltage [97], due to the fact that the charges in this lead screen the Coulomb interactions. However, nowadays the self-assembly arrays fabricated onto insulating substrates in general do not have a gate electrode. In these arrays the screening of long-range is less effective. However, when two conductors are close enough to each other, the charge in their surfaces screen the interaction between the charges in these conductors, then as a result of the proximity of other conductors the interaction is modified with respect to a $1/r$ Coulomb law [112, 113]. The screening depends on the shape of the nanoparticles. For the case of spherical nanoparticles the screening is less important than in the case of cubic islands [112], but larger than for thin disks [113].

In this thesis we take into account the static screening due to the presence of other conductors. As we want to study the effect of the long-range interaction, for simplicity we have considered that the electrodes are two large spherical leads. The screened interaction potential is obtained from two numerical methods [114] which had been developed (by the group before this thesis) to calculate the inverse capacitance matrix of an array of spheres. The effect of the screening is included in the inverse capacitance matrix where the electrostatic interactions are defined. The effect of the screening is included in the potential of disorder, and is given by

$$\phi_i^{dis} = \sum_{j=1}^{N} \tilde{C}_{ij}^{-1} Q_j^{sc} + \phi_i^{dis-bare} \tag{4.1}$$

with Q_j^{sc} the screening charges and $\phi^{dis-bare}$ the initial disorder potential at the islands, see section 2.2.3.

As in the case of short-range interactions, the system is composed of N metallic spheres of radius r^{isl} and the distance between the surfaces of two nanoparticles is d, see Fig. 4.1. When d/r^{isl} decreases, the range of interaction increases, because when the charges are closer they feel more the effects of the charges in other conductors. The effect of the screening starts to be important for $d/r^{isl} < 1-2$. In experimental arrays when the metallic nanoparticles are capped with thiols $d/r^{isl} \sim 0.5$, while in arrays self-assembled via other types of molecules, like DNA, there are larger values, $d/r^{isl} \sim 7$ [10].

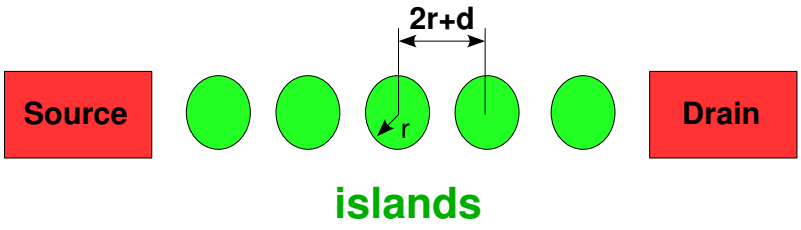

Figure 4.1: Schematic diagram of a one-dimensional nanoparticle array between two metallic electrodes.

In Fig. 4.2 (a) we can see how C_{ii}^{-1}, $C_{i,i+1}^{-1}$ and the excitonic energy E_i^{e-h} depend on the distance between the particles, d/r^{isl} for the case of an array with $N = 50$ equal-sized islands without electrodes, at the center of the array. On the other hand, the dependence of $C_{i,i+j}^{-1}$ on j for different distances can be observed in Fig. 4.2 (b), where it is compared with a $1/r$ law. At short distance the screened interaction potential decreases and at large distances it increases. When the particles are very close, there is a bump in the renormalized interaction. The effect of screening is negligible for $d/r \sim 3$.

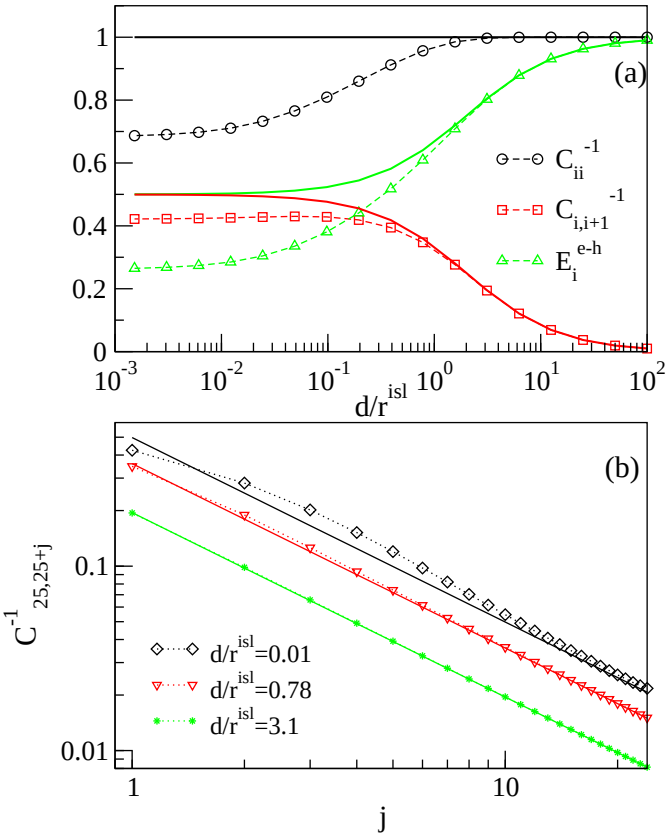

Figure 4.2: (a) Island inverse capacitance C_{ii}^{-1}, nearest-neighbor interaction $C_{i,i+1}^{-1}$ and excitonic energy, all in units of $(C^{isl})^{-1}$, at the center of a 50 nanoparticle array (without electrodes) as a function of the interisland separation. Solid-lines give the value obtained with a $1/r$ interaction between charges. (b) Decay of the interaction potential from the center of a 50 nanoparticle array (without electrodes) as a function of island position for different values of d/r^{isl}. Inverse capacitances are given in units of $(C^{isl})^{-1}$. Solid lines correspond to an unscreened $1/r$ law. In (a) and (b) dashed and dotted lines are included as a guide to the eye. From Bascones et al [114].

4.2 Threshold Voltage

Clean arrays

The threshold voltage is the minimun voltage at which the current starts to flow through the array. As we saw in the previous chapter, in the case of short range interaction in a clean array, the charge cannot flow freely through the array because there is no potential drop at the inner junctions. However, for long range interactions the polarization potential drop at the bulk junctions, $\Phi_i^{pol} = \Lambda_i^{\alpha} V = (\lambda_i^{\alpha} - \lambda_{i-1}^{\alpha})V$, is finite (Eqs. (2.8) - (2.9)). As a consequence, once the electron-hole pair is created, the charge can flow through the array. Thus, the threshold voltage is equal to the minimun voltage which allows the creation of an electron-hole pair.

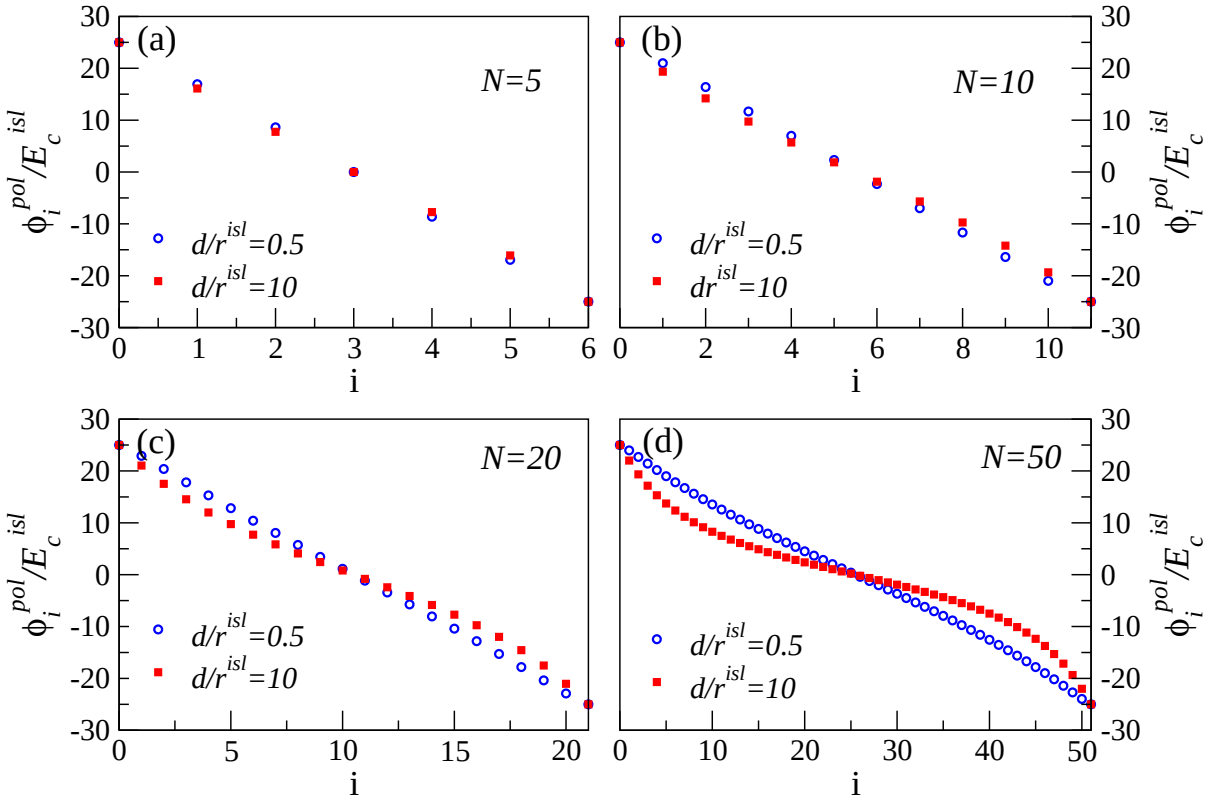

Figure 4.3: Polarization potential at the islands as a function of the position for $V = 50E_c^{isl}$ and symmetrically biased arrays with different length and two different values of d/r^{isl}, $d/r^{isl} = 0.5$ and $d/r^{isl} = 10$. (a) $N = 5$. (b) $N = 10$. (c) $N = 20$. (d) $N = 50$.

In order to create an electron-hole pair in a junction i of an uncharged array (i.e. there are no excess charges), the cost in energy is $\Delta E = E_i^{e-h} - \Lambda_i^{\alpha} V$. We can define a junction dependent threshold voltage for creating an electron-hole pair $V_i^{TH,\alpha} = E_i^{e-h}/\Lambda_i^{\alpha}$. While in the onsite limit $V_i^{TH,\alpha}$ is finite only at one or both contact junctions and infinite at the bulk, with long-range interactions this is finite at every junction, see Eqs. (2.8) - (2.9). It is larger at the junctions close to the biasing leads. Due to the smaller value of the excitonic energy and the larger potential drop at the contact junctions, V_i^{TH} is smallest at these junctions. Then the threshold voltage is controlled by the contact junctions.

The threshold voltage depends on the number of islands N, d/r^{isl} and α. A priori we could think that for a given d/r^{isl} and α if the threshold is given by the minimun voltage which allows the creation of an electron-hole pair and as after that, the charge can flow freely through the array, the threshold would be independent of the number of nanoparticles in the array. However, the polarization potential drop at the junctions depends on the number

of nanoparticles. The longer the array, the more homogeneous the potential of polarization at the islands, see Fig. 4.3. Then the potential drop at the contact junctions is smaller when N increases. As a result, the threshold voltage increases with increasing N, see Fig. 4.4 (a) where the threshold is represented as a function of the number of islands in the array N, for a clean symmetrically biased array with different spacing between array sites. $d/r^{isl} = 0.5$ is the pure long range limit. We also study $d/r^{isl} = 10$ because it has interactions among islands that are finite yet but small and this situation can seem quite similar to the onsite case that is often used to describe experiments [1, 64, 79]. When the spacing between the electrodes increases, the potential drop at the contact junctions decreases until it reaches the minimun value possible, which corresponds to the interaction between an electrode and its closest island. Main figure in Fig. 4.4 (b) shows the dependence of the threshold voltage on the spacing between arrays sites for clean arrays with $\alpha = 1/2$ and different sizes.

In Figs. 4.4 (a) and (b), the values of the threshold voltage which are estimated when the electrostatic interactions are calculated by the Coulomb law $1/r$ (without screening), are included as dashed lines. As we can observe in the system studied the threshold voltage is barely sensitive to the screening.

Unlike the case of short-range interaction where the dependence of the threshold voltage on α showed peaks structure (Fig. 3.2 (b)), for long range interactions the threshold voltage varies smoothly with α, as we can observe in the inset in Fig. 4.4 (b), where the threshold voltage of clean arrays is represented for several array parameters as a function of α normalized to the value for a symmetrically biased array. The peaks in the onsite limit indicate the number of charges that have to be accumulated to allow the flow of charge. In the case of long range interaction once the charge enters the array it can flow freely, because it is not necessary to accumulate charge in the array and the peaks do not appear. The dependence of the threshold voltage on α decreases as N increases and as d/r^{isl} decreases because the applied voltage drops more homogenously at the array junctions. If the polarization potential drops linearly this dependence disappears completely, and the threshold voltage of clean arrays would be $V_T = (N+1)E_c^{isl}$.

In the same way as in the onsite limit, for long range interactions the disorder in resistances does not affect the threshold voltage.

Charge disordered arrays

When there is charge disorder in the array the situation is more complex with long range interactions than with short range ones. In the onsite limit, only the junctions with step-up ($\Phi^{dis} > 0$) prevent the flow of current, and a charge gradient has to be created in these

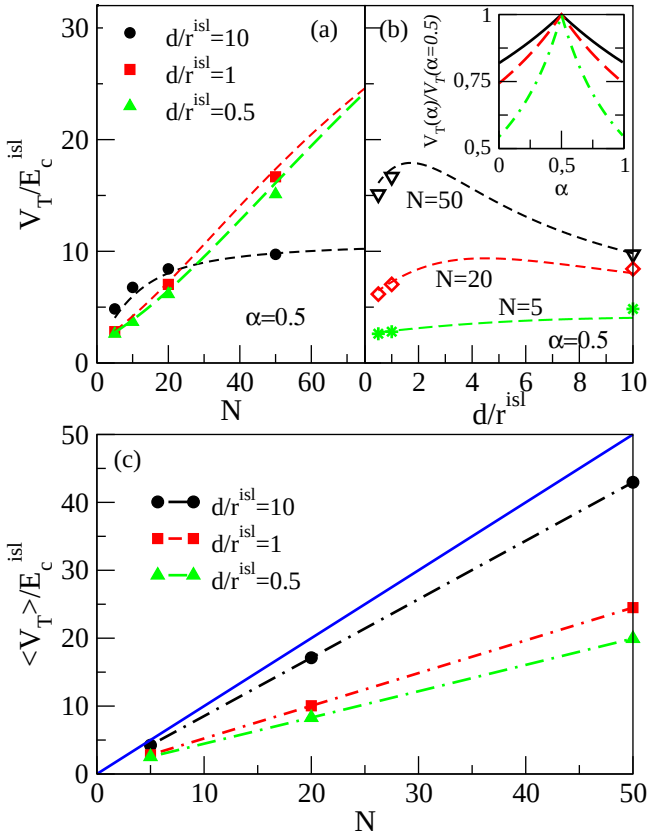

Figure 4.4: (a) and main figure in (b): With symbols it is respectively plotted the threshold voltage V_T of symmetrically biased arrays $\alpha = 0.5$, with no disorder as a function of number of islands N and of array spacing d/r^{isl} for the inverse capacitances calculated as [114]. The dashed lines are estimates for V_T that use a r^{-1} interaction to approximate the polarization potential drops across the contact junctions Λ_1^α and Λ_{N+1}^α. Inset in (b): Threshold voltage of clean arrays for several array parameters as a function of α normalized to the value for a symmetrically biased array. From top to bottom $d/r^{isl} = 0.5, N = 50$; $d/r^{isl} = 0.5, N = 20$; and $d/r^{isl} = 10, N = 50$. (c) Average threshold voltage of disordered arrays versus the array length at three different array spacings. The solid line shows the dependence of the average threshold on array length in the limit of onsite interactions.

junctions to allow the flow. Whereas, in the case of long range interactions and thanks to the finite polarization potential drop at the inner junctions, the flow of current is prevented only by the step-upwards junctions at which the disorder potential step is larger than the polarization potential drop. Consequently, the threshold voltage for charge disordered arrays is reduced in the case of long range interactions with respect to the onsite limit.

For charge disordered arrays and long-range interactions, the threshold voltage can be smaller or larger than the threshold found in the clean case, depending on whether d/r^{isl} is

small or large. This is a consequence of the fact that there are two different behaviors that compete to determinate the threshold voltage, and depending on d/r^{isl} one is more important than the other.

First behavior: Sometimes the tunneling process at a given junction can become possible with a small increase in the applied voltage, even if the polarization potential drop is a little smaller than the energy cost for the tunneling. When the applied voltage allows the creation of an electron-hole pair, in the cases where the disorder potential is small, the total potential at a given junction can be negative and thus allows the flow of charges through the array. The interaction between charges in different islands decreases the energy for the entrance of charges with opposite sign and increases the one for the entrance of charges with the same sign. This effect dominates for small d/r^{isl}, and the threshold voltage is smaller in the disordered case than in the clean one, see Fig. 4.6 (b) where the $I-V$ curves are represented for ordered and disordered arrays with different values of d/r^{isl}.

Second behavior: The other possibility is that the entrance of more charges and the creation of a charging potential gradient occurs in the same way as in onsite case. This last situation happens more often. In the case in which there are accumulation of charges in the array, the threshold voltage increases. In arrays with large d/r^{isl}, the voltage drop at the bulk junctions is small and the charges have to be accumulated to allow the flow of current. On average V_T of large arrays will increase compared to the clean array threshold voltage, see Fig. 4.6 (b).

On average the threshold voltage depends linearly on the number of islands in the array, see Fig. 4.4 (c), where the average threshold voltage is represented as a function of the length of the array for disordered arrays with several d/r^{isl}. When the array spacing decreases, the average thresholds decrease below the threshold values of the arrays in the onsite limit.

4.3 Flow of Current

In this section we will discuss the three main voltage regimes which can be distinguished in the $I-V$ curve. Although the three regimes are the same as in the case of onsite limit, there are several differences between both ranges of interactions.

4.3.1 Voltages close to threshold

For voltages very close to the threshold, the $I-V$ characteristics have a power-law behavior $I \sim (V-V_T)^{\zeta}$. For long-range interations as for the onsite case, $\zeta = 1$. This means that there is a linear dependence on $V-V_T$. For an array of dots capacitively coupled to their nearest neighbors, Kaplan et al [89] found that the power-law in the extremely long-range

limit ($C >> C_o$) is also linear.

As it occurs in the case of short-range interactions, this linear behavior is due to the fact that there is a junction that acts as a bottleneck, and the energy for the tunneling process through this junction linearly depends on the bias voltage. In the case of a clean array, the junction that acts as a bottleneck and controls the transport is a contact junction, and the current is given by

$$I \sim \frac{\Lambda_1^\alpha}{R_1}(V - V_T) \tag{4.2}$$

when the bottleneck is the source junction, while in the case where it is the drain junction the current is

$$I \sim \frac{\Lambda_{N+1}^\alpha}{R_{N+1}}(V - V_T) \tag{4.3}$$

with $\Lambda_i^\alpha = \lambda_i^\alpha - \lambda_{i-1}^\alpha$ the coefficient which controls the polarization potential drop at given function, see Eqs. (2.8) and (2.9). For symmetrically biased arrays as in the onsite interaction, the charge can enter into the array through both contact junctions if the number of nanoparticles in the array is odd, whereas for N even the flow of current requires that charge enters through both junctions. Then for $\alpha = 1/2$, $\Lambda_1^{1/2}/R_1$ and $\Lambda_{N+1}^{1/2}/R_{N+1}$ have to be added in the expression for the slope as in Eqs. (3.5) and (3.6).

Contrary to the short-range interaction case, the slope of this linearity depends, not only on the junction resistance and on α, but also on the number of islands and on d/r^{isl}. In Figs. 4.5 (a) and (b), where the $I - V$ curves are represented in logarithmic scale for different arrays, the dependence of the current on these parameters can be observed. As for α, the dependence on the number of nanoparticles and d/r^{isl} enters via Λ_i^α. When Λ_i^α changes, the potential drop at the bottleneck junction varies. The smaller the potential drop at the contact junctions, the smaller the slope of the current. For $\alpha \neq 1/2$, increasing the number of nanoparticles in the array and decreasing d/r^{isl}, as we mentioned above, decreases the polarization potential at the contact junction, and consequently the slope decreases. In a similar way, the polarization potential depends on α. Thus, when it changes the polarization potential drop is modified. Fig. 4.5 (b) shows the dependence of the slope on how symmetrically the array is biased.

Moreover, the slope depends on the junction resistances, as in the case of short-range interactions, as we can see in Fig. 4.5 (c) in which the $I - V$ curves are represented for arrays with different configurations of disorder in resistances.

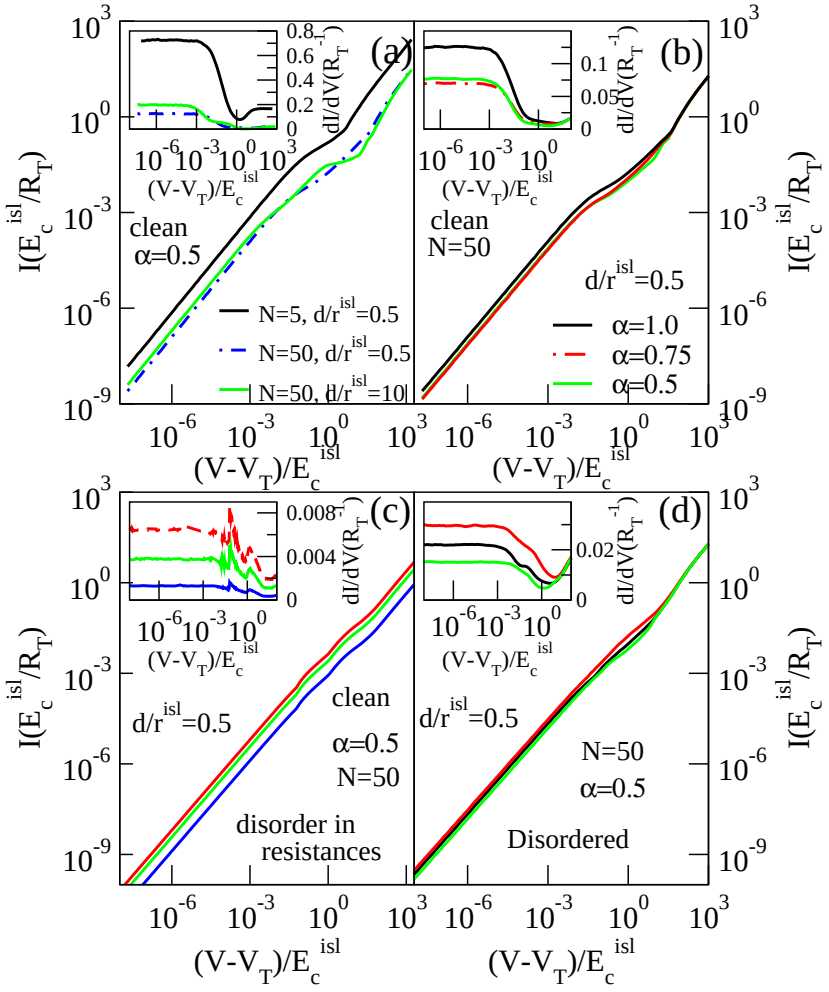

Figure 4.5: I-V curves of ordered arrays with long-range interaction at voltages very close to threshold. The insets show the derivatives of the I-V curves. (a) shows how varying the length and spacing of symmetrically biased arrays modifies the slopes of the linear regimes. (b) In a similar way, the slope depends on how symmetrically is the array biased. (c)plots the I-V curves and derivatives corresponding to clean arrays with equal length, d/r^{isl} and α but different junction resistances. Resistances in these plots vary randomly in between $(5-11)R_T$, $(8-21)R_T$ and $23-83R_T$ in top, middle and lower curves. (d)I-V curves corresponding to three different realizations of charge-disordered arrays with all junction resistances equal $N = 50$ and $\alpha = 0.5$.

One of the main characteristics that appears in this regime occurs when there is charge disorder in the array. Contrary to the onsite limit, the slope of the low-voltage linear current depends on the charge disorder configuration, see main figure and inset of Fig. 4.5 (d). This is a consequence of the fact that in disordered arrays with long range interactions, the bottleneck is not necessarily a contact junction but it can be a junction in the bulk. This depends on the disorder configuration. The slope of the linear dependence can then be controlled by Λ_i^α with $i \neq 1, N+1$. As Λ_i^α depends on the interaction of the charges in the islands with

the charges in the electrodes, the slope is generally larger when the bottleneck junction lies closer to the edge of the array, i.e. closer to the electrodes. While if the bottleneck junction lies in the middle of the array, the slope is smaller.

The linear regime appears for several orders of magnitude, but it ends at voltages $V - V_T \sim 10^{-2} E_c^{isl}$, much lower than the values used in experiments to check the power-law dependence close to threshold.

4.3.2 Intermediate voltage regime

The loss of linearity of the current as in the onsite limit, dissapears when the junction that acts as a bottleneck ceases to be it. This happens when two processes have comparable rates. In order to understand this sublinear behavior, we can assume that the flow of one charge through the array occurs in a sequence of $N+1$ tunneling processes, and consider a bottleneck process with rate $\Gamma_i = R_i^{-1} \Lambda_i^\alpha \tilde{V}$ where $\tilde{V} = V - V_T$, and another process in the sequence with rate $\Gamma_j = R_j^{-1}(E_j^T + \Lambda_j^\alpha \tilde{V})$. Where E_j^T is the gain in energy of the second process at the threshold voltage. If these two processes have rates much smaller than the rest of processes in the sequence, the current can be approximated by

$$I \sim \frac{1}{\tau_i + \tau_j} = \frac{R_i^{-1} \Lambda_i^\alpha \tilde{V}}{1 + \frac{R_i^{-1} \Lambda_i^\alpha \tilde{V}}{R_j^{-1}(E_j^T + \Lambda_j^\alpha \tilde{V})}} \sim R_i^{-1} \Lambda_i^\alpha \tilde{V} \left(1 - \frac{R_i^{-1} \Lambda_i^\alpha \tilde{V}}{R_j^{-1} E_j^T} \right) \tag{4.4}$$

The slope and the loss of linearity depend on the resistance of the junctions, on the number of nanoparticles in the array, on d/r^{isl} and on how the array is biased. The last three dependences enter via Λ_i^α. The more homogeneous the values of Λ_i^α through the array, the longer the linear behavior. Thus, in a clean array with long range interaction, the linear behavior is lost for larger voltages when the arrays are shorter, and d/r^{isl} and α are smaller than in a longer array with d/r^{isl} and α large. However, for charge disordered arrays with long range of interaction, it is not so easy to make a prediction, because the polarization potential drop in a junction does not increase homogeneously, then if the junction has a small energy gain but large Λ_i^α, it can increase this gain more than other junctions when the applied voltage increases.

In this regime of intermediate voltages the current shows smooth steps. Decreasing d/r^{isl} the steps are smoothed, and for small d/r^{isl} they practically disappear, see Fig. 4.6 (a) where the I-V curves are represented for arrays with different interaction ranges and lengths. In order to compare, all the curves have been plotted as a function of $(V - V_T)$. The staircase profile is different in all the cases. This is due to the way the flow of charge is allowed in the array. The top curve corresponds to a clean array with $N = 50$ islands and short range

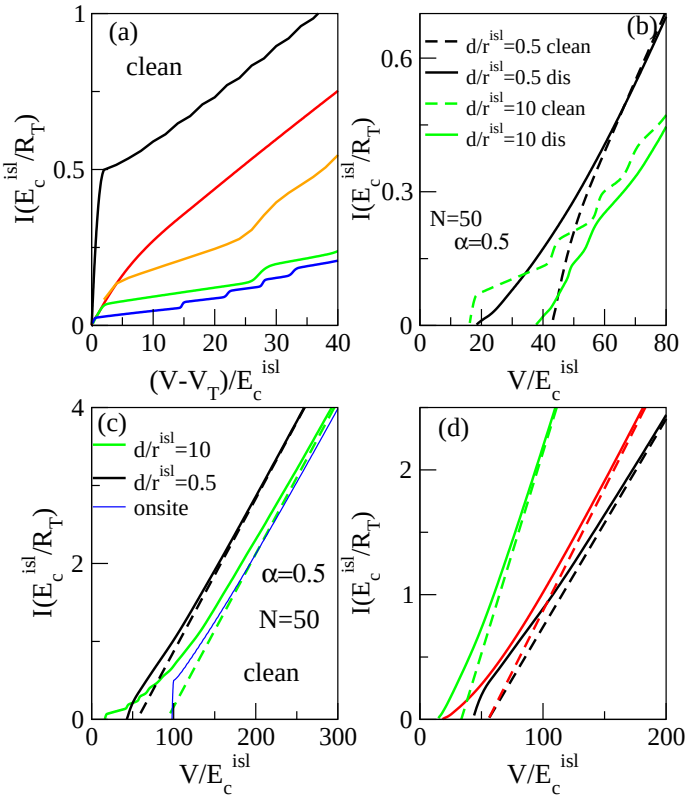

Figure 4.6: In (a) and (b) the I-V characteristics show the Coulomb staircase and correspond to arrays with homogeneous resistances. (a) From top to bottom, the first four curves correspond to $\alpha = 0.5$ and respectively to $N = 50$ with onsite interaction; $N = 50$ with $d/r^{isl} = 0.5$; $N = 30$ with $d/r^{isl} = 10$; $N = 50$ with $d/r^{isl} = 10$. The lowest curve corresponds to a $N = 50$ and $\alpha = 1$ and $d/r^{isl} = 10$. The threshold voltage has been substracted. V_T equals $98, 43, 14, 16$ and $9.7E_c^{isl}$ respectively. (b) I-V curves for disordered arrays with $d/r^{isl} = 0.5, 10$. The clean case is included for comparison. (c) I-V at high voltages for clean arrays with homogeneous resistances, from top to bottom solid lines correspond to $d/r^{isl} = 0.5$, $d/r^{isl} = 10$ and onsite interactions. The dashed lines give the asymptotic predictions for $d/r^{isl} = 0.5$ and 10. (d) I-V curves in a large voltage scale corresponding to $d/r^{isl} = 0.5$ symmetrically biased arrays. From top to bottom $N = 30$ and $N = 50$ disordered arrays with homogeneous resistances and a $N = 50$ clean array with the first resistance ten times larger than the other ones. Dashed lines give the asymptotic predictions. The slope of both $N = 50$ curves differ, but their offset voltages are the same.

interactions. We remember that to allow the flow of current through the array in the onsite limit, a charge gradient has to be created in all the junctions. As a consequence, there is a large jump in the current close to the threshold. In the case of long range interactions it is not necessary to create a charge gradient to allow the flow of current, because there is finite polarization potential drop at the inner junctions. For the case of $d/r^{isl} = 10$, the nanoparticles are very separated from each other, and the interaction between the charges in different islands is small. As a result, the potential drop at the inner junctions is small and the charge

flows slowly through these junctions, yielding a staircase structure. However, for $d/r^{isl} = 0.5$ the steps practically disappear. This is because the polarization potential drop at the inner junctions is larger and more homogeneous, then once the charge enters into the array, it can flow more easily.

When there are steps in the current, their width depends on α. For completely asymmetric biased arrays ($\alpha = 0, 1$) the step width is smaller than in symmetrically biased arrays ($\alpha = 1/2$). Contrary to the onsite case, for long range interactions the step width is not fixed. Because the interactions between the charges in different islands are finite, the charges in the array influence in the energy cost to add one charge into the array from the electrodes.

Charge disorder affects the current, see Fig. 4.6 (b), where $I - V$ curves are plotted for clean and disordered arrays with different d/r^{isl}. Unlike in the onsite case, the steps are sharper in the clean case than with disorder for $d/r^{isl} = 10$. Although specially interesting is the $I - V$ curve for the disordered case with $d/r^{isl} = 0.5$. It looks superlinear, similar to what would be found if a power-law larger than unity is present at these voltages. We have observed that this approximate superlinear type dependence is common in disordered arrays with small d/r^{isl}. If experimentally the power-law behavior expected close to threshold is measured at these voltages (larger than those at which the linear behavior is predicted) the exponent of the power-law could be erroneously assigned a value larger than one. It occurs in experimental studies of disordered arrays in two dimensions, that we will study in detail in the following chapter.

4.3.3 Linear behavior at high voltages

At high voltages there is a linear behavior of the current with the voltage. The asymptotic prediction of the current Eq. (3.8) is not restricted to onsite interactions, but applies also to the long-range limit. We remember that this prediction is given by

$$I_{asympt} \sim \frac{1}{R_{sum}} \left(V - \sum_{i=1}^{N+1} E_i^{e-h} \right) \tag{4.5}$$

The slope in current is independent of the range of interactions, the bias parameter α and the charge disorder. The slope only depends on the resistance of the junctions and is given by R_{sum}^{-1}. There is a good agreement between the numerical results and the asymptotic predictions, as we can see in Fig. 4.6 (c), where $I - V$ curves are plotted for symmetrically biased arrays with homogeneous resistances and different range of interaction.

However, the offset voltage at which the asymptotic current cuts the zero current axis, depends on the range of interaction [95, 115]. This is because the offset voltage is given by the

addition of the excitonic energies, which depend on the range of interaction Eq. (2.5). In general, the offset voltage is different from the value of threshold. In particular the $d/r^{isl} = 10$ curve has a smaller threshold and larger offset than the $d/r^{isl} = 0.5$, see Fig. 4.6 (c). The offset increases linearly with N, and is always larger for $d/r^{isl} = 10$ than for $d/r^{isl} = 0.5$. From Eq. (2.5) we can see that the excitonic energy is smaller when the interaction between the charges in both conductors is larger, and this occurs in the case in which the islands are close. For this reason $V_{offset} = \sum_{i=1}^{N+1} E_i^{e-h}$ is smaller in the case of $d/r^{isl} = 0.5$ than for $d/r^{isl} = 10$.

The disorder in resistance affects the slope in the same way for both short and long range of interactions, see Fig. 4.6 (d) where $I - V$ curves correspond to clean symmetrically biased arrays with different length, and when the number of nanoparticles is the same, with different configuration of resistances. For the cases of arrays with the same length but different configuration of resistances, their slope is different but V_{offset} is the same in both cases.

4.4 Potential drop through the array

In this section we analyze the effect of the long-range interactions in the potential drop through the array. There are three regimes with different behavior. These regimes are the same that appear in the current. The differences with respect to the onsite case are a consequence of a finite polarization potential drop at the bulk junctions for the case of long range interaction.

4.4.1 Low-voltage regime

For voltages close to the threshold the transport is governed by a bottleneck junction, where the time associated to the tunneling process of this junction is much larger than the time corresponding to the processes through the rest of the junctions in the array. Thus, the average potential drop is almost the same as the potential drop at the threshold. We remember that in a clean array with long-range interactions the threshold voltage is the minimun bias voltage which allows the creation of an electron-hole pair. Once the charge is in the array, it can flow freely through the array due to the polarization potential at the inner junctions, without creating a charge gradient as occurs in the onsite limit. Then, for voltages very close to threshold, the potential drop reflects the polarization potential drop $(\lambda_i^\alpha - \lambda_{i-1}^\alpha)V$ at each junction, as we can see in the main figure of Fig. 4.7 (b) where the average total potential drop and the polarization potential drop at the junctions are plotted. The average potential drop at the islands as a function of the position can be seen in Fig. 4.8.

The potential drop depends on the number of nanoparticles in the array N, the bias asymmetry α and on the range of interactions d/r^{isl}. These dependences can be observed in Fig. 4.7

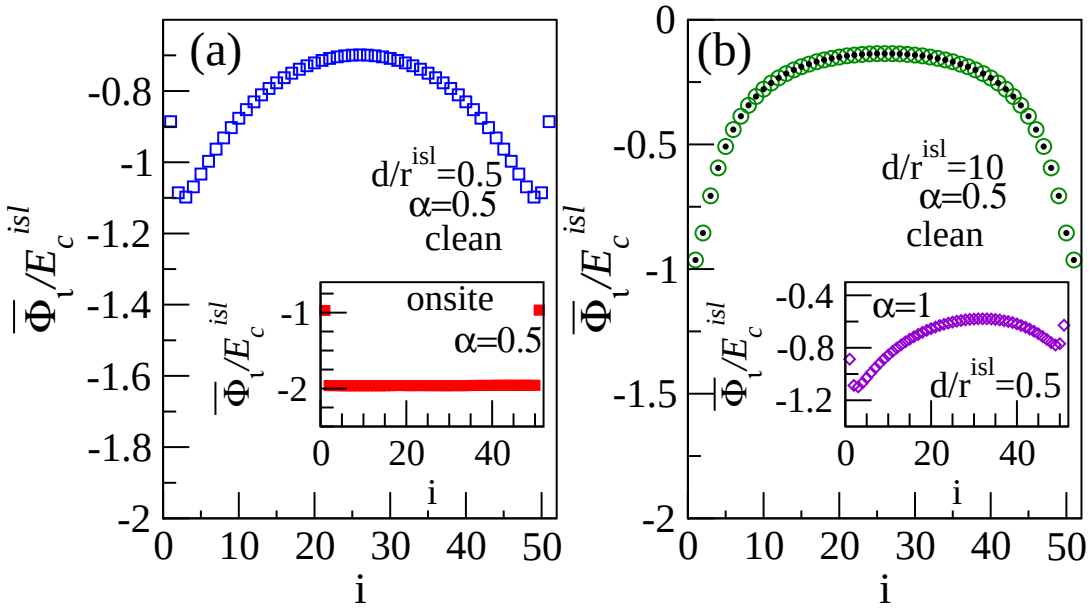

Figure 4.7: Average voltage drop at the junctions as a function of the position for a voltage close to threshold, $N = 50$ clean arrays with different parameters. Main figures are for $\alpha = 0.5$ and long-range interaction. The average potential drop essentially equals the polarization potential for each value of d/r^{isl}, which is plotted as filled small dots in (b) for comparison. This behavior contrasts with the potential due to the charge gradient which has to be created in the onsite case, shown in the inset of (a). As shown by comparing main figure in (a) with the inset in (b) a change in the value of α modifies the potential drop through the array.

where the average potential drop is represented at the junctions as a function of the position for different array parameters. The potential drop in the long-range case is very different to the one found in the onsite limit (inset of Fig. 4.7 (a)), because in this last case the potential drop at the inner junctions is a consequence of the charge accumulation at the islands. On the other hand, the dependence with α can be observed in the main figure in Fig. 4.7 (a) and the inset of the (b).

Disorder in resistances

In general, the dependence of the potential drop on the value of the resistance is extremely weak, except in the case where one junction has a value of resistance much larger than the others. But to observe any effect due to this large resistance, this must be too much large $R \sim 10^9 R_T$. In this particular case, the charge potential is necessary to allow the flow of charge through the array, and as a result the total potential drop depends on the resistances.

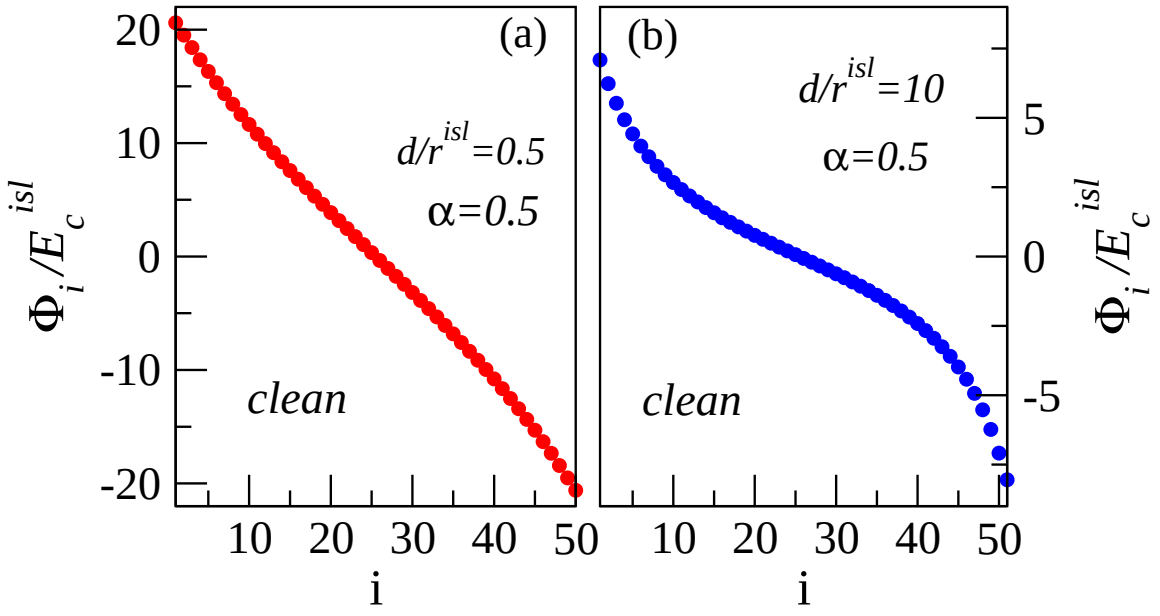

Figure 4.8: Average voltage drop at the islands as a function of the position for a voltage close to threshold, $N = 50$ clean arrays with $\alpha = 0.5$ and long-range interaction. (a) $d/r^{isl} = 0.5$. (b) $d/r^{isl} = 10$.

Charge disordered arrays

For charge disordered arrays with long-range interaction in some cases once charge is allowed to enter into the array it can flow. Generally, this occurs when d/r^{isl} is small because the polarization potential drop can overcames the up-step in the disorder potential. Then the average potential drop is approximately the sum of the disorder potential and the polarization potential. In general, when this happens the threshold voltage is smaller than the one in the clean case as the disorder potential reduces the polarization potential drop necessary in at least one of the contact junctions. For large d/r^{isl} it is more probable that one or more charges remain stacked in the array, similarly to the case with onsite interactions. The charge potential due to these stacked charges contributes to the average potential drop.

4.4.2 Intermediate-voltage regime

In clean arrays at intermediate voltages in the Coulomb staircase regime, as in the onsite case the potential drop shows almost periodic oscillations, with the number of maxima increasing in pairs from one step to the next one in the $I-V$ curve, for $d/r^{isl} = 10$. This can be seen in Fig. 4.9 (a) where the average potential drop is plotted at the junctions as a function of the position for a clean symmetrically biased array. However, in the case of $d/r^{isl} = 0.5$ represented in Fig. 4.9 (b), for all the voltages the number of maxima is always two, i.e. it has not increased in this range of voltages but oscillations are smoothed with increasing bias

voltage. This is because there is only one step in the current, see Fig. 4.6 (a).

In the same way that in the onsite limit, when charge or resistance disorder are present in the array, the oscillations dissapear.

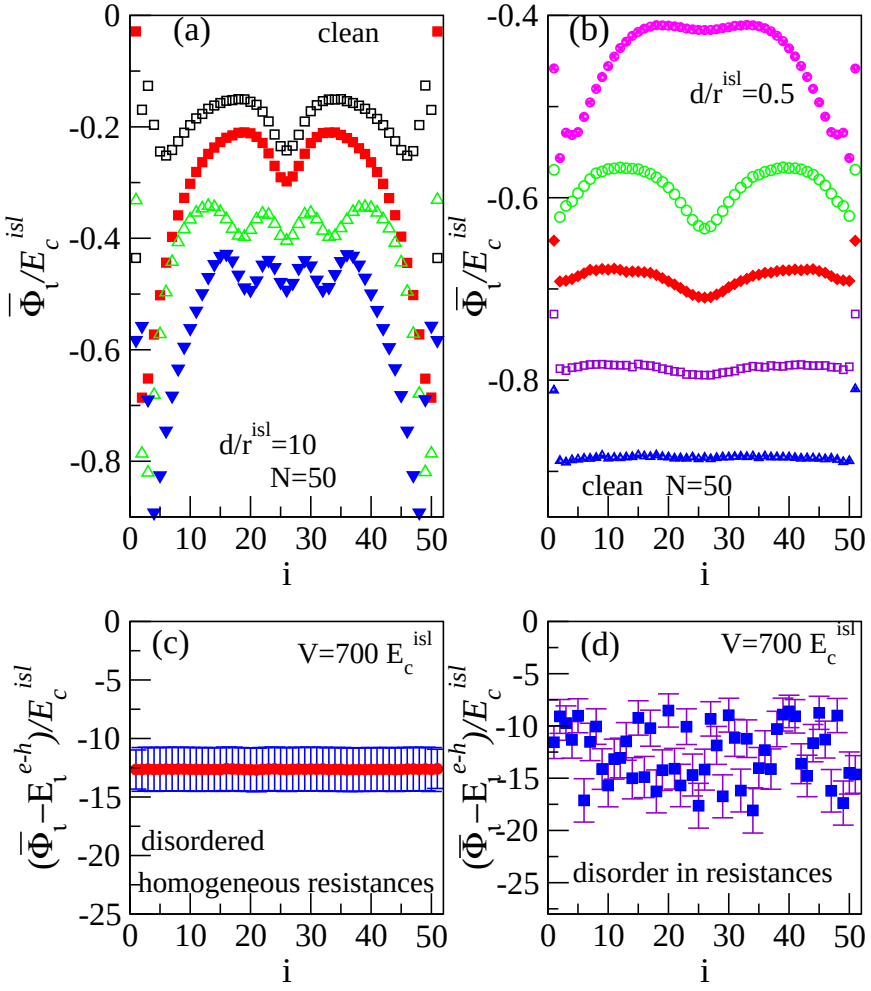

Figure 4.9: Average potential drop at the array junctions at intermediate (upper figures) and high voltages (lower figures) for $\alpha = 0.5$ and $N = 50$. Upper figures correspond to clean arrays. Curves in (a) are for $d/r^{isl} = 10$ and (from top to bottom) $V = 20, 32, 44, 56 E_c^{isl}$. In (b) $d/r^{isl} = 0.5$ and $V = 46, 60, 70, 80, 90 E_c^{isl}$. In (c) and (d) the excitonic energy has been substracted from the average potential drop at high voltages. Once this term is substracted the average potential drop is completely homogeneous through the array in (c) where there is charge disorder, and all resistances are equal but not in (d) which corresponds to a clean array but with resistances which vary randomly between $(5-11)R_T$.

4.4.3 High-voltage regime

At high voltages, in the same way as in the case of short-range interaction, for the long-range case the potential drops linearly only after subtracting from each junction the excitonic energy. Expression (3.10) is also valid for long-range interactions for both ordered and disordered arrays. In Fig. 4.9 (c) we can see that as expected, in the absence of resistance disorder, once the excitonic energy is substracted the potential drops homogeneously through the array even if there is charge disorder, while it is proportional to the resistance value when resistances are not homogeneous, as shown in Fig. 4.9 (d).

4.5 Summary

In this chapter we have analyzed the effect of the long-range interaction in the transport through ordered and disordered one-dimensional arrays. We have included the screening in the interactions. The screening is produced by the proximity of the other conductors. When the islands are very close to each other, the interaction between the charges in different conductors is reduced with respect to a $1/r$ law. The effect of the screening starts to be relevant when $d/r^{isl} \sim 1-2$. For large d/r^{isl} the interaction approaches the $1/r$ law. Besides, the long-range interactions screen the disorder potential and induce correlations between the values of ϕ^{dis} at the islands.

In the same way as in the onsite case, the current is blocked up to a threshold voltage value V_T. This threshold voltage is independent of the resistances of the junctions. For long-range interaction, there is a finite polarization potential drop at the inner junctions which facilitates the flow of charge. Thus, in a clean array the threshold voltage is given by the minimun voltage which allows the creation of an electron-hole pair. For the case of charge disordered arrays, there are two effects that compete to determine the V_T. The threshold voltage can increase or decrease with respect to the clean case depending on the effect that dominates. The first effect appears when there are step-up junctions due to the disorder potential ($\phi^{dis} > 0$), as a result, the charge can be accumulated at the islands, increasing V_T. In the second effect, the disorder potential distribution can reduce the energy to create an electron-hole pair, then the threshold voltage decreases. The latest effect dominates for small d/r^{isl}, while the first for large d/r^{isl}.

The $I-V$ curve shows three different regimes of behavior. At voltages close to the threshold, the current linearly depends on $(V-V_T)$. The linear dependence appears for several orders in magnitude, however the loss of linearity occurs for voltages probably too small to be observed experimentally. We have analyzed the linear dependence numerically and analytically. This dependence is due to the fact that a junction acts as a bottleneck and that the change

in energy for tunneling at this junction depends linearly on bias voltage. In the clean case this junction is a contact junction. However, in the disordered case, the bottleneck junction can be a bulk junction, because there is polarization potential drop at the inner junctions. Thus, the slope in current depends on the charge disorder configuration, unlike the onsite case. Futhermore, the slope also depends on the resistance of the junctions, the number of nanoparticles, and on the bias parameter α.

At intermediate voltages there is the Coulomb staircase regime. The steps are smoother than in the onsite case, and for small d/r^{isl} the $I-V$ curve cannot show stepwise behavior. Contrary to the onsite case, the step width is not fixed. This is a consequence of the fact that the interactions between the charges in different islands influence in the energy cost for adding a charge from the electrodes.

At high voltages the current depends linearly on the bias voltages. We have predicted the asymptotic $I-V$ curve that cuts the zero current axis at a finite offset voltage which is given by the sum of the excitonic energies of all the junctions, and its value depends on the range of interaction. On the other hand, the slope of the current is given by the addition of the resistances in series and it is equal to the value in the onsite case, i.e. it is independent of the d/r^{isl}.

Besides, we have studied the effect of the long-range interaction in the potential drop through the array. At voltages close to threshold the potential drop through the array reflects the polarization potential drop Λ_i^α due to the electrodes.

At intermediate voltages an oscillatory voltage drop through the array, similar to the one found for the onsite case is obtained for large values of d/r^{isl}. For small d/r^{isl}, although there are oscillations, the largest number of maxima that we have found is two. This is because the $I-V$ curves reaches the high-voltage regime without showing stepwise behavior.

At high voltages as in the case of short-range interactions, for the long-range ones the proportionality between the potential drop and the junction resistance, is only recovered once the excitonic energy is substracted.

In conclusion, the $I-V$ curves are modified by the effect of the long-range interactions. This modification is mostly due to the finite polarization potential drop at the inner junctions. Larger differences between both ranges of interactions appear at low voltages.

5 Transport through two-dimensional nanoparticle arrays

In this chapter I will analyze the transport properties through two-dimensional nanoparticle arrays, emphasizing the main differences with respect to the one-dimensional case. The most important point in this study is that I will show that the commonly used scaling hypotesis to fit $I-V$ curves at voltages close to threshold does not describe the electronic transport in these systems. I will consider short range interactions, zero temperatures and symmetrically biased arrays. I will explain how the disorder affects the transport properties. Besides the charge and resistance disorder, in this system I will analyze the case where there are vacancies in the array or structural disorder. This type of disorder appears in the nanoparticle arrays when they are synthesized experimentally. Futhermore, I will study different lattice geometries. I will first give a brief introduction of the previous works done in two-dimensional arrays, and our motivation to study them. After that I will explain the threshold voltage, the flow of current and the potential drop through the array.

5.1 Introduction

In the last two decades, most experimental [1, 21, 24, 79, 97, 98, 116–124] and theoretical [64, 67, 90, 88, 91, 125] studies have focused on the possible power-law behavior of the current $(V-V_T)$ through two dimensional disordered arrays for voltages close to threshold. For a system with the conductors capacitively coupled with $C << C_o$ (i.e. practically short-range interactions), where C is the coupling capacitance between nearest neighbors and C_o is the capacitance of the conductor itself, Middleton and Wingreen [64] predicted that in the Coulomb blockade regime the $I-V$ characteristic follows a scaling behavior

$$I \propto (V-V_T)^{\zeta} \tag{5.1}$$

which depends on the dimensionality of the system. Analytically they obtained $\zeta = 1$ for one-dimensional arrays and $\zeta = 5/3$ in two dimensional infinite arrays; while their numerical results for finite arrays with square lattice gave $\zeta = 2.0 \pm 0.2$ for a range of voltages of $(V/V_T - 1) \sim 0.02 - 100$. Their prediction is based on the assumption that close to threshold the current flows through N_{ch} independent channels, each of them driving a current linearly dependent on $(V-V_T)$. For one-dimensional arrays there is only one channel, thus, $\zeta = 1$.

In two-dimensional arrays, on the basis of a mapping of the current flow to a model of interface growth, the Kadar-Parisi-Zhang (KPZ) model [126]. Neglecting the role of the contact junctions in determining the current, they concluded that $N_{ch} \sim (V/V_T - 1)^{2/3}$, which together with the linear current of a one-dimensional channel gives $\zeta = 5/3$. Other theoretical studies also found numerically $\zeta = 2$, Roux and Herrmann [88], and Reichhardt and Olson Reichhardt [90]. The later using a model with a $1/r$ interaction between the charges in the islands for arrays with square lattice and not very large size (from $20x20$ to $60x60$). However, in this work the system instead of electrodes has periodic boundary conditions. In more recent studies Suvakov and Tadić [91, 125] obtained that the scaling depends strongly on the structure of the array, finding $\zeta \sim 3.9$ for arrays with topological inhomogeneity, whereas for more homogeneous structure $\zeta \sim 2.7$. This means that ζ is larger in arrays with more number of voids. They relate the value of the scaling with the number of paths that the charge can follow through the array to be transfered from one electrode to the other. Thus, they argue that different geometries have different conducting paths, and as a consequence the current is affected by the geometry, yielding different values of the scaling. For the limit of an array of dots capacitively coupled to their nearest neighbors and $C >> C_o$, Kaplan et al [89] found a scaling exponent with a value equal to $\zeta = 1.7 \pm 0.1$.

The prediction of Middleton and Wingreen has been considered basic and correct. So much so, that since then in all the experimental work the $I - V$ characteristics have been systematically discussed in terms of these power laws. Several experimental works have given a wide range of values of the scaling exponent, from $\zeta = 1$ to 5.2, in general $\zeta \geq 2$. This large variation has been associated with different facts, such as in the arrays there are different types of disorder or the possibility that the system does not have exactly the same dimension. In Fig. 5.2 one can observe the $I - V$ curves and the scaling exponent obtained in different experiments. In some cases a dependence of the scaling on the sample has been observed. Kurdak et al [97] for two 40x40 square arrays of Al islands obtained for one sample $\zeta = 2.01 \pm 0.04$, while for the other $\zeta = 1.58 \pm 0.04$. The difference between both samples was that they were fabricated on different GaAs/AlAs heteroestructures. For polydisperse nanocrystals, Wybourne et al [116] got $\zeta = 1.6$ for electron-beam patterned samples and $\zeta = 2.1$ for non-patterned ones. Recently, variations much larger $1 < \zeta < 5.2$ have been found by Tan et al [122] for CoFe nanoparticles arrays fabricated with different ligands. Whereas Duruöz et al [21] had $1.4 < \zeta < 1.7$ for one sample, 200x200 arrays of GaAs quantum dots, varying the gate voltage. Rimberg et al [98] obtained $\zeta = 1.80 \pm 0.16$ for square arrays with $N = 40x38$ small metallic islands (Al). Black et al [24] found $2.2 < \zeta < 2.7$ when they studied arrays of Co-nanocrystals with hexagonal form. Bose et al [118] got $\zeta = 2.2$ for arrays of microscopic iron plaquettes deposited epitaxially on MgO. Other studies have focused in the effect of structural disorder, i.e. in the influence of the topology on ζ. Blunt et al [92] obtained for arrays with large areas witout islands $\zeta = 4.35$, whereas for arrays with low

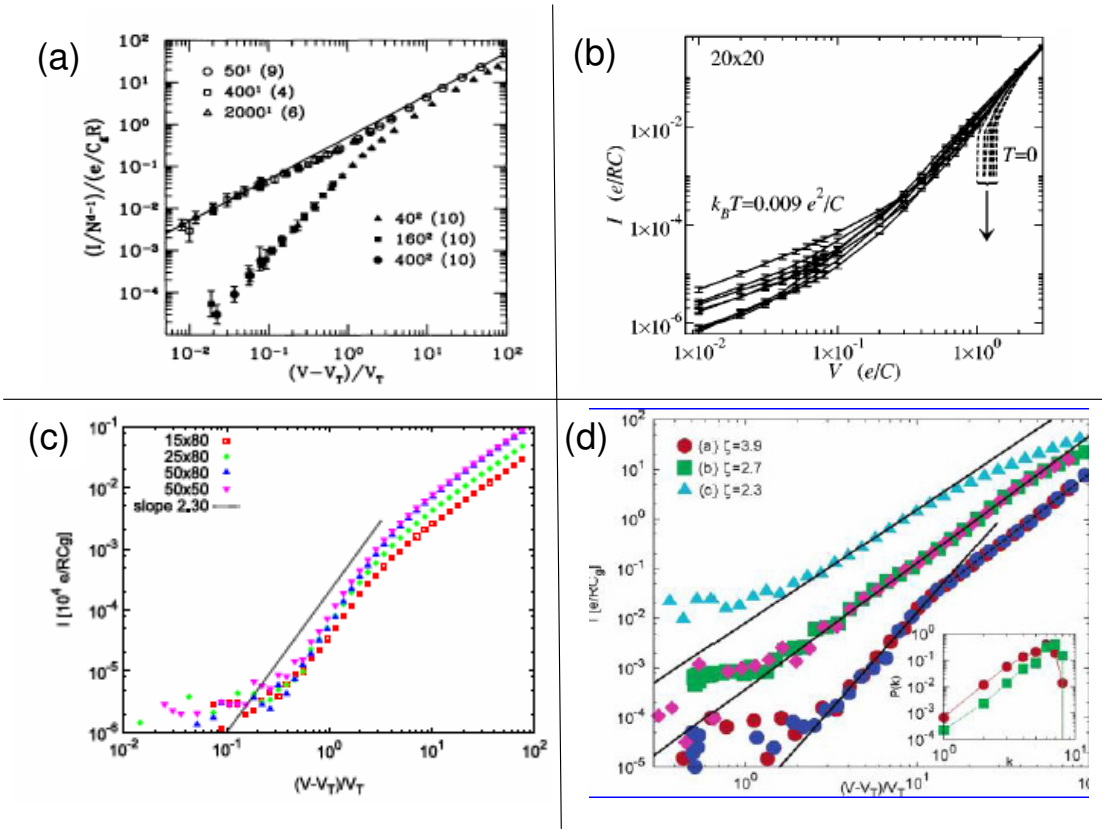

Figure 5.1: $I - V$ curves in logarithmic scales for different numerical simulations. (a) For one and two dimensional arrays of various sizes. In 2D-arrays the exponent obtained is $\zeta = 2$, from Middleton and Wingreen [64]. (b) For an array with $20x20$ islands and long-range interaction $\zeta = 1.7$ from Kaplan et al [89]. (c) For regular triangular array with quenched charge disorder and several sizes, from Suvakov and Tadic [125]. (d) For cellular nanoparticle networks with different void density and one without voids. ζ increases when the void density increases, from Blunt et al.[92].

void fraction the scaling is reduced to 2.8. Parthasarathy et al [1] observed a power-law scaling with $\zeta = 2.25 \pm 0.1$ for structurally ordered arrays with triangular lattice. For this same system Parthasarathy et al [79] found that the scaling is independent of the temperature. Other groups [19, 117] have also obtained temperature independendent exponent, however Sacher et al [121] observed a slight increase with the temperature. Romero and Drndic [19] obtained $2.1 < \zeta < 2.6$ for nanocrystal arrays of $PbSe$. Ruffino et al [117] for disordered arrays of $TiSi_2$ nanocrystals found $1.99 < \zeta < 2.06$. The nanostructure arrays of these experiments have been fabricated by different techniques, such as electron-beam lithography or self-assembly. As we can see in all these experiments the scaling is not related to the size of the array. Moreover, experimentally the scaling exponent can have any value, which makes

us wonder if the theoretical prediction [64] is correct.

On the other hand, as it can be seen in Figs. 5.1 and 5.2 the range of voltages in which

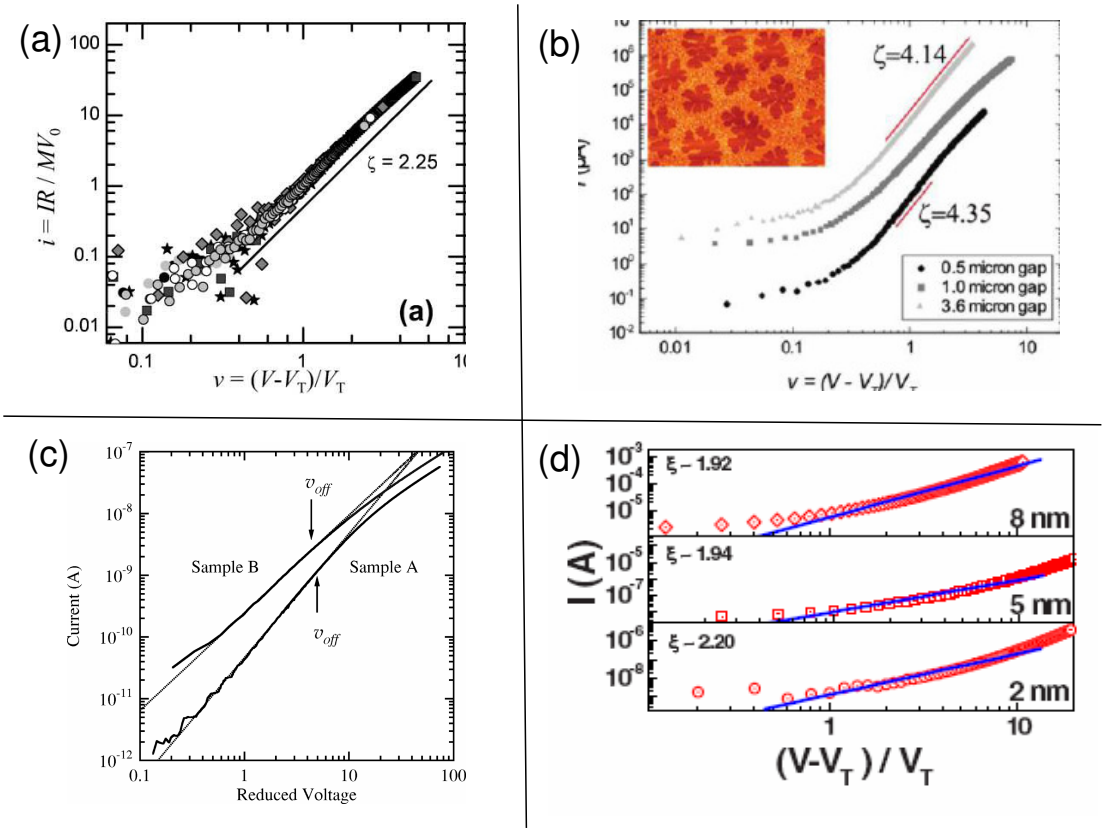

Figure 5.2: Experimental $I - V$ curves in logarithmic scale. (a) Data from seven monolayers with long-range structural disorder, from Parthsarathy et al. [1]. (b) For a nanoparticle assembly, for different range of gap widths, from Blunt et al [92]. (c) For two different samples, see text. The scaling depens on the same $\zeta_A = 2$ and $\zeta_B = 1.58$, from Kurdak et al [97]. (d) For different samples of granular systems consisting of Fe plaquettes over which silver nanospheres, from Bose et al [118].

the scaling exponent has been obtained in the experiments and numerical simulations is somewhere in the region $(V/V_T - 1) \sim 0.04 - 10$. As we show in the one-dimensional case see section 3.2.1, this range of voltage is not sufficiently close to threshold.

Once we have studied and understood the flow of current for voltages close to threshold in one-dimensional arrays, we expect that in the two-dimensional case the current depends linearly on $(V - V_T)$. This is due to the fact that the physics that controls the transport at this

voltage regime is the same for both one and two-dimensional arrays. It is possible that this linear regime is very small, i.e. for a few orders of magnitude, and above it, a new regime can appear where the power-law has a scaling larger than one. For this reason we will study in detail the transport through two-dimensional nanoparticle arrays. Specially, we will study symmetrically biased arrays ($\alpha = 1/2$), in which the charge can enter through both electrodes. We remember that the arrays are given by m x k, where m is the number of rows and k of the columns.

5.2 Threshold Voltage

We first study the threshold voltage at which the scaling regime starts. As we know, the threshold voltage is the minimun voltage at which the current can flow through the array, and it is controlled by the changes in energy in tunneling. For two-dimensional arrays the threshold voltage is given by the minimun number of junctions necessary to transfer the charge from one electrode to the other. In the following, we will explain the threshold voltage for different cases.

5.2.1 Clean Arrays

Square lattice

Specially, in the onsite limit at zero temperature, the threshold voltage of a two-dimensional array with square lattice is equal to the threshold voltage of a clean one-dimensional array with the same length, i.e the number of islands in the one-dimensional case is equal to the number of columns in the two-dimensional array with square lattice. This is due to the fact that there will be a finite current if the charge is able to be transferred from one electrode to the other, and in the case of two-dimensional array with square lattice the minimun path that the charge must follow to cross all the array is one row, see Fig. 5.3 (a) in which the minimun path is represented schematically.

We remember that at zero temperature only the tunneling processes with gain in energy are possible, $\Gamma(\Delta E) = -\Delta E/R\Theta(-\Delta E)$. As we saw in the case of clean one-dimensional arrays, with short range interaction there is no polarization potential drop at the inner junctions, then if the array is uncharged there is no gain in energy and the tunneling processes at the inner junctions are forbbiden. A charge gradient has to be created at these junctions to allow the flow of charge through the array. For a clean two-dimensional array with square lattice this situation occurs in each row. Thus, charge gradients are created in each row under the same conditions. Therefore, the threshold voltage depends on the length of the array but it is independent of the number of rows, as we can see in Fig. 5.4 (a), in which the I-V characteristics are represented for arrays with different size, but all of them with the same

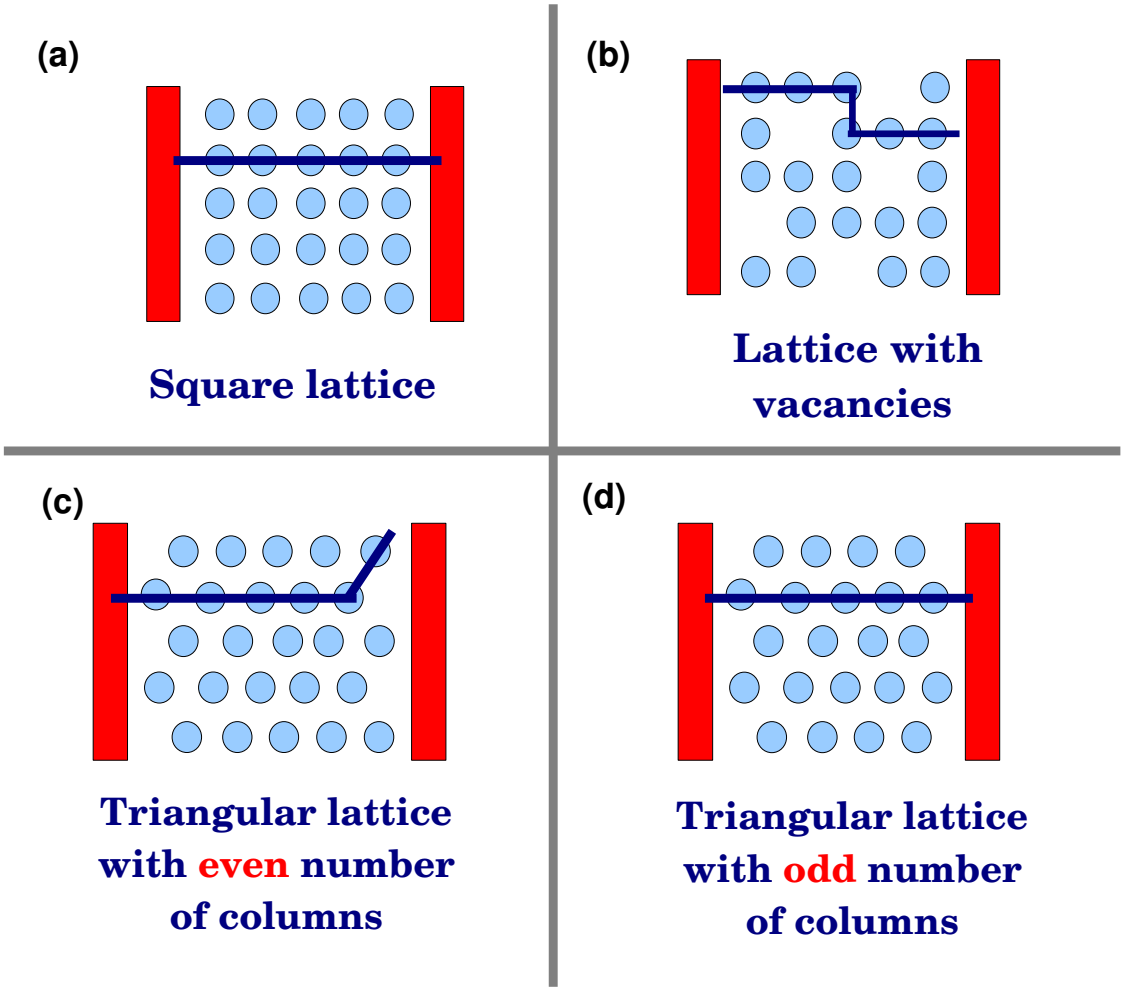

Figure 5.3: Schematic diagrams of the different types of two-dimensional nanoparticle arrays with the minimun path that the charge must follow to across the array from one electrode to the other. (a) Array with square lattice, where m is the number of rows and k the number of columns. (b) Lattice with vacances. (c) Triangular lattice with even number of columns. (d) Triangular lattice with odd number of columns

number of columns, $k = 20$. The current is the only quantity that depends on the number of rows, as we will explain in more detail in the next section.

Triangular lattice

In the case of arrays with triangular lattice, all the rows are not situated at the same distance to the electrodes, i.e. the distance between the first island and the source electrode in an even row is d, whereas in an odd one is $3d/2$, see Figs. 5.3 (c) and (d). The tunneling processes

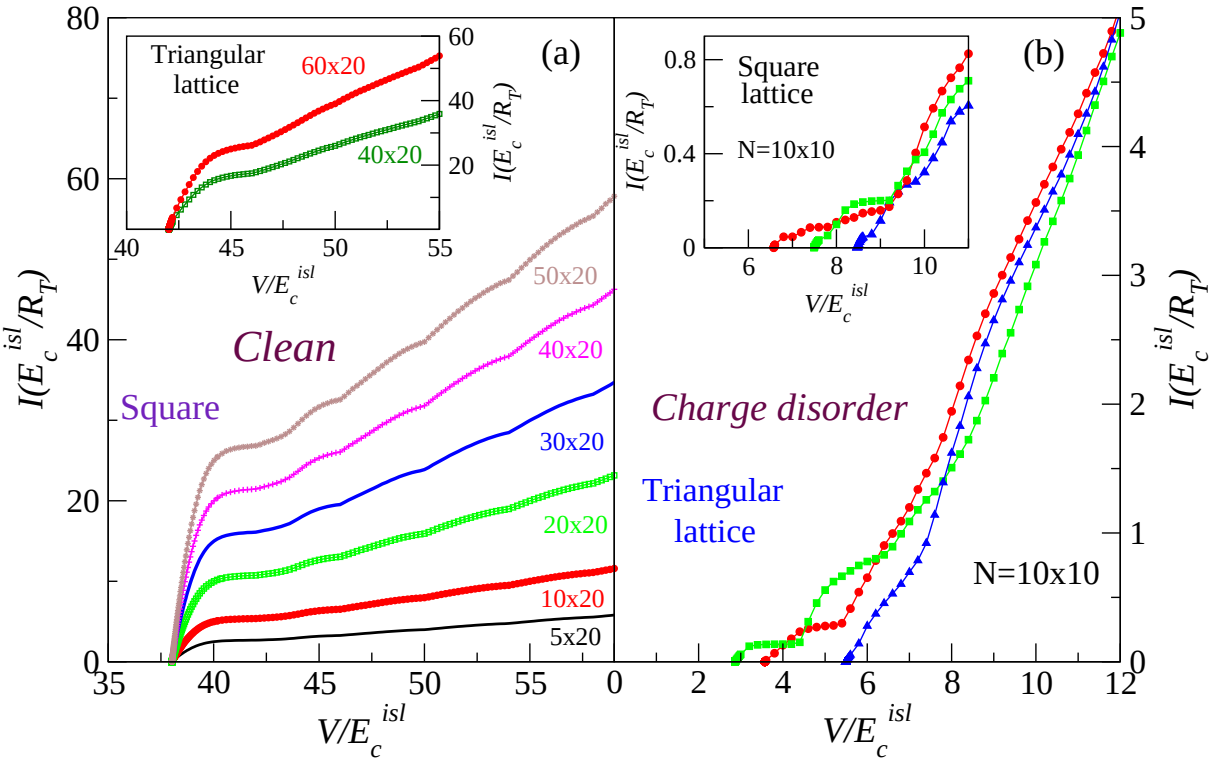

Figure 5.4: (a) Main (inset) figure: I-V curves for clean arrays with square (triangular) lattice with different number of rows, but equal number of columns $k = 20$. Threshold voltage is independent of the number of rows.(b)Main (inset) figure: I-V curves for $N = 10x10$ arrays with triangular (square) lattice with different charge disorder configurations.

are only allowed at first neighbors, d, while at the other one are forbbiden. Thus, the charge cannot enter/exit the array through the contact junctions in which the distance between the island and the electrode is $3d/r$. The case in which the closest nanoparticles to the source electrode is in odd rows, has also been considered . The results obtained in both cases are the same because the arrays studied are symmetrically biased.

There are two different cases: odd and even number of columns.

Odd number of columns

In the case where k is odd, the charge can be transferred from one electrode to the other one across the whole array without change of row, then the threshold voltage is given by the number of islands that there are in this row, see Fig. 5.3 (d). Here, as in the case of square lattice, the charge gradient is created through the row.

Even number of columns

However, for arrays with an even number of columns, as we only allow the tunneling processes between nearest neighbors, the input and output of the charges is restricted to specific rows. For example, in the case of the array represented in Fig. 5.3 (c), input/output of charge is restricted to even/odd rows from the source/drain electrode. As a consequence, the charge cannot enter into the array and leave it by the same row, then the charge has to change of row to be transferred through the array. Fig. 5.3 (c) shows the path with the minimun number of junctions that the charge must follow to go from one electrode to the other.

As in the case of arrays with square lattice, threshold voltage is independent of the number of rows see inset in Fig. 5.4 (a).

In the same way that in one-dimensional array, for symmetrically biased arrays there is an even-odd effect. Thus, the threshold voltage is given by $V_T = 2n_{mp}E_c^{isl}$ when n_{mp} that is the number of islands in the minimun path, is odd and $V_T = 2(n_{mp}-1)E_c^{isl}$ when n_{mp} is even.

5.2.2 Disordered Arrays

For the case of charge disordered arrays, the threshold voltage depends on array configuration of disorder ϕ^{dis}, see Fig. 5.4 (b). Besides, for short-range interaction the theshold voltage is reduced with respect to the clean case because here there are finite potential drops at the inner junctions. We know from the one-dimensional case that the charge gradient necessary to allow the flow of charge only is created at the junctions that prevent the flow of charge ($\Phi^{dis} > 0$). But in a two-dimensional array the charge can move in more directions, then the charge gradient is not created at all the junctions that prevent the flow, because the charge can change of row if it is more favorable energetically. For this reason and unlike the clean case, for charge disordered arrays the threshold voltage can be affected by the number of rows, although not in a generic and systematic way. The threshold voltage in arrays with charge disorder has previously been studied by theoretical [30, 31, 64, 94, 89, 95] and experimental [1, 21, 24, 86, 96, 78, 97–101] groups.

5.2.3 Vacancies

For arrays with vacancies or voids but without charge disorder, the threshold voltage is given by the number of islands in the minimun path between both electrodes, as in the case of clean arrays without disorder. As a result, the current starts to flow at voltages larger than $V_T = 2n_{mp}E_c^{isl}$ for n_{mp} odd and $V_T = 2(n_{mp}-1)E_c^{isl}$ when n_{mp} is even, in the same way that in the clean case. Fig. 5.3 (b) shows a schematic diagram of the minimun path in a clean array

with vacancies, where the charge dodges these vacancies to cross all the array. The threshold voltage is affected by the position of the voids. This can be observed in Fig. 5.5. In the main figure, the $I-V$ characteristic for square arrays with $N = 10x10$ islands and different vacancies configuration are represented. The vacancies are distributed randomly over the array. The number of vacancies in the configurations A and B is 10, whereas in C and D is 20. As we can see the configurations A and C have the same threshold voltage despite having different number of vacancies. This also occurs in the triangular lattice represented in the inset of Fig. 5.5, where the threshold is equal for a clean array with size $N = 10x10$ [1] and only one void and for the case of an array with the same size and 10 vacancies. However, the threshold voltage depends on the position of the vacancies, as can be observed in the cases of the configurations C and D that with the same number of voids have different values of threshold, see main fig 5.5.

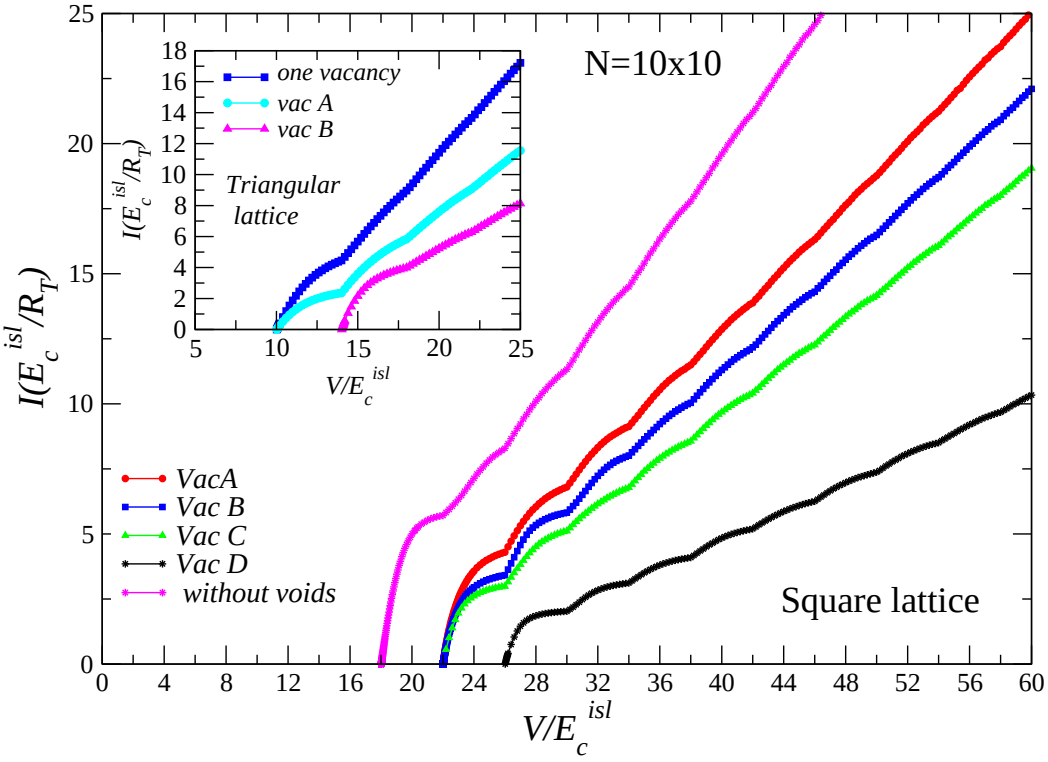

Figure 5.5: Main figure: I-V curves for clean arrays with square lattice with $N = 10x10$ islands and different vacancies configurations. The case without vacancies is included for comparison. The number of vacancies in the configurations A and B is 10, and in C and D 20. The vacancies are randomly dispersed over the arrays. Inset: $I-V$ curves for triangular arrays of size $N = 10x10$ where the configurations A and B have 10 and 12 vacancies respectively.

[1] The size in arrays with triangular lattice indicates the number of rows x columns, however the total number of islands in the array is different. Specifically, in this case there are $10x5$ islands

5.3 Flow of Current

Once there is current flow through the two-dimensional array as in the one-dimensional case, it is affected by different factors such as the different types of disorder, the lattice geometries, the size of the array or the charging energy, leading a strongly non-linear function of the current with the voltage. Contrary to general believe in which the current shows a power-law behavior $I \sim (V/V_T - 1)^{\zeta}$ with $\zeta = 5/3$ (see above), the current depends linearly on voltage close to threshold. At higher voltages we find steps over a range of superlinear behavior for large charge disordered arrays. But in general, this superlinear behavior cannot be described in terms of a power-law. A second linear regime appears at very high voltages.

5.3.1 Linear dependence close to threshold

So far, most of the studies done in these systems considered that the current shows a power-law behavior for voltages close to threshold as a consequence of the conducting channels in the array. It means that at the threshold voltage there is a minimun path, but for larger voltages in a two-dimensional array new paths for the conduction will be possible, resulting in a particular current dependence on the voltage. As the number of conducting channels depends on the lattice geometry, structural or charge disorders, in some works the scaling exponent has been related to the topology of the array [91, 125]. However, for voltages very close to the threshold the power-law does not depend on the number of conduncting paths. As shown below in two-dimensional arrays as in the one-dimensional case there is a linear dependence on the voltage, with $\zeta = 1$. Moreover, this linear behavior is independent of the lattice geometry and the different types of disorder, as we can see in Fig. 5.6. where the $I - V$ curves in logarithmic scale and their derivatives are represented for different array parameters.

The linear dependence for voltages close to the threshold in two-dimensional arrays is a consequence of the existence of a bottleneck junction which controls the current in a path, in the same way as in the one-dimensional case seen in chapter 3. In two-dimensional arrays this behavior appears in all the possible minimun paths through the array at the same time, as a result, the slope of the current is affected by the number of minimun conducting paths, but not the linear dependence.

This linear dependence can be demonstrated analytically for arrays without disorder. We remember that in one-dimensional arrays the current at voltages close to the threshold can be approximated by the tunneling rate of the junction that acts as bottle-neck, see section 3.2.1. As for short-range interactions the junctions that act as a bottleneck are the contact ones the current resulting is

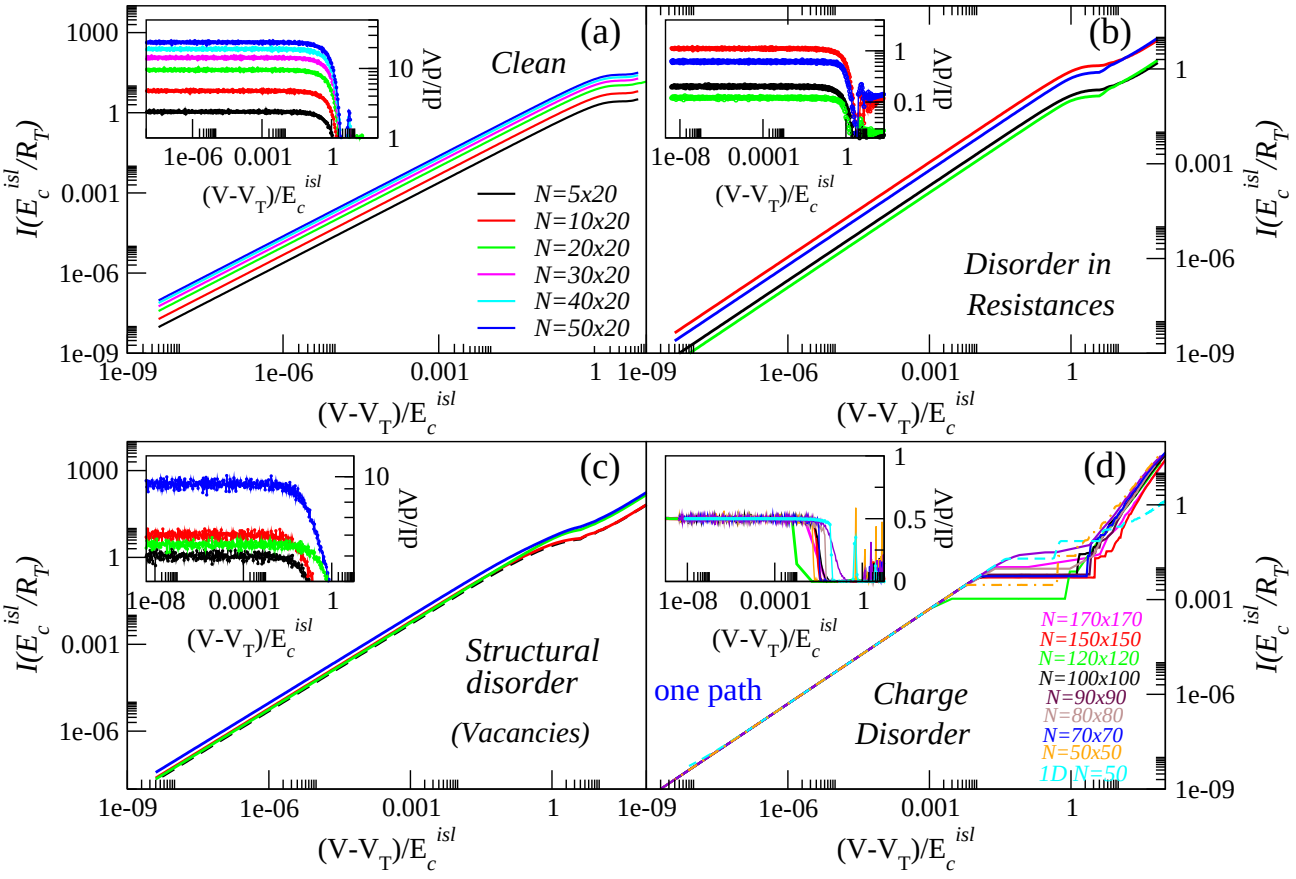

Figure 5.6: Main figure: I-V curves in logarithmic scales for different array parameters. The insets show the derivatives (in units of $1/R_T$) of curves plotted in the main figures. (a) $I-V$ curves corresponding to arrays without any type of disorder, for square lattice and equal number of columns. (b) $I-V$ curves for arrays with disorder in resistances, which values vary randomly between $(20-84)R_T$ and $(5-11)R_T$ for $N = 20x20$ and $N = 20x38$ square and triangular lattices, respectively. (c) $I-V$ curves for arrays with structural disorder for both square and triangular lattices, with $N = 10x10$ and $N = 20x20$ respectively. (d) $I-V$ curves for charge disordered arrays for square and triangular lattices. One-dimensional array with $N = 50$ nanoparticles is included for comparison. Only a single channel contributes to the current.

$$I = \frac{1}{R_{bn}}(V - V_T) \tag{5.2}$$

where R_{bn} is the resistance of the bottleneck junction. For two-dimensional arrays the current is determined by the tunneling rates across the bottle-neck junctions in the different paths.

As we saw in chap. 3 for the one-dimensional case when the arrays are symmetrically biased, at voltages close to threshold the slope of current depends on whether the number of

islands is even or odd. In two-dimensions the current depends not only on the number of islands in the minimun path, but also on the lattice geometry of the array. We study each lattice separately.

Square lattice

We remind from one-dimensional case that when the array is symmetrically biased and the number of islands is odd, the flow of charge can be controlled by any of the two contact junctions, due to the charge gradient created within the array, see subsection 3.2.1. Thus, to determinate the current both contact junctions have to be taken into account. In a clean two-dimensional array with square lattice each row is a minimun path. Then, the current is given by the different channels that conduce in parallel

$$I = m_{minpath}\left(\frac{1}{R_1} + \frac{1}{R_{N+1}}\right)\frac{1}{2}(V - V_T) \tag{5.3}$$

where $m_{minpath}$ is the number of rows that are contributing to the current. In particular, for clean arrays with square lattice $m_{minpath}$ is qual to the number of rows.

For an even number of islands in the minimun path, the charge gradient is created in all junctions except one, see subsection 3.2.1. As a consequence, the charge has to enter into the array through both contact junctions to allow the flow of current. This situation occurs in each row, leading a current equal to

$$I = m_{minpath}\frac{2}{R_1 + R_{N+1}}\frac{1}{2}(V - V_T) \tag{5.4}$$

The dependence of the current with the number of conducting channels can be clearly observed in Fig. 5.6 (a), where the $I - V$ curves are represented in logarithmic scale for two-dimensional clean arrays, all of them with the same minimun path but with different number of conducting channels, that in the case of square lattice is equal to the number of rows. The dependence of the slope of the current is better seen in dI/dV plotted in the inset.

Triangular lattice

In the case of nanoparticle arrays with triangular lattice, at voltages close to the threshold the current depends not only on the number of islands in the minimun path, but also on whether the number of columns is even or odd.

Odd number of columns

For clean symmetrically biased arrays with triangular lattice and odd number of columns,

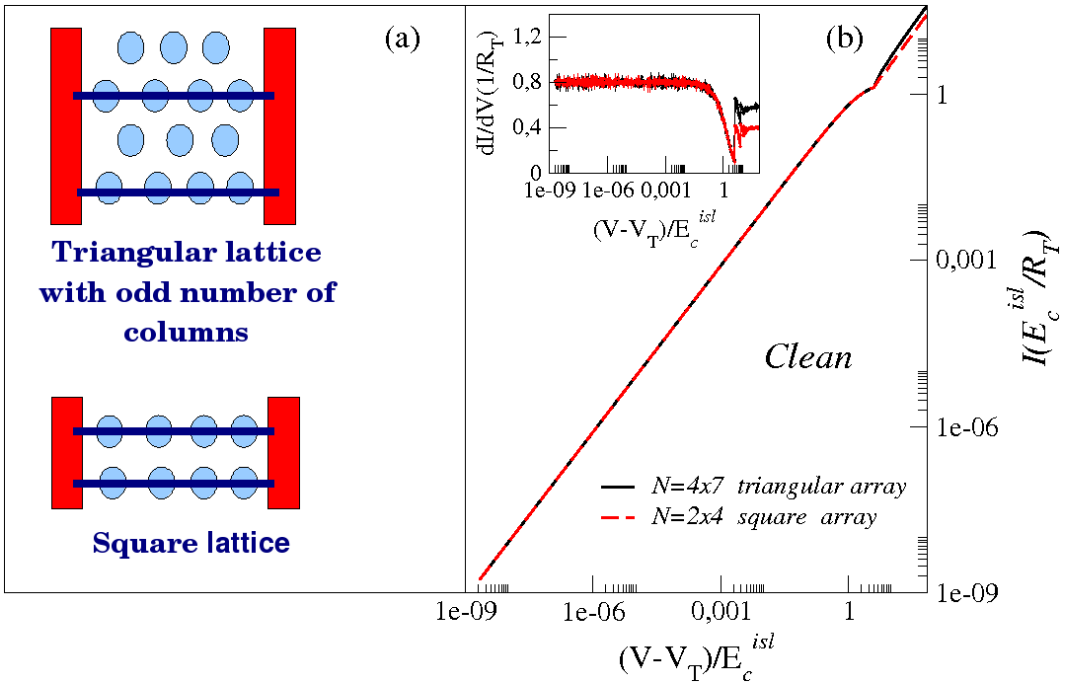

Figure 5.7: (a) Schematic diagram of the conducting paths in two clean arrays, one with triangular lattice and odd number of columns and the other with square lattice. (b) Main figure: I-V curves in logarithmic scales for two clean arrays, one with square lattice and $N = 2x4$, and the other with triangular lattice and $N = 4x7$. The inset shows the derivatives (in units of $1/R_T$) of curves plotted in the main figures.

there are rows in which the entrance and exit of charge are forbbiden because the first and last islands in the row are not nearest neighbors of the electrodes, see Fig. 5.7 (a). For $V \simeq V_T$, only the rows that allow the transference of charge from one electrode to the other will contribute to the current. This can be clearly seen if we compare the $I - V$ curves for a triangular array with odd number of columns with the case of a square lattice with equal number of rows than the number of conducting rows in the triangular array, and both of them with the same minimun path. The current obtained is equal in both arrays see Fig. 5.7 (b). When the triangular array has an odd number of columns, the current is given by Eqs. 5.3 and 5.4 for an odd and even number of nanoparticles in the minimun path, respectively.

Even number of columns

In order to transfer one charge from one electrode to the other in a triangular array with even number of columns, it is necessary that the charge changes of row, see Fig. 5.3(c). Then, the smallest array in which there is current is one with two rows and two columns.

Odd number of islands in the minimun path

The smallest array in which there is current for a number of columns given is represented

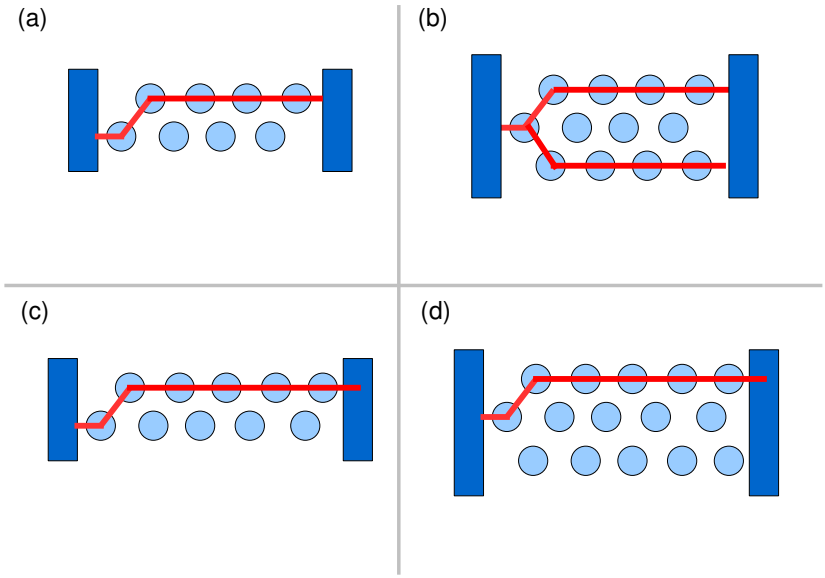

Figure 5.8: Schematic diagrams of the paths followed by the charge in different clean triangular arrays with even number of columns and odd and even number of islands in the path. (a) $N = 2x8$ triangular array, is the smallest array where there is current for this number of columns. The minimum path has odd number of islands. (b)Possible paths in a $N = 3x8$ clean array. (c) $N = 2x10$ triangular array, is the smallest array where there is current for this number of columns. The minimun path has even number of islands. (d) In the case of $N = 3x10$, the third row hardly contributes to the current at voltages close to threshold.

in Fig. 5.8 (a), and as it can be seen the two rows are necessary to allow the flow of charge. Unlike in square arrays where if there are two rows, these contribute fully to the current (Eq 5.3), in the specific case of this triangular lattice each row contributes the half. If we add one row more, Fig. 5.8 (b), its contribution to the current is the half too. Thus, the current is equal to

$$I = \frac{m}{2}\left(\frac{1}{R_1} + \frac{1}{R_{N+1}}\right)\frac{1}{2}(V - V_T) \tag{5.5}$$

regardless of whether the number of rows is even or odd.

Even number of islands in the minimun path

However, for the case of arrays with triangular lattice and even numbers of columns and n_{mp}, the current depends on whether the number of rows is even or odd.For even n_{mp} the

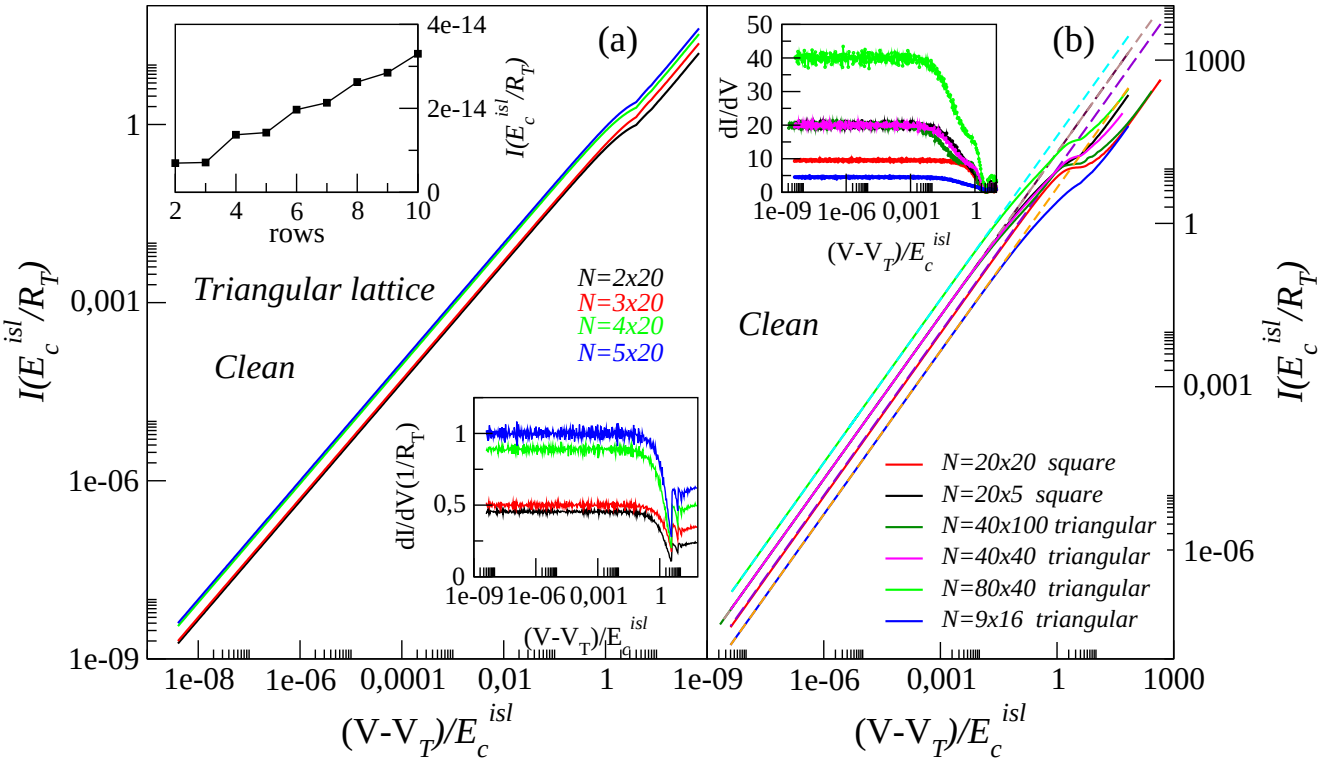

Figure 5.9: (a) Main figure: $I-V$ curves in logarithmic scale for clean arrays with triangular lattice all of them with even number of columns and odd number of islands in the minimun path. Bottom inset: derivatives (in units of $1/R_T$) of the curves plotted in the main figure. Top inset: Current as a function of the number of rows in arrays with 42 columns and triangular lattice at the threshold voltage. (b) Main figure: $I-V$ curves in logarithmic scale for clean arrays with square and triangular lattices (solid lines) with their theoretical predictions (dashed lines). Inset: derivatives (in units of $1/R_T$) of the curves plotted in the main figure.

charge has to enter through the two contact junctions to allow the flow of charge see Fig. 5.8 (c). For this reason, if in the array there is one row more, see Fig. 5.8 (d), although there is one contact junction more through which the charge can enter or exit, this third row hardly contributes to the current at $V \simeq V_T$, see Fig. 5.9 (a). There is something like an even-odd effect with respect to the rows, as we can see in the top inset of Fig. 5.9 (a), where the current is represented as a function of the number of rows for arrays with 42 columns in the triangular lattice at V_T. Therefore, the current is approximately equal to Eq (5.6) for even m and to Eq (5.7) when m is odd.

$$I = \frac{m}{2}\left(\frac{2}{R_1 + R_{N+1}}\right)\frac{1}{2}(V - V_T) \tag{5.6}$$

$$I = \frac{m-1}{2}\left(\frac{2}{R_1 + R_{N+1}}\right)\frac{1}{2}(V - V_T) \tag{5.7}$$

Fig. 5.9 (b) shows good agreement between the numerical results and the theoretical predictions (dashed lines) for the $I - V$ curves at voltages close to the threshold, for different clean arrays with square and triangular lattices.

On the other hand, the slope of current is affected by disorder in resistances and the vacancies' configuration, see insets in Fig. 5.6 (b) and (c).

Linear behavior close to threshold in charge disordered arrays

As we previously mentioned, most of the works have focused on the study of $I - V$ curves at voltages close to the threshold for charge disordered arrays. It was predicted that the current shows a scaling power-law behavior at these voltages [64]. They assumed that the current is given by independent channels which depends linearly on $(V - V_T)$. They considered that at threshold voltage there was only one conducting channel, and with the increase of the voltage new channels opened. The number for opening channels depended on the voltage.

In the three types of arrays studied until now, clean, with disorder in resistances, and with voids, different conducting channels contribute to the current. These channels are the minimun paths at the threshold voltage. On the contrary, in charge disordered arrays very close to the threshold there is only one path that contributes to the current independently of the size of the array, as we can observe in Fig. 5.6 (d). This can be clearly seen by the derivative of the $I - V$ curves, which is the same for one and two-dimensional arrays with homogeneous contact resistance, see inset in Fig. 5.6 (d). In both cases the current is controlled only by one contact junction, through which the charges enter into the array. As we have explained before (section 5.2.2), to allow the flow of charge in charge disordered arrays it is necessary to create a charge gradient at the junctions that prevent it. But in two-dimensional case the charge can move in different directions, thus the charge chooses the direction in which it is easiest to overcome the disorder potential. Therefore, the single conducting channel in these arrays corresponds to the path that allow the flow of charge with the smallest number of charges piled-up.

In this thesis we have demostrated that for voltages close to threshold, the electronic transport is governed by the contact junction that acts as a bottle-neck, and not by the lattice as has been considered by different groups until now. A linear dependence on $(V - V_T)$ does

not mean scaling on $(V - V_T)/V_T$ as it was predicted in [64]. This is seen in Fig. 5.6 (d) in which all the $I - V$ curves, corresponding to arrays with different V_T, show the same current in the linear regime in units of $V - V_T$. The whole lattice determines V_T, but a single contact junction controls the slope in current close to threshold. Moreover, this fact can be clearly seen in Fig. 5.10 (a) where the $I - V$ curves are represented for two charge disordered arrays with $N = 150x150$ islands, one of them with all junction resistances equal and the other with the contact junction resistances 1000 times smaller than the resistance of the inner junctions (between islands). In spite that the current through both arrays shows linear behavior for voltages very close to threshold, in the case of the array with small contact resistances the current is three orders of magnitude larger, confirming the importance of the contact junctions. Besides with increasing voltage, the loss of linearity occurs before in the case with smaller contact resistances. This is because in this case the transport is controlled by the lattice for smaller voltages than in the homogeneous resistances case due to the tunneling rate at the contact junction.

On the other hand, the scaling behavior predicted by Middleton and Wingreen for charge disordered arrays is based on the assumption that for voltages close to threshold the current flows through independent channels that depend on the dimensionality of the array. However, their numerical and analytical results do not match. They argue that this discrepancy is due to the finite-size effect. We have studied an extreme case of a very large array with a size of 1000x10 nanoparticles, and for voltages close to threshold the current shows linear behavior, see Fig. 5.10 (b).

To summarize, for two dimensional arrays as in the one-dimensional case the current has a linear dependence on $(V - V_T)$ at voltages close to threshold. This is because the transport is controlled by a contact junction. Moreover, this linear behavior occurs in clean and disordered arrays with square or triangular lattice and in the presence of vacancies for several orders in magnitude. The loss of linearity appears at values of $(V - V_T)$ similar to those found in one-dimensional arrays, much smaller than the voltages at which the experiments and the previous numerical simulations have been done.

5.3.2 Intermediate regime of voltages

At intermediate voltages between the two linear regimes at low and high voltages there is another regime with different behavior. This regime coincides with the voltage range in which all previous experiments and theoretical studies that tried to find a power-law at voltages close to threshold, have been done. It should be noted that most experiments interpreted in terms of power laws very small ranges of voltages, see Fig. 5.2. Sometimes they are less than an order in magnitude. For such small ranges we cannot speak of power-laws. We can be

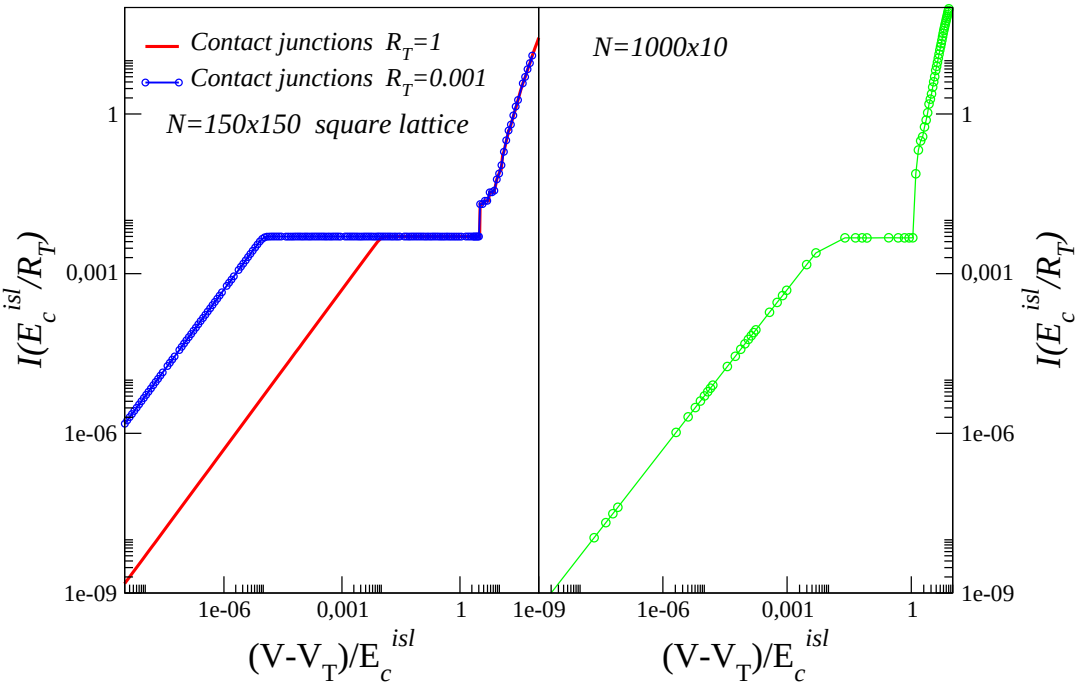

Figure 5.10: (a)$I-V$ curves in logarthmic scale for two 150x150 square lattice arrays with the same charge disorder configuration. In one of them the tunnel resistance of the contact junctions is 1000 times smaller. (b) $I-V$ curve for a charge disordered array with 1000x10 and square lattice.

sure that the observed behavior is a power-law when the power-law behavior is obseved at least in two orders in magnitude.

As in the one-dimensional case, for two-dimensional arrays the loss of linearity occurs when the transport becomes controlled by one or several inner junctions, yielding a staircase profile in the current. Remember that this is because in the onsite limit at an inner or bulk junction the change in energy of a tunneling process is independent of the voltage (see chapter 3). The current has kinks at those voltages, which allow new transport processes. It means that the change from one step to the next one is associated with the opening of a new conducting channel.

For arrays without charge disorder, the current shows a big jump, that increases with the number of rows in the clean case, see Fig. 5.4 (a). Whereas for arrays with structural disorder or disorder in resistances, the height of the jump depends on the vacancies and resistances configurations respectively, see Fig. 5.5 for the case with voids. As we explained in the one-dimensional case, this jump occurs as a result of having to create a charge gradient through all the array to allow the flow of charge. Once the charge gradient is created, the charge can flow easily from one electrode to the other. As in one-dimension, for symmetrically biased

arrays the width of the steps is $4E_c^{isl}$, and for clean arrays the kinks in the current appear at the same position in both dimensions. Moreover, the position of the kinks are not affected by the disorder in resistances or vacancies.

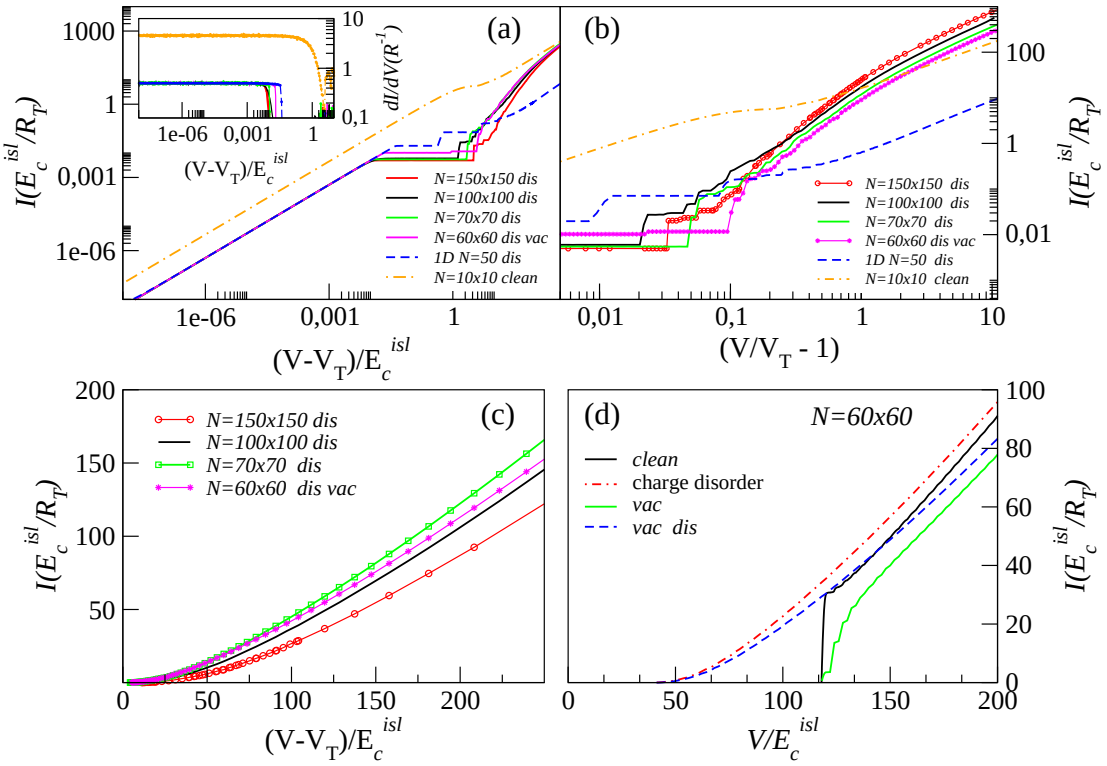

Figure 5.11: (a) Main figure: $I-V$ curves at low voltages in logarithmic scale corresponding to 2D disordered arrays of different size, a N=50 islands disordered 1D array and a clean N=10x10 square-lattice 2D clean array. N=60x60 square lattice has structural disorder (vacancies) besides the charge disorder. Inset: derivativ of the $I-V$ curves plotted in the main figure. (b) Same as in main figure in (a) but in different voltage regime and with the axis scaled differently. (c) Same as in (c) for selected curves in normal scale with the same axis as in (a). (d) $I-V$ curves for 60x60 square array clean, with charge disorder, structural disorder and one with charge and structural disorder.

Charge disordered arrays

For charge disordered arrays the current shows clear steps with horizontal plateaux as we can see in Fig. 5.11 (a) and (b), where the $I-V$ curves are represented for arrays with different size. Fig. 5.11 (a) shows the loss of linearity, which is sublinear. In Fig. 5.11 (b) the same curves are represented in the regime of intermediate voltages with the axis scaled dif-

ferently, in the same way that the previous works. This is done to see if there is a scaling law $(V/V_T - 1)$ as it was predicted by Middleton and Wingreen [64]. Similar staircase profile had been observed experimentally by Kurdak et al [97], see Fig. 5.2 (c). The width of the steps depends on the charge disorder configuration, see Fig. 5.4 (b). For large disordered arrays within a range of voltages steps smooth up to look like superlinear behavior which resembles a power-law, see Fig. 5.11 (c). Note that this superlinear behavior only appears when there is charge disorder in the arrays, see Fig. 5.11 (d) in which the $I - V$ curves are represented for $N = 60x60$ nanoparticles with square lattice in different cases, clean, with charge disorder, with structural disorder and with structural disorder besides the charge disorder.

In this regime of voltages it is where the experiments have been done, see Fig. 5.2. For this reason, we want to know if this superlinear behavior can be described in terms of a power-law. We fit the $I - V$ curves obtained numerically from our simulation to a scaling power-law as the one proposed by Middleton and Wingreen

$$I = a(V/V_T - 1)^{\zeta} \tag{5.8}$$

In Fig. 5.12 (a) and (b) the $I - V$ curves of a charge disordered array with $N = 150x150$ islands and square lattice are represented with their fittings for several ranges of voltage, that are similar to the ones used to fit the results obtained experimentally. The threshold voltage used to obtain $(V/V_T - 1)$ is calculated theoretically. Our numerical results fit perfectly with the power-law given by Eq.(5.8), and the values of the exponents that we obtain are similar to the ones discussed previously in the literature, remember that there is a wide range ($1 < \zeta < 5.2$). However, the scaling exponent strongly depends on the length of the range of voltage. Specially, for the case represented in Fig. 5.12 (a)-(b) the scaling exponent varies between 1.39 and 2.63. We have also studied arrays with different sizes and we found variations in the values of the scaling exponent as we can see in the next table. This means that the current-voltage dependence is not given by a power-law. The fitting exponent ζ is meaningless.

Further to explore this issue we use a different method to perform the fitting. If the current was described by a power-law like the one discussed above we could determine the scaling exponent ζ and the threshold voltage V_T from the representation of

$$\frac{I}{dI/dV} = \frac{1}{\zeta}(V - V_T) \tag{5.9}$$

This method has been used to extract the threshold voltage and the scaling exponent by several experimental groups [121, 122, 127]. However, we note that the values of the threshold obtained from the fitting of the curves are different from the true ones, which can be calculated theoretically. In Fig. 5.12 (c) and (d) we show these functions $I/(dI/dV)$ us V and their

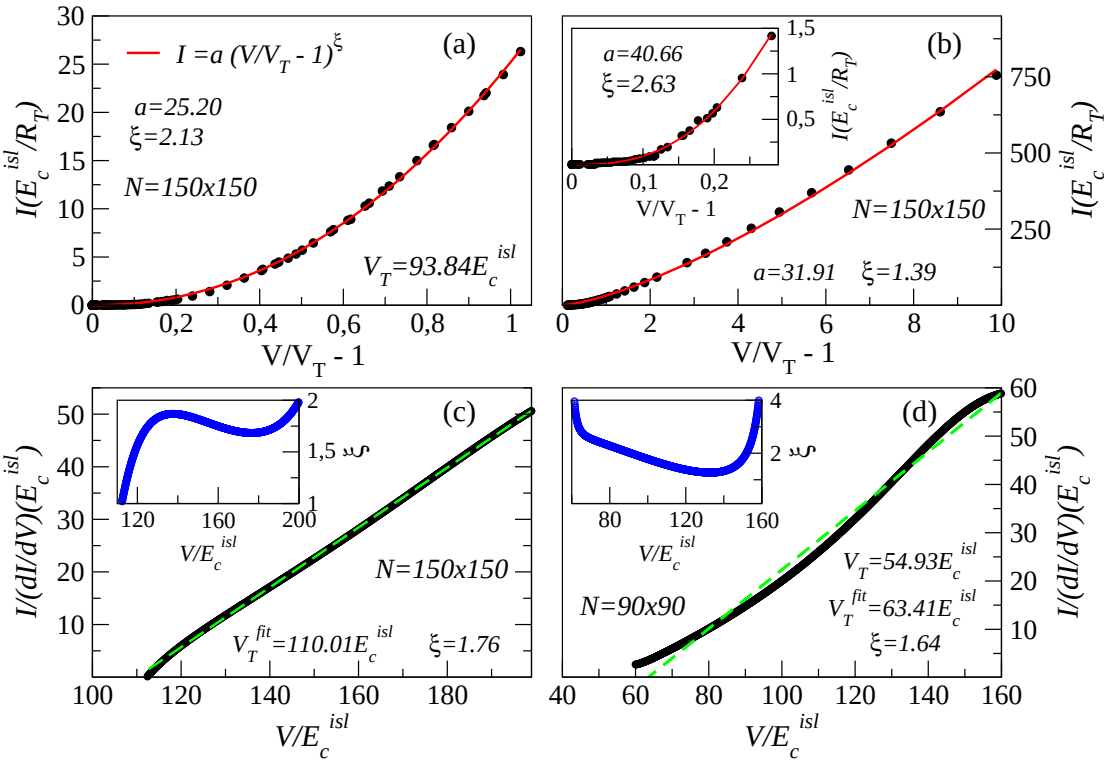

Figure 5.12: (a) and (b) Main figures and inset: $I-V$ curves with their fittings to a power-law $I = a(V/V_T - 1)^{\zeta}$ for the same charge disordered array with $N = 150x150$ and square lattice and several ranges of voltage. (c) and (d) Main figures: $I/(dI/dV)$ as a function of the voltage with their fitting to $\zeta^{-1}(V - V_T^{fit})$ for $150x150$ and $90x90$ charge disordered arrays. Insets: Values of ζ extracted from the derivatives of (c) and (d), according to: $\zeta^{-1} = d(I/(dI/dV))/dV$.

corresponding fitting parameters for two charge disordered arrays with different size. One with $N = 150x150$ and the other with $N = 90x90$, both of them with square lattice. As the derivatives give a lot of noise, in order to avoid this noise and clearly see $I/(dI/dV)$, the $I-V$ curves had been previously fitted to a high order polynomial. Due to the fact that the polynomial fitting induces spurious voltage dependences at smallest voltages, these have not been represented. V_T^{fit} is the threshold voltage obtained from the fitting, whereas V_T is the true one. Not only are the threshold voltages wrong, but also the fittings for the array with $N = 90x90$ are very bad, because $I/(dI/dV)$ is not linear in voltage. Moreover, for this case the values of V_T vary with the range of voltages.

Scaling exponent can be determined easily from the derivative of $I/(dI/dV)$, which should be a constant, see (5.9). But as we can see in the insets in Fig. 5.12 (c) and (d) where the scaling is represented as a function of the voltage, it is far from being a constant. This confirms that contrary to what has been believed in the past two decades, the current is not described

	SCALINGS		
ARRAYS	[0:1]	[0:0.6]	[0:0.3]
60X60	1.98	2.06	1.90
70X70	2.02	2.04	2.16
80X80	2.19	2.17	1.93
90X90	1.95	2.14	2.51
100X100	2.01	2.05	1.81
120X120	1.94	2.01	1.87
150X150	2.12	2.27	2.65
170X170	2.00	2.06	2.10

Figure 5.13: Scaling for charge disordered arrays with different sizes and square lattice for several ranges of voltages.

by a power-law at this range of voltages.

5.3.3 Linear behavior at high voltages

At high voltages the current depends linearly on the bias voltage as it occurs in the one-dimensional case. This linear dependence appears in clean arrays, with charge disorder, disorder in resistances or with structural disorder for both square and triangular lattices, see Fig. 5.14 (a) and (b). As in one-dimensional arrays, for this range of voltages the charge does not feel the presence of the charge disorder. Thus, at high voltage in two-dimensional charge disordered arrays many channels contribute to the current, contrary to what happens in the linear behavior at low voltages, in which only a single channel contributes. On the other hand, the current strongly depends on the structural disorder or voids.

At high voltages the charge can flow through all the junctions in the array thanks to the large charge gradient created at each of the junctions. For this reason at this regime of voltages the average current depends on the lattice of the array and on the configuration of vacancies.

Square lattice

In the case of arrays with square lattice without voids or disorder in the resistances, the charge gradient existent at high voltages ensures that all the tunneling processes to the right

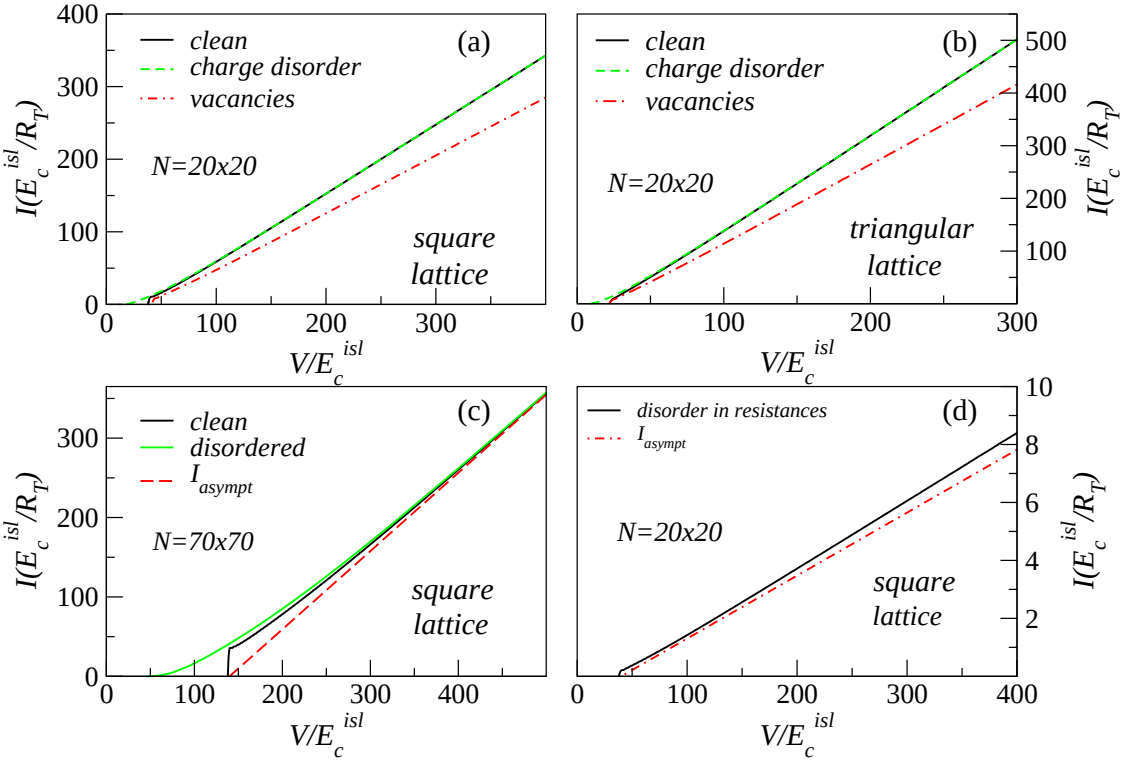

Figure 5.14: (a) $I-V$ curves at high voltages for a square lattice $N = 20x20$ array corresponding to clean, charge disordered and with structural disorder (vacancies). (b) Same that in (a) but the arrays have triangular lattice. (c) $I-V$ curves for clean and charge disordered arrays with $N = 70x70$ and square lattice. Theoretical prediction is included for comparison. (d) $I-V$ curve for $N = 20x20$ square lattice array with disorder in resistances $(20-84)R_T$. The asymptotic $I-V$ curve has been derived using a potential drop equal to the one corresponding to adding the resistances in series.

decrease the energy. Thus, in this array the vertical junctions barely contribute to the current, and the charges follow the minimun paths in the array that are the rows. The current can be approximated by the following asymptotic curve

$$I_{asympt} \sim \frac{m}{(k+1)R_T}\left(V - V_{offset}\right) \tag{5.10}$$

with m and k the number of rows, and of columns respectively, and V_{offset} the offset voltage at which the asymptotic current extrapolates to zero. For a square lattice $V_{offset} = 2kE_c$ equals the V_{offset} in one-dimensional arrays. This equation is valid for clean and charge disordered arrays, as can be observed in Fig. 5.14 (c).

The voltage at which the high linear behavior is reached , V_{linear}, does not depend on the number of rows m, but depends on the length of the array or number of columns k. The

linear behavior starts approximately at the same values in 1D and 2D arrays, and it is approximately $V_{linear} \sim 8kE_c$, consistent with the behavior observed in the experiments [24, 98] and in the calculations of Middleton and Wingreen [64].

In the case of one-dimensional arrays with disorder in resistances, we remember that the current is given by $I = (V - V_{offset})/R_{sum}$, where R_{sum} is the addition in series of all the resistances. However, in two-dimensional arrays with non-homogeneous resistances the current cannot be approximated by $I = \sum_{i=rows}(V - V_{offset}/R_{sum,i})$, with $R_{sum,i}$ the sum of the junctions resistances in a row i, as we can see in Fig. 5.14 (d), where the current and this approximation have been represented for an array with square lattice and disorder in resistances. The reason why the current cannot be approximated by this equation, is because in two-dimensional arrays the charge can move in several directions, then, if there is a large resistance the charge can meander and avoid it. This effect is clearly observed in the potential drop through the array that we will explain in the next section.

Triangular lattice

Unlike the case of arrays with a square lattice, for arrays with a triangular lattice we cannot predict analytically the average current at high voltages. At these voltages thanks to the charge gradients created through the array there are finite potential drops at all diagonal junctions, leading to a lot of paths that can be followed by the charges. Different paths contribute to the current but not all of them do it in the same way. The problem is that we cannot determinate the paths that the charges follow because there are too many possibilities. Contrary to the case of low voltages or square lattice, in triangular arrays at high voltages not only the minimun paths contribute to the current, as we can see in Fig. 5.15. In this figure the $I - V$ curves are represented for two clean arrays, one with triangular lattice $N = 4x7$ and the other with square lattice $N = 2x4$. If only the minimun paths contribute to the current, both $I - V$ curves should be equal, as occurs at low voltages see Fig. 5.7, but it does not happen.

For arrays with triangular lattice the offset voltage is determinated by the length of the different paths that contribute to the current. For this reason we have not been able to calculate V_{offset} analytically. However, we can calculate V_{offset} extrapolating the polinomial at which the current fits at high voltages. The values obtained confirm that paths with different length contribute to the current. In general, the offset voltage depends on the length and width of the nanoparticle array.

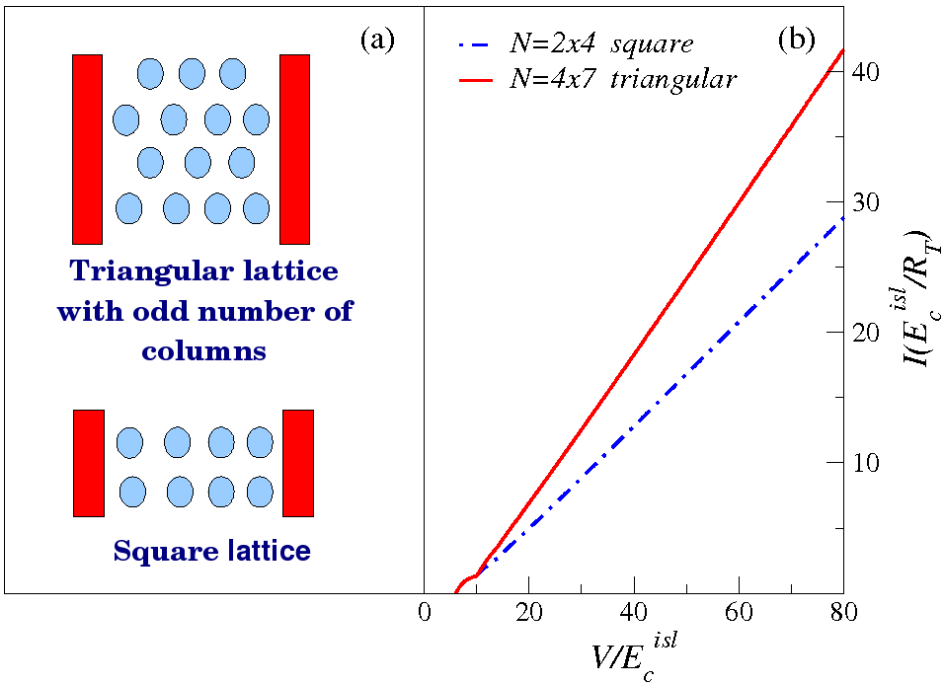

Figure 5.15: (a) Schematic diagram of two clean arrays, one with triangular lattice and odd number of columns $N = 4x7$ and the other with square lattice $N = 2x4$. (b) I-V curves for two clean arrays represented in (a).

Arrays with vacancies

In the same way as for the case of triangular lattice, for arrays with structural disorder or voids we cannot predict the asymptotic behavior analytically. Let us consider an array with square lattices and vacancies. To go from one electrode to the other one the charge has to avoid the vacancies. Thus, the charge gradients are created at horizontal and vertical junctions. For large values of voltages the charge gradients are created through all junctions in the array, and as a consequence a lot of possible paths appear. The paths that contribute to the current can have different length as in the case of clean triangular arrays.

5.4 Potential drop through the array

In this section we analyze the potential drop through two-dimensional nanoparticle arrays, and how it is affected by the lattice or the different types of disorders, such as the structural disorder or non-homogeneous resistances. We study the potential drop in the different regimes of voltages that appear in the current. In order to understand the differences between both square and triangular lattices we first focus on the clean case. And after that we analyze the effect of the disorder.

5.4.1 Clean

Square lattice

For clean two-dimensional nanoparticle arrays with square lattice, the potential drop in each row is similar to the potential drop in the one-dimensional case. This occurs for the three different regimes of voltages that the current shows.

As we already know, at low voltages the transport is governed by a bottleneck junction. As tunnel through this junction required larger time than tunnel through the rest of the junctions, most of the time, the charge state in the array is the necessary to allow the flow of charge, i.e. the charge state at threshold. In two-dimensional arrays with square lattice the potential drop reflects the charge state or charge gradient necessary to allow that one charge will be transfered from one electrode to the other in each row, see Fig. 5.16 (a).

For intermediate voltages the average potential drop shows almost periodic oscillations when it is represented at the junctions as a function of the positions in a row, in the same way that in one-dimensional case (subsection 3.3.2). Remember that the oscillations in the voltage drop indicate oscillations in the charge density. The number of oscillations changes at the values of voltages, at which the I-V curve shows the steps in the Coulomb staircase regime. For voltages in a same step the number of maxima/minima does not change. While, from one step to the next one, the number of oscillations increases. The change in the number of oscillations is associated with the entrance of new charges in the array. In two-dimensional symmetrically biased arrays they increase in pairs in each row, see Fig. 5.16 (c). As we saw in the one-dimensional case, for this type of arrays ($\alpha = 0.5$) there is an even-odd effect. For arrays with odd number of islands in the minimun conducting path, that in this case is a row, at the center of the array the average potential drop always shows a minimun, while in the case of rows with even number of islands there is a maximun.

In the high-voltage linear regime, in two as in one-dimensional arrays the average potential drop at the horizontal junctions in a row is homogeneous only once the excitonic energy is substracted. This is because the values of the excitonic energy of the contact and bulk junctions are different. For two-dimensional arrays the analytic calculation of the average potential drop in each row is obtained in a similar way as Eq. (3.10) and it is given by

$$\bar{\Phi}_i = E_i^{e-h} + \frac{R_T}{R_{sum,i}} \left(V - V_{offset} \right) \tag{5.11}$$

with $R_{sum,i}$ the sum in series of the junction resistances in row i. This equation is valid for homogeneous resistances, and as we can see in Fig. 5.16 (b) it gives a good aproximation of

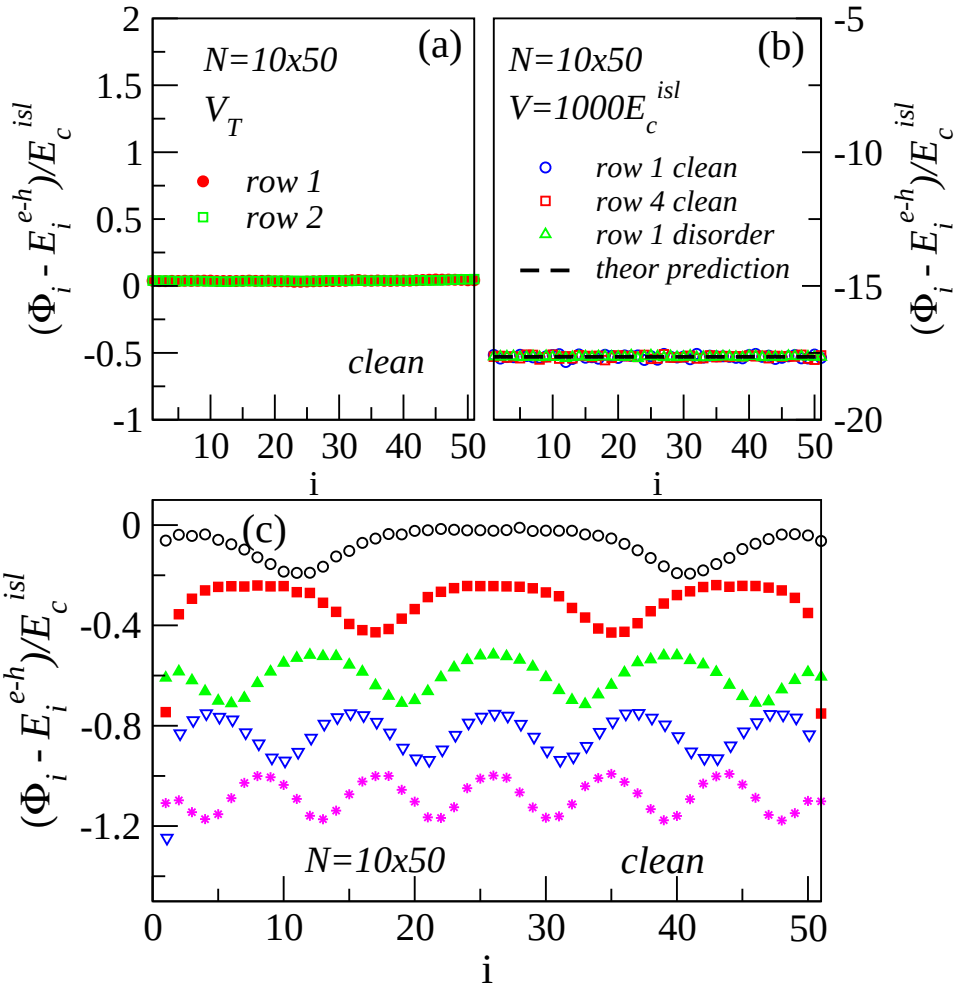

Figure 5.16: Average potential drop at the junctions as a function of the position for a clean array $N = 10x50$ with square lattice and the excitonic energy substrated. (a) at the threshold voltage for two different rows. (b) At high voltages ($V = 1000E_c^{isl}$), for two rows in the clean array, one row in a charge disordered array and the theoretical prediction.(c) At several values of the bias voltage, for which the current shows the Coulomb staircase regime, see Fig. 5.17 (a). From top to bottom $V = 104, 106, 108, 110, 112E_c^{isl}$. Curves have been vertically displaced to avoid overlap.

the average potential drop. The case with disorder in resistances will be studied in a later subsection.

Triangular lattice

In triangular arrays with even number of columns, to transfer one charge from one electrode to the other, the charge has to change of row, see Fig. 5.3 (c). In each row the charge can enter only through one contact junction and at the other one the potential drop is zero. Thus, the potential drop through a row is similar to the case of completely asymmetric biased arrays

with $\alpha = 1$ or $\alpha = 0$ studied for 1D arrays in section 3.3, see Fig. 5.18 (a) and Fig. 3.8 (a). The potential drop reflects the charge gradient created in the row to allow the flow of charge at threshold voltage.

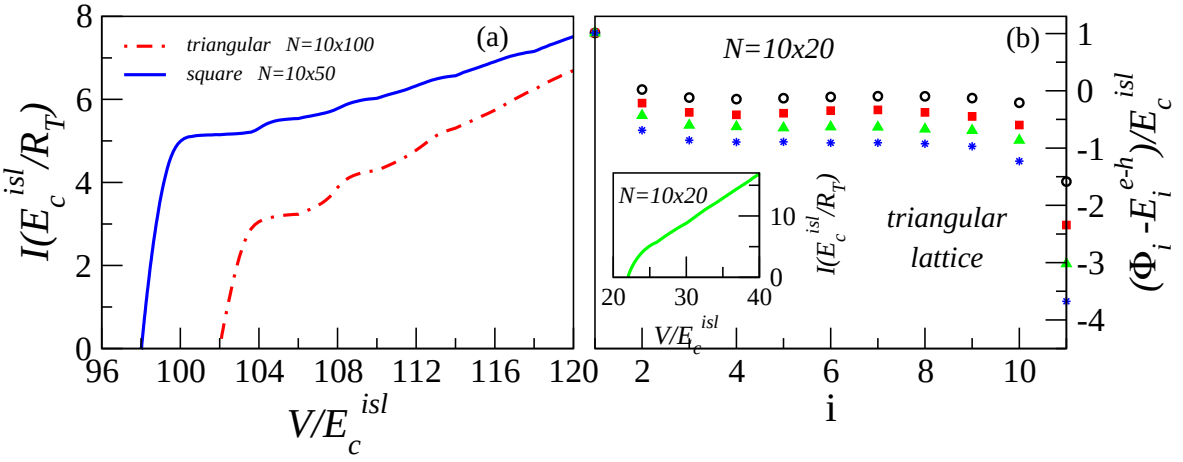

Figure 5.17: (a) $I-V$ curves for two clean arrays. One with $N = 10x50$ and square lattice and the other with $N = 10x100$ and triangular lattice. (b) Main figure: Average potential drop at the junctions as a function of the position for the third row in a clean array with $N = 10x20$ and triangular lattice at several voltages. From top to bottom $V = 24, 28, 32, 36 E_c^{isl}$. The number of islands in each row is 10. Inset: $I-V$ curve for a clean array with $N = 10x20$ and triangular lattice.

For intermediate voltages, the potential drop shows oscillations when the array is long enough. For example, in the case of N=10x20 the oscillations are very weak, see Fig. 5.17 (b), while they can clearly be seen in a clean array N=10x100, see Figs. 5.18 (b) and (c) . Unlike in the case of arrays with square lattice in which the potential drop shows oscillations in each row, for triangular lattice the potential drop at the first and last rows does not show oscillations, see Fig. 5.18 (b). Charges at these rows are not ordered because while they enter the array through the contact junctions of these rows they change row as they flow.

On the other hand, the rest of the rows show oscillations that depend on the possibility of the charges to enter/exit the array through the source or drain contact junction. For the junctions where there are maxima in an even row there are minima in an odd row and vice versa, see Fig. 5.18 (b). As in the case of a completely asymmetric biased array with $\alpha = 1, 0$ the number of maxima or minima only increases one by one from one step to the next one in the regime of the Coulomb staircase showed by the current, see Fig. 5.18 (c). This is because the charge can only enter into the array from one electrode.

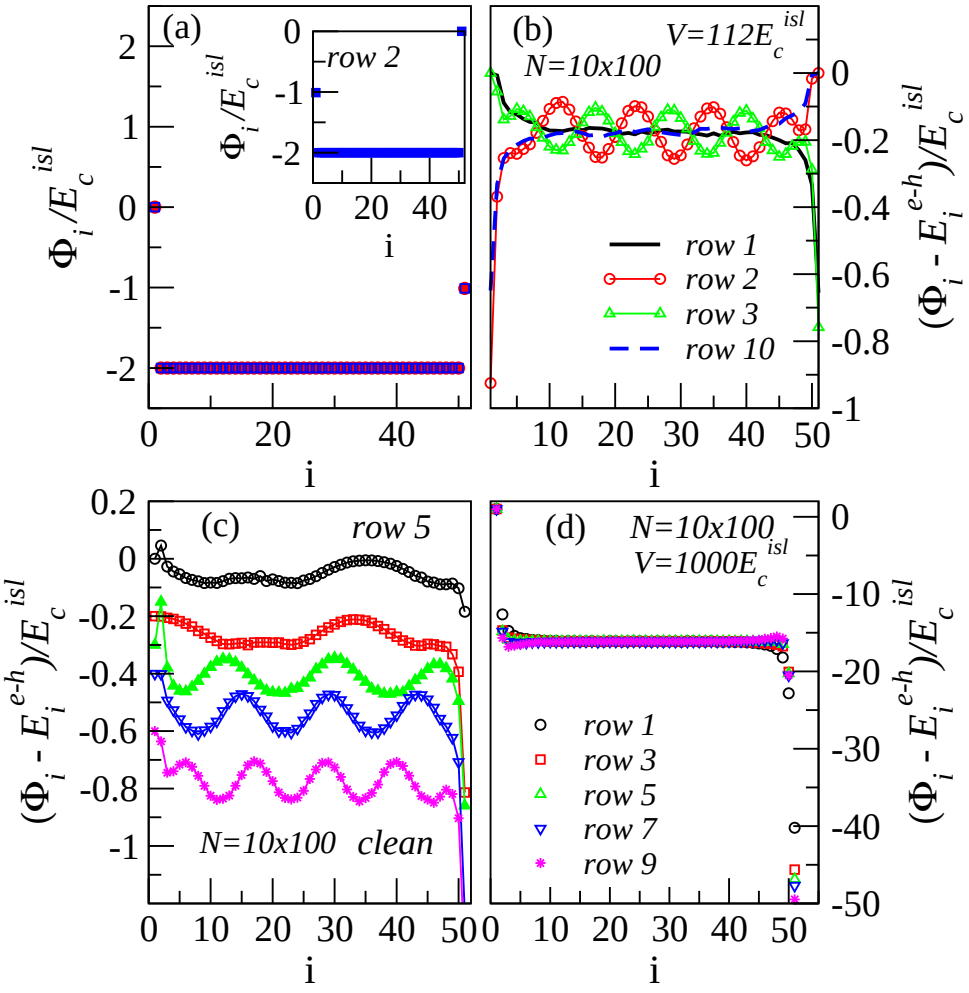

Figure 5.18: (a) Main figure: Average potential drop at the junctions as a function of the position for a clean array $N = 10x100$ with triangular lattice at V_T in two odd rows. The number of islands in each row is 50. Inset: the same for an even row. (b), (c) and (d) Average potential drop at the junctions as a function of the position for a clean array $N = 10x100$ with triangular lattice and the excitonic energy substrated. (b) At $V = 112E_c^{isl}$ for the first, the last and two bulk rows. (c) At several values of the bias voltage , for which the current shows the Coulomb staircase, see Fig. 5.17 (a). From top to bottom $V = 104, 106, 108, 110, 112E_c^{isl}$. Curves have been vertically displaced to avoid overlap. (d) For odd rows at high voltages ($V = 1000E_c^{isl}$).

At high voltages in two-dimensional arrays with triangular lattice the potential drop at the diagonal junctions is very important for the transport. Unlike in the case of square lattices in which at the vertical junctions the potential drop is very small and practically does not contribute to the transport, for triangular lattice the potential drop at the diagonal junctions is fundamental to transfer one charge from one electrode to the other. As we saw before, in this regime of voltage there are a lot of paths which can be follow by the charge what com-

plicates to make analytical predictions. However, from the study of the potential drop at the horizontal junctions in the rows we can observe that there are paths that contribute more to the current than others. Fig. 5.18 (d) shows the potential drop at the junctions as a function of the position for the odd rows in a triangular lattice with N=10x100, and as we can see, in average, larger number of charges exit out the array through certain contact junctions. For even rows we find the same behavior but in the other contact junction. Eq (5.11) is not valid for this type of lattice.

5.4.2 Charge disorder

The effect of the charge disorder in the potential drop through two-dimensional arrays is similar to that found in the one-dimensional case. At low voltages the potential drop reflects the charge state of the array at the threshold voltage. Unlike the one-dimensional case in which all the junctions with upwards steps ($\Phi_{dis} > 0$) are charged, for two-dimensional case not all the junctions with upwards steps are charged. This is a consequence of the fact that in two dimensions the charge can move in several directions and follows the energetically most favorable way.

For intermediate voltages, the charge disorder alters the charge motion and the charges cannot be periodically ordered into the array. As a result there are not oscillations in the potential drop.

In the high voltage regime, the potential drop is not affected by the presence of charge disorder in the array, and Eq (5.11) is valid in the case of square lattice, see Fig. 5.16 (b).

5.4.3 Disorder in resistances

The potential drop through the array strongly depends on the disorder in resistances. We remember that at high voltages in the one-dimensional case when one junction resistance is larger than the rest, the potential drop with the excitonic energy substracted is proportional to the resistance of the junction (section 3.3). However, in two-dimensional arrays this does not occur because if there is a large resistance the charge can meander and avoid it. Let us consider the case of square lattice with $N = 10x50$ islands in which at the middle junction in the first row there is a resistance equal to $10R_T$. Although the larger resistance is at the first row, in the neighboring rows the potential drop is also affected by this resistance, see Fig. 5.19 where the average potential drop is represented at the junctions with the excitonic energy substracted in this array for several rows. Only in rows far enough from this resistance, the potential drop is independent of it. This is the case of the tenth row represented in the left inset in Fig. 5.19 with the theoretical prediction Eq (5.11). However, in the row with

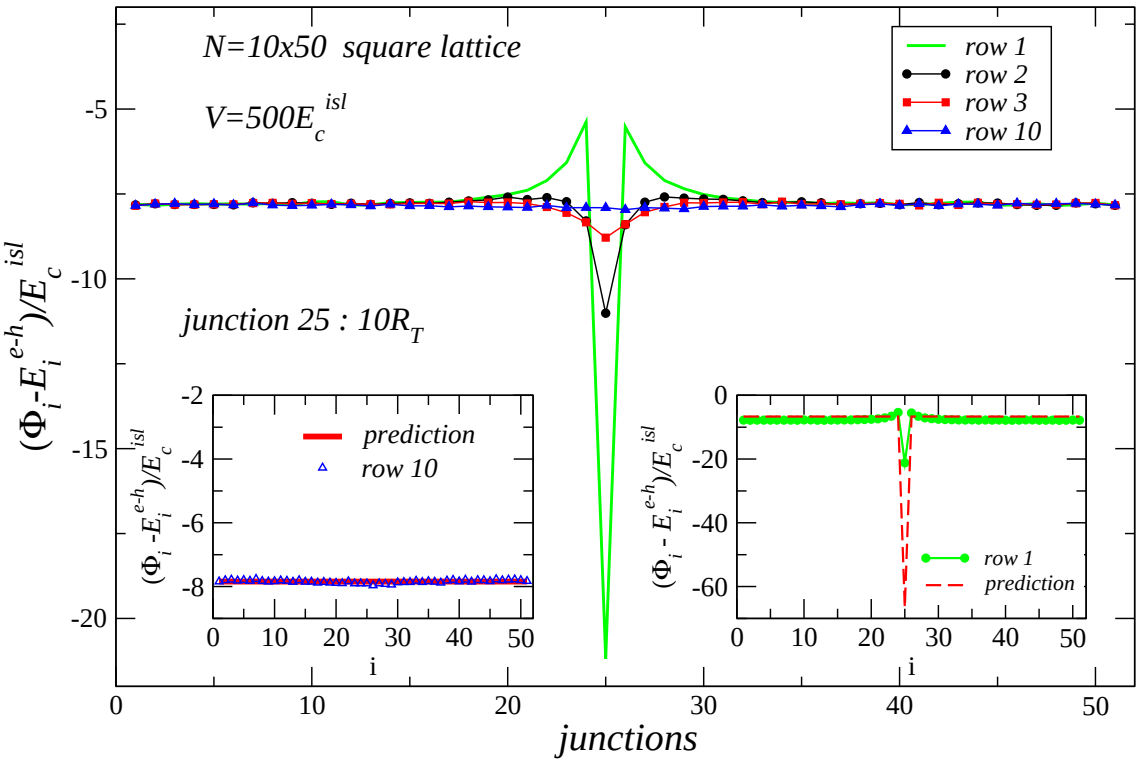

Figure 5.19: Main figure: Average potential drop with the excitonic energy substrated at the junctions as a function of the position for a clean array with $N = 10x50$ nanoparticles and square lattice with the junction 25 in the first row ten times larger than the rest. The potential drop is represented by rows. Insets: average potential drop for the first and tenth rows with the theoretical prediction.

the largest resistance and the neighboring rows this prediction is not valid, see right inset Fig. 5.19.

5.4.4 Structural disorder or Vacancies

For arrays with structural disorder, the potential drop depends on the configuration of the vacancies. In particular, at intermediate voltages, the potential drop can show oscillations depending on the localization of the vacancies.

At high voltages the potential drop shows a similar effect to the case of disorder in resistance that we have just seen. The charge meanders and avoids the vacancies in the array.

5.5 Summary

In this chapter we have analyzed the transport properties through two-dimensional nanoparticle arrays when they are placed between two metallic electrodes. And how they are affected by the geometry of the lattice and the different types of disorder such as charge disorder, disorder in resistances or structural disorder. The main differences with respect to the one-dimensional case have been also studied.

As in the one-dimensional case, in two-dimensional arrays there is a threshold voltage V_T below which the current is blocked. In the clean case the V_T depends on the length of the array, but it is independent of the number of rows. This means that V_T depends on the number of islands in the minimun path, n_{mp}, that the charge has followed to be transferred from one electrode to the other. For symmetrically biased arrays ($V_o = V/2$ and $V_{N+1} = -V/2$), $V_T = 2n_{np}E_c^{isl}$ for odd n_{mp} and $V_T = 2(n_{np} - 1)E_c^{isl}$ for even n_{mp}. The even-odd effect shown by V_T as a function of n_{mp} for this type of arrays also occurs in two dimensions. For arrays with structural disorder in which the flow of charge through the array is possible, the threshold voltage is given by the same equations. On the contrary, in charge disordered arrays V_T depends on the array configuration of disorder and can be affected by the number of rows in the array. This is due to the fact that in two-dimensional arrays the charge can meander, then if the change of row is more favorable energetically than to create a charge gradient at a upward junction, the charge will change of row.

The $I - V$ characteristic shows that there are three regimes of voltages with different behavior. Contrary to general belief used in the past two decades, for voltages close to threshold in two-dimensional arrays the current depends on $(V - V_T)$ linearly. The transport in this range of voltages is controlled by the contact junctions that act as a bottleneck, in the same way that in the one-dimensional case. The linear behavior is observed in clean and charge disordered arrays with square or triangular lattice and in presence of structural disorder or disorder in resistances. This linear dependence has been reproduced numerically at least for five orders in magnitude and has been demostrated analytically.

At intermediate voltages there is another regime, that coincides with the voltage range in which all the previous works done until now considered erroneously the one close to threshold as they did not explore small enough voltages. For not very large arrays the current shows steps, this is the called Coulomb staircase regime that depends on the parameters of the array. As we explained in section 3.2.2 the origin of the steps is that a bulk junction, in which ΔE is independent of the applied voltage, controls the transport. For large charge disordered arrays although there are steps, these are very smooth, and the current shows a superlinear behavior which resembles a power-law. However, in this thesis we have de-

mostrated that this is not a real power-law. We show that although the fittings of the $I-V$ curves to a power-law scaling curve are good, the fitting parameters depend on the range of voltages (which are in any case very small) and the values obtained for V_T are wrong.

For high voltages there is a linear behavior. This dependence in the current appears for all the arrays studied, clean, charge disordered, with disorder in resistances, or with vacancies in both square and triangular lattice. For this regime of voltages the charge does not feel the presence of the charge disorder as in the one-dimensional case. However, the $I-V$ curves depend on the structural disorder and the disorder in resistances. In two-dimensional arrays we have predicted the asymptotic $I-V$ characteristic for square lattice in the cases of clean and charge disordered arrays. The offset voltage obtained from the extrapolation of the asymptotic $I-V$ is equal to the offset in the one-dimensional case. For triangular lattice or with disorder in resistances or with voids in the array the asymptotic current cannot be calculated analytically because in these cases at the diagonal and vertical junctions the potential drops are finite and very important for the transport. As a result, the charge can follow a lot of different paths that we have not be able to determine.

In order to understand better the transport in two-dimensional nanoparticle arrays, we have studied the potential drop through the array, and how it is affected by different parameters of the array. For voltages close to threshold the potential drop reflects the charge state of the array that allows the flow of charge from one electrode to the other. In clean square lattice the potential drop at the junctions as a function of the position is the same in all the rows. On the other hand, for triangular lattice with even number of columns there is only one contact junction in each row through which the charge can enter/exit the array, and the potential drop obtained is similar to the case of completely asymmetric biased arrays ($V_o = V, V_{N+1} = 0$).

At intermediate voltages, for two-dimensional clean arrays the potential drop at the junctions shows periodic oscillations for both square and triangular lattices. These oscillations are asociated with the correlated motion of the charges. As in the one dimensional case, in presence of charge disorder or resistance disorder in the array there are no oscillations. However, the potential drop for arrays with voids can show oscillations, depending on the vacancies configurations.

In the linear regime at high voltages, unlike the one-dimensional case, for two-dimensional arrays the potential drop at the junction is only proportional to the resistance junction once the excitonic energy was substracted for homogeneous resistances. In the case in which there is one junction resistance larger than the rest the charge meanders and avoids it. As a result, the potential drop at this junction is smaller than the potential drop at a junction with the same resistance for one-dimensional arrays.

Summary of Part I

In the first part of this thesis I have studied the transport properties through one and two-dimensional metallic nanoparticle arrays between non-magnetic electrodes at zero temperature. And how these properties are affected by different parameters arrays such as the charge and resistance disorder or the way the array is biased. Two range of interactions have been considered: short and long-range. The transport is treated at the sequential tunneling level and the tunneling processes are only allowed between nearest neighbords. I study the system in the regime of classical Coulomb blockade $\delta << K_B T << E_c$.

At zero temperature, in these systems there is a threshold voltage below which the current vanishes. The threshold voltage values obtained in the different cases studied in this thesis are given by:

Short-range interactions

- One-dimensional arrays
  - Clean or with resistance disorder:
    - symetrically biased arrays: *even-odd effect*
      - $V_T = 2E_c^{isl}N$ for odd N
      - $V_T = 2E_c^{isl}(N-1)$ for even N
    - completely asymmetric biased arrays:
      - $V_T = 2E_c^{isl}(N-1)$
  - Charge disorder
    - $V_T = 2E_c^{isl}N$
- Two-dimensional arrays
  - Clean or with resistance disorder or vacancies:
    - symetrically biased arrays: *even-odd effect*
      - $V_T = 2n_{minpath}E_c^{isl}$ for odd $n_{minpath}$
      - $V_T = 2(n_{minpath}-1)E_c^{isl}$ for even $n_{minpath}$
  - Disorder:
    - depends on the charge configuration disorder

Long-range interactions

- One-dimensional arrays
  - Clean:
    - V_T is the minimun voltage which allows the creation of an electron-hole pair
  - Charge disorder:
    - two effects compete that can increase or decrease V_T with respect to the clean case:
      - *Large* d/r^{isl} : charge accumulation induced by the up-steps in the disorder potential distribution, increasing V_T
      - *Small* d/r^{isl}: disorder potential distribution can reduces the energy to create a nelectron-hole pair, decreasing V_T

In one and two-dimensional arrays, for short and long-range interaction the $I-V$ curves shows three different regimes of behavior. Two linear behaviors, one at voltages close to threshold and another at high voltages. In between these two linear regime the current increases showing Coulomb staircase profile.

At voltages very close to threshold $I \propto (V - V_T)$. This is because the junction that controls the entrance of charge into the array acts as a bottleneck junction. This linear dependence has been obtained analytically and numerically. The linear behavior occurs for clean arrays, with charge or resistance disorder and in the two-dimensional case for arrays with voids. The previous controversy on the power-law behavior close to thershold in one-dimensional arrays has been resolved. In two-dimensional arrays, contrary to the general belief the current does not show a scaling power-law behavior. This is very important because in the experimental works done, the $I-V$ curves have been interpreted in terms of a power-law, and from this power-law they obtained values of V_T, ζ and conclusions.

In one-dimensional arrays, for short-range interactions and voltages close to threshold, the slope in current is independent of the number of nanoparticles in the array, but depends on the resistance of the bottleneck junction and the bias asymmetry parameter α that indicates how the array is biased. For long-range interactions, the slope in current also depends on the number of nanoparticles in the array. For two-dimensional clean arrays and short-range interactions, the slope of current depends on the resistance of the bottleneck junction and on the number of conducting channels through the array. In the charge disordered arrays there is only one conducting channel, contrary to the general belief.

At intermediate voltages we find the Coulomb staircase regime which is a consequence of the fact that the transport is controlled by a bulk junction, which tunneling rate is independent

of voltage. At this regime the transport strongly depends on the parameters of the arrray. For short-range interactions the step width depends on α and on the presence of charge disorder in the array. In the limit of long-range interactions, the steps are smoother than in the onsite case, and the step width is not fixed.

In two-dimensional arrays for large disordered arrays if the steps are very smooth, the current looks superlinear, which resemble a power-law. This regime of voltages has been erroneously considered close to the threshold by the previous works. In this thesis it has been demostrated that this behavior is not a power-law. A similar superlinear dependence is obtained in one-dimensional arrays with charge disorder and long-range interactions.

At high voltages there is a linear dependence on the bias voltages. The current is independent of the charge disorder, but depends on the resistance disorder of the junctions. The asymptotic prediction has been done in this thesis for the one-dimensional case and for two-dimensional arrays with square lattice. The asymptotic $I - V$ curve cuts the zero current axis at the V_{offset}. This offset voltage is given by the of sum of the excitonic energies of all the junctions, $V_{offset} = \sum_{i=1}^{N+1} E_i^{e-h}$. Thus, V_{offset} depends on the range of interaction but not on the dimensionality. Slope in current is given by the inverse of the sum of the junctions resistances in serie in each conducting channel through the array. For two dimensional arrays with triangular lattice, vacancies or resitance disorder, due to the possibility of meandering the slope of the linear dependence is not given by the inverse of the sum of resistances in series.

So far, the potential drop has not been studied theoretically. For voltages close to the threshold with short-range interactions, the potential drop through the array reflects the charge gradient created through the array to allow the current flow. This occurs in both one and two-dimensional arrays. For long-range limit, the potential drop reflects the polarization potential.

At intermediate voltages, for clean arrays the potential drop at the junctions shows oscillations. The oscillations reflects the correlation of the charges. These oscillations appear in one and two-dimensional arrays with square and triangular lattice in both ranges of interactions. Charge and resistance disorder destroy the oscillations. However in two-dimensional arrays with vacancies the oscillations can appear, depending on the configuration of vacancies.

At high voltages, the potential drop at the junctions is only proportional to the value of the resistance once the excitonic energy is substracted. This occurs in the one-dimensional case. However, in two-dimensional arrays this only happens in the case of homogeneous

resistances.

Part II

Ferromagnetic Electrodes

6 Introduction to the interplay bewteen ferromagnetism and charging effects

In this chapter I will give a brief introduction to the interplay between ferromagnetism and charging effects. I will first give an overview of the works done until now. After that, I will explain our model. Finally I will study the case of a single metallic nanoparticle placed between two ferromagnetic electrodes.

6.1 Overview

A new research field appears when the spin degree of freedom is added to the conventional charge-based electronics: *Spintronics*. Due to the interplay between the charging effects and ferromagnetism, spintronics offers new applications in electronic devices. Thanks to these applications the new devices have some advantages with respect to the older devices, such as greater data storage in the hard drives, or the possibility of non-volatility, or increase the data processing speed with a lower cost in consumption. As a consequence, in the last two decades a lot of theoretical and experimental works has been done [128–133].

In a ferromagnetic material the majority of electrons have a given spin whereas the rest or the minority have the other spin. In a non-magnetic metal, the density of states for the majority and the minority of the electrons at the Fermi level are the same, $\nu_{maj}(E_F) = \nu_{min}(E_F)$. Thus, the spin polarization p, that is given by $p = (\nu_{maj} - \nu_{min})/(\nu_{maj} + \nu_{min})$, is equal to zero. However, in ferromagnetic metals, such as Ni, Fe or Co, the densities of states at the Fermi level are different $\nu_{maj}(E_F) \neq \nu_{min}(E_F)$ and $p \neq 0$, see Fig. 6.1 in which a schematic diagram of the density of states in a ferromagnet is represented. One possibility to obtain spin polarized electrons in a non-magnetic metal is to have an unpolarized current through a ferromagnetic material [134]. This means that when a ferromagnet is connected to a non-magnetic metal and a current passes through them, in the non-magnetic metal the electrons are spin polarized thanks to the ferromagnet.

In order to study the interplay of ferromagnetism and the charging effects, different systems have been sandwiched between two ferromagnetic electrodes, nanoparticles [135–138], quantum dots [139–141], molecules [142] or carbon nanotubes [143–147]. However, most of

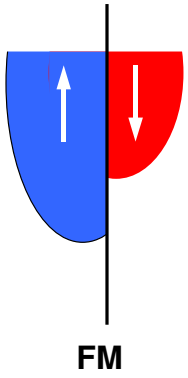

Figure 6.1: Schematic diagram of the density of states in a ferromagnet.

the works are focused on systems with a single magnetic junction, with a large magnetoresistance [148–152]. Magnetic tunneling junctions consist of two ferromagnetic conductors separated by a thin insulator. Depending on the orientation of the magnetic moment of the ferromagnets one can define two special magnetic configurations, parallel (P) and antiparallel (AP), see Fig. 6.2. When the magnetic configuration of the system varies, there is a change in the resistance of the junction, that is known as magnetoresistance. This magnetoresistance can be defined in terms of the resistance for both magnetic orientations as $MR = (R_{AP} - R_P)/R_P$. The first study on tunneling through a magnetic tunnel junction was done by Julliere in 1975 [148], showing that the resistance depends on the orientation of the magnetic moments of the electrodes. The model of Julliere is based on two assumptions. First, it is assumed that the spin of electrons is conserved in each tunneling process, thus the conductance is given by the two independent spin channels. The second assumption is that the tunneling conductance for each spin is proportional to the product of the density of states at the Fermi level of ferromagnetic electrodes. Thus, the Julliere tunnel magnetoresistance is given by

$$TMR^{Jul} = \frac{2p_1p_2}{1 - p_1p_2} \tag{6.1}$$

for the case in which each electrode has different polarization, $p_1 \neq p_2$. When the spin polarization is equal in both electrodes $TMR^{Jul} = 2p^2/(1 - p^2)$. In this model the TMR is independent of the insulator, however for magnetic tunnel junctions there are works that have studied the dependence of the magnetoresistance on the height, on width and on the material of the insulator [153]. In this thesis as in Julliere's model these dependences are neglected.At first, Julliere's work did not attract much attention because the TMR had a value of 14% at low temperature $4.2K$. The first time that the TMR was measured at room temperature was in 1991 by Miyazaki although the effect was very small 2.7%. Large values of TMR

Figure 6.2: Schematic diagram of a ferromanget/insulator/ferromagnet in both magnetic configurations, parallel and antiparallel.

at room temperature were obtained in 1995 by two different groups [151, 152]. This and the discovery of magnetoresistance in magnetic multilayers, giant magnetoresistance, [154] in 1988 not only promoted the fundamental study of these systems but also a great commercial interest. A lot of effort has been devoted to the study and fabrication of magnetic tunnel junctions with large values of TMR at room temperature [155–164].

However, the Julliere value of the TMR is not valid when there is a metallic area inserted between the ferromagnetic electrodes. In this case not only are there tunneling processes, but also the spin can flip and change its sign inside the metallic area. The TMR vanishes except if the spin flip processes are of little importance in the metal. When the spin relaxation time is long, the tunneling electrons do not change their spin inside the metal, and spin accumulation appears in the conductor in the case of antiparallel configuration [165]. The spin accumulation affects the transport through the system and consequently the TMR that is given by $(I_p - I_{ap})/I_{ap}$. In the case of one non-magnetic insertion the TMR is the half of Julliere's value because in the system there are two junctions. The TMR is reduced by increasing the number of metallic non-magnetic insertions, N, separated by tunnel barriers:

$$TMR^N = \frac{TMR^{Jul}}{2\left(N + \frac{(1-p^2)(N-1)^2}{4}\right)} \tag{6.2}$$

where all the tunnel barriers separating the metallic insertions are supposed to be equivalent [166]. The reduction of the TMR with the number of metallic regions is expected as it is only via the spin accumulation that the information about the relative magnetic orientation of the electrodes is transferred.

The spin accumulation is a non-equilibrium effect that occurs at the interfaces between materials with different spin polarization. The first system in which the spin accumulation was measured consisted in a ferromagnetic (FM)/non-magnetic (NM) metallic interface and it was done by Johnson and Silsbee in 1985 [165]. In this system, because there is a finite spin polarization in the ferromagnetic layer, the number of electrons with spin up/down in the ferromagnetic layer is different to the number of electrons with spin up/down in the non-magnetic one. In order to compensate this difference the spins are accumulated at the interface between the two layers. The first measurement of spin accumulation at room temperature was done by Jedema et al [167]. The spin accumulation will be very important in the transport properties through these systems.

In the case in which there are metallic insertions between two ferromangetic electrodes, when the size of these insertions is very small, the charging effects are relevant and new phenomena appear in the current [30] and in the magnetoresistance [170]. So far, the study of the interplay between the charging effects of the nanoparticles and the ferromagnetism of the electrodes has been restricted to the cases of one [135, 167, 168, 171–188] and two nanoparticles [169, 189, 190]. Most of the works done have focused in the case of a single nanoparticle. There are different studies where the island between the ferromagnetic electrodes is non-magnetic [172, 174–177, 181, 183] or ferromagnetic [171, 180, 183, 185]. The case in which the island and one electrode are ferromagnetic whereas the other electrode is non-magnetic has also been studied [135, 168, 183]. These works have analyzed the spin accumulation and its effect in the transport properties through the island. For equal spin polarization in both electrodes, spin accumulation only appears for the AP orientation. However, in the case of polarization asymmetry, in which each electrode has different spin polarization, there is spin accumulation in both P and AP configurations [172, 177, 183]. The current flow depends on the magnetic configuration. Due to the charging effects, a finite polarization of the electrodes can induce regions of negative differential conductance as can be observed in Fig. 6.3 (a) where the $I - V$ curves are represented for a single nanoparticle in the limit of long spin relaxation time for both magnetic configurations [168]. The $I - V$ curves in P and AP orientations are very different, leading to oscillations and changes of sign in the TMR, depending on specific set-up, see bottom in Fig. 6.3 (a) that shows the TMR corresponding to the $I - V$ curves represented in the top of the same figure. The oscillations and the changes of sign in the TMR have been clearly observed in experimental works, see Fig. 6.3 (b). For the case of two nanoparticles, three different cases have been studied. The first corresponds to the case in which the two islands and the electrodes are ferromagnetic [189]. In the second case, both islands and one electrode are ferromagnetic while the other one is non-magnetic [169]. And in the third there are two non-magnetic islands placed between two ferromagnetic electrodes [190]. In this last case for equal spin polarization in both electrodes contrary to the

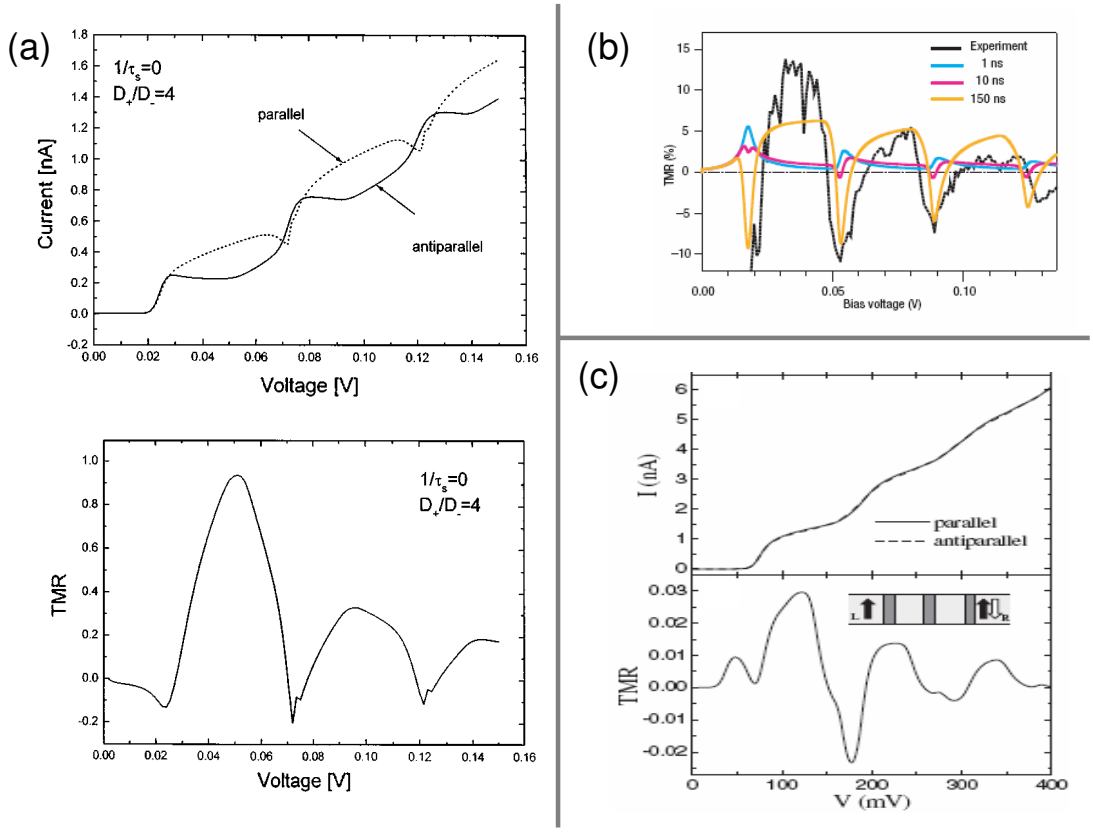

Figure 6.3: (a) Top: $I-V$ curves for parallel and antiparallel configurations in the limit of infinite spin relaxation time for the case of a single nanoparticle, from Barnaś and Fert [168]. D_+/D_- is the spin asymmetry in the density of electron states D_σ at the Fermi level on the island. Bottom: TMR as a function of the voltage from [168]. (b) TMR as a function of the voltage for a single nanoparticle for different values of the spin-relaxation time from Yakushiji et al [135] (c) Top: $I-V$ curves in the P and AP orientations for array with $N=2$ non-magnetic islands from Weymann and Barnaś [169]. Bottom: resulting TMR as a function of the voltage.

case of a single nanoparticle, there is spin accumulation in both P and AP configurations when the spin relaxation time is long. Spin accumulation is equal in both islands for AP orientation, whereas for P configuration it has opposite sign in each island. The oscillations and the change of sign in the TMR also appears in the case of two islands see bottom in Fig. 6.3 (c), in which the TMR as a function of the voltage is represented for the case of two non-magnetic islands between ferromagnetic electrodes. The $I-V$ curves for both magnetic configurations are represented on top in Fig. 6.3 (c). However, the effects due to the interplay between ferromagnetism and charging effects in one and two nanoparticles are very small compared to the results obtained in this thesis in the case of arrays with $N \geq 3$ nanoparticles,

that we will see in chapters 7 and 8. In the last section of this chapter I will describe in detail the case of a single nanoparticle.

Besides the spin accumulation and the magnetoresistance, the spin current and the spin polarization of the current have been studied in several works [165, 191–194]. The spin current is the difference between the current flows of each spin, $I_{up} - I_{down}$. This quantity will be finite when the current flow of electrons with a given spin is larger than the current flow for electrons with opposite spin. The spin polarization of the current is given by

$$\frac{I_{up} - I_{down}}{I} \tag{6.3}$$

6.2 Model

For the case of ferromagnetic electrodes, there are little changes in our model with respect to the model for non-magnetic electrodes explained in chapter 2. In this section we will see these changes in the one-dimensional case, because as we saw in chapter 2 the model is the same for two-dimensional arrays.

The system under study consists of an array of N metallic nanoparticles placed between two ferromagnetic electrodes with spin polarization p. All the conductors are separated by high tunneling barriers with a resistance much larger than the quantum of resistance. We consider the classical Coulomb blockade, $\delta \ll K_B T < E_c^{isl}$. Unlike in the case of non-magnetic electrodes in which we assume that $\delta = 0$, here δ is kept finite in order to allow the spin accumulation in the islands. The value of δ does not influence the $I - V$ curves and spin accumulation values if the following condition is met $\delta << K_B T$. δ only affects the number of electrons with spin σ, $N_{i\sigma}$, which absolute value goes like $\sim 1/\delta$ and the time needed to reach the steady state as we will see in subsection 6.2.4.

We consider two magnetic orientations, parallel and antiparallel, see Fig. 6.4, where the system is represented for both configurations. The densities of states of the ferromagnetic electrodes are given by

$$\nu_{maj} \sim \frac{1+p}{2} \tag{6.4}$$

$$\nu_{min} \sim \frac{1-p}{2} \tag{6.5}$$

where ν_{maj} and ν_{min} are the majority and the minority of the electrons with a given spin, respectively. In our model we introduce the ferromagnetic polarization of the electrodes via the tunneling resistance. The resistances are spin dependent. The total resistance of the junction is given by the addition of both spin resistances. At the contact junctions, between the

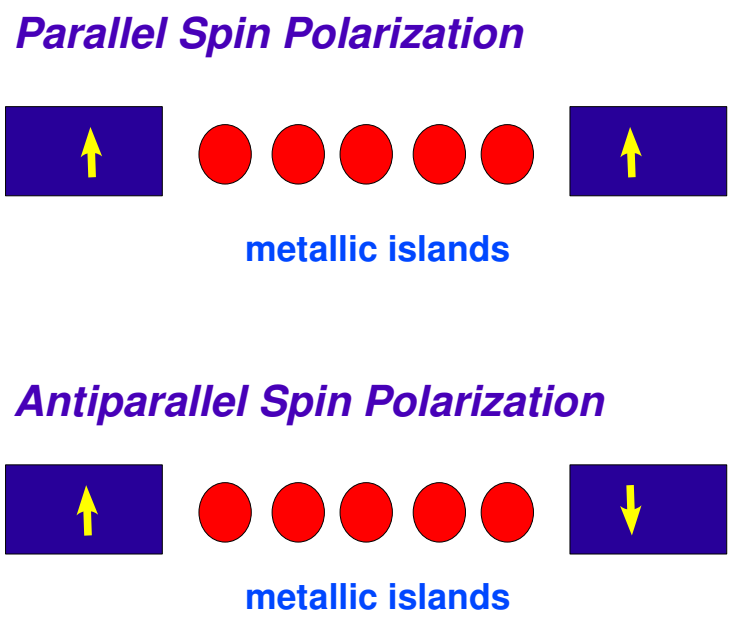

Figure 6.4: Schematic diagram of a nanoparticle array placed between two ferromangetic electrodes for both P and AP magnetic configurations.

electrode and the island, the resistance for the spin σ is equal to $2R_T(1 \pm p)^{-1}$. Plus (minor) signs are assigned to majority (minority) spin carriers. At the inner junctions R_σ is equal to $2R_T$, once the resistances of both spins are added the junction resistance of the non-magnetic case studied in the first part of the thesis is recovered, R_T.

The transport is between nearest neighbors and it is treated at the sequential tunneling level. The probability of a tunneling process is similar to the non-magnetic case, but now it depends on the spin, and it is given by

$$\Gamma_\sigma(\Delta E_\sigma) = \frac{1}{R_\sigma} \frac{\Delta E_\sigma}{exp(\Delta E_\sigma / K_B T) - 1} \tag{6.6}$$

where ΔE_σ is the change in energy of electrons with spin σ due to the tunneling process. Remember that this equation is derived assuming a continuum spectrum $\delta = 0$. For finite δ its use is justified assuming a broadening of the energy levels of order $\delta/2$.

We consider that the spin relaxation time is infinite.

Some works for the determination of the spin polarization considered different effects such

as the Magneto-Coulomb [170, 195, 196], spin-orbit effects [197], and the role of the metal insulator interface [198]. In this thesis these effects are neglected.

6.2.1 Electrostatic interactions

We have studied different ranges of interaction, the onsite limit and long range limit. In the onsite limit the interactions are restricted to the charges in the same conductor. This type of interaction is explained in detail in section (2.1.1).

For the long range limit, in which the interactions between charges in different conductors are finite, we will study an exponentially decaying interaction, typical of capacitively coupled islands. This type of long range interaction will be explained in chapter 8.

6.2.2 Potential drop: Spin Potential

As for non-magnetic electrodes, in the case of ferromagnetic electrodes to understand the transport in these systems it will be fundamental to understand the potential drop through the array. At the electrodes the potential are $\phi_0 = V_0$ and $\phi_{N+1} = V_{N+1}$. We will focus only on symmetrically biased arrays, where the potential at the electrodes is given by $\phi_0 = V/2$ and $\phi_{N+1} = -V/2$. At the islands the potential can be decomposed in four terms

$$\phi_i = \phi_i^{dis} + \phi_i^{pol} + \phi_i^{ch} + \phi_i^{\sigma} \tag{6.7}$$

ϕ_i^{dis} is the disorder potential, ϕ_i^{pol} is the polarization potential and ϕ_i^{ch} the charge potential. These potentials are present in the nanoparticles when the electrodes are non-magnetic, see section 2.2 in which the first three terms are explained in detail. Here a new potential appears at the islands because δ is finite, the spin potential ϕ_i^{σ}. In the same way that the charge potential depends on the charge state at each moment, the spin potential depends on the spin state during the simulation. There are two different spin potentials because we consider that the two possible spins of the electron are two independent reservoirs of charge [181]. These potentials are given by

$$\phi_i^{\sigma} = N_{i,\sigma}\delta \tag{6.8}$$

where δ is the level spacing, and $N_{i,\sigma}$ the number of electrons with spin σ at island i.

The spin accumulation at the islands is defined as

$$\phi_i^{\sigma} - \phi_i^{-\sigma} = (N_{i,\sigma} - N_{i,-\sigma})\delta \tag{6.9}$$

On the other hand, the charge that contributes to the ϕ_i^{ch} is determined by the total excess charge at the island $Q_i = N_{i,\sigma} + N_{i,-\sigma}$.

6.2.3 Simulation

The simulation to calculate the current is the same as the simulation used in the non-magnetic case, section (2.3). Only the number of possible tunneling processes changes. In the case of a one-dimensional array between two metallic electrodes, we saw that the number of possible processes is $2(N+1)$, corresponding to the hop to the left or to the right. However, when the leads are ferromagnetic as we distinguish between spin up and spin down, the total number of possible hopping events is the double, $4(N+1)$. For the two-dimensional case the number of possible processes is larger because the electron can move in more directions.

The simulations become increasingly costly as the temperature increases. I will focus on the study of these systems at low temperatures. For low temperatures the electrons flow in the same direction in all the relevant tunneling processes. However, when the temperature increases the electrons become frequently stacked between two islands, and computation is impossible. For this reason this computational method is appropiate for low temperatures.

6.2.4 Equilibration

It is important to note that the equilibration of the different systems does not occur for the same number of iterations N_{eq}. In particular, the system with ferromagnetic electrodes and metallic islands needs a great number of iterations to be equilibrated. Moreover, its equilibration strongly depends on the level spacing. The smaller δ the larger the number of charges necessary to equilibrate the system. For example for $\delta = 10^{-4}$ the number of charges that have to arrive at the drain electrode to equilibrate the system is $Q_{drain} \geq 10^7$, while for $\delta = 10^{-6}$ it is larger $Q_{drain} \geq 10^9$ (this implies a greater number of iterations). This situation can clearly be observed in Fig. 6.5 (a) in which the current is represented as a function of the Q_{drain} for two different values of δ. For $\delta = 10^{-4}$ the system is equilibrated for these Q_{drain} but not in the case of $\delta = 10^{-6}$. Besides, this equilibration depends on the polarization and the magnetic configuration of the electrodes. The system equilibrates before for the P orientation than for the AP one, although the charges necessary are of the same order. On the other hand, the system equilibrates faster in the case in which the electrodes are non-magnetic than when they are ferromangetic, see Figs. 6.5 (b) and (c).

6.3 One Nanoparticle

As we already saw in the first chapter (section 1.2), at zero temperature in order to add one electron unto a nanoparticle a cost in energy is necessary, the charging energy. Due to this cost in energy, the current is blocked at voltages below the threshold voltage, V_T. For $V > V_T$,

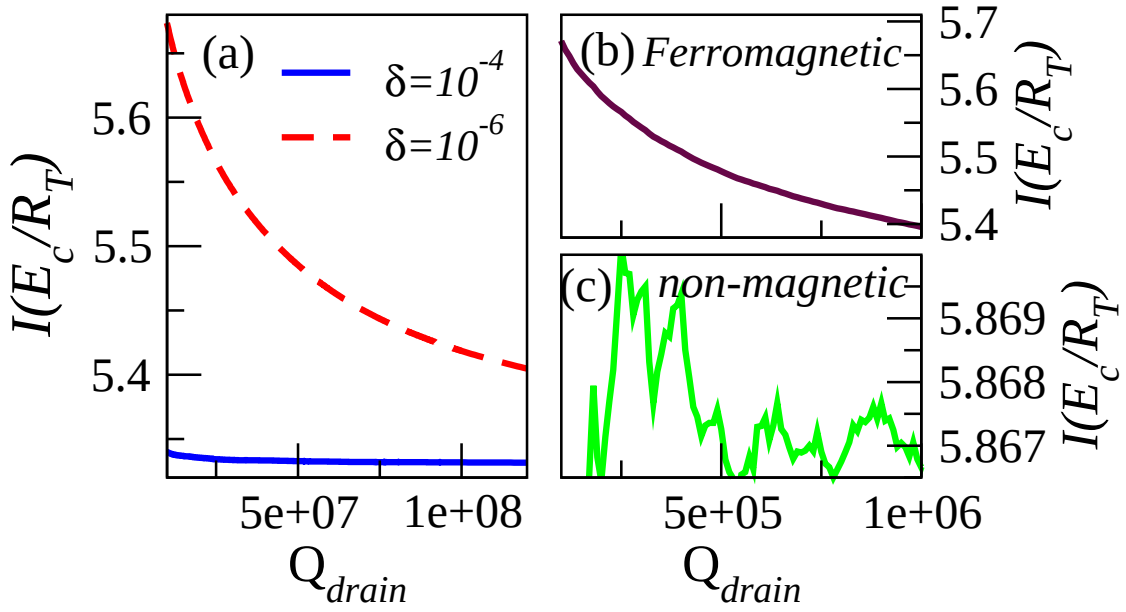

Figure 6.5: (a) Current as a function of the Q_{drain}, number of charges that arrive at the drain electrode, for $\delta = 10^{-4}$ and $\delta = 10^{-6}$ in the case of P-orientation for an array with $N = 12$ islands and $p = 0.7$. The equilibration depends on δ. At this range of Q_{drain} the system is equilibrated for $\delta = 10^{-4}$ but not for $\delta = 10^{-6}$. (b) and (c) Current as a function of the Q_{drain}, for an array with $N = 12$ islands placed between ferromagnetic electrodes (b), and non-magnetic electrodes (c). In (b) $p = 0.7$ and $\delta = 10^{-4}$ for AP-orientation.

the current is a non-linear function of the voltage. When the nanoparticle is placed between two ferromagnetic electrodes there is a finite spin polarization at the electrodes. The interplay between ferromagnetism and discrete charging controls the electronic transport through the nanoparticle. We consider the case in which the spin relaxation time is much longer than the time between successive tunneling processes and take it as infinite. This means the electrons do not change their spin inside the nanoparticle. Here we assume $R_1 = R_2$ and equal spin polarization in both electrodes. The case of different polarization in each electrode will be explained in chapter 8. We know from Eq. 6.6 that the probability of a tunneling process depends on the resistance. As a result of the spin polarization, the resistance at the contact junctions are spin dependent. This favors that electrons with a given spin have more probability to enter or exit the nanoparticle than the other electrons depending on the polarization of the electrodes. The current is strongly sensitive to the magnetic orientation of the electrodes, as we can see in Fig. 6.6 (a), in which the $I - V$ curves are represented for both magnetic configurations and for the case of non-magnetic electrodes. For P orientation the current has the same value that in the non-magnetic case. However, in the AP orientation the current is smaller than in the other cases. This is a consequence of the spin dependence of the resistances.

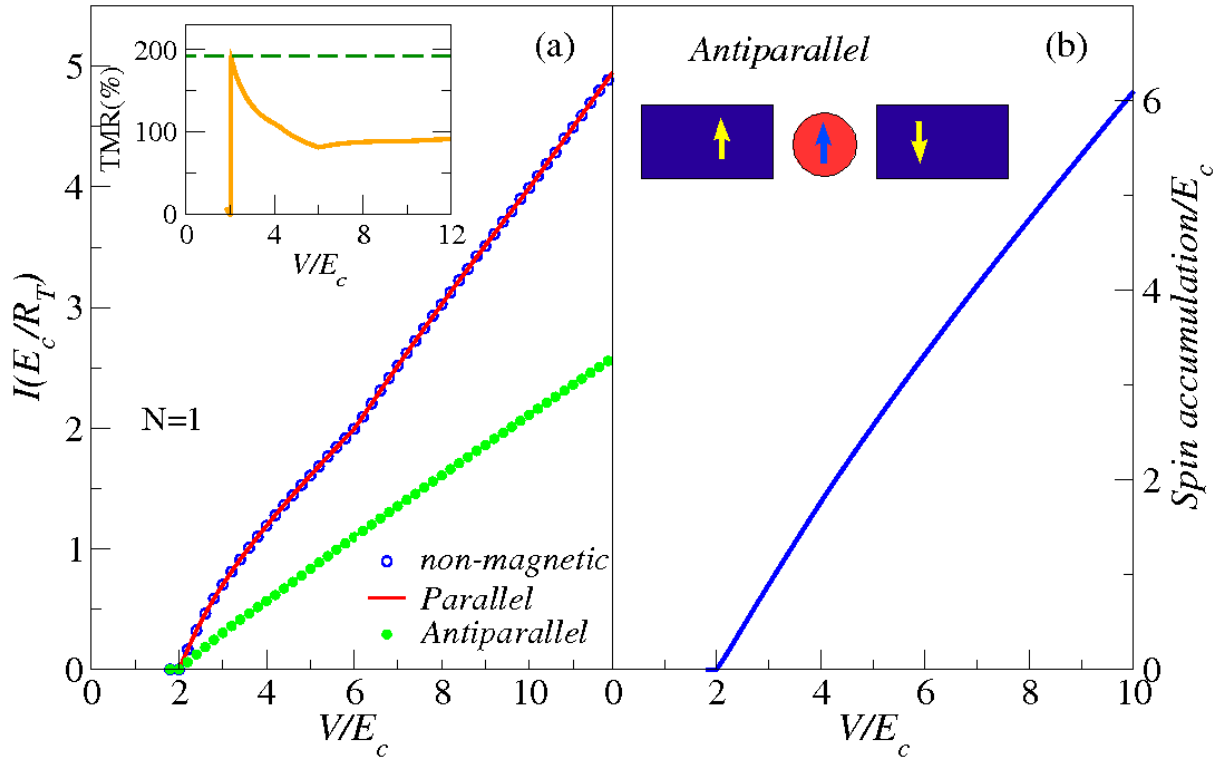

Figure 6.6: (a) Main figure: I-V curves of a single island placed in between two metallic (non-magnetic) or ferromagnetic electrodes for p = 0.7 with P and AP orientation of the electrode magnetizations. Inset in (a): the corresponding TMR is shown as a function of voltage where the Julliere's TMR is marked with a dashed line. (b) Main figure: Spin accumulation for a single island and AP arrangement. Inset in (b): Sketch of the device and the spin accumulation for AP orientation. The arrow in the island shows the spin with largest potential.

6.3.1 Parallel spin polarization

For P orientation, the majority of the electrons have the same spin in both electrodes. All the electrons that enter into the nanoparticle can exit it without being accumulated. For this reason in the P orientation there is no spin accumulation. The current is equal to the current in the case of non-magnetic electrodes. This can clearly be seen from the spin resistances. For a given spin the resistance of entrance and exit to the nanoparticle are equal if the spin polarization of both electrodes is the same, $R_{1\uparrow} = R_{2\uparrow} = 2R_T(1+p)^{-1}$ and $R_{1\downarrow} = R_{2\downarrow} = 2R_T(1-p)^{-1}$.

Spin current

In the P orientation at both contact junctions $R_\uparrow < R_\downarrow$. As the probability of a tunneling process is inversely proportional to its resistance for equal change in energy ΔE (see Eq. 6.6), more electrons with spin up than with spin down will try to enter into the island and to

leave it, see Fig. 6.7 (a). Thus, the current of spin up will be larger than with spin down $I_\uparrow > I_\downarrow$, resulting in a finite spin current ($I_\uparrow - I_\downarrow \neq 0$).

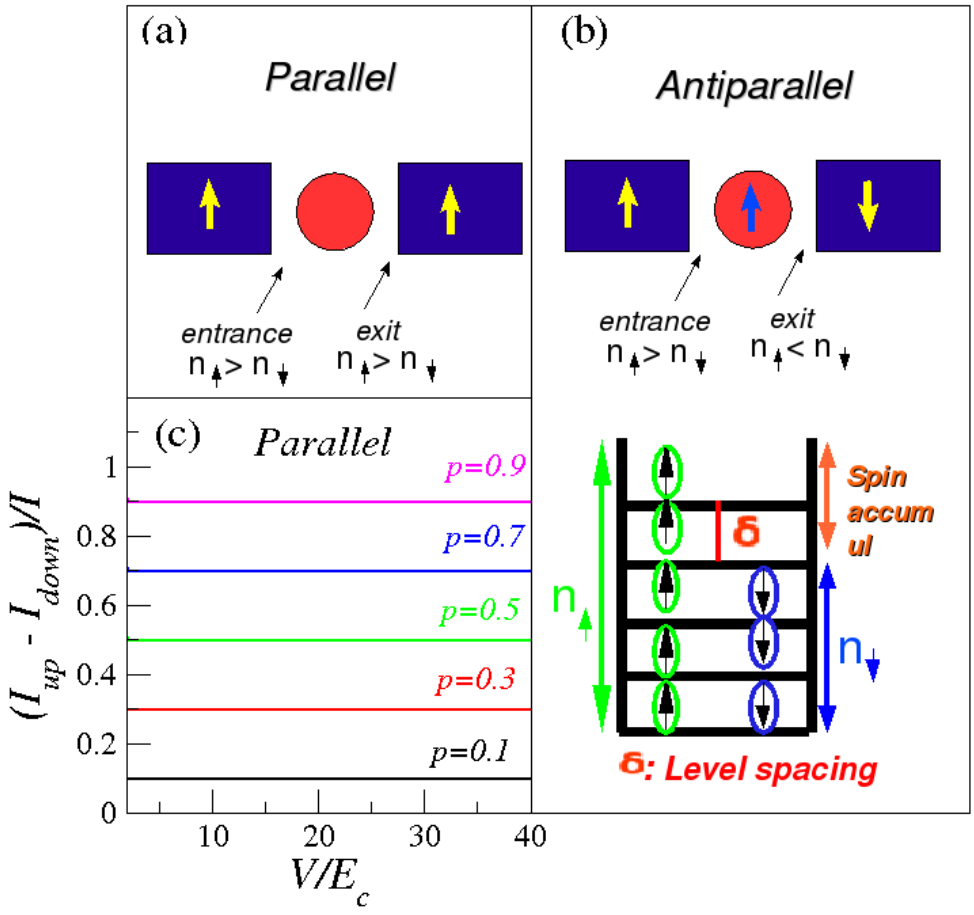

Figure 6.7: (a) Schematic diagram of a single nanoparticle placed between two ferromagnetic electrodes in the P orientation. (b) Schematic diagrams for of the system and the spin accumulation the case with AP orientation. (c) Spin polarization of the current as a function of the voltage for different values of p. The spin polarization of the current is constant and equal to p.

Spin polarization of current

For the case of one nanoparticle the spin polarization of the current is independent of voltage and equal to p, see Fig. 6.7 (c) in which the spin polarization of the current is represented as a function of the voltage for several values of polarization.

6.3.2 Antiparallel spin polarization

For AP orientation the majority of the electrons in one electrode have a given spin whereas in the other electrode the majority of the electrons have the opposite spin. Thus, the number

of electrons that will try to enter unto the nanoparticle with a given spin will be different to the number of electrons with the same spin that will try to leave the nanoparticle. As a result, the spin accumulation appears in the island to equilibrate the ratio between entrance and exit of spin up and spin down electrons. Bottom in Fig. 6.7 (b) shows a schematic diagram of the spin accumulation that is given by $(N_{i,\sigma} - N_{i,-\sigma})\delta$. Spin accumulation depends on voltage, increases monotously above V_T, see Fig. 6.6 (b).

Unlike in the parallel case, for AP orientation there is no spin current through the system because the current flow for spin up and down are equal when there is the same spin polarization in both electrodes. This is as a consequence of the fact that in AP configuration $R_{1\uparrow} = R_{2\downarrow} = 2R_T(1+p)^{-1}$ and $R_{1\downarrow} = R_{2\uparrow} = 2R_T(1-p)^{-1}$, and the symmetry of the array.

6.3.3 TMR

The inset in Fig. 6.6 (a) shows the TMR corresponding to a single nanoparticle as a function of the bias voltage V. For $V >> E_c$ charging effects are not important and the TMR equals half of the Julliere's value, as expected for a double tunnel junction. As the voltage is reduced the TMR first decreases slightly and then increases until V_T where it suddenly jumps to zero. The maximun TMR, found at threshold voltage equals Julliere's value given in Eq. 6.1.

7 Transport through metallic nanoparticle arrays placed between ferromagnetic electrodes

In this chapter I will study the spin accumulation and the transport properties through metallic nanoparticle arrays when they are placed between two ferromagnetic electrodes. I will analyze the $I-V$ characteristics in these systems, highlighting the main differences with respect to the case in which the electrodes are non-magnetic, studied in the first part of this thesis. I will also see in detail the tunnel magnetoresistance. In this chapter I will focus in the study of one and two-dimensional arrays without disorder (clean) and in the case of short-range interaction.

7.1 Introduction

As we have seen in the previous chapter, the interplay between ferromagnetism and the charging effects controls the electronic transport through a single nanoparticle placed between two ferromagnetic electrodes. Charging effects are strongly enhanced in nanoparticle arrays. Here we show that the spin accumulation has a very strong effect in the transport properties of metallic nanoparticle arrays placed in between ferromagnetic electrodes when $N \geq 3$ islands. The observed behavior is qualitatively different to the cases of one and two islands. In nanoparticle arrays when the spin relaxation time is long, spin accumulation appears not only for antiparallel orientation, as it occurs in the case of a single island, but also for parallel one of the electrodes' magnetic moments. In the last case, the threshold voltage at which current starts to flow is reduced with respect to the case of non-magnetic electrodes. There is a new regime with large oscillations in the current and negative differential resistance for voltages below V_T in the non-magnetic case, see Fig. 7.1 in which the $I-V$ characteristics are represented for a one-dimensional clean array in both magnetic configurations and for the non-magnetic case. For this range of voltages there is a huge enhancement of the differential magnetoresistance. This unexpected behavior can be understood thanks to the study of the potential drop through the array.

In this chapter we assume that the spin polarization p is equal in both electrodes. Whenever not specified the calculations reported in this chapter correspond to $p = 0.7$, $\delta = 10^{-5}$

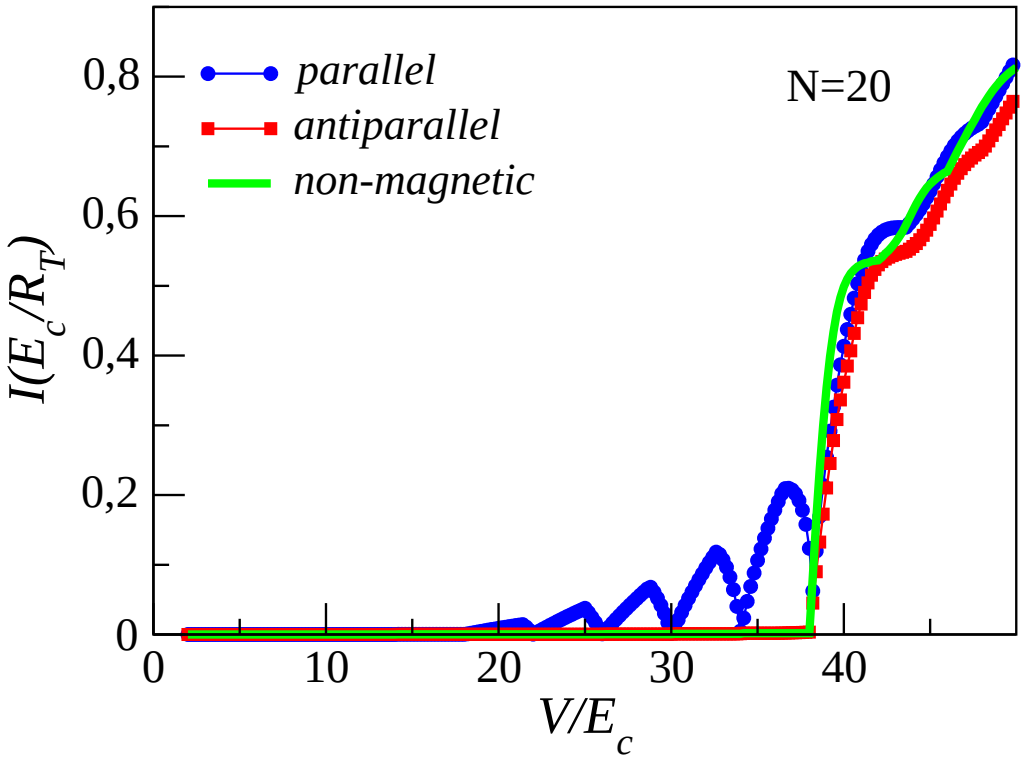

Figure 7.1: I-V curves for a clean array with N = 20 nanoparticles placed between ferromagnetic electrodes in parallel and antiparallel arrangement. $p = 0.7$, $\delta = 10^{-5}$ and $K_BT = 10^{-4}E_c$. The I-V curve corresponding to non-magnetic electrodes is plotted to serve as a reference.

and $K_BT = 10^{-4}$ in order to meet the condition $\delta << K_BT$.

We will first analyze the one-dimensional arrays when the spin relaxation time is infinite, and after that we will see the main differences in the two-dimensional case.

7.2 One-dimensional nanoparticle arrays

7.2.1 Spin accumulation

As a result of the spin accumulation at the islands, the transport through nanoparticle arrays shows different behaviors. For this reason we will start this chapter explaining the spin accumulation in both magnetic configurations.

Unlike in the case of a single nanoparticle, for nanoparticle arrays there is spin accumulation in both parallel and antiparallel orientations. However, the position dependence of the spin accumulation at the islands is very different in both cases, see figs . 7.3 (a) and (b).

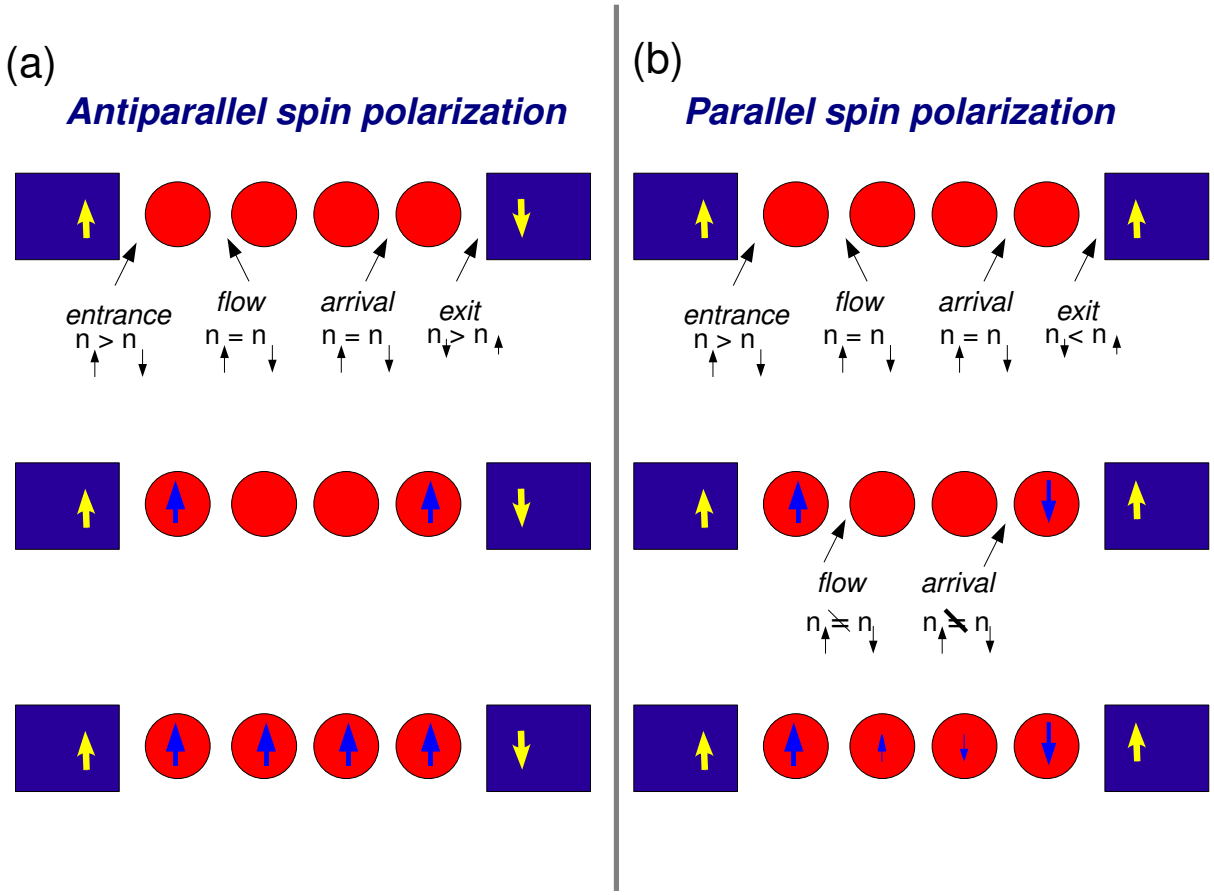

Figure 7.2: Schematic diagrams of the creation of spin accumulation in the islands in antiparallel (a) and parallel (b) orientions.

Antiparallel orientation

For AP orientation at the source junction the spin resistances are $R_\uparrow = 2R_T(1+p)^{-1}$ and $R_\downarrow = 2R_T(1-p)^{-1}$. As $R_\uparrow < R_\downarrow$ and the probability of a tunneling process is inversely proportional to its resistance, more electrons with spin up than with spin down will try to enter into the array through this contact junction. At the inner junctions as the spin resistances are equal for both spins, $R_\uparrow = R_\downarrow$, equal number of electrons can flow from the first to the second island in which there are not excess electrons, see top Fig. 7.2 (a). As a result, the spin accumulation at the first island is positive, spin up. On the contrary, through the drain junction more electrons with spin down than with spin up will try to exit the array because at this contact junction $R_\uparrow > R_\downarrow$. Equal number of electrons for each spin can reach the last island from the neighboring one. As a consequence, at the last island the spin accumulation, $(N_{i,\sigma} - N_{i,-\sigma})\delta$, is positive as it occurs in the first one, see middle in Fig. 7.2 (a). Once the spin accumulation is created at the first and last islands, the probability of the tunneling

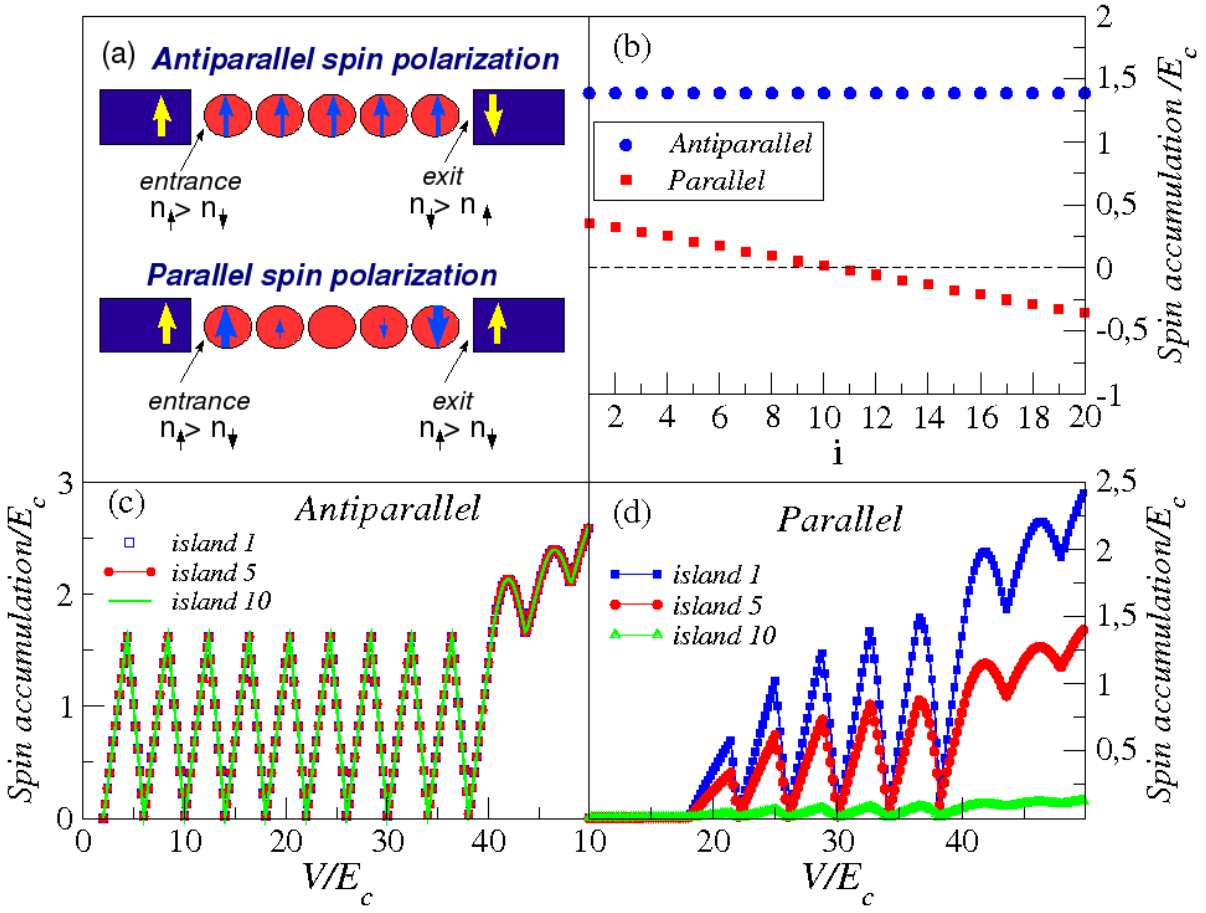

Figure 7.3: (a) Schematic diagrams of the spin accumulation in a clean array with $N = 5$ islands and antiparallel (top) and parallel (bottom) configurations. (b) Spin accumulation at the islands as a function of the position for both magnetic orientations. (c) Spin accumulation as a function of the voltage at the first, fifth and tenth islands in the antiparallel case. The spin accumulation for voltages below V_T is a consequence of the finite temperature. (d) Same that in (c) for the parallel configuration.

process for a given spin at the inner junctions depends on spin accumulation at these islands. Thus, at the rest of the islands more electrons with spin up than with spin down will try to enter into the islands while more electrons with spin down than with spin up will try to exit, leading positive spin accumulation in all the islands. Thus, for AP orientation the spin accumulation is very homogeneous through the array, i.e. it is practically equal in all the islands, see Figs. 7.3 (a) and (b). In the schematic diagram in Fig. 7.2 (a) and on top in Fig. 7.3 (a) the arrows in the islands show the spin with largest potential.

Spin accumulation strongly depends on voltage, as we can see in Fig. 7.3 (c) in which the spin accumulation is represented as a function of the voltage at the first, the fifth and the

tenth islands in a clean array with $N = 20$ islands. The dependence on voltage is equal in each island for the antiparallel case.

Parallel orientation

For P orientation, more electrons with spin up than with spin down will try to enter/exit the array. This is because $R_\uparrow < R_\downarrow$ in both contact junctions. At the first island the spin accumulation is created as in the first island in the AP configuration. However, the spin accumulation at the last island has opposite sign. This is because more electrons with spin up than with spin down exit the array, and the number of electrons with spin up that exit the array is larger than the number of electrons with spin up that reach this island from the neighboring one. As a result, the spin accumulation, $(N_{i,\sigma} - N_{i,-\sigma})\delta$, is negative, see middle in Fig. 7.2 (b) in which the arrows represent the largest potential at the two islands. The spin accumulation in the rest of the islands depends on the spin accumulation in the first and the last islands. This means that depending on the electrons accumulated in these islands, the charge and spin gradients created at the inner junctions between the first or last island and its neighboring one will favor more the tunneling processes of electrons with a given spin than with the other. Thus, the spins will be accumulated in the islands to allow the flow of electrons. In the case of P configuration, the spin accumulation changes its sign within the array, as we can see in Fig. 7.3 (b). For equal spin polarization in both electrodes the change of sign occurs at the center of the array. As we said before the value of spin accumulation at the first island is the same as in the last one but with opposite sign. This happens along the array, with the second and penultimate islands, etc. The spin accumulation depends on the position of the islands, see Fig. 7.3 (d) in which the spin accumulation is represented as a function of the voltage for three different islands in a clean array with $N = 20$ islands. As can be observed in this figure spin accumulation also depends on voltage, showing oscillations.

Unlike in the antiparallel case, for parallel orientation there is an even-odd effect in the spin accumulation. In arrays with an even number of nanoparticles there is spin accumulation in each island. However, for an odd number, there is no spin accumulation in the island placed at the center of the array, see sketch on bottom in Fig. 7.3 (a). This effect is a consequence of the symmetry polarization, i.e. equal spin polarization in both electrodes. In this case and P orientation, as the central island is placed at the same distance of both electrodes, the number of electrons for a given spin that arrive and exit the central island is the same. Thus, there is a fast passage of electrons through the central island, without being accumulated. This even-odd effect only occurs in symmetrically biased arrays with equal spin polarization in both electrodes.

7.2.2 Spin potential drop

Here we highlight the potential drop created by the spin accumulation: *spin potentials*. The spin potential drop at the islands depends on the magnetic configuration of the electrodes.

In the case of antiparallel orientation the spin-up and spin-down potentials at one island are very similar to the spin-up and spin-down in the other islands, i.e. the change in the spin potential varies very little between the islands, see Fig. 7.4 (a). Thus, the spin potential at the junctions will be very small, and in general it barely contributes to the tunneling processes.

However, for parallel configuration the spin potentials depend on the position of the island, see Fig. 7.4 (b) in which the spin-up and spin-down are represented at the islands as a function of the position. The spin potentials change their sign within the array. As the value of the spin potential is different in each island, at the inner junctions, $\Phi_{i,\sigma} = \phi_{i,\sigma} - \phi_{i-1,\sigma}$, there are finite spin potential drops which strongly contribute to the transport, as we will see in detail in the following sections.

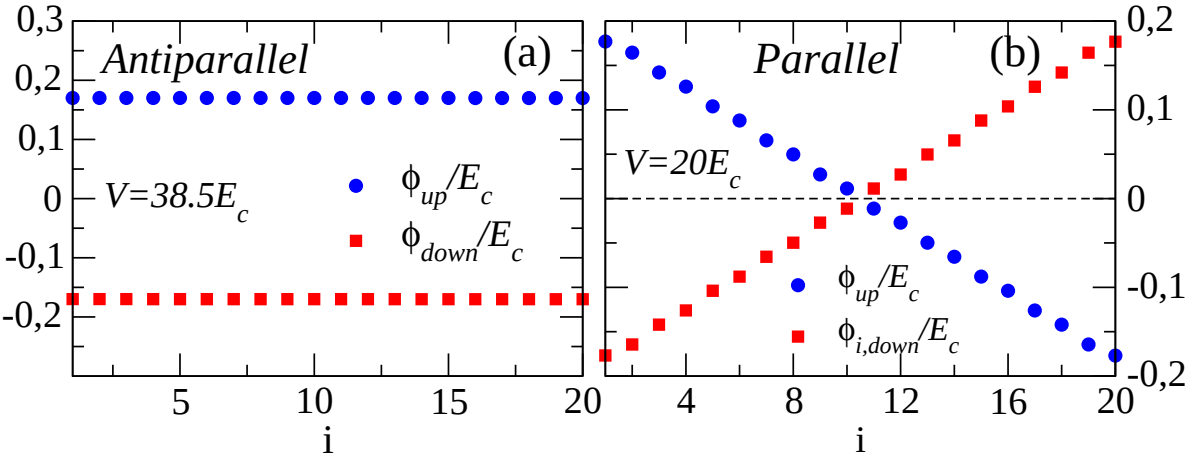

Figure 7.4: Spin potentials at the islands as function of the position for a clean array with $N = 20$ islands at $V = 38.5E_c$ and at $V = 20E_c$ corresponding to antiparallel (a) and parallel (b) orientation of the magnetization electrodes respectively.

7.2.3 Threshold Voltage

As we already know, the threshold voltage is the minimun voltage at which the current starts to flow through the array at zero temperature. In order to allow the spin accumulation at the islands we consider that δ is finite, and to ensure $\delta << K_B T$, the temperature is finite. Under these conditions there is a very small current for voltages below the true threshold. As this current is really small, the effect due to the finite temperature below threshold is neglected.

Thanks to the influence of the spin accumulation the threshold voltage is modified with respect to the case of non-magnetic electrodes.

We remind that in the case of non-magnetic electrodes for a clean array with short-range interactions the polarization potential drop is only finite at the contact junctions, while the rest of junctions prevent the flow of charge for voltages below the threshold due to the lack of potential drop, see sections 2.2 and 3.1. Thus, to allow the flow of charge through the array a charge gradient has to be created at the inner junctions. The threshold voltage is given by $V_T \sim 2NE_c^{isl}$, with N the length of the array and E_c^{isl} the charging energy.

In the same way as in the non-magnetic case, for short-range interaction in a clean array placed between ferromagnetic electrodes there is no polarization potential drop at the inner junctions. And a charge gradient has to be created at these junctions to transfer one electron from one electrode to the other. However, at the same time that the charge gradient is created within the array, the spin gradients are created too, and they can favor the current flow at smaller voltages. As we saw in the previous section, the spin potential depends on the magnetic configuration, and does not always favor the flow of charge.

Antiparallel orientation

In the antiparallel case, as the spin potentials are very homogeneous through the array, at the inner junctions potential drops are very small and barely contribute to the change in energy for the tunneling processes, see Fig. 7.4 (a). Thus, the current flow is allowed by the charge gradient as it happens in the case of non-magnetic electrodes. For this reason the threshold voltage and $I-V$ curves in the AP orientation and non-mangetic case are quite similar, see Fig. 7.1. However, sometimes very small spin gradients can be created through the array, allowing some tunneling processes which are forbidden if there is only a charge gradient through the array. As a result, the threshold voltage can slightly be modified with respect to the value found in the non-magnetic case, see Fig. 7.5 (a).

Parallel orientation

For P orientation the threshold voltage is reduced with respect to the non-magnetic case, as a result of the spin potentials through the array. Spin up (down) potential decreases (increases) producing potential drops at the junctions between the islands which oppose (favor) the current flow, see Fig. 7.4 (b). Thus, the spin charge gradient necessary to allow the flow of electrons with spin up decreases. With the reduction of the number of charges which have to be accumulated at the first or last island to allow the current flow, the threshold is reduced. This effect can be clearly observed in Fig. 7.5 (a) in which the threshold voltage of clean arrays is represented as a function of the number of islands for the cases of ferromagnetic

and non-magnetic electrodes.

The threshold voltage depends on the spin polarization p, increasing with the decrease of p, see Fig. 7.5 (b). This is because the spin up potential created within the array favors the flow of electrons with spin up, however the spin down potential prevents the flow of electrons with spin down. The flow of spin-down electrons is allowed via the charge potential left by the spin-up ones. The threshold voltage is determined by the charge gradient created to transfer spin-up electrons from one electrode to the other. Thus, the larger p, the larger the number of electrons with spin up and smaller the electrons with spin down that will enter/exit the array. As a consequence, the charge gradient will be created with less charges accumulated and the current will start to flow at smaller voltages.

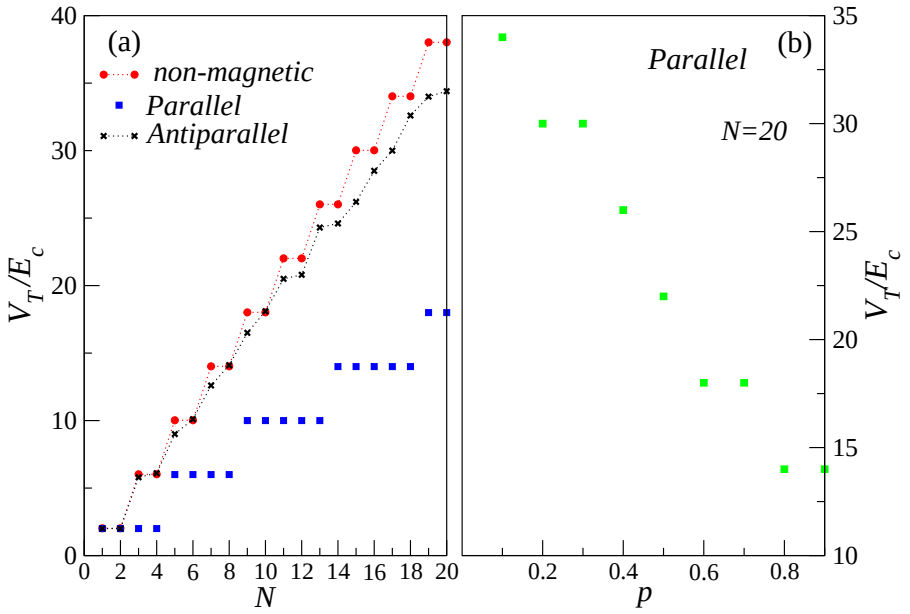

Figure 7.5: (a) Threshold voltage of clean arrays as a function of the number of islands N for the P and AP orientations with $p = 0.7$ and non-magnetic case. (b) Threshold as a function of the spin polarization p for a clean array with $N = 20$ islands for parallel orientation.

7.2.4 Regime with negative differential conductance in the parallel orientation

The most interesting regime in the current appears in P magnetic orientation at voltages smaller than the threshold obtained in the case of non-magnetic electrodes, see Fig. 7.6 (a). There is current at these voltages thanks to the potential gradient created by the spin accumulation. The current shows large oscillations, in which there are ranges of voltages where the current decreases when the voltage increases, corresponding to negative differential con-

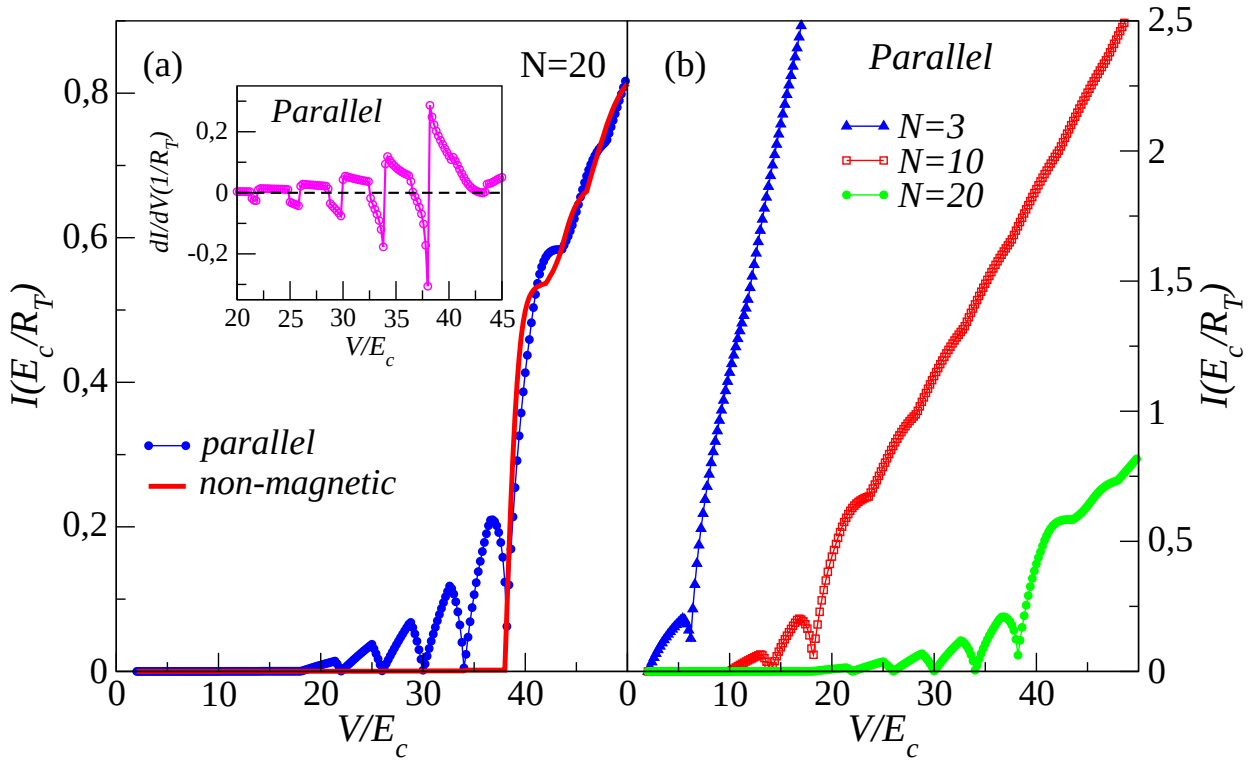

Figure 7.6: (a) Main figure: I-V curves for an N = 20 array with ferromagnetic electrodes in parallel arrangement. The I-V curve corresponding to nonmagnetic electrodes is plotted to serve as a reference. Inset: Differential conductance corresponding to N = 20 and parallel arrangement. (b) I-V curves for arrays of different sizes and parallel orientation of the electrode magnetizations. The number of peaks in the I-V curve increases with the size of the array.

ductance, see the inset of Fig. 7.6 (a). The negative differential conductance that we have obtained for arrays with $N \geq 3$ islands is much larger than the values found in the case of a single nanoparticle [135, 168], see Fig. 6.3. The number of peaks in the current depends on the number of islands. The larger the number of islands the larger the number of peaks, see Fig. 7.6 (b).

This oscillating behavior is a consequence of the potential drop at the inner junctions. The potential gradients created through the array can favor or prevent the tunneling processes for a given spin. In Fig. 7.4 (b) it can clearly be observed that for P orientation, the spin up potential favors the tunneling processes of electrons with spin up, while the spin down potential prevents the processes with spin down. However the spin polarization of the current is not completely spin polarized, see Fig. 7.7 (b). This means that there is a flow of spin-down and spin-up electrons in the system. The flow of spin-down electrons is mediated by the charge gradient created through the array by the passage of spin-up electrons. Once this

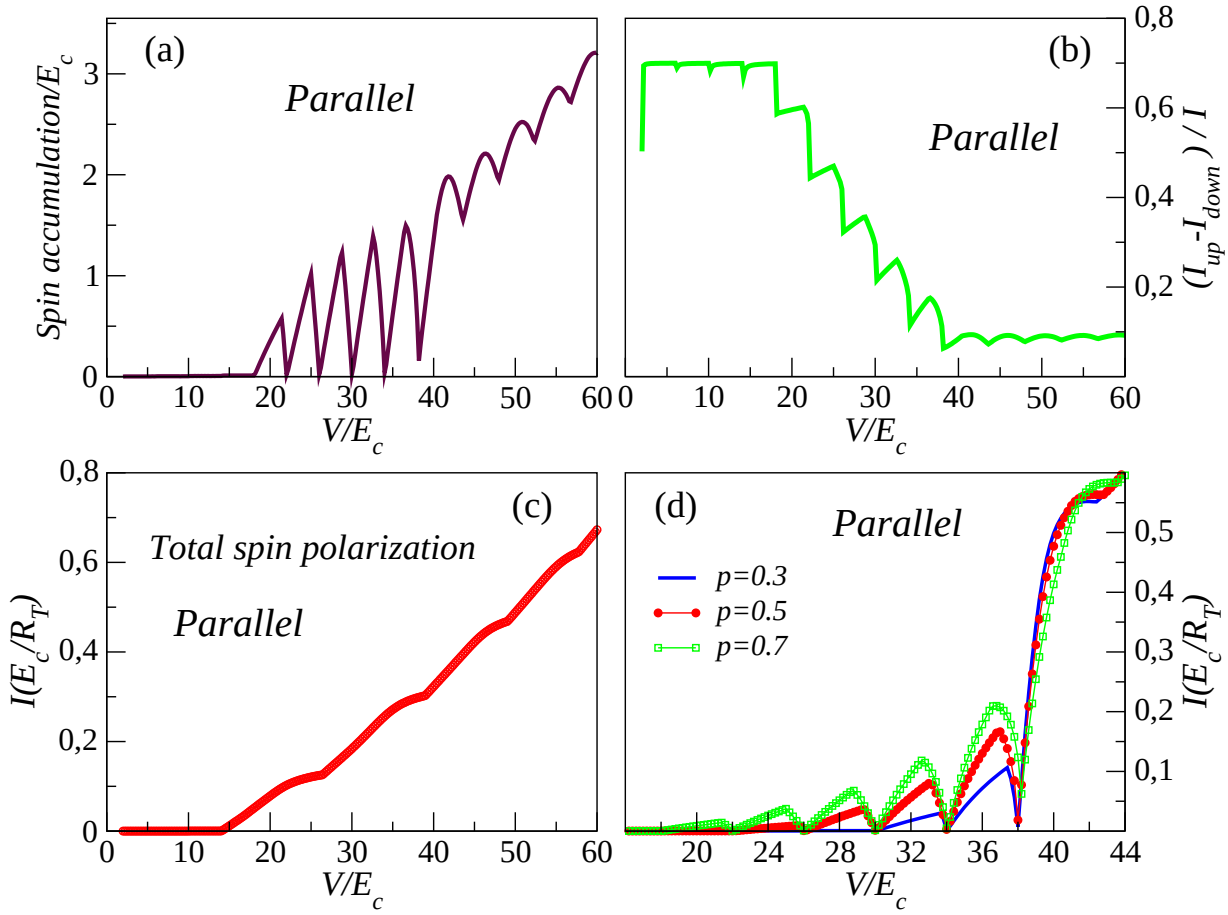

Figure 7.7: (a) Spin accumulation as a function of the voltage in the first island of a clean array with $N = 20$ islands and $p = 0.7$ in the paralell orientation. (b) Spin polarization of the current as a function of the voltage for the same array used in (a). (c) $I - V$ curves for the same array but with total spin polarization $p = 1$ in the parallel orientation and for the case with non-magnetic electrodes. (d) $I - V$ curves for a clean array with $N = 20$ islands for several values of p in the parallel case.

charge gradient is created, the tunneling processes for electrons with spin up and down are possible. When the entrance of charge into the array costs less energy for electrons with spin-down than with spin-up thanks to the voltage drop, a new conduction channel is opened for spin-down electrons and closed for spin-up ones. When this new channel for spin-down electrons is opened, the charges that were accumulated can flow and the spin accumulation decreases, leading to the decrease of current with the increase of voltage. Once the conducting channel is also opened for spin-up electrons, the spin accumulation increases again. The opening of new conducting channels for a given spin is the origin of the oscillations in the spin accumulation and as a result in the current. As we can see in Fig. 7.6 (a) and Figs. 7.7 (a) and (b), the spin accumulation, the current and the spin polarization of the current are

correlated, the oscillations appear in the three cases at the same voltages.

If the tunneling processes are only allowed for electrons with a given spin, this regime with negative differential conductance dissapears. This occurs when the spin polarization of the electrodes is total, $p = 1$, as we can see in Fig. 7.7 (c) in which the $I - V$ curve is represented for a clean array with $N = 20$ islands in the case of parallel orientation with $p = 1$. One example of materials with total spin polarization are the half metals [199], which are often used in experiments because they are very good spin injectors and detectors.

The number of peaks or oscillations in the current not only depends on the number of islands in the array, but also depends on the spin polarization p, see Fig. 7.7 (d). The larger p the larger number of peaks.

7.2.5 Linear dependence at High Voltages

At high voltages there is a linear dependence in both magnetic configurations, as it occurs in the non-magnetic case, see Fig. 7.8 (a) and (b). At these voltages the different gradients created through the array ensure that all the tunneling processes to the right for spin-up and spin-down electrons will be possible as a result of the decrease in energy in these processes. The current is given by the addition of the spin-up and spin-down current, $I = I_\uparrow + I_\downarrow$. Thus, the average current at high voltages is given by

$$I_{asympt} \sim (\frac{1}{R_{sum\uparrow}} + \frac{1}{R_{sum\downarrow}}) \left(V - \sum_{i=1}^{N+1} E_i^{e-h} \right) \tag{7.1}$$

with $R_{sum\uparrow} = \sum_{i=1}^{N+1} R_{i\uparrow}$, and $R_{sum\downarrow} = \sum_{i=1}^{N+1} R_{i\downarrow}$, the addition in series of all the junction resistances for a given spin. $R_{sum\uparrow}$ and $R_{sum\downarrow}$ depend on the magnetic configuration of the electrodes. For parallel orientation $R_{sum,\sigma} = \frac{4}{1\pm P} + 2(N-1)$, where plus (minor) sign corresponds to spin-up (spin-down). For the antiparallel case the addition of the resistances for each spin is equal, $R_{sum,\sigma} = \frac{4}{1-P^2} + 2(N-1)$. Thus, the asymptotic $I - V$ curves are given by

$$I_{asympt}^{P} \sim \frac{2 + (N-1)(1-p^2)}{4 + 4(N-1) + (1-p^2)(N-1)^2} \left(V - \sum_{i=1}^{N+1} E_i^{e-h} \right) \tag{7.2}$$

$$I_{asympt}^{AP} \sim \frac{1-p^2}{2 + (1-p^2)(N-1)} \left(V - \sum_{i=1}^{N+1} E_i^{e-h} \right) \tag{7.3}$$

These analytical predictions (7.2) and (7.3) for parallel and antiparallel orientation respectively, are compared with the numerical results in Fig. 7.8 (a) and (b), and as we can see

there is a good agreement between them. The slope of current, that is the addition of $R_{sum\uparrow}$ and $R_{sum\downarrow}$ in parallel, depends on the spin polarization and on the number of islands.

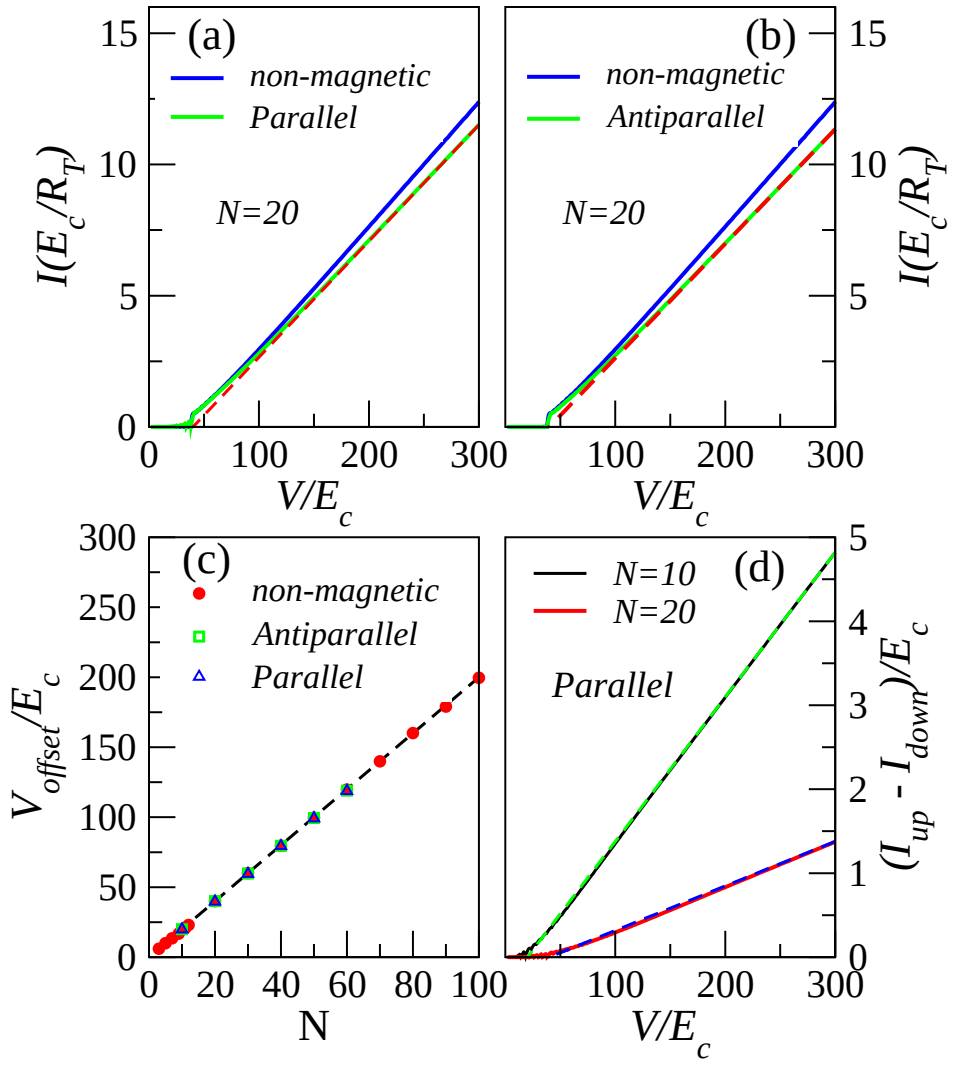

Figure 7.8: (a) and (b) $I-V$ curves at high voltages for a clean array with $N = 20$ and $p = 0.7$ for parallel and antiparallel orientations, respectively. The theoretical prediction (dashed lines) and the non-magnetic case are included for comparison. (c) V_{offset} as a function of the number of islands, for the non-magnetic case, the parallel and antiparallel orientations. The analytical prediction is included (dashed line). (d) Spin current as a function of voltage (solid lines) for two clean arrays with $N = 10$ and $N = 20$ islands, $p = 0.7$. Their theoretical asymtotic predictions are included (dashed lines).

The asymptotic I-V curve cuts the zero current axis at a finite offset voltage $V_{offset} = \sum_{i=1}^{N+1} E_i^{e-h}$. This voltage is independent of the magnetic orientation and equal to the V_{offset}

in the case of non-magnetic electrodes, see Fig. 7.8 (c) in which the V_{offset} is represented as a function of the number of islands for both magnetic configurations and the non-magnetic case. This is due to the fact that the V_{offset} only depends on the excitonic energy, which is equal in both systems.

As in the case of a single nanoparticle there is only spin current in the parallel configuration. For the antiparallel case there is no spin current. This is because $R_{sum,\sigma}$ is equal for both spines. The average spin current for the parallel orientation is given by

$$(I_\uparrow - I_\downarrow)_{asympt} \sim \frac{2p}{4+4(N-1)+(1-p^2)(N-1)^2}\left(V - \sum_{i=1}^{N+1} E_i^{e-h}\right) \tag{7.4}$$

As for the total current, the slope depends on the spin polarization and on the length of the array. Fig. 7.8 (d) shows the spin current as a function of the voltage for two arrays with different size.

At high voltages the spin polarization of the current saturates to

$$\frac{2p}{2+(N-1)(1-p^2)} \tag{7.5}$$

For $N = 1$ the value of saturation is equal to p, as we already saw in section 6.3. In a general case, the value at which the spin polarization of current satures depends on N and p.

7.2.6 TMR

The most interesting region in the TMR appears the regime of voltages with negative differential conductance in the parallel orientation. In this regime we find the largest differences in the current depending on the magnetic configuration. The TMR depends strongly on voltage, showing the same peaks characteristic of the current in the parallel orientation, see Fig. 7.9 in which the TMR is represented as a function of the voltage for arrays with different size.

However, the most amazing results are the extremely large values obtained for the TMR. There is a huge enhancement of the tunnel magnetoresistance in nanoparticle arrays with respect to the case of a single nanoparticle. They are more than two orders of magnitude larger in arrays with $N \geq 3$ islands than in the case of a single nanoparticle, see the inset in Fig. 7.9. The largest value of the magnetoresistance is for a clean array with $N = 3$ islands. These large values originate in the almost zero current found for AP orientation at these voltages.

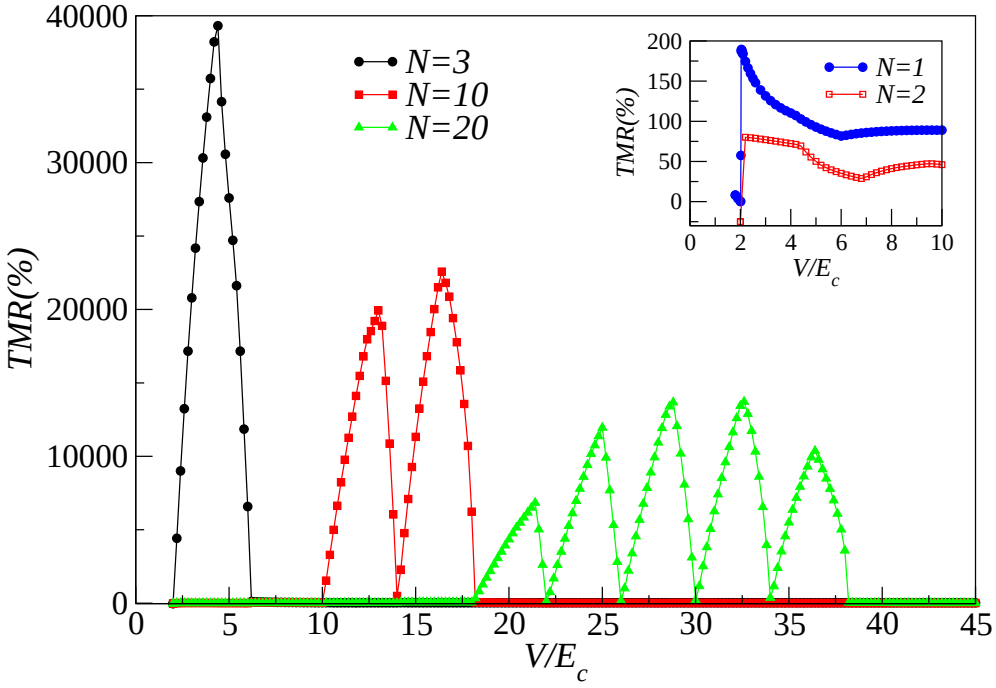

Figure 7.9: Tunneling magnetoresistance as a funtion of bias voltage. Main figure: for different array sizes. Inset: for a single nanoparticle.

For arrays with $N = 2$ nanoparticles, the value of the TMR is even smaller than the TMR of a single nanoparticle, see inset in Fig. 7.9. The behavior in this array is different to the behavior in arrays with more than two islands. This is due to the fact that in arrays with more than two islands in the parallel orientation the new regime which appears at smaller voltages than the metallic threshold voltage is a consequence of the spin accumulation. This means that if there is no spin accumulation in the array, there is no current at these voltages. However, as we explained in section 3.1 for the case of two islands when the array is symmetrically biased, there is current through the array once a charge enters into the array and a hole exits, and it occurs without spin accumulation. Thus, in a clean $N = 2$ array the threshold voltage is equal for both magnetic configurations, and the $I - V$ curves are of the same order leading a value of TMR small if we compare with the TMR in arrays with more than two islands.

On the other hand, as in the parallel orientation the number of peaks in the current depends on the spin polarization, the peaks in TMR are determined by p. At high voltages, the value of TMR in the absence of charging effects (Eq.6.2) is recovered. The TMR depends on the number of islands N and the spin polarization.

7.3 Two-dimensional nanoparticle arrays

The case of two-dimensional nanoparticle arrays has been studied in order to know how the interplay between ferromagnetism and charging effects is affected by the dimensionality of the array. Naively, we could wonder if the change from one to two dimensions could have a large effect on the current and on the TMR as it occurs when the system increases from a single nanoparticle to a clean array with more than two islands.

In a two-dimensional clean array placed between non-magnetic electrodes with m x k particles where m is the number of rows and k the number of nanoparticles in each row, the current is $I \sim mI_1$, with I_1 the current through one row, see section 5.3. For two-dimensional arrays between ferromagnetic electrodes we could expect the same behavior regardless the spin accumulation through the array. In the following sections we will see that this is what actually happens and consequently the value of the TMR is not much affected by the dimensionality of the array.

7.3.1 Spin accumulation

In two-dimensional arrays with square lattice, the spin accumulation is equal in each row. This can be clearly seen if we study the spin accumulation at different islands of an array with $N = 3x5$, see Fig. 7.10 (a). For parallel configuration, in each row the spin accumulation changes its sign. Moreover, the islands placed at the same position in the rows have the same spin accumulation, see Fig. 7.10 (b) in which the spin accumulation is represented as a function of the voltage at different islands. In the antiparallel case all the islands have equal spin accumulation, see Fig. 7.10 (c).

7.3.2 Flow of current

As in the case of non-magnetic electrodes, for ferromagnetic electrodes the current can be approximated by the contribution of the current through each row. This occurs for both parallel and antiparallel magnetic orientations. In Fig. 7.11 (a) the $I - V$ curves are represented for a one-dimensional array with $N = 5$ nanoparticles and for a two-dimensional array with $N = 3x5$ nanoparticles. As we can observe, once the $I - V$ curve for the two-dimensional case is divided by the number of rows, the current in a row is very similar to the current in the one-dimensional system. Only little differences appear around the metallic threshold, that is equal in both arrays when they are placed between non-magnetic electrodes, $V_T = 10E_c$.

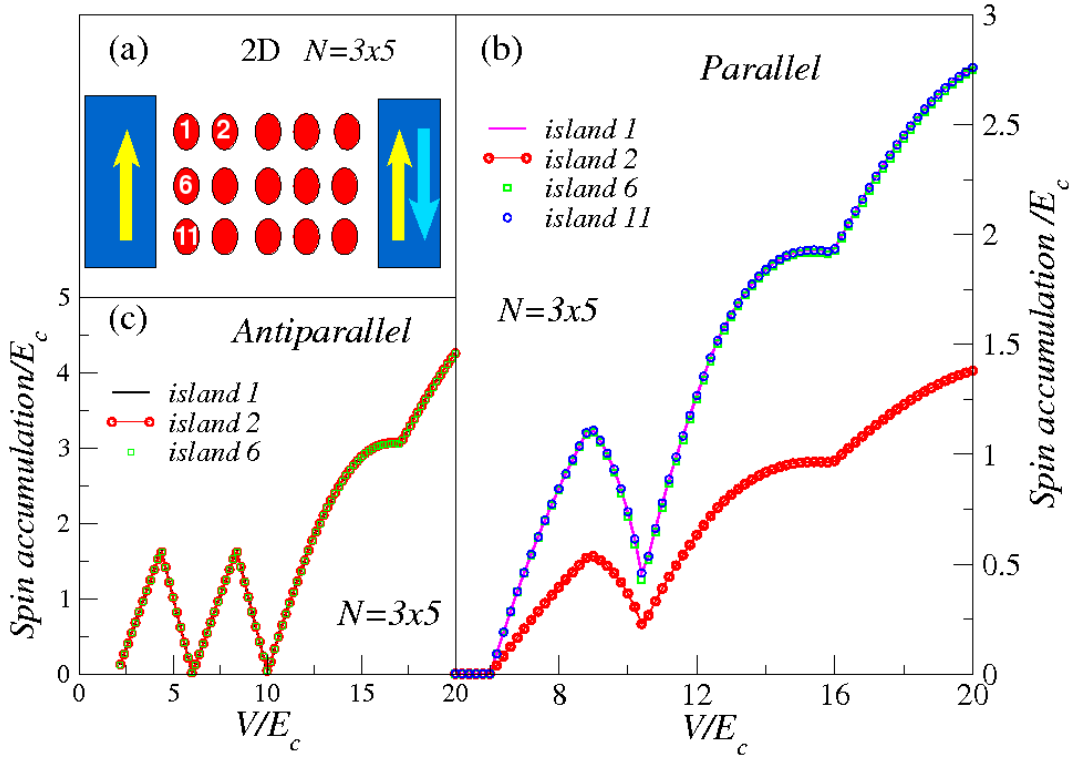

Figure 7.10: (a) Schematic diagram of a two-dimensional array $N = 3x5$ placed between two ferromagnetic electrodes. The number that appears in some of the islands indicates the number of the island. (b) and (c) Spin accumulation as a function of the voltage at different islands in the array represented in (a) for parallel and antiparallel orientation, respectively.

7.3.3 TMR

In a two-dimensional clean array with square lattice, as the current is approximately given by the current in a one-dimensional array with the same length multiplied by the number of rows in both parallel and antiparallel configurations, the value of the TMR, $(I_p - I_{ap})/I_{ap}$, does not change much, see fig .7.11 (b), in which the TMR for one and two-dimensional cases is represented as a function of the voltage. Only at the top of the peak a small difference can be observed.

7.4 Summary

In this chapter we have studied the interplay between ferromagnetism and charging effects in nanoparticle arrays placed between ferromagnetic electrodes, and how it affects the transport properties. So far, previous works have focused in the cases of one or two nanoparticles. I have analyzed one and two-dimensional clean arrays without any type of disorder. Here, I have only considered two-dimensional arrays with square lattice. In this thesis I have studied

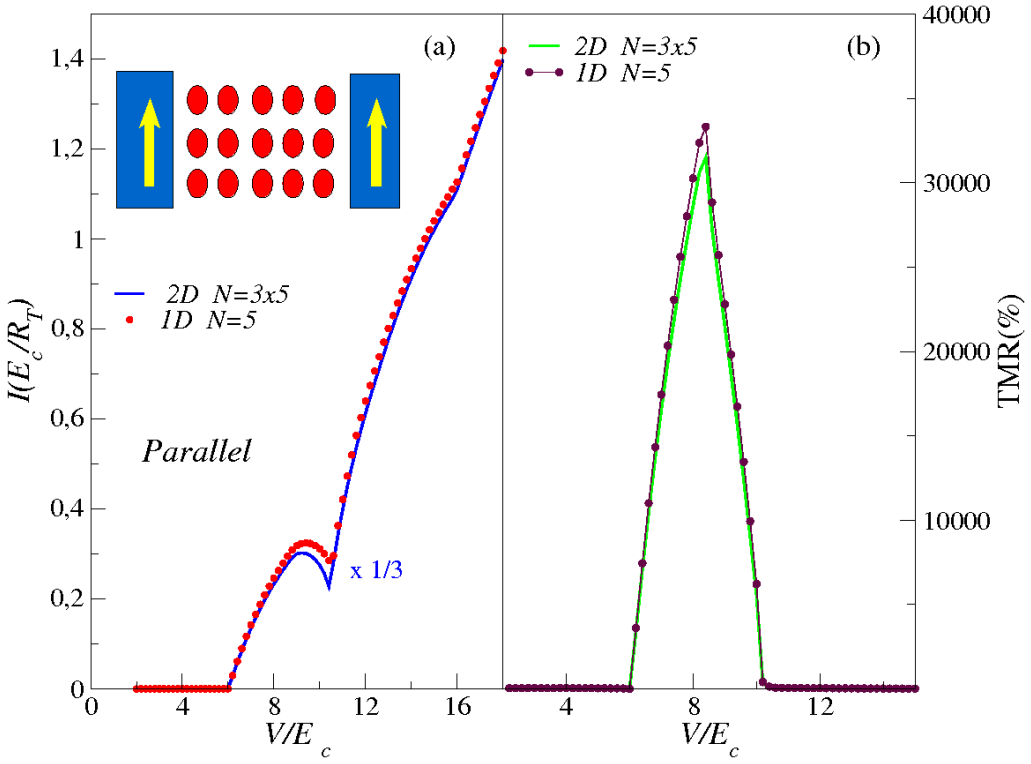

Figure 7.11: (a) $I-V$ curves in one and two-dimensional arrays with parallel orientation: 1D (N=5), 2D (N=3x5) and $p = 0.7$. The $I-V$ curve in 2D has been divided by 3, the number of rows in the array. (b) TMR as a function of the voltage for the arrays in (a).

the differences in the current for P and AP orientations of the electrodes polarization. In this chapter I have considered the case of equal spin polarization in both electrodes.

Unlike the case of a single non-magnetic nanoparticle in which there is only spin accumulation in the AP orientation in the limit of long spin relaxation time, in nanoparticle arrays there is spin accumulation in both P and AP configurations. The spin accumulation is different in both cases. For the AP orientation the spin accumulation is practically equal in each island. However, in the parallel case the spin accumulation changes its sign within the array.

The current is a non-linear function of the voltage in P and AP orientations, although its profile is quite different at some ranges of voltage. We have found that in the antiparallel case, the spin accumulation is homogeneous through the array, and it barely contributes to the change in energy of tunneling processes, so the $I-V$ curves are quite similar to the non-magnetic case. However, in the parallel orientation, a new regime with negative differential conductance appears at voltages smaller than the metallic threshold voltage. This unexpected behavior is a consequence of the inhomogeneous spin gradient created through the array.

The oscillations of the current correlate with the oscillations of the spin accumulation, of the spin polarization of the current and the tunnel magnetoresistance. The number of oscillations increases with the increase of nanoparticle in the array. There is a strongly voltage dependent spin polarization of current in the case of parallel orientation. For the antiparallel case there is not spin current.

There is a huge enhancement of the magnetoresistance in nanoparticle arrays with respect to the case of a single nanoparticle. TMR can be two orders in magnitude large in arrays than in the single island case. This large effect in the TMR is a consequence of the large differences between the $I - V$ curves in both magnetic orientations.

The dimensionality of the array does not affect the value of the TMR. This is due to the fact that in two-dimensional arrays with square lattice the current can be approximated by the contribution of the current of the different conducting channels, that in this case are the rows. Thus, the current is equal to the current in a clean one-dimensional array with the same length multiplied by the number of rows. But this occurs in both magnetic configurations, therefore the TMR is practically equal in one and two-dimensional arrays.

8 Effect of the disorder and long-range interaction in metallic nanoparticle arrays between ferromagnetic electrodes

In this chapter I will analyze how differences in polarization, temperature, disorder and the long-range interactions affect the transport properties discussed in previous chapter. I will first study the case in which there is polarization asymmetry. After that, the dependences on the temperature will be analyzed. The effects of different types of disorder such as disorder in resistances or charge disorder will be studied in detail. Finally, I will analyze the effect of the long-range interactions in the transport for this type of systems.

8.1 Introduction

Until now we have studied the spin accumulation and the transport properties through clean metallic nanoparticle arrays placed between two ferromagnetic electrodes when the polarization of the electrodes is equal and the electrostatic interactions are restricted to the interaction between charges in a same conductor, onsite limit. However, the electrode polarization asymmetry, the different types of disorder or the long-range interaction affect the transport properties. There are qualitative differences with respect to the clean case for both one island and nanoparticle arrays. Here, we will study how the interplay between ferromagnetism and charging effects is affected by the electrode polarization asymmetry, the temperature, the different types of disorder (charge and resistance disorder) and the long-range interactions. As in the previous chapter, for all the cases we will focus in the study of spin accumulation, the flow of current and the tunnel magnetoresistance, highlighting the main differences with respect to the clean case.

In all the cases studied in this chapter except in the case of electrode polarization asymmetry, we consider equal spin polarization in each electrode, $p_1 = p_2 = p$.

8.2 Electrode polarization asymmetry

Before addressing the effect of the polarization asymmetry in nanoparticle arrays I discuss the single island case.

8.2.1 One Nanoparticle

Spin accumulation

For a single nanoparticle and electrode polarization asymmetry ($p_1 \neq p_2$) there is spin accumulation in both P and AP magnetic configurations, unlike the case with equal spin polarization in both electrodes, in which there is only spin accumulation for the AP orientation. With $p_1 \neq p_2$, if the chemical potentials for both spins at the islands are equal, the number of electrons that will try to enter into the nanoparticle with a given spin will be different to the number of electrons with the same spin that will try to exit the nanoparticle. Thus, the spin accumulation appears in order to equilibrate the ratios for entrance and exit from the island of spin up and down electrons. This happens in both magnetic configurations, see Fig. 8.1 (a) and (b) in which the spin accumulation is represented as a function of the voltage with the source polarization $p_1 = 0.7$ and different values of drain polarization p_2. As it can be observed the spin accumulation depends on voltage, on spin polarization, and on the magnetic configuration. If we fix the polarization of the source electrode,p_1 equal to 0.7, and we vary the values of the spin polarization of the drain electrode p_2, in the AP case the spin accumulation increases with p_2, while in the P orientation it decreases when p_2 increases. This is a consequence of the ratios between the entrance and exit from the island of electrons with a given spin. For AP orientation, the larger p_2 the larger the difference between the number of electrons for a given spin that enter and exit from the island. Thus, the spin accumulation will increase with the increase of p_2 in order to compensate this difference, see Fig. 8.1 (a). On the contrary, in the P orientiation as the majority of the electrons in the both electrodes have the same spin, there will be more spin accumulation when the difference between the polarization of both electrodes is larger, see Fig. 8.1 (b).

Flow of current

The current is a non-linear function of the voltage and strongly depends on the magnetic orientation of the electrodes, as it occurs in the case of equal spin polarization in both electrodes. The $I-V$ curves depend on the spin polarization, see Fig. 8.1 (c) in which the $I-V$ curves are represented for P and AP orientations in the inset and main figure respectively. In the high voltage linear regime the current can be approximated by

$$I_{asympt} \sim \frac{2-p_1^2-p_2^2}{4-(p_1 \pm p_2)^2}\left(V-\sum_{i=1}^{N+1} E_i^{e-h}\right) \tag{8.1}$$

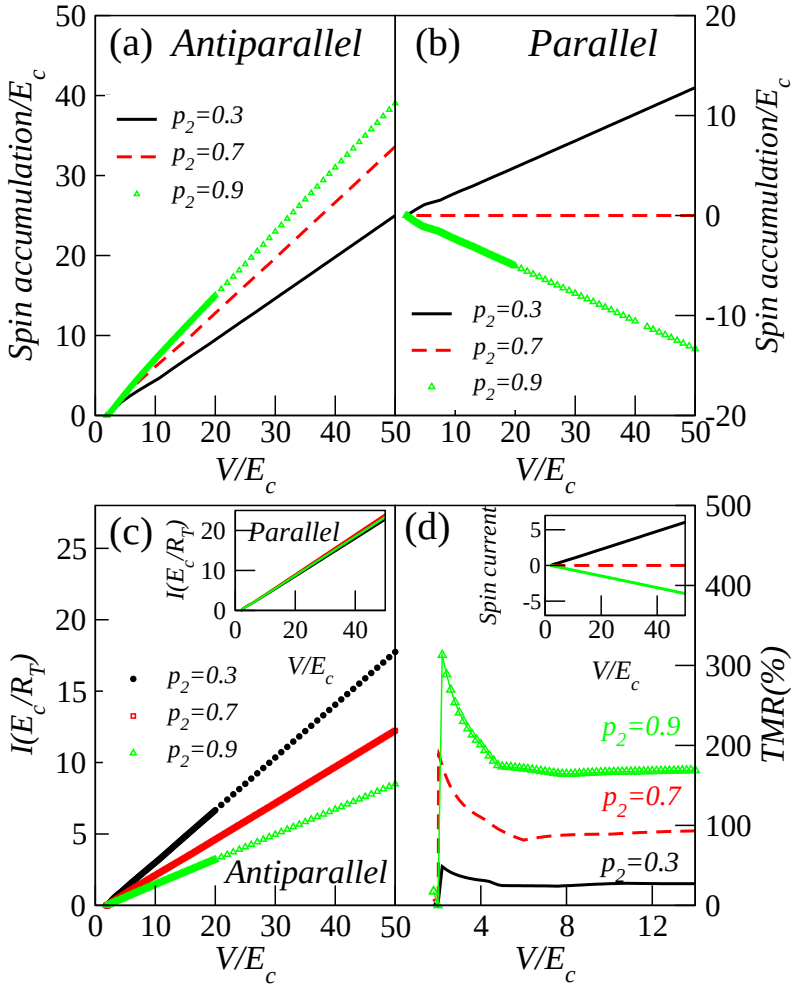

Figure 8.1: (a) and (b) Spin accumulation as a function of the voltage for a single nanoparticle with source polarization $p_1 = 0.7$ and several values of the drain electrode p_2, for AP and P orientations respectively. (c) $I - V$ curves for a single nanoparticle with $p_1 = 0.7$ and different values of p_2 for P (inset) and AP (main figure) orientations. (d) Main figure: TMR as a function of the voltage corresponding to the $I - V$ curves in (c). Inset: Spin current as a function of the voltage for a single nanoparticle with $p_1 = 0.7$ and different values of p_2, from top to bottom $p_2 = 0.3, 0.7, 0.9$. The spin current is given in units of (E/R_T). The case with equal spin polarization in both electrodes is included for comparison.

with upper and lower signs corresponding to P and AP configurations respectively.

Another difference with respect to the case with equal spin polarization is that for $p_1 \neq p_2$ there is a finite spin current in the AP orientation, see inset in Fig. 8.1 (d). The spin current in both magnetic configurations depends on voltage and on the spin polarization of the

electrodes. At high voltages the spin current average is given by

$$(I_\uparrow - I_\downarrow)_{asympt} \sim \frac{p_1 \pm p_2 \mp p_1^2 p_2 - p_1 p_2^2}{4 - (p_1 \pm p_2)^2} \left(V - \sum_{i=1}^{N+1} E_i^{e-h} \right) \tag{8.2}$$

with upper and lower signs corresponding to P and AP configurations respectively. In the antiparallel case for $p_1 < p_2$ the spin current will be negative.

TMR

The value of TMR depends on the spin polarization of the electrodes, p_1 and p_2, see Fig. 8.1 (d), in which the TMR is represented as a function of the voltage with $p_1 = 0.7$ and different values of p_2. At high voltages TMR saturates to

$$TMR = \frac{4 p_1 p_2}{4 - (p_1 + p_2)^2} \tag{8.3}$$

8.2.2 Nanoparticle arrays

In nanoparticle arrays, when the electrodes have different spin polarization, the spin gradients created through the array are modified with respect to the case with $p_1 = p_2$. As a consequence, the $I - V$ characteristics can be modified. In the AP orientation there is current flow below the metallic threshold, showing a regime which can have negative differential conductance. Before explaining this regime, we will see the spin accumulation created through the array when $p_1 \neq p_2$.

Spin accumulation

In the case of nanoparticle arrays and electrode polarization asymmetry, there are several differences in the spin accumulation with respect to the case in which $p_1 = p_2$. For both magnetic configurations the spin accumulation has different values in all the islands. Thanks to this inhomogeneous spin accumulation, the spin gradients created through the array allow the flow of current for voltages smaller than the non-magnetic threshold in both P and AP orientation. The change in spin accumulation between the first and last island of the array is much larger when the electrode magnetizations are parallel than when they are antiparallel, as shown in Fig. 8.2 (a) and (b).

For P orientation, when there is equal spin polarization in both electrodes, the spin accumulation changes its sign at the center of the array. However, when the spin polarization of the electrodes is different, this change of sign does not always occur. Furthermore, if there is a change of sign, in general it will not happen at the center of the array. The change on sign depends on the polarization of the electrodes, as we can see in Fig. 8.2 (a), where the

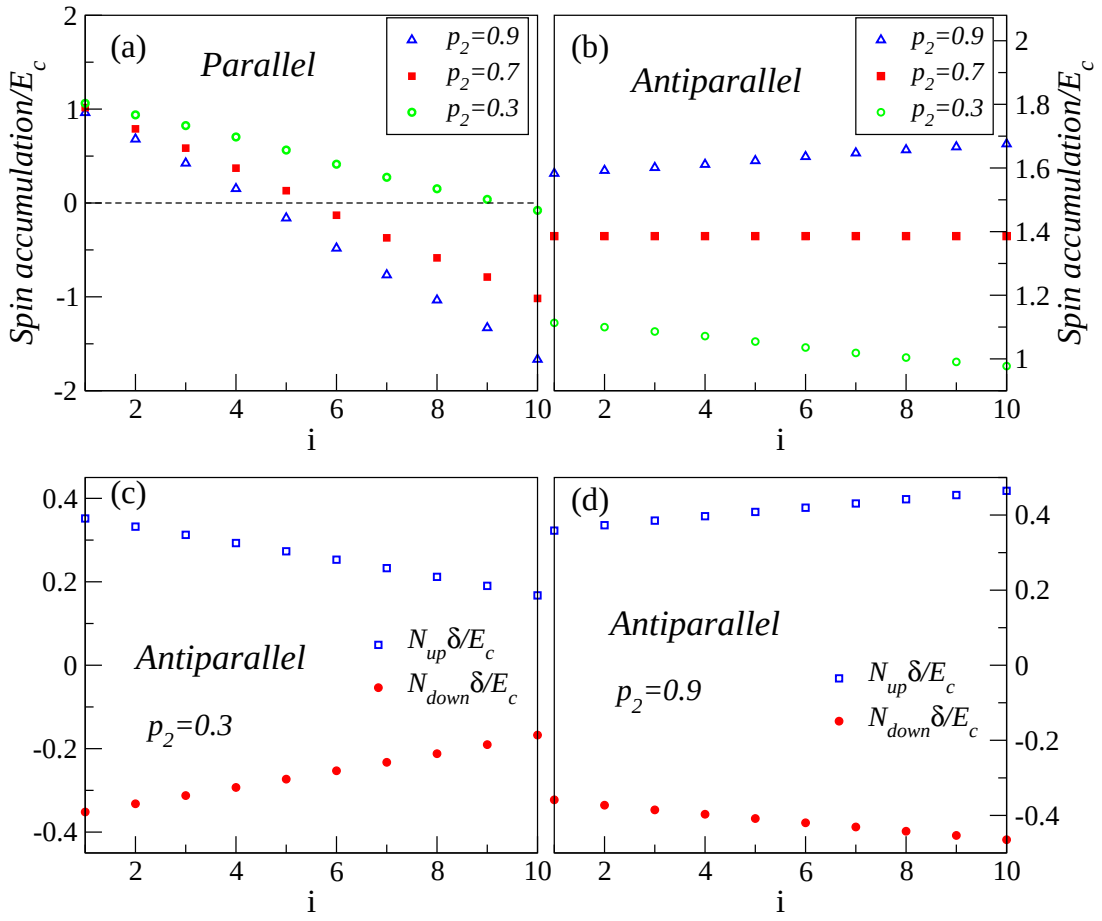

Figure 8.2: (a) and (b) Spin accumulation at the islands as function of the position for a clean array with $N = 10$ islands, source polarization $p_1 = 0.7$ and different drain polarizations p_2 at $V = 16E_c$ for P and AP configuration respectively. (c) Spin potentials at the islands as a function of the position for a clean array with $N = 10$ islands, $p_1 = 0.7$ and $p_2 = 0.3$ at $V = 19E_c$ in the AP orientation. (d) same that in (c) for $p_2 = 0.9$.

spin accumulation is represented at the islands as a function of the position for a clean array with $N = 10$ islands and different values of p_2 when p_1 is fixed. As a result of the electrode polarization asymmetry, the even-odd effect that there is in the case with $p_1 = p_2$ dissapears, and there is spin accumulation at the central island in a clean array with odd number of islands.

For AP orientation the spin accumulation does not change its sign within the array, at least in the cases analyzed in this thesis. The spin accumulation can increase or decrease along the array depending on the spin polarization of the electrodes. When $p_1 < p_2$ the spin accumulation increases, whereas for $p_1 > p_2$ it decreases, see Fig. 8.2 (b). The fact that the spin accumulation can increase or decrease implies that the spin gradients created through

the array sometimes favor the flow of spin-up electrons and prevent the flow of spin-down electrons, while other times the electrons which flow is favored have spin-down. This effect can be clearly seen in Fig. 8.2 (c) and (d), where the spin potentials for the two cases are represented as a function of the position. This behavior is different to the case of P orientation in which the spin gradients always favor the flow of spin-up electrons and prevent the flow of spin-down electrons.

Flow of current

For different spin polarization asymmetry, the threshold voltage at which the current starts to flow is reduced with respect to the case with non-magnetic electrodes in both P and AP configurations.As explained in previous section, this is due to the spin gradients created through the array. The spin potentials have different values at the islands, and as a result, there are finite potential drops at the inner junctions, that depending on the spin, favor or prevent the flow of electrons with a given spin.

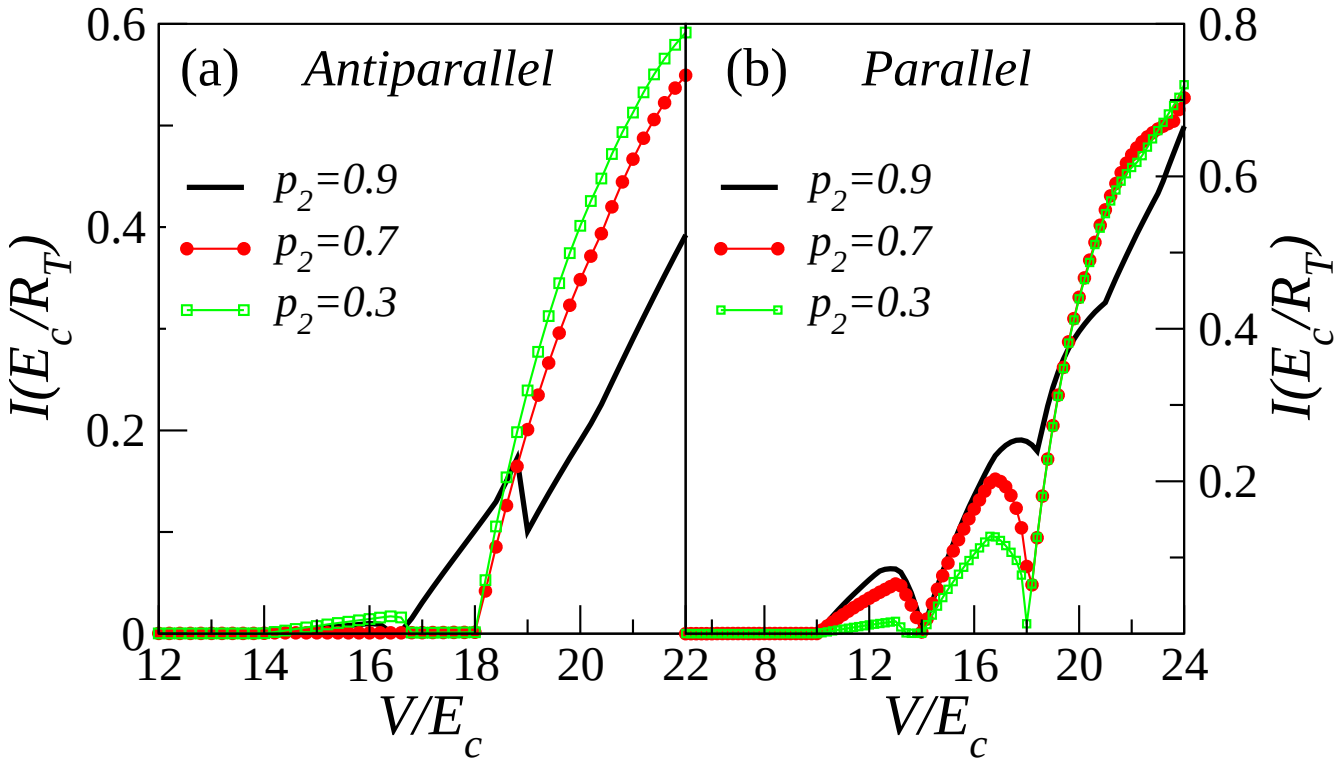

Figure 8.3: (a) and (b) $I-V$ curves for a clean array with $N = 10$ islands, source polarization $p_1 = 0.7$ and different drain polarizations p_2 for AP and P orientations respectively.

In the case of P orientation the regime with negative differential conductance does not disappear when spin polarization asymmetry is present. The current depends on the spin po-

larization of the electrodes, increasing when p_2 increases if p_1 is fixed, see Fig. 8.3 (b). The shape of the $I-V$ curves barely changes. The origin of this regime is the same as in the case of $p_1 = p_2$, see subsection 7.2.4.

The main difference that appears when $p_1 \neq p_2$ is that in the AP orientation there is a new regime for voltages smaller than the metallic threshold in which the current shows peaks, see Fig. 8.3 (a). The shape of these peaks is more irregular and their height notably reduced with respect to those found in the P orientation. The appearence of these peaks will have an influence on the shape of the TMR, see below.

In the case of $p_1 \neq p_2$ there are spin gradients in both magnetic orientations. The difference between them is that in the P case the spin-up electrons are always favored by the spin potential, however, in the AP case the spin that is favored by the spin gradient depends on the spin polarization of the electrodes, as we already saw in Fig. 8.2 (c) and (d).

For $p_1 \neq p_2$ there is spin current not only in the P orientation but also in the AP one, as it occurs for a single nanoparticle case. Fig. 8.4 shows the spin polarization of the current as a function of the voltage for a clean array with $N = 10$ islands and $p = 0.7$ for different values of p_2 for P (a) and AP (b) orientation. The case in which $p_1 = p_2$ is included for comparison. For the AP orientation the spin polarization of the current can be positive or negative depending on the value of p_2 with respect to p_1 when this one is fixed. When $p_2 > p_1$, $I_\uparrow < I_\downarrow$. However, in the P orientation although the spin polarization of the current depends on the values of p_1 and p_2 there is no change of sign because the current flow for spin-up electrons is always larger than for spin-down ones. At high voltages the spin polarization saturates to

$$\frac{I_\uparrow - I_\downarrow}{I} = \frac{(p_1 \pm p_2)(1 \mp p_1 p_2)}{(1 - p_1^2 p_2^2) + N(1 - p_1^2)(1 - p_2^2)} \tag{8.4}$$

with upper and lower signs corresponding to P and AP configurations respectively.

TMR

With spin polarization asymmetry there are peaks in the TMR, but their shape is strongly modified with respect to the case in which $p_1 = p_2$, see Fig. 8.5. The change in the shape of the TMR is mainly due to the peaks in the $I-V$ curve that appear for AP orientation. The values of the TMR have the same order of magnitude as in the case of equal polarization in both electrodes. The shape of the peaks in the TMR depend on the complicated way on the polarization and on the voltage.

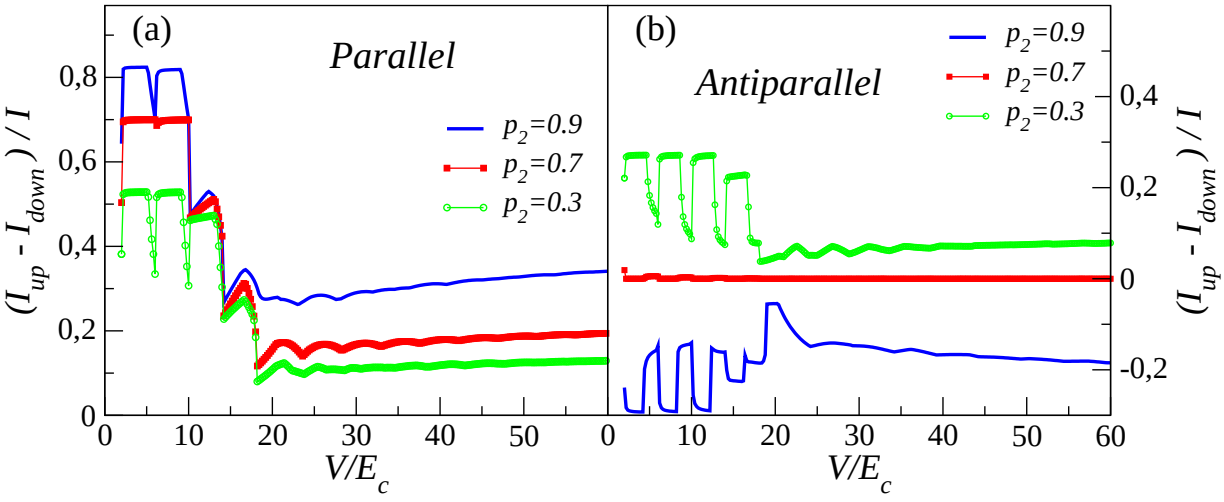

Figure 8.4: (a) and (b) Spin polarization of the current as function of the voltage for a clean array with $N = 10$ islands, source polarization $p_1 = 0.7$ and different drain polarizations p_2 for P and AP configuration respectively.

8.3 Dependence on the temperature

At zero temperature only the processes with gain in energy are possible. This means that the processes with cost in energy ($\Delta E > 0$) or without it ($\Delta E = 0$) are forbidden. In the AP orientation there is a small current below the non-magnetic threshold when there is a finite temperature. If the temperature is zero, the current will extrapolate to zero. This small current is mostly a consequence of the fact that at finite temperature the tunneling processes at the inner junctions, which do not have cost in energy, are allowed with a probability which increases linearly with temperature

$$\Gamma_\sigma(\Delta E_\sigma) = \frac{K_B T}{R_\sigma} \tag{8.5}$$

with $R_\sigma = 2R_T$. Thus, the current increases with the temperature in the AP case. In Fig. 8.6 (a) the $I - V$ curves are represented for a clean array with $N = 5$ islands and two different temperatures for AP orientation. The largest effect of temperature is seen for $V < V_T$ with V_T the non-magnetic threshold.

For P configuration the current below the non-magnetic threshold is a consequence of the spin potential gradients created through the array. The tunneling processes at the inner junctions have a finite energy gain. And the current through the array is much less sensitive to the temperature. We can observe this in Fig. 8.6 (b) in which the $I - V$ curves are represented for the same array with two different temperatures.

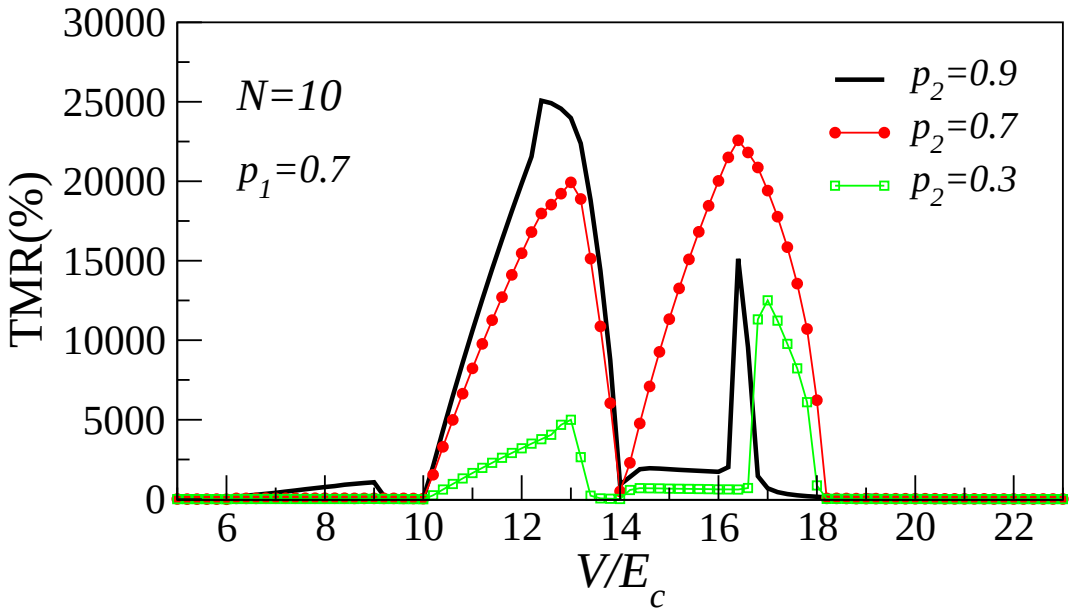

Figure 8.5: TMR as a function of the voltage for a clean array with $N = 10$ islands, source polarization $p_1 = 0.7$ and different drain polarizations p_2.

The dependence of the current on the temperature in the AP orientation strongly affects the TMR, which is inversely proportional to the temperature, see main Fig. 8.6 (c), in which the TMR is represented as a function of the temperature for a clean array with $N = 5$ islands at a given voltage. The TMR decreases dramatically with the increase of temperature. The strong dependence of the TMR on the temperature is not a simple consequence of the weakening of Coulomb blockade. As shown in the top inset of Fig. 8.6 (c) the temperature dependence of the TMR corresponding to the single island case $N = 1$ is much weaker at $K_B T \ll E_c$, because the tunneling processes involved are thermally activated, contrary to the zero energy cost relevant at the inner junctions of a long array.

8.4 Disorder in resistances

In this section I will analyze how the resistance disorder affects the transport properties in nanoparticle arrays. There is resistance disorder when not all the junctions resistances are equal, section 1.3.2. I will consider equal spin polarization in both electrodes. I will first discuss briefly the case of a single nanoparticle in order to highlight the main effects that appear in the nanoparticle arrays.

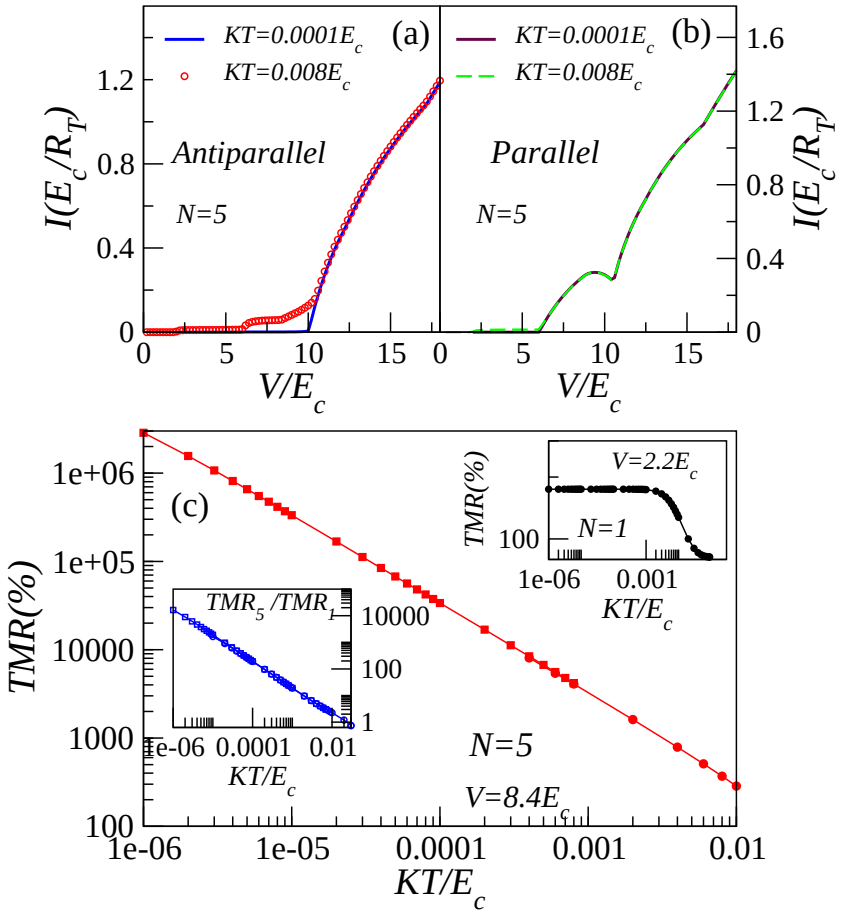

Figure 8.6: (a) and (b) I-V curves for an $N = 5$ array with P and AP orientations,respectively, for two different temperatures. The effect of temperature is much stronger for the AP orientation, as expected. (c) TMR as a function of temperature for a clean $N = 5$ array and a voltage $V = 8.4E_c$. Top inset: TMR as a function of temperature for a single island and $V = 2E_c$. It shows a much weaker temperature dependence, what is emphasized in the lower inset where the dependence of the relative values of the TMR as a function of temperature are represented.

8.4.1 One island

For the case of a single nanoparticle when the resistance of one junction is larger than the other one, the shapes of the current is affected by the values of the resistances. These dependence can be observed in Figs. 8.7 (a) and (b) in which the $I - V$ curves are represented for different values of resistances in the P and AP orientations respectively. In both magnetic configurations, the larger the resistance of one of the junctions, the smaller the current. At high voltages the current has a linear behavior which can be calculated analitically, the slope of these asymptotic curves for both magnetic orientations are given by

$$S_p = \frac{1}{R_1 + R_2} \tag{8.6}$$

$$S_{ap} = \frac{(R_1 + R_2)(1 - p^2)}{(R_1^2 + R_2^2)(1 - p^2) + 2R_1R_2(1 + p^2)} \tag{8.7}$$

The main difference with respect to the case without resistance disorder is that there is spin

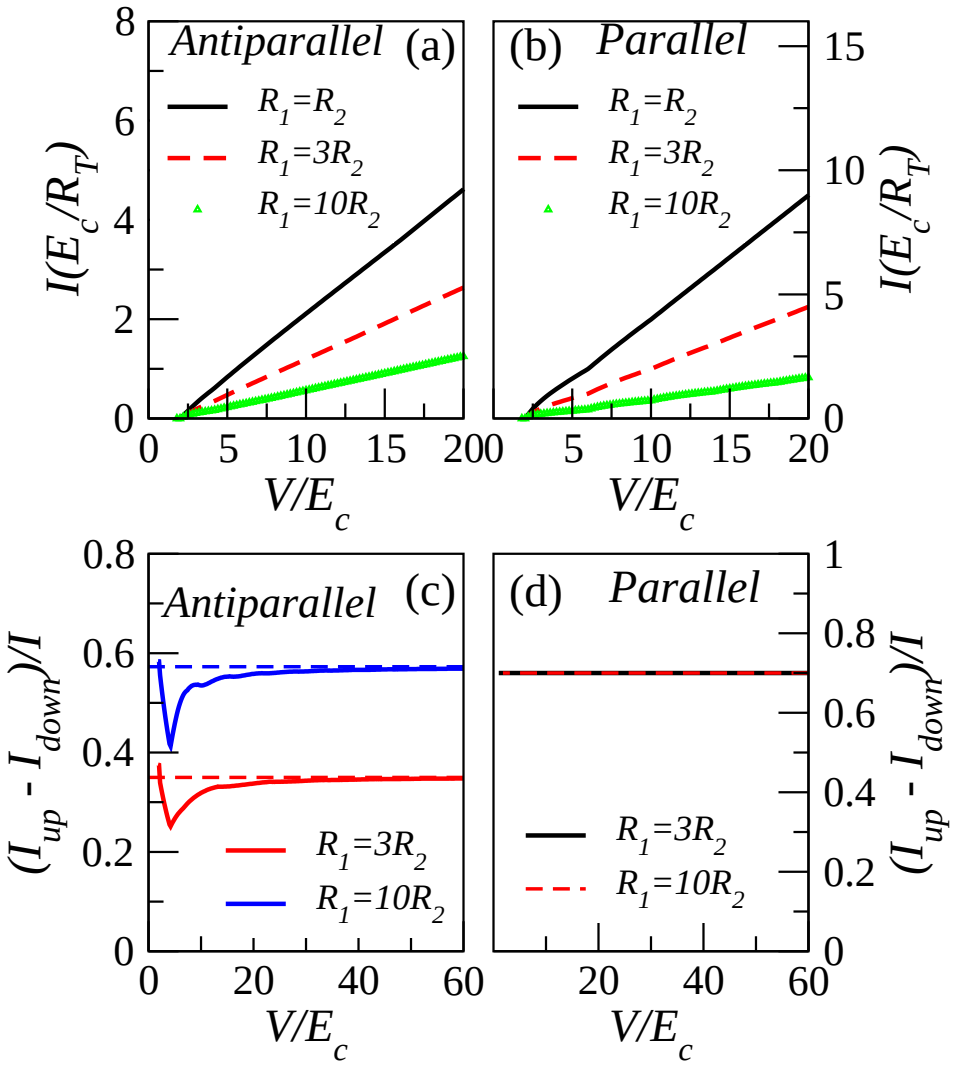

Figure 8.7: (a) and (b) I-V curves for a single nanoparticle when the resistance at the first contact junction is larger than the other resistance, $3R_T$ and $10R_T$, in AP and P orientions respectively. The case with $R_1 = R2$ is included for comparison. (c) and (d) Spin polarization of the current as a function of the voltage for the same cases that in (a) and (b) for AP and P configurations respectively. In (c) The dashed lines are the theoretical predictions at high voltages.

current in the AP orientation when one of the resistances is larger than the other one. The vanishing of the spin current in the absence of resistance disorder was linked to $R_{1\uparrow} = R_{2\downarrow}$ and $R_{1\downarrow} = R_{2\uparrow}$. This is not true anymore when resistance disorder is present. As $R^{\uparrow}_{sum} \neq R^{\downarrow}_{sum}$, $I_{up} \neq I_{down}$, leading to a finite spin current. With resistance disorder, there is spin polarization

of the current in both magnetic configurations, see Fig. 8.7 (c) and (d). At high voltages the spin polarization of the current saturates to a value, which in the case of P orientation is equal to p. However, for AP orientation the saturation also depends on the resistances

$$\frac{I_{\uparrow}^{AP} - I_{\downarrow}^{AP}}{I^{AP}} = \frac{p(R_1 - R_2)}{(R_1 + R_2)} \tag{8.8}$$

As in the clean case without any kind of disorder, there is only spin accumulation in the

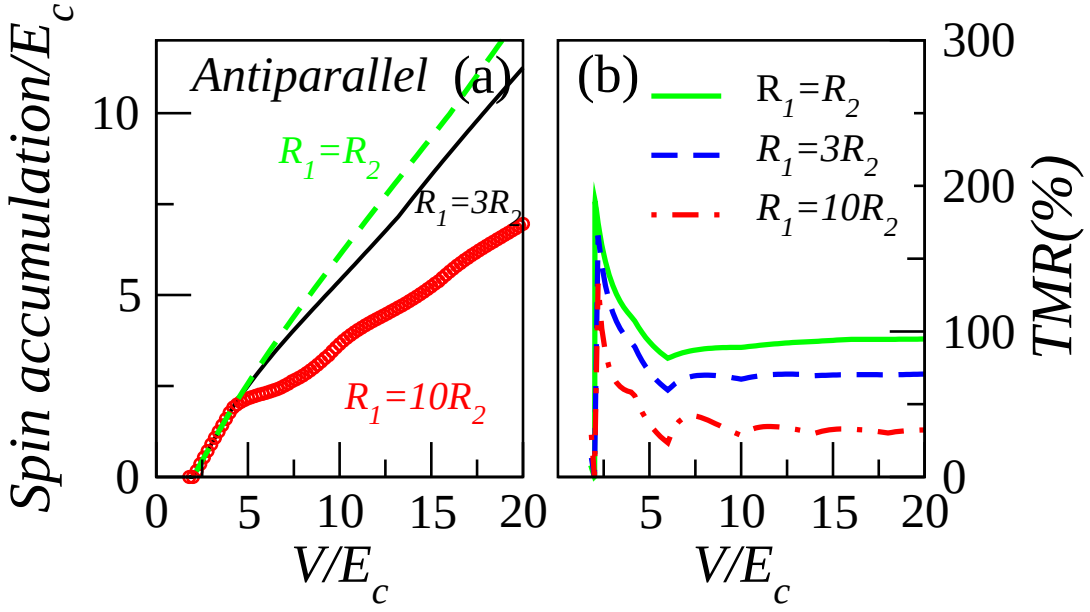

Figure 8.8: (a) Spin accumulation as a function of the voltage for a single nanoparticle when the resistance at the first contact junction is larger than the other resistance, $3R_T$ and $10R_T$, in AP orientation. The case with equal resistances $R_1 = R_2$ is included for comparison. (b) TMR as a function of the voltage corresponding to the $I - V$ curves represented in (a) and (b) of Fig. 8.7.

AP orientation. The spin accumulation strongly depends on the values of resistances and the spin polarization, as can be observed in Fig. 8.8 (a) in which the spin accumulation is represented as a function of the voltage for different values of resistances and p.

The TMR depends on the resistances, but the TMR is of the same order as the TMR in the clean case, see Fig. 8.8(b).

8.4.2 Nanoparticle arrays

In nanoparticle arrays, we model the resistance disorder by means of junction resistances randomly assigned and varying between two values. Although the current depends on the configuration of resistance disorder, the profile of the current is equal to the profile in the

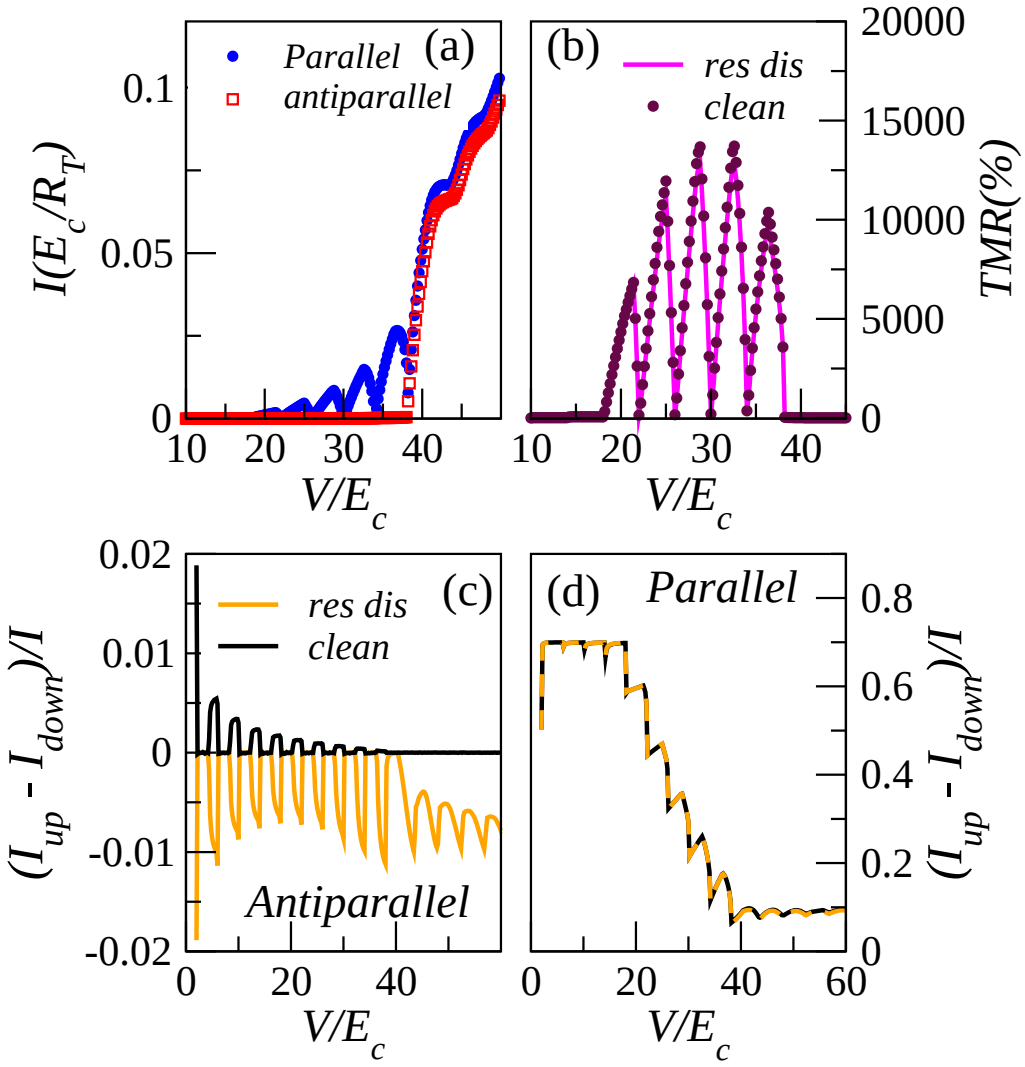

Figure 8.9: (a) I-V curves for a $N = 20$ array with the junction resistances randomly assigned varying between $(10 - 22)R_T$, for both magnetic configurations and $p = 0.7$. (b) TMR as a function of the voltage for the same array that in (a) compared with the one corresponding to a resistance disorder free array. (c) and (d) Spin polarization of the current for AP and P arrangements respectively for $N = 20$ arrays with $p = 0.7$ in the cases with and without resistance disorder. In the array with resistance disorder, it is randomly assigned varying between $(10 - 22)R_T$.

clean case for both magnetic orientations. This means that the $I - V$ characteristics show the same regimes of behavior found in the clean case, and the resistance disorder configurations only affect the value of the current. For AP orientation the current shows a threshold voltage equal to the one found for the case of non-magnetic electrodes. For P orientation the threshold voltage is reduced and the regime with negative differential conductance appears in presence of resistance disorder, as in the clean case. Fig. 8.9 (a) shows the I-V curves for P and AP configurations corresponding to an array with $N = 20$ islands and resistance

disorder, being the junction resistances randomly assigned and varying between $(10-22)R_T$.

The high values of the TMR are not affected by the resistance disorder, as we can see in Fig. 8.9 (b) in which the TMR corresponding to an array with resistance disorder is compared with the TMR of a clean array without resistance disorder. The TMR is equal in the two cases in the regime with peaks. Although the current decreases with the resistance disorder with respect to the clean case, in both magnetic orientations the current is reduced by the same factor. Thus, the TMR is almost equal in a clean array in presence and absence of resistance disorder.

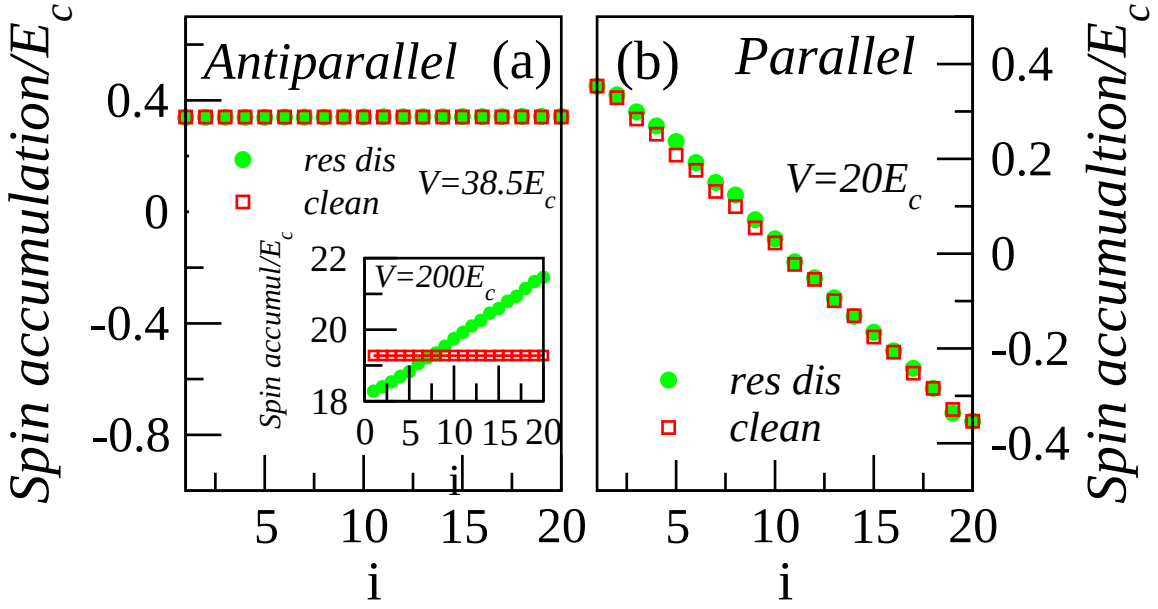

Figure 8.10: (a) Main (inset) figure: Spin accumulation at the islands for two $N = 20$ arrays, one with resistance disorder and the other disorder free, at $V = 38.5E_c$ ($V = 200E_c$) in the AP orientation. (b) Same that in (a) for P orientation at $V = 20E_c$. In the case with resistance disorder, all the junction resistances are randomly assigned varying between $(10-22)R_T$.

Unlike the case without resistance disorder, there is spin current in the antiparallel orientation when resistance disorder is present in the array, see Fig. 8.9 (c). This behavior also occurs in the case of a single nanoparticle with a resistance larger than the other. At high voltages there is a finite spin polarization of the current. Its sign and dependence on voltage change for different configurations of the resistance disorder. The spin polarization of the current that appears for voltages smaller than the non-magnetic threshold is a consequence of the finite temperature. For P orientation the spin polarization of the current is equal to the one found when there is no resistance disorder in the array, see Fig. 8.9 (d).

As the $I-V$ curves for arrays with resistance disorder have the same profile as the ones found for the case without any type of disorder, the spin accumulation must be quite similar to the spin accumulation in the clean case. This situation occurs for the voltages at which there are peaks in the P orientation and for voltages close to the threshold voltage for the non-magnetic case, as we can observe in Figs. 8.10 (a) and (b). For the AP case the spin accumulation is homogeneous through the array, and in the P orientation the spin accumulation changes sign within the array. For both magnetic orientation the spin accumulation for arrays with and without resistance disorder is equal. However, at higher voltages the spin accumulation depends on the resistance disorder configuration, and some differences appear with respect to the resistance disorder free case. At these voltages, for AP orientation when there is resistance disorder in the array, spin gradients are created through the array, unlike the case without resistance disorder, see inset on Fig. 8.10 (a).

8.5 Charge disorder

The charge disorder is really important in self-assembled nanoparticle arrays, see section 1.3.2. As in the case of non-magnetic electrodes studied in chapter 3, the charge disorder strongly affects the tranport properties through nanoparticle arrays when they are placed between two ferromagnetic electrodes. The effect of the charge disorder in the current can be observed in Fig. 8.11 (a), in which the $I-V$ curves are represented for clean and charge disordered arrays between ferromagnetic electrodes for P and AP orientations. The I-V curves of the disordered arrays strongly differ when compared with the clean case. In charge disordered arrays the threshold voltage is reduced with respect to the clean non-magnetic threshold voltage in both magnetic configurations. However, the main effect produced by the charge disorder is that the strong dependence of the current on the magnetic orientation of the electrodes has disappeared. As a result the $I-V$ curves in both magnetic configurations are very similar, leading to a very small magnetoresistance compared with the TMR found in the clean case or in the case with resistance disorder studied in the previous section, see Fig. 8.11 (b) and Fig. 8.9 (b). The TMR has been reduced four orders of magnitude by the charge disorder.

In clean arrays for the P orientation thanks to the spin gradients created through the array, there is a finite current for voltages smaller than the non-magnetic threshold. For AP orientation the spin accumulation is very homogeneous within the array, and the spin potentials created barely contribute to the tunneling processes. As a result, the small current that appears below the non-magnetic threshold is due to the finite temperature. This different behavior produces the large TMR values.

In charge disordered arrays there are spin gradients, being even larger than in the clean

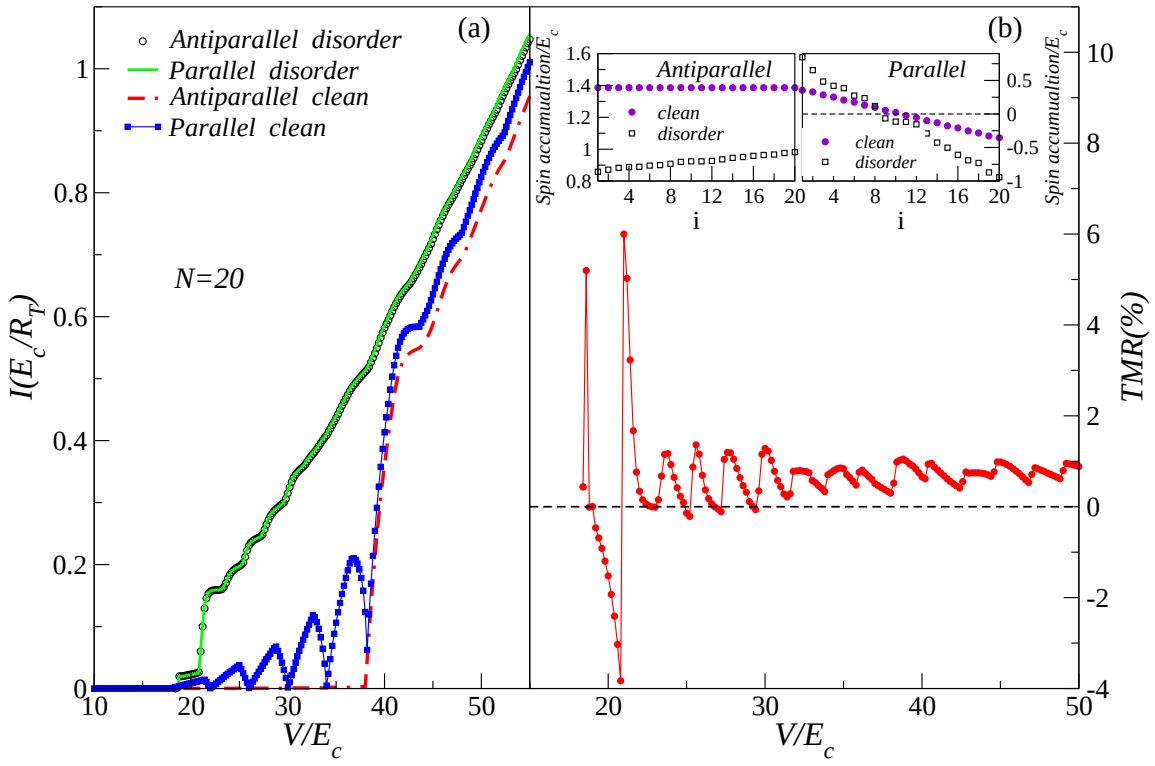

Figure 8.11: (a) I-V curves for $N = 20$ clean and charge disordered arrays, with source and drain polarization p=0.7 with P and AP configurations. (b)Main figure: TMR as a funtion of the voltage for the charge disordered array used in (a). Insets. Comparison of the spin accumulation gradient created in the clean and charge disordered arrays in (a) at $V = 20E_c^{isl}$ with AP (left) and P (right) orientations.

case, see insets in Fig. 8.11 (b). However, in these arrays there are also random disorder potentials at the islands, which result in finite potential drops at the inner junctions, and which can facilitate or prevent the flow of charge. Thus, contrary to the clean case in which all the tunneling processes through the inner junctions do not cost energy, in the disordered case the tunneling processes at the junctions that prevent the current flow (upwards steps) cost energy. The change in potential due to spin accumulation is too small to overcome such energy cost or to modify significatively the tunneling rates through the junctions with downward steps in disorder potential. Thus, to allow the current flow through the array a charge gradient has to be created at the upwards junctions. The resulting current shows a staircase profile which depends on the charge disorder configuration.

8.6 Long-range interaction

In this section I analyze how long-range interactions influence in the transport properties in metallic nanoparticle arrays placed between two ferromagnetic electrodes. As discussed previously, in the long-range limit the interactions are between charges in different conductors. Unlike in the first part of this thesis, in which the long-range interaction studied is close to the $1/r$ Coulomb law, see chapter 4, in this case the interaction used is of the type of exponential decay. This interaction is a good approximation when the islands are capacitively coupled to the neighboring ones or for screened interactions. A similar approximation has been frequently used in previous studies of nanoparticle arrays [30, 64, 105]. The electrostatic interaction between two conductors is given by

$$C_{\alpha\beta}^{-1} = C_{\alpha\alpha}^{-1} e^{|\alpha-\beta|/a_0} \tag{8.9}$$

where α and β label indicate the two conductors involved in the interaction. a_o is considered as an effective interaction or screening length and is measured in units of distance between the centers of the two nanoparticles.

For long-range interaction the polarization potential drop, which is a consequence of the interaction with the electrodes, is proportional to the bias voltage applied to the array. For exponentially decaying interactions the polarization potential at the islands is given by

$$\phi_\alpha^{pol} = \frac{V}{2}\left(e^{-\alpha/a_0} - e^{-|N+1-\alpha|/a_0}\right) \tag{8.10}$$

In the long-range limit, the polarization potential drop at the inner junctions ($\Phi_\alpha = \phi_\alpha - \phi_{\alpha-1}$) increases when increasing the length of the interactions, see chapter 4. For long-range interactions with an exponential decay interaction the polarization potential drop also increases with the increase of interaction length, as can be observed in Fig. 8.12 (a), in which ϕ_α^{pol} is represented at the islands as a function of the position for several values of length of interaction.

For long-range interactions in a clean array without charge disorder, once a charge has entered into the array it is able to flow from one electrode to the other, even in the absence of a charge gradient, due to the finite polarization potential drops at the inner junctions. And the threshold voltage is given by the voltage which allows an electron to enter the array or a hole to leave it, see section 4.2. Unlike in the onsite limit with ferromagnetic electrodes, in which the current below the non-magnetic threshold voltage is allowed thanks to the spin accumulation in the P case, for long-range limit the current can flow without the help of the spin accumulation. This means that the current in the case of long-range limit is determined by the interplay between the long-range of the interactions and by the spin accumulation.

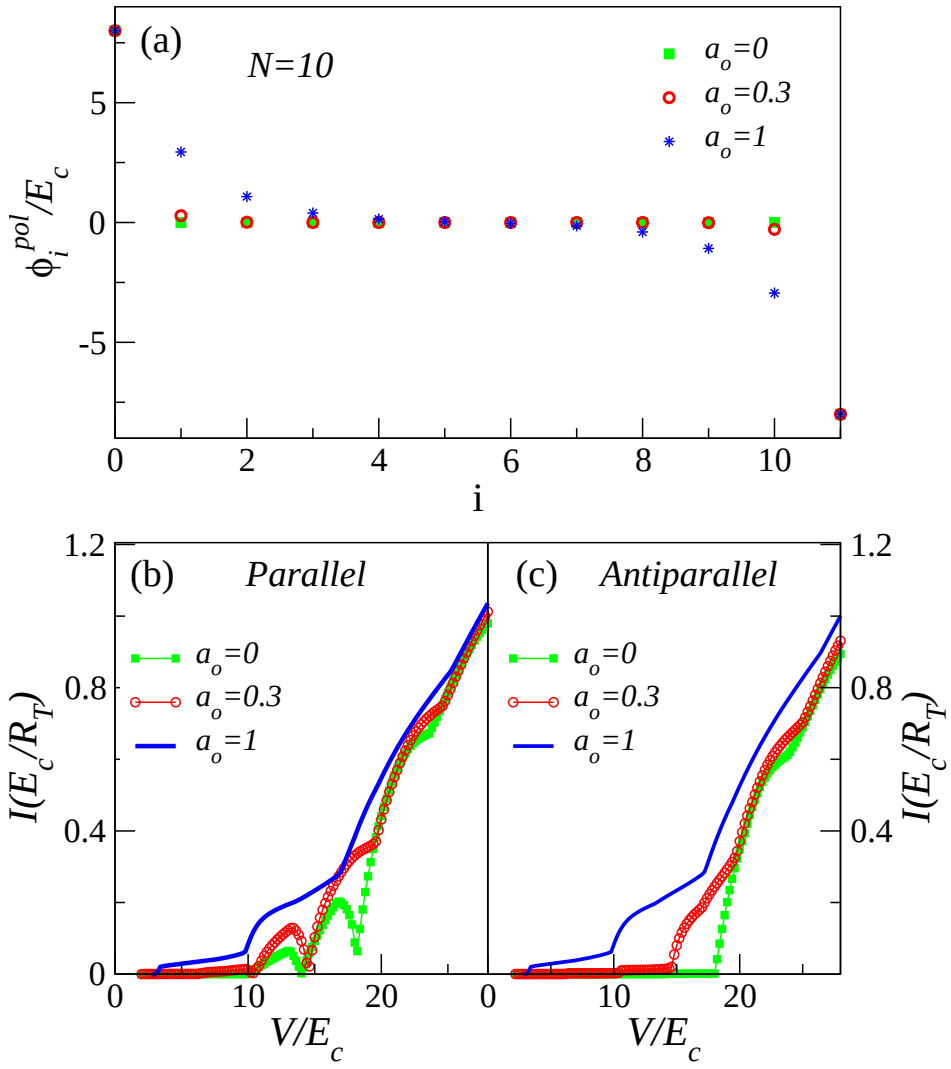

Figure 8.12: (a) Polarization potential at the islands and electrodes for an array with $N = 10$ islands at $V = 16E_c$ and several values of a_0, the range of the interactions, $a_0 = 0$ refers to the onsite interaction limit discussed in previous sections. (b) and (c) I-V curves corresponding to the same values of a_0 in (a) for P and AP orientation, respectively.

Thus, the larger a_o the smaller the influence of the spin accumulation on the transport. This can be observed in Figs. 8.12 (b) and (c) in which the $I - V$ curves are represented for several values of a_o in both P and AP orientations respectively. $a_o = 0$ is the case of short-range interaction. For P orientation there are oscillations in the current for small values of a_o, however for large a_o the oscillations disappear. The threshold voltage is similar for P and AP configurations. Morover, the long-range of the interactions affects the step width and height.

As for the parallel case the amplitude of the oscillations in the current decreases when a_o increases, and in the AP orientation the threshold voltage is reduced when a_o increases, the

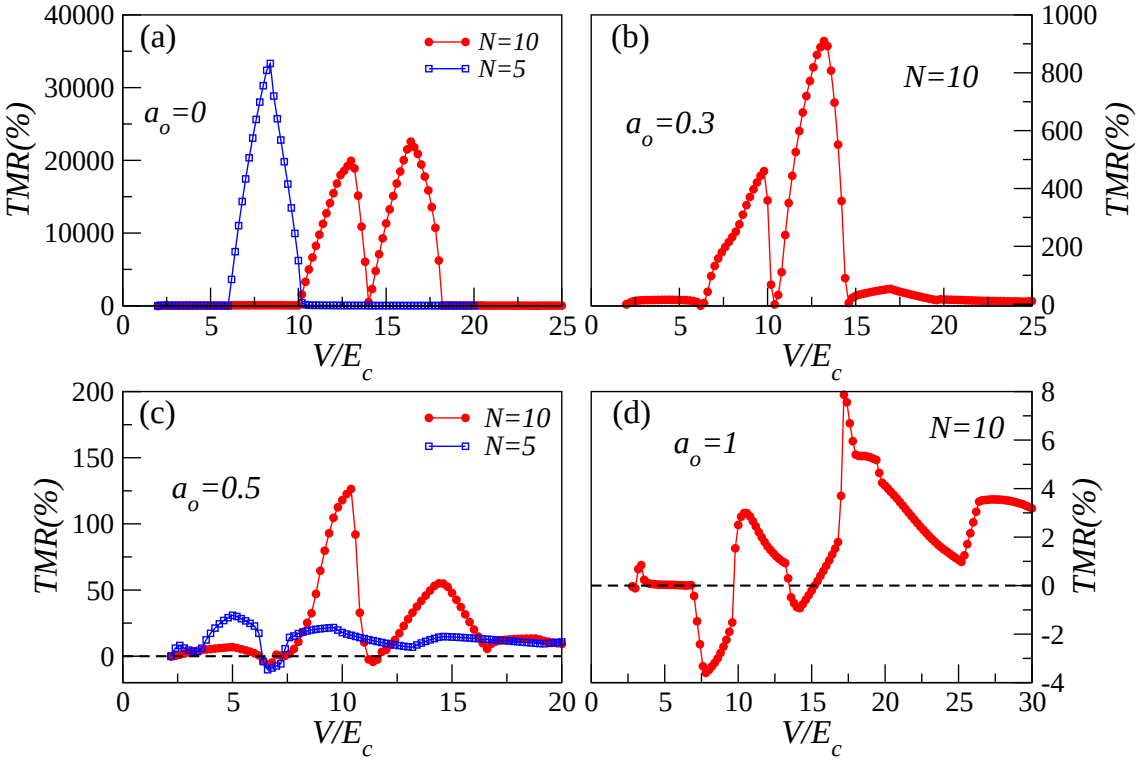

Figure 8.13: (a) to (d) TMR as a function of voltage for an $N = 10$ array for $a_0 = 0, 0.3, 0.5$ and 1, respectively. In (a) and (c) the TMR of an $N = 5$ array with the same a_0 is included. The reduction of the oscillations amplitude with a_0 is faster in shorter arrays.

values of the TMR decrease when the long-range of interaction increases. This effect can be clearly observed in Fig. 8.13, in which the TMR as a function of the voltage is represented for several values of a_o. Note the different scale of the TMR axis in the figures. Comparing Fig. 8.13 (a) and (d) we can see that there are approximately four orders of magnitude less for $a_o = 1$ than for the onsite-limit.

On the other hand, the reduction of the TMR for a given interaction length depends strongly on the array length, as seen in Fig. 8.13 (c) for two arrays with different size. The longer the array, the weaker the reduction in the magnitude of the oscillations. This dependence appears because the polarization potential drops at the junctions between particles is larger for smaller N.

8.7 Summary

In this chapter I have studied how the polarization asymmetry of the electrodes, the temperature, resistance or charge disorder and long-range interactions affect the transport properties

through the metallic nanoparticle arrays when they are placed between two ferromagnetic electrodes.

In nanoparticle arrays the main difference that appears when the spin polarization of the electrodes is different with respect to the case in which it is equal, is that there is a new regime with peaks for voltages smaller than the non-magnetic threshold in the AP orientation. For the P case, the magnitude of the oscillations in the current does not change very much with respect to the case with equal polarization in both electrodes. Although the shape of the peaks in TMR are strongly modified when there is electrode polarization asymmetry, the values of TMR are of the same order as the one found for $p_1 = p_2$.

The current in the AP orientation is more strongly affected by the temperature than in the P one. And the TMR depends on temperature, decreasing when it increases.

For arrays with resistance disorder, the current depends on the resistance disorder configuration, but the current shows the same regimes as in the case with all the resistances equal. Except at very high voltages, the TMR is not affected by the resistance disorder and the values obtained are equal than in the case without resistance disorder. For the case of a single nanoparticle there is only spin accumulation in the AP orientation. For resistance disordered arrays the current is spin polarized in both P and AP orientations.

The charge disorder destroys the spin dependence of the current on the magnetic configuration of the electrodes. As a consequence the $I - V$ curves in both magnetic configurations are very similar, resulting in very small values of the TMR. In some systems like self-assembled arrays this kind of disorder seems unavoidable because of charges quenched on the substracte. However, in other devices like epitaxially grown pillars the disorder will be probably less important, what makes them a better candidate to observe these effects.

The long-range interactions affect the transport properties. When the arrays are placed between two ferromagnetic electrodes, the current is determined by the interplay between the long-range of the interactions and the spin accumulation. The effect of the latter decreases when the long-range of interaction increases. Thus, for very large values of a_o the oscillations disappears and the values of the TMR are very much reduced with respect to the short range interaction. The effect of the long-range of interaction is less important in long arrays.

Summary of Part II

In this part of the thesis we have seen how the interplay between ferromagnetism and charging effects controls the electronic transport through metallic nanoparticle arrays when they are placed between two ferromagnetic electrodes.

For clean nanoparticle arrays with equal spin polarization in both electrodes and short range interactions, when the spin relaxation time is long, spin accumulation not only appears in the AP orientation, as it occurs in the case of a single nanoparticle, but also in the P configuration. While the spin accumulation is quite homogeneous through the array in the AP orientation, for the P one the spin accumulation changes its sign within the array. In this last case, we have seen that the spin accumulation has a very strong effect in the transport properties.

The current is a strongly non-linear function of the voltage for both magnetic configurations. The main differences with respect to the case with non-magnetic electrodes studied in the first part of this thesis occur for P orientation. In this case, we have found that not only the threshold voltage at which the current starts to flow is reduced with respect to the non-magnetic case, but also a new regime with negative differential conductance appears at voltages smaller than the non-magnetic threshold. This unexpected regime originates in the inhomogeneity of the spin potentials created through the array by the spin accumulation.

We have seen that the oscillations that appear in the current, spin accumulation and spin polarization of the current in the P orientaion not only are correlated between them, but also with the oscillations in the TMR. Besides, the number of oscillations depends on the size of the array, increasing with the number of nanoparticles.

The values of TMR that we have obtained in nanoparticle arrays can be up several orders in magnitude larger than those found in the case of a single nanoparticle.

We have analyzed how these effects are affected by a polarization asymmetry of the electrodes, the dimensionality of the array, the temperature, resistance or charge disorder and long-range interactions. The regime with negative differential conductance and the oscillations in the TMR are robust to several of the modifications that can appear in an experiment.

The dimensionality of the array does not affect the value of the TMR. We have found similar values of TMR for one and two-dimensional arrays with square lattice. This occurs because in two-dimensional arrays with square lattice each row can be approximated as a conducting channel which contributes to the current. Thus, the current increases with the number of rows in both P and AP magnetic orientations, resulting in similar values of TMR that those found in a one-dimensional case.

A similar situation has been obtained in nanoparticle arrays with resistance disorder. The TMR is not affected by this type of disorder. Although the current depends on the resistance disorder configuration, the $I - V$ curves show the same regime as in the case without any kind of disorder.

For electrode polarization asymmetry, $p_1 \neq p_2$, we have found that the regime with peaks in the current and negative differential conductance not only appears in P orientation, but also in the AP one. Although the shape of the peaks can be strongly modified depending on the asymmetry, the magnitude of the oscillations in the TMR does not change much.

The TMR depends on the temperature, decreasing when it increases. The huge enhancement of the TMR in nanoparticle arrays occurs at low temperature. For this reason, in the experiments the temperature should be kept as small as can be possible, taking into account that $K_B T << E_c$.

We have seen that the charge disorder destroys the spin dependence of the current on the magnetic configurations of the electrodes. As a result, the TMR is practically eliminated. This type of disorder should be avoided in the experiments. Although in systems like self-assembly arrays that is impossible because of charges quenched on the substracte, there are other devices such as the pillars grown epitaxially in which the charge disorder is expected to be less important.

In many arrays the long-range part of the interaction is screened by mobile charges in neigbour conductors. If this does not happen the TMR can be suppressed with respect to the onsite interactions case. As we have observed this effect is less important in long arrays. Thus, if the length of the interaction has to be taken into account the oscillations and large values of the TMR will be better observed in long arrays.

Publications

Part of the work presented in this thesis has given rise to the following publications:

- "*Electronic correlations and disorder in transport through one-dimensional nanoparticle arrays*"

  E. Bascones, V. Estévez, J.A. Trinidad and A.H. MacDonald, Phys. Rev. B **77**, 245422 (2008).

- "*Enhancement of the magnetoresistance and negative differential conductance of nanostructures arrays*"

  V. Estévez and E. Bascones, Phys. Rev. B **83**, 020408(R) (2011).

- "*Absence of scaling in transport through two-dimensional nanoparticle arrays*"

  V. Estévez and E. Bascones, arXiv:1011.0605.

- "*Robustness of the magnetoresistance of nanoparticle arrays*"

  V. Estévez and E. Bascones, arXiv:1012.3887.

Bibliography

[1] R. Parthasarathy, X. Lin, and H. M. Jaeger. *"Electronic Transport in Metal Nanocrystal Arrays: The Effect of Structural Disorder on Scaling Behavior"*. Phys. Rev. Lett. **87**, 186807 (2001). (cited on pages 1, 9, 10, 11, 14, 59, 73, 75, 76, and 80)

[2] R. L. Whetten, J. T. Khoury, M. M. Alvarez, S. Murthy, I. Vezmar, Z. L. Wang, P. W. Stephens, C. L. Cleveland, W. D. Luedtke, and U. Landman. *"Nanocrystal gold molecules"*. Advanced Materials **8**, 428 (1996). (cited on p. 1)

[3] C. P. Collier, R. J. Saykally, J. J. Shiang, S. E. Henrichs, and J. R. Heath. *"Reversible Tuning of Silver Quantum Dot Monolayers Through the Metal-Insulator Transition"*. Science **277**, 1978 (1997). (cited on p. 1)

[4] G. Markovich, C. P. Collier, S. E. Henrichs, F. Remacle, R. D. Levine, and J. R. Heath. *"Architectonic Quantum Dot Solids"*. Acc. Chem. Res. **32**, 415 (1999). (cited on p. 1)

[5] H. Brune, M. Giovannini, K. Bromann, and K. Kern. *"Self-organized growth of nanostructure arrays on strain-relief patterns"*. Nature **394**, 451 (1998). (cited on p. 1)

[6] C. Chin. *"Fabrication of metallic nanoparticle arrays"*. Journal of Young Investigators **16** (2007). (cited on pages 1 and 2)

[7] J. D. Le, Y. Pinto, N. C. Seeman, K. Musier-Forsyth, T. A. Taton, and R. A. Kiehl. *"DNA-Templated Self-Assembly of Metallic Nanocomponent Arrays on a Surface"*. Nano Lett. **4**, 2343 (2004). (cited on p. 1)

[8] Y. Lin, A. Boker, J. He, K. Sill, H. Xiang, C. Abetz, X. Li, J. Wang, T. Emrick, S. Long, Q. Wang, A. Balazs, and T. P. Russell. *"Self-directed self-assembly of nanoparticle/copolymer mixtures"*. Nature **434**, 55 (2005). (cited on p. 1)

[9] K. Elteto, X. Lin, and H. M. Jaeger. *"Electronic transport in quasi-one-dimensional arrays of gold nanocrystals"*. Phys. Rev. B **71**, 205412 (2005). (cited on pages 1 and 34)

[10] J. Zhang, Y. Liu, Y. Ke, and H. Yan. Periodic Square-Like gold nanoparticle arrays templated by Self-Assembled 2D DNA nanogrids on a surface. Nano Lett. **6**, 248 (2006). (cited on pages 1, 11, and 56)

[11] T. P. Bigioni, X. Lin, T. T. Nguyen, E. I. Corwin, T. A. Witten, and H. M. Jaeger. *"Kinetically driven self assembly of highly ordered nanoparticle monolayers"*. Nature Mat. **5**, 265 (2006). (cited on p. 1)

[12] J. Liao, L. Bernard, M. Langer, C. Schönenberger, and M. Calame. *"Reversible Formation of Molecular Junctions in 2D Nanoparticle Arrays"*. Advanced Materials **18**, 2803 (2006). (cited on p. 1)

[13] S. S. Mark, M. Bergkvist, X. Yang, L. M. Teixeira, P. Bhatnagar, E. R. Angert, and C. A. Batt. *"Bionanofabrication of Metallic and Semiconductor Nanoparticle Arrays Using S-Layer Protein Lattices with Different Lateral Spacings and Geometries"*. Langmuir **22**, 3763 (2006). (cited on p. 1)

[14] C. B. Murray, C. R. Kagan, and M. G. Bawendi. *"Self-Organization of CdSe Nanocrystallites into Three-Dimensional Quantum Dot Superlattices"*. Science **270**, 1335 (1995). (cited on p. 1)

[15] D. V. Talapin, E. V. Shevchenko, A. Kornowski, N. Gaponik, M. Haase, A. L. Rogach, and H. Weller. *"A New Approach to Crystallization of CdSe Nanoparticles into Ordered Three-Dimensional Superlattices"*. Advanced Materials **13**, 1868 (2001). (cited on p. 1)

[16] N. Y. Morgan, C. A. Leatherdale, M. Drndić, M. V. Jarosz, M. A. Kastner, and M. Bawendi. *"Electronic transport in films of colloidal CdSe nanocrystals"*. Phys. Rev. B **66**, 075339 (2002). (cited on p. 1)

[17] V. J. Porter, T. Mentzel, S. Charpentier, M. A. Kastner, and M. G. Bawendi. *"Temperature-, gate-, and photoinduced conductance of close-packed CdTe nanocrystal films"*. Phys. Rev. B **73**, 155303 (2006). (cited on p. 1)

[18] D. Yu, C. Wang, B. L. Wehrenberg, and P. Guyot-Sionnest. *"Variable Range Hopping Conduction in Semiconductor Nanocrystal Solids"*. Phys. Rev. Lett. **92**, 216802 (2004). (cited on p. 1)

[19] H. E. Romero and M. Drndic. *"Coulomb Blockade and Hopping Conduction in PbSe Quantum Dots"*. Phys. Rev. Lett. **95**, 156801 (2005). (cited on pages 1 and 75)

[20] T. Feng, H. Yu, M. Dicken, J. R. Heath, and H. A. Atwater. *"Probing the size and density of silicon nanocrystals in nanocrystal memory device applications"*. App. Phys. Lett. **86**, 033103 (2005). (cited on p. 1)

[21] C. I. Durüz, R. M. Clarke, C. M. Marcus, and J. Harris. *"Conduction Threshold, Switching, and Hysteresis in Quantum Dot Arrays"*. Phys. Rev. Lett. **74**, 3237 (1995). (cited on pages 1, 2, 14, 73, 74, and 80)

[22] K. Xu, L. Qin, and J. R. Heath. *"The crossover from two dimensions to one dimension in granular electronic materials"*. Nature Nanotech. **4**, 368 (2009).
(cited on pages 1 and 34)

[23] S. Sun, C. B. Murray, D. Weller, L. Folks, and A. Moser. *"Monodisperse FePt Nanoparticles and Ferromagnetic FePt Nanocrystal Superlattices"*. Science **287**, 1989 (2000).
(cited on p. 1)

[24] C. T. Black, C. B. Murray, R. L. Sandstrom, and S. Sun. *"Spin-Dependent Tunneling in Self-Assembled Cobalt-Nanocrystal Superlattices"*. Science **290**, 1131 (2000).
(cited on pages 1, 14, 73, 74, 80, and 96)

[25] V. F. Puntes, P. Gorostiza, D. M. Aruguete, N. G. Bastus, and A. P. Alivisatos. *"Collective behaviour in two-dimensional cobalt nanoparticle assemblies observed by magnetic force microscopy"*. Nature Mat. **3**, 263 (2004). (cited on p. 1)

[26] F. X. Redl, K. Cho, C. B. Murray, and S. O'Brien. *"Three-dimensional binary superlattices of magnetic nanocrystals and semiconductor quantum dots"*. Nature **423**, 968 (2003).
(cited on pages 1 and 3)

[27] E. V. Shevchenko, D. V. Talapin, N. A. Kotov, S. O'Brien, and C. B. Murray. *"Structural diversity in binary nanoparticle superlattices"*. Nature **439**, 55 (2006). (cited on p. 1)

[28] J. L. Wasserman, K. Lucas, S. H. Lee, A. Ashton, C. T. Crowl, and N. Marković. *"Fabrication of one-dimensional programmable-height nanostructures via dynamic stencil deposition"*. The Review of Scientific Instruments **79**, 073909 (2008). PMID: 18681718.
(cited on p. 2)

[29] F. Solá, O. Resto, A. Biaggi-Labiosa, and L. F. Fonseca. *"Growth and characterization of branched carbon nanostructures arrays in nano-patterned surfaces from porous silicon substrates"*. Micron **40**, 80 (2009). (cited on p. 3)

[30] H. Grabert, M. H. Devoret, and N. A. T. O. S. A. Division. *Single charge tunneling: Coulomb blockade phenomena in nanostructures* (Plenum Press, 1992).
(cited on pages 5, 6, 13, 14, 20, 33, 39, 80, 116, and 161)

[31] K. Likharev. *"Single-electron transistors: Electrostatic analogs of the DC SQUIDS"*. Magnetics, IEEE Transactions on **23**, 1142 (1987). (cited on pages 6, 13, 14, 39, and 80)

[32] K. Mullen, E. Ben-Jacob, R. C. Jaklevic, and Z. Schuss. *"I-V characteristics of coupled ultrasmall-capacitance normal tunnel junctions"*. Phys. Rev. B **37**, 98 (1988).
(cited on pages 6, 14, and 39)

[33] B. Laikhtman. *"Current-voltage characteristic of double normal tunnel junctions"*. Phys. Rev. B **43**, 2731 (1991). (cited on pages 6, 14, and 39)

[34] J. Wan, K. A. McGreer, L. I. Glazman, A. M. Goldman, and R. I. Shekhter. *"Two-state approximation in the Coulomb-blockade theory: Simple analytical results for a double-tunnel junction"*. Phys. Rev. B **43**, 9381 (1991). (cited on pages 6, 14, and 39)

[35] M. Amman, R. Wilkins, E. Ben-Jacob, P. D. Maker, and R. C. Jaklevic. *"Analytic solution for the current-voltage characteristic of two mesoscopic tunnel junctions coupled in series"*. Phys. Rev. B **43**, 1146 (1991). (cited on pages 6, 14, 33, and 39)

[36] A. E. Hanna and M. Tinkham. *"Variation of the Coulomb staircase in a two-junction system by fractional electron charge"*. Phys. Rev. B **44**, 5919 (1991). (cited on pages 6, 14, 33, and 39)

[37] M. Stopa. *"Coulomb staircase and Wigner crystalline states in single-electron tunneling through one-dimensional arrays"*. Phys. Rev. B **64**, 193315 (2001). (cited on pages 7, 39, and 48)

[38] C. J. Gorter. *"A possible explanation of the increase of the electrical resistance of thin metal films at low temperatures and small field strengths"*. Physica **17**, 777 (1951). (cited on p. 8)

[39] C. A. Neugebauer and M. B. Webb. *"Electrical Conduction Mechanism in Ultrathin, Evaporated Metal Films"*. Jour. of App. Phys. **33**, 74 (1962). (cited on p. 8)

[40] I. Giaever and H. R. Zeller. *"Superconductivity of Small Tin Particles Measured by Tunneling"*. Phys. Rev. Lett. **20**, 1504 (1968). (cited on p. 8)

[41] J. Lambe and R. C. Jaklevic. *"Charge-Quantization Studies Using a Tunnel Capacitor"*. Phys. Rev. Lett. **22**, 1371 (1969). (cited on p. 8)

[42] C. T. Black, D. C. Ralph, and M. Tinkham. *"Spectroscopy of the Superconducting Gap in Individual Nanometer-Scale Aluminum Particles"*. Phys. Rev. Lett. **76**, 688 (1996). (cited on p. 8)

[43] D. C. Ralph, C. T. Black, and M. Tinkham. it "Gate-Voltage Studies of Discrete Electronic States in Aluminum Nanoparticles". Phys. Rev. Lett. **78**, 4087 (1997). (cited on p. 8)

[44] O. Agam, N. S. Wingreen, B. L. Altshuler, D. C. Ralph, and M. Tinkham. *"Chaos, Interactions, and Nonequilibrium Effects in the Tunneling Resonance Spectra of Ultrasmall Metallic Particles"*. Phys. Rev. Lett. **78**, 1956 (1997). (cited on p. 8)

[45] D. G. Salinas, S. Guëron, D. C. Ralph, C. T. Black, and M. Tinkham. *"Effects of spin-orbit interactions on tunneling via discrete energy levels in metal nanoparticles"*. Phys. Rev. B **60**, 6137 (1999). (cited on p. 8)

[46] S. Guéron, M. M. Deshmukh, E. B. Myers, and D. C. Ralph. *"Tunneling via Individual Electronic States in Ferromagnetic Nanoparticles"*. Phys. Rev. Lett. **83**, 4148 (1999). (cited on p. 8)

[47] D. Davidović and M. Tinkham. *"Spectroscopy, Interactions, and Level Splittings in Au Nanoparticles"*. Phys. Rev. Lett. **83**, 1644 (1999). (cited on p. 8)

[48] D. Davidović and M. Tinkham. *"Fine structure in the energy spectra of ultrasmall Au nanoparticles"*. Phys. Rev. B **61**, R16359 (2000). (cited on p. 8)

[49] L. L. Sohn, L. P. Kouwenhoven, and G. Schön. *Mesoscopic electron transport* (Springer, 1997). (cited on p. 8)

[50] J. H. F. Scott-Thomas, S. B. Field, M. A. Kastner, H. I. Smith, and D. A. Antoniadis. *"Conductance Oscillations Periodic in the Density of a One-Dimensional Electron Gas"*. Phys. Rev. Lett. **62**, 583 (1989). (cited on p. 8)

[51] S. J. Tans, A. R. M. Verschueren, and C. Dekker. *"Room-temperature transistor based on a single carbon nanotube"*. Nature **393**, 49 (1998). (cited on p. 8)

[52] P. Lafarge, H. Pothier, E. R. Williams, D. Esteve, C. Urbina, and M. H. Devoret. *"Direct observation of macroscopic charge quantization"*. Zeitschrift für Physik B Condensed Matter **85**, 327 (1991). (cited on p. 9)

[53] U. Meirav, P. L. McEuen, M. A. Kastner, E. B. Foxman, A. Kumar, and S. J. Wind. *"Conductance oscillations and transport spectroscopy of a quantum dot"*. Zeitschrift für Physik B Condensed Matter **85**, 357 (1991). (cited on p. 9)

[54] L. P. Kouwenhoven, N. C. Vaart, A. T. Johnson, W. Kool, C. J. P. M. Harmans, J. G. Williamson, A. A. M. Staring, and C. T. Foxon. *"Single electron charging effects in semiconductor quantum dots"*. Zeitschrift für Physik B Condensed Matter **85**, 367 (1991). (cited on p. 9)

[55] L. P. Kouwenhoven, A. T. Johnson, N. C. Vaart, A. Enden, C. J. P. M. Harmans, and C. T. Foxon. *"Quantized current in a quantum dot turnstile"*. Zeitschrift für Physik B Condensed Matter **85**, 381 (1991). (cited on p. 9)

[56] P. Sheng and B. Abeles. *"Voltage-Induced Tunneling Conduction in Granular Metals at Low Temperatures"*. Phys. Rev. Lett. **28**, 34 (1972). (cited on p. 9)

[57] P. Sheng, B. Abeles, and Y. Arie. *"Hopping Conductivity in Granular Metals"*. Phys. Rev. Lett. **31**, 44 (1973). (cited on p. 9)

[58] J. S. Helman and B. Abeles. *"Tunneling of Spin-Polarized Electrons and Magnetoresistance in Granular Ni Films"*. Phys. Rev. Lett. **37**, 1429 (1976). (cited on p. 9)

[59] J. J. Shiang, J. R. Heath, C. P. Collier, and R. J. Saykally. *"Cooperative Phenomena in Artificial Solids Made from Silver Quantum Dots: The Importance of Classical Coupling"*. The Journal of Physical Chemistry B **102**, 3425 (1998). (cited on p. 9)

[60] S. Kim, G. Medeiros-Ribeiro, D. A. A. Ohlberg, R. S. Williams, and J. R. Heath. *"Individual and Collective Electronic Properties of Ag Nanocrystals"*. The Journal of Physical Chemistry B **103**, 10341 (1999). (cited on p. 9)

[61] Sampaio, K. C. Beverly, and J. R. Heath. *"DC Transport in Self-Assembled 2D Layers of Ag Nanoparticles"*. The Journal of Physical Chemistry B **105**, 8797 (2001). (cited on p. 9)

[62] I. S. Weitz, J. L. Sample, R. Ries, E. M. Spain, and J. R. Heath. *"Josephson Coupled Quantum Dot Artificial Solids"*. The Journal of Physical Chemistry B **104**, 4288 (2000). (cited on p. 9)

[63] A. Courty, A. Mermet, P. A. Albouy, E. Duval, and M. P. Pileni. *"Vibrational coherence of self-organized silver nanocrystals in f.c.c. supra-crystals"*. Nature Mat. **4**, 395 (2005). (cited on p. 9)

[64] A. A. Middleton and N. S. Wingreen. *"Collective transport in arrays of small metallic dots"*. Phys. Rev. Lett. **71**, 3198 (1993). (cited on pages 9, 12, 13, 15, 33, 34, 52, 55, 59, 73, 75, 76, 80, 88, 89, 92, 96, and 161)

[65] M. Shin, S. Lee, K. W. Park, and E. Lee. *"Geometrically Induced Multiple Coulomb Blockade Gaps"*. Phys. Rev. Lett. **80**, 5774 (1998). (cited on p. 9)

[66] D. M. Kaplan, V. A. Sverdlov, and K. K. Likharev. *"Subelectron transport in single-electron-tunneling arrays"*. Phys. Rev. B **65**, 193309 (2002). (cited on pages 9 and 55)

[67] D. M. Kaplan, V. A. Sverdlov, and K. K. Likharev. *"Shot noise in frustrated single-electron arrays"*. cond-mat/0303477 (2003). (cited on pages 9 and 73)

[68] Y. A. Kinkhabwala, V. A. Sverdlov, and K. K. Likharev. *"A numerical study of Coulomb interaction effects on 2D hopping transport"*. J. Phys.: Condens. Matter **18**, 2013 (2006). (cited on p. 9)

[69] I. S. Beloborodov, A. V. Lopatin, V. M. Vinokur, and K. B. Efetov. *"Granular electronic systems"*. Rev. Mod. Phys. **79**, 469 (2007). (cited on p. 9)

[70] I. S. Beloborodov, A. Glatz, and V. M. Vinokur. *"Transport properties of semiconducting nanocrystal arrays at low temperatures"*. Phys. Rev. B **75**, 052302 (2007). (cited on p. 9)

[71] T. B. Tran, I. S. Beloborodov, X. M. Lin, T. P. Bigioni, V. M. Vinokur, and H. M. Jaeger. *"Multiple Cotunneling in Large Quantum Dot Arrays"*. Phys. Rev. Lett. **95**, 076806 (2005). (cited on p. 9)

[72] A. Altland, L. I. Glazman, and A. Kamenev. *"Electron Transport in Granular Metals"*. Phys. Rev. Lett. **92**, 026801 (2004). (cited on p. 9)

[73] Y. L. Loh, V. Tripathi, and M. Turlakov. *"Effective charging energy for a regular granular metal array"*. Phys. Rev. B **72**, 233404 (2005). (cited on p. 9)

[74] K. B. Efetov and A. Tschersich. *"Transition from insulating to non-insulating temperature dependence of the conductivity in granular metals"*. Europhys. Lett. **59**, 114 (2002). (cited on p. 9)

[75] J. Zhang and B. I. Shklovskii. Density of states and conductivity of a granular metal or an array of quantum dots. Phys. Rev. B **70**, 115317 (2004). (cited on p. 9)

[76] D. S. Novikov, B. Kozinsky, and L. S. Levitov. *"Correlated electron states and transport in triangular arrays"*. Phys. Rev. B **72**, 235331 (2005). (cited on p. 9)

[77] M. M. Fogler, S. V. Malinin, and T. Nattermann. *"Coulomb Blockade and Transport in a Chain of One-Dimensional Quantum Dots"*. Phys. Rev. Lett. **97**, 096601 (2006). (cited on p. 9)

[78] A. Bezryadin, R. M. Westervelt, and M. Tinkham. *"Self-assembled chains of graphitized carbon nanoparticles"*. App. Phys. Lett. **74**, 2699 (1999). (cited on pages 9, 10, 14, 23, 34, and 80)

[79] R. Parthasarathy, X. Lin, K. Elteto, T. F. Rosenbaum, and H. M. Jaeger. *"Percolating through Networks of Random Thresholds: Finite Temperature Electron Tunneling in Metal Nanocrystal Arrays"*. Phys. Rev. Lett. **92**, 076801 (2004). (cited on pages 11, 25, 59, 73, and 75)

[80] K. Elteto, E. G. Antonyan, T. T. Nguyen, and H. M. Jaeger. *"Model for the onset of transport in systems with distributed thresholds for conduction"*. Phys. Rev. B **71**, 064206 (2005). (cited on pages 11 and 25)

[81] K. C. Beverly, J. F. Sampaio, and J. R. Heath. *"Effects of Size Dispersion Disorder on the Charge Transport in Self-Assembled 2-D Ag Nanoparticle Arrays"*. The Journal of Physical Chemistry B **106**, 2131 (2002). (cited on p. 11)

[82] F. Remacle, C. P. Collier, G. Markovich, J. R. Heath, U. Banin, and R. D. Levine. *"Networks of Quantum Nanodots: The Role of Disorder in Modifying Electronic and Optical Properties"*. The Journal of Physical Chemistry B **102**, 7727 (1998). (cited on p. 11)

[83] F. Remacle, K. C. Beverly, J. R. Heath, and R. D. Levine. *"Conductivity of 2-D Ag Quantum Dot Arrays: Computational Study of the Role of Size and Packing Disorder at Low Temperatures"*. The Journal of Physical Chemistry B **106**, 4116 (2002). (cited on p. 11)

[84] A. S. Cordan, A. Goltzené, Y. Hervé, M. Mejias, C. Vieu, and H. Launois. *"Electron transport in metallic dot arrays: Effect of a broad dispersion in the tunnel junction dimensions"*. Jour. of App. Phys. **84**, 3756 (1998). (cited on p. 11)

[85] A. Pépin, C. Vieu, M. Mejias, Y. Jin, F. Carcenac, J. Gierak, C. David, L. Couraud, H. Launois, A. S. Cordan, Y. Leroy, and A. Goltzené. *"Temperature evolution of multiple tunnel junction devices made with disordered two-dimensional arrays of metallic islands"*. App. Phys. Lett. **74**, 3047 (1999). (cited on p. 11)

[86] A. S. Cordan, Y. Leroy, A. Goltzené, A. Pépin, C. Vieu, M. Mejias, and H. Launois. *"Temperature behavior of multiple tunnel junction devices based on disordered dot arrays"*. Jour. of App. Phys. **87**, 345 (2000). (cited on pages 11, 14, and 80)

[87] Y. Leroy, A. S. Cordan, and A. Goltzené. *"Variance analysis of the Coulomb blockade parameters in nanometer-size disordered arrays"*. Jour. of App. Phys. **90**, 953 (2001). (cited on p. 11)

[88] S. Roux and H. J. Herrmann. *"Disorder-Induced Nonlinear Conductivity"*. Europhys. Lett. **4**, 1227 (1987). (cited on pages 12, 73, and 74)

[89] D. M. Kaplan, V. A. Sverdlov, and K. K. Likharev. *"Coulomb gap, Coulomb blockade, and dynamic activation energy in frustrated single-electron arrays"*. Phys. Rev. B **68**, 045321 (2003). (cited on pages 12, 13, 15, 34, 61, 74, 75, and 80)

[90] C. Reichhardt and C. J. O. Reichhardt. *"Temperature and ac effects on charge transport in arrays of metallic dots"*. Phys. Rev. B **68**, 165305 (2003). (cited on pages 12, 15, 23, 33, 73, and 74)

[91] M. Šuvakov and B. Tadić. Collective charge fluctuations in single-electron processes on nanonetworks. Journal of Statistical Mechanics: Theory and Experiment **2009**, P02015 (2009). (cited on pages 12, 73, 74, and 82)

[92] M. Blunt, F. Suvakov, C. P. Pulizzi, E. Martin, A. Pauliac-Vaujour, A. Stannard, B. Rushforth, P. Tadic, and P. P. Moriarty. *"Charge transport in cellular nanoparticle networks: meandering through nanoscale mazes"*. Nano Lett. **7**, 855 (2007). (cited on pages 12, 13, 74, 75, and 76)

[93] Y. Xue and M. A. Ratner. *"Microscopic theory of single-electron tunneling through molecular-assembled metallic nanoparticles"*. Phys. Rev. B **68**, 235410 (2003). (cited on p. 12)

[94] G. Schön and A. D. Zaikin. *"Quantum coherent effects, phase transitions, and the dissipative dynamics of ultra small tunnel junctions"*. Phys. Rep. **198**, 237 (1990). (cited on pages 13 and 80)

[95] N. Bakhvalov, G. Kazacha, K. Likharev, and S. Serdyukova. *"Statics and dynamics of single-electron solitons in two-dimensional arrays of ultrasmall tunnel junctions"*. Physica B: Condensed Matter **173**, 319 (1991). (cited on pages 13, 66, and 80)

[96] W. Chen, H. Ahmed, and K. Nakazoto. *"Coulomb blockade at 77 K in nanoscale metallic islands in a lateral nanostructure"*. App. Phys. Lett. **66**, 3383 (1995). (cited on pages 14 and 80)

[97] I. Kurdak, A. J. Rimberg, T. R. Ho, and J. Clarke. *"Activated transport and scaling behavior in the current-voltage characteristics and Coulomb-blockade oscillations of two-dimensional arrays of metallic islands"*. Phys. Rev. B **57**, R6842 (1998). (cited on pages 14, 15, 55, 73, 74, 76, 80, and 92)

[98] A. J. Rimberg, T. R. Ho, and J. Clarke. *"Scaling Behavior in the Current-Voltage Characteristic of One- and Two-Dimensional Arrays of Small Metallic Islands"*. Phys. Rev. Lett. **74**, 4714 (1995). (cited on pages 14, 73, 74, 80, and 96)

[99] C. Schönenberger, H. van Houten, and H. C. Donkersloot. *"Single-Electron Tunnelling Observed At Room Temperature by Scanning-Tunnelling Microscopy"*. Europhys. Lett. **20**, 249 (1992). (cited on pages 14, 39, and 80)

[100] T. A. Fulton and G. J. Dolan. *"Observation of single-electron charging effects in small tunnel junctions"*. Phys. Rev. Lett. **59**, 109 (1987). (cited on pages 14 and 80)

[101] E. Bar-Sadeh, Y. Goldstein, C. Zhang, H. Deng, B. Abeles, and O. Millo. *"Single-electron tunneling effects in granular metal films"*. Phys. Rev. B **50**, 8961 (1994). (cited on pages 14, 39, and 80)

[102] S. Jha and A. A. Middleton. *"Effects of Disorder on Electron Transport in Arrays of Quantum Dots"*. cond-mat/0511094 (2005). (cited on pages 15, 34, and 55)

[103] N. Bakhalov, G. Kazacha, K. Likharev, and S. Serdyukova. *"Single-electron solitons in one-dimensional tunnel structure"*. Sov. Phys. JETP **68**, 581 (1989). (cited on pages 15, 25, 26, and 55)

[104] G. Y. Hu and R. F. O'Connell. *"Exact solution for the charge soliton in a one-dimensional array of small tunnel junctions"*. Phys. Rev. B **49**, 16773 (1994). (cited on pages 15, 29, 30, 52, and 55)

[105] J. A. Melsen, U. Hanke, H. Müller, and K. Chao. *"Coulomb blockade threshold in inhomogeneous one-dimensional arrays of tunnel junctions"*. Phys. Rev. B **55**, 10638 (1997). (cited on pages 15, 55, and 161)

[106] C. A. Berven and M. N. Wybourne. *"Effect of self-capacitance on the tunneling thresholds in linear arrays of nanoparticles"*. App. Phys. Lett. **78**, 3893 (2001). (cited on pages 15 and 55)

[107] S. Semrau, H. Schoeller, and W. Wenzel. *"Designable electron transport features in one-dimensional arrays of metallic nanoparticles: Monte Carlo study of the relation between shape and transport"*. Phys. Rev. B **72**, 205443 (2005). (cited on p. 15)

[108] N. Metropolis and S. Ulam. *"Monte carlo method"*. Journal of the American Statistical Association **44**, 335 (1949). (cited on p. 26)

[109] H. G. Katzgraber. *"Introduction to Monte Carlo Methods"*. 0905.1629 (2009). (cited on p. 26)

[110] D. N. Tsigankov, E. Pazy, B. D. Laikhtman, and A. L. Efros. *"Long-time relaxation of interacting electrons in the regime of hopping conduction"*. Phys. Rev. B **68**, 184205 (2003). (cited on p. 27)

[111] J. Sample, K. Beverly, P. Chaudhari, F. Remacle, J. Heath, and R. Levine. *"Imaging Transport Disorder in Conducting Arrays of Metallic Quantum Dots: An Experimental and Computational Study"*. Advanced Materials **14**, 124 (2002). (cited on p. 44)

[112] K. K. Likharev and K. A. Matsuoka. *"Electron-electron interaction in linear arrays of small tunnel junctions"*. App. Phys. Lett. **67**, 3037 (1995). (cited on p. 55)

[113] C. B. Whan, J. White, and T. P. Orlando. *"Full capacitance matrix of coupled quantum dot arrays: Static and dynamical effects"*. App. Phys. Lett. **68**, 2996 (1996). (cited on p. 55)

[114] E. Bascones, V. Estévez, J. A. Trinidad, and A. H. MacDonald. *"Electronic correlations and disorder in transport through one-dimensional nanoparticle arrays"*. Phys. Rev. B **77**, 245422 (2008). (cited on pages 55, 57, and 60)

[115] U. Geigenmüller and G. Schön. *"Single-Electron Effects in Arrays of Normal Tunnel Junctions"*. Europhys. Lett. **10**, 765 (1989). (cited on p. 66)

[116] M. Wybourne, L. Clarke, M. Yan, S. Cai, L. Brown, J. Hutchison, and J. Keana. *"Coulomb-Blockade Dominated Transport in Patterned Gold-Cluster Structures"*. Japanese Journal of Applied Physics **36**, 7796 (1997). (cited on pages 73 and 74)

[117] F. Ruffino, A. M. Piro, G. Piccitto, and M. G. Grimaldi. *"Electronic collective transport in disordered array of C49-phase TiSi[sub 2] nanocrystals in Si"*. Jour. of App. Phys. **101**, 024316 (2007). (cited on pages 73 and 75)

[118] S. K. Bose, R. Sharma, and R. C. Budhani. *"Percolative spin-dependent transport in mesoscopic epitaxial Fe plaquettes of tailored connectivity"*. Phys. Rev. B **78**, 115403 (2008). (cited on pages 73, 74, and 76)

[119] R. P. Tan, J. Carrey, M. Respaud, C. Desvaux, P. Renaud, and B. Chaudret. *"High-field and low-field magnetoresistances of CoFe nanoparticles elaborated by organometallic chemistry"*. Jour. of App. Phys. **103**, 07F317 (2008). (cited on p. 73)

[120] T. Okamoto, H. Maki, Y. Oba, S. Yabuuchi, T. Sato, and E. Ohta. *"Electrical detection of ferromagnetism in Pd nanoparticles by magnetoresistance measurement"*. Jour. of App. Phys. **106**, 023908 (2009). (cited on p. 73)

[121] R. Sachser, F. Porrati, and M. Huth. *"Hard energy gap and current-path switching in ordered two-dimensional nanodot arrays prepared by focused electron-beam-induced deposition"*. Phys. Rev. B **80**, 195416 (2009). (cited on pages 73, 75, and 92)

[122] R. P. Tan, J. Carrey, C. Desvaux, L. Lacroix, P. Renaud, B. Chaudret, and M. Respaud. *"Magnetoresistance and collective Coulomb blockade in superlattices of ferromagnetic CoFe nanoparticles"*. Phys. Rev. B **79**, 174428 (2009). (cited on pages 73, 74, and 92)

[123] Y. C. Ou, S. F. Cheng, and W. B. Jian. *"Size dependence in tunneling spectra of PbSe quantum-dot arrays"*. Nanotechnology **20**, 285401 (2009). (cited on p. 73)

[124] M. Son, J. Im, K. Wang, S. Oh, Y. Kim, and K. Yoo. *"Surface plasmon enhanced photoconductance and single electron effects in mesoporous titania nanofibers loaded with gold nanoparticles"*. App. Phys. Lett. **96**, 023115 (2010). (cited on p. 73)

[125] M. Šuvakov and B. Tadić. Modeling collective charge transport in nanoparticle assemblies. J. Phys.: Condens. Matter **22**, 163201 (2010). (cited on pages 73, 74, 75, and 82)

[126] M. Kardar, G. Parisi, and Y. Zhang. *"Dynamic Scaling of Growing Interfaces"*. Phys. Rev. Lett. **56**, 889 (1986). (cited on p. 74)

[127] M. G. Ancona, W. Kruppa, R. W. Rendell, A. W. Snow, D. Park, and J. B. Boos. *"Coulomb blockade in single-layer Au nanocluster films"*. Phys. Rev. B **64**, 033408 (2001). (cited on p. 92)

[128] S. A. Wolf, D. D. Awschalom, R. A. Buhrman, J. M. Daughton, S. von Molnar, M. L. Roukes, A. Y. Chtchelkanova, and D. M. Treger. *"Spintronics: A Spin-Based Electronics Vision for the Future"*. Science **294**, 1488 (2001). (cited on p. 113)

[129] S. Maekawa and T. Shinjõ. *"Spin dependent transport in magnetic nanostructures"* (Taylor & Francis, 2002). (cited on p. 113)

[130] M. Johnson. *"Spintronics"*. The Journal of Physical Chemistry B **109**, 14278 (2005). (cited on p. 113)

[131] C. Chappert, A. Fert, and F. N. V. Dau. *"The emergence of spin electronics in data storage"*. Nature Mat. **6**, 813 (2007). (cited on p. 113)

[132] S. Bandyopadhyay and M. Cahay. *"Introduction to Spintronics"* (CRC Press, 2008), 1 edition. (cited on p. 113)

[133] I. Zutic, J. Fabian, and S. D. Sarma. *"Spintronics: Fundamentals and applications"*. Rev. Mod. Phys. **76**, 323 (2004). (cited on p. 113)

[134] J. S. Moodera, X. Hao, G. A. Gibson, and R. Meservey. *"Electron-Spin Polarization in Tunnel Junctions in Zero Applied Field with Ferromagnetic EuS Barriers"*. Phys. Rev. Lett. **61**, 637 (1988). (cited on p. 113)

[135] K. Yakushiji, F. Ernult, H. Imamura, K. Yamane, S. Mitani, K. Takanashi, S. Takahashi, S. Maekawa, and H. Fujimori. *"Enhanced spin accumulation and novel magnetotransport in nanoparticles"*. Nature Mat. **4**, 57 (2005). (cited on pages 113, 116, 117, and 135)

[136] A. Bernand-Mantel, P. Seneor, K. Bouzehouane, S. Fusil, C. Deranlot, F. Petroff, and A. Fert. *"Anisotropic magneto-Coulomb effects and magnetic single-electron-transistor action in a single nanoparticle"*. Nature Phys. **5**, 920 (2009). (cited on p. 113)

[137] M. M. Deshmukh and D. C. Ralph. *"Using Single Quantum States as Spin Filters to Study Spin Polarization in Ferromagnets"*. Phys. Rev. Lett. **89**, 266803 (2002). (cited on p. 113)

[138] Y. Wei, C. Malec, and D. Davidovic. *"Saturation of spin-polarized current in nanometers scale aluminium grains"*. Phys. Rev. B **76**, 195327 (2007). (cited on p. 113)

[139] Y. Chye, M. E. White, E. Johnston-Halperin, B. D. Gerardot, D. D. Awschalom, and P. M. Petroff. *"Spin injection from (Ga,Mn)As into InAs quantum dots"*. Phys. Rev. B **66**, 201301 (2002). (cited on p. 113)

[140] J. Wunderlich, T. Jungwirth, B. Kaestner, A. C. Irvine, A. B. Shick, N. Stone, K.-Y. Wang, U. Rana, A. D. Giddings, C. T. Foxon, R. P. Campion, D. A. Williams, and B. L. Gallagher. *"Coulomb Blockade Anisotropic Magnetoresistance Effect in a (Ga,Mn)As Single-Electron Transistor"*. Phys Rev. Lett. **97**, 077201 (2006). (cited on p. 113)

[141] K. Hamaya, S. Masubuchi, M. Kawamura, T. Machida, M. Jung, K. Shibata, K. Hirakawa, T. Taniyama, S. Ishida, and Y. Arakawa. *"Spin transport through a single*

self-assembled InAs quantum dot with ferromagnetic leads". Applied Physics Lett. **90**, 053108 (2007). (cited on p. 113)

[142] A. N. Pasupathy, R. C. Bialczak, J. Martinek, J. E. Grose, L. A. K. Donev, P. L. McEuen, and D. C. Ralph. *"The Kondo Effect in the Presence of Ferromagnetism"*. Science **306**, 86 (2004). (cited on p. 113)

[143] K. Tsukagoshi, B. W. Alphenaar, and H. Ago. *"Coherent transport of electron spin in a ferromagnetically contacted carbon nanotube"*. Nature **401**, 572 (1999). (cited on p. 113)

[144] B. Zhao, I. Mönch, H. Vinzelberg, T. Mühl, and C. M. Schneider. Spin-coherent transport in ferromagnetically contacted carbon nanotubes. App. Phys. Lett. **80**, 3144 (2002). (cited on p. 113)

[145] S. Sahoo, T. Kontos, J. Furer, C. Hoffmann, M. Gräber, A. Cottet, and C. Schönenberger. *"Electric field control of spin transport"*. Nature Phys. **1**, 99 (2005). (cited on p. 113)

[146] L. E. Hueso, J. M. Pruneda, V. Ferrari, G. Burnell, J. P. Valdes-Herrera, B. D. Simons, P. B. Littlewood, E. Artacho, A. Fert, and N. D. Mathur. *"Transformation of spin information into large electrical signals using carbon nanotubes"*. Nature **445**, 410 (2007). (cited on p. 113)

[147] J. Hauptmann, J. Paaske, and P. Lindelof. *"Electric-field-controlled spin reversal in a quantum dot with ferromagnetic contacts"*. Nature Phys. **4**, 373 (2008). (cited on p. 113)

[148] M. Julliere. *"Tunneling between ferromagnetic films"*. Phys. Lett. A **54**, 225 (1975). (cited on p. 114)

[149] T. Miyazaki, N. Tezuka, and S. Kumagai. Spin-polarized tunneling magnetoresistive effect in ferromagnet/insulator/ferromagnet junctions. Physica B **237-238**, 256 (1997). (cited on p. 114)

[150] J. C. Slonczewski. *"Conductance and exchange coupling of two ferromagnets separated by a tunneling barrier"*. Phys. Rev. B **39**, 6995 (1989). (cited on p. 114)

[151] J. S. Moodera, L. R. Kinder, T. M. Wong, and R. Meservey. *"Large Magnetoresistance at Room Temperature in Ferromagnetic Thin Film Tunnel Junctions"*. Phys. Rev. Lett. **74**, 3273 (1995). (cited on pages 114 and 115)

[152] T. Miyazaki and N. Tezuka. *"Giant magnetic tunneling effect in Fe/Al2O3/Fe junction"*. Journal of Magnetism and Magnetic Materials **139**, L231 (1995). (cited on pages 114 and 115)

[153] P. LeClair, a. H. W. B. Hoex, J. Kohlhepp, H. Swagten, and W. de Jonge. *"Sign reversal of spin polarization in Co/Ru/Al2O3/Co magnetic tunnel junctions"*. Phys. Rev. B **64**, 100406(R) (2001). (cited on p. 114)

[154] M. N. Baibich, J. M. Broto, A. Fert, F. N. V. Dau, F. Petroff, P. Etienne, G. Creuzet, A. Friederich, and J. Chazelas. *"Giant Magnetoresistance of (001)Fe/(001)Cr Magnetic Superlattices"*. Phys. Rev. Lett. **61**, 2472 (1988). (cited on p. 115)

[155] W. H. Butler, X. Zhang, T. C. Schulthess, and J. M. MacLaren. *"Spin-dependent tunneling conductance of Fe|MgO|Fe sandwiches"*. Phys. Rev. B **63**, 054416 (2001). (cited on p. 115)

[156] M. Bowen, V. Cros, F. Petroff, A. Fert, C. M. Boubeta, J. L. Costa-Krämer, J. V. Anguita, A. Cebollada, F. Briones, J. M. de Teresa, L. Morellón, M. R. Ibarra, F. Güell, F. Peiró, and A. Cornet. *"Large magnetoresistance in Fe/MgO/FeCo(001) epitaxial tunnel junctions on GaAs(001)"*. App. Phys. Lett. **79**, 1655 (2001). (cited on p. 115)

[157] J. Faure-Vincent, C. Tiusan, E.Jouguelet, F. Canet, M. Sajieddine, C. Bellouard, E. Popova, M. Hehn, F. Montaigne, and A.Schuhl. *"High tunnel magnetoresistance in epitaxial Fe/MgO/Fe tunnel junctions"*. Appl Phys Rev. Lett. **82**, 4507 (2003). (cited on p. 115)

[158] S. Yuasa, T. Nagahama, A. Fukushima, Y. Suzuki, and K. Ando. *"Giant room-temperature magnetoresistance in single-crystal Fe/MgO/Fe magnetic tunnel junctions"*. Nat. Mater. **3**, 868 (2004). (cited on p. 115)

[159] S. S. P. Parkin, C. Kaiser, A. Panchula, P. M. Rice, B. Hughes, M. Samant, and S. Yang. *"Giant tunnelling magnetoresistance at room temperature with MgO (100) tunnel barriers"*. Nature Mat. **3**, 862 (2004). (cited on p. 115)

[160] D. D. Djayaprawira, K. Tsunekawa, M. Nagai, H. Maehara, S. Yamagata, N. Watanabe, S. Yuasa, Y. Suzuki, and K. Ando. *"230 % room-temperature magnetoresistance in CoFeB/MgO/CoFeB magnetic tunnel junctions"*. Appl. Phys. Lett. **86**, 092502 (2005). (cited on p. 115)

[161] M. Lee, J.Hayakawa, S. Ikeda, F. Matsukura, and J.Ohno. *"Giant tunnel magnetoresistance and high annealing stability in CoFeB/MgO/CoFeB magnetic tunnel junctions with synthetic pinned layer"*. Appl. Phys. Lett. **89**, 042506 (2006). (cited on p. 115)

[162] S. Yuasa, A. Fukushima, H. Kubota, Y. Suzuki, and K. Ando. *"Giant tunneling magnetoresistance up to 410temperature in fully epitaxial Co/MgO/Co magnetic tunnel junctions with bcc Co(001) electrodes"*. Appl Phys Lett. **89**, 042505 (2006). (cited on p. 115)

[163] Y. Lee, J. Hayakawa, S. Ikeda, F. Matsukura, and H. Ohno. *"Effect of electrode composition on the tunnel magnetoresistance of pseudo-spin-valve magnetic tunnel junction with a MgO tunnel barrier"*. App. Phys. Lett. **90**, 212507 (2007). (cited on p. 115)

[164] J. Hauch, M. Fonin, M. Fraune, P.Turban, R.Guerrero, F. Aliev, J. Mayer, U. Rüdiger, and G. Güntherodt. *"Fully epitaxial Fe(110)/MgO(111)/Fe(110) magnetic tunnel junctions: Growth, transport, and spin filtering properties"*. App. Phys. Lett. **93**, 083512 (2008). (cited on p. 115)

[165] M. Johnson and R. H. Silsbee. *"Interfacial charge-spin coupling: Injection and detection of spin magnetization in metals"*. Phys. Rev. Lett. **55**, 1790 (1985). (cited on pages 115, 116, and 118)

[166] V. Estévez and E. Bascones. *"Enhancement of the magnetoresistance and negative differential conductance of nanostructure arrays"*. Phys. Rev. B **83**, 020408 (2011). (cited on p. 115)

[167] F. J. Jedema, A. T. Filip, and B. J. van Wees. *"Electrical spin injection and accumulation at room temperature in an all-metal mesoscopic spin valve"*. Nature **410**, 345 (2001). (cited on p. 116)

[168] J. Barnaś and A. Fert. *"Effects of spin accumulation on single-electron tunneling in a double ferromagnetic microjunction"*. Europhys. Lett. **44**, 85 (1998). (cited on pages 116, 117, and 135)

[169] I. Weymann and J. Barnasacute. *"Negative differential conductance and magnetoresistance oscillations due to spin accumulation in ferromagnetic double-island devices"*. Phys. Rev. B **73**, 033409 (2006). (cited on pages 116 and 117)

[170] K. Ono, H. Shimada, and Y. Ootuka. *"Enhanced Magnetic Valve Effect and Magneto-Coulomb Oscillations in Ferromagnetic Single Electron Transistor"*. J. Phys. Soc. Jpn. **66**, 1261 (1997). (cited on pages 116 and 120)

[171] J. Barnaś and A. Fert. *"Magnetoresistance Oscillations due to Charging Effects in Double Ferromagnetic Tunnel Junctions"*. Phys. Rev. Lett. **80**, 1058 (1998). (cited on p. 116)

[172] J. Barnas and A. Fert. *"Interplay of spin accumulation and Coulomb blockade in double ferromagnetic junctions"*. Journal of Magnetism and Magnetic Materials **192**, 391 (1999). (cited on p. 116)

[173] S. Takahashi and S. Maekawa. *"Effect of Coulomb Blockade on Magnetoresistance in Ferromagnetic Tunnel Junctions"*. Phys. Rev. Lett. **80**, 1758 (1998). (cited on p. 116)

[174] A. Brataas, Y. V. Nazarov, J. Inoue, and G. E. W. Bauer. *"Spin accumulation in small ferromagnetic double-barrier junctions"*. Phys. Rev. B **59**, 93 (1999). (cited on p. 116)

[175] H. Imamura, S. Takahashi, and S. Maekawa. *"Spin-dependent Coulomb blockade in ferromagnet/normal-metal/ferromagnet double tunnel junctions"*. Phys. Rev. B **59**, 6017 (1999). (cited on p. 116)

[176] G. Michalek, J. Martinek, J. Barnas, and B. Bulka. *"Therory of spin effect on Coulomb blockade of single-electron tunneling in ferromagnetic systems"*. Ann. Phys. (Leipzig) **8**, 507 (1999). (cited on p. 116)

[177] J. Martinek, J. Barnas, G. Michalek, B. R. Bulka, and A. Fert. *"Spin effects in single-electron tunneling in magnetic junctions"*. Journal of Magnetism and Magnetic Materials **207**, 1 (1999). (cited on p. 116)

[178] A. N. Korotkov and V. I. Safarov. *"Nonequilibrium spin distribution in a single-electron transistor"*. Phys. Rev. B **59**, 89 (1999). (cited on p. 116)

[179] L. F. Schelp, A. Fert, F. Fettar, P. Holody, S. F. Lee, J. L. Maurice, F. Petroff, and A. Vaurès. *"Spin-dependent tunneling with Coulomb blockade"*. Phys. Rev. B **56**, R5747 (1997). (cited on p. 116)

[180] J. Barnasacute, J. Martinek, G. Michalstrokek, B. R. Bulstrokka, and A. Fert. *"Spin effects in ferromagnetic single-electron transistors"*. Phys. Rev. B **62**, 12363 (2000). (cited on p. 116)

[181] J. Martinek, J. Barnaś, S. Maekawa, H. Schoeller, and G. Schön. *"Spin accumulation in ferromagnetic single-electron transistors in the cotunneling regime"*. Phys. Rev. B **66**, 014402 (2002). (cited on pages 116 and 120)

[182] I. Weymann, J. König, J. Martinek, J. Barnasacute, and G. Schön. *"Tunnel magnetoresistance of quantum dots coupled to ferromagnetic leads in the sequential and cotunneling regimes"*. Phys. Rev. B **72**, 115334 (2005). (cited on p. 116)

[183] F. Ernult, K. Yakushiji, S. Mitani, and K. Takanashi. *"Spin accumulation in metallic nanoparticles"*. J. Phys.: Condens. Matter **19**, 165214 (2007). (cited on p. 116)

[184] T. Koda, S. Mitani, M. Mizuguchi, and K. Takanashi. *"Spin Accumulation in Cr Nanoparticles in Single Electron Tunneling Regime"*. Magnetics, IEEE Transactions on **46**, 2060 (2010). (cited on p. 116)

[185] S. Mitani. *"model for the detection of spin accumulation in a ferromangetic double tunnel junction"*. Journal of Physics: Conference Series **200**, 052015 (2010). (cited on p. 116)

[186] M. Zaffalon and B. J. van Wees. Zero-Dimensional spin accumulation and spin dynamics in a mesoscopic metal island. Phys. Rev. Lett. **91**, 186601 (2003). (cited on p. 116)

[187] M. Zaffalon and B. J. van Wees. Spin injection, accumulation, and precession in a mesoscopic nonmagnetic metal island. Phys. Rev. B **71**, 125401 (2005). (cited on p. 116)

[188] T. Kimura, Y. Otani, and J. Hamrle. *"Switching Magnetization of a Nanoscale Ferromagnetic Particle Using Nonlocal Spin Injection"*. Phys. Rev. Lett. **96**, 037201 (2006). (cited on p. 116)

[189] H. Shimada and Y. Ootuka. *"Magnetic-field-driven single-electron pump"*. Phys. Rev. B **64**, 235418 (2001). (cited on p. 116)

[190] I. Weymann and J. Barnaś. *"Spin-dependent transport thro double-island single-electron devices"*. phys. stt. sol. (b) **243**, 239 (2006). (cited on p. 116)

[191] M. Johnson and R. H. Silsbee. *"Coupling of electronic charge and spin at a ferromagnetic-paramagnetic metal interface"*. Phys.Rev. B **37**, 5312 (1988). (cited on p. 118)

[192] M. Johnson. *"Spin polarization of gold films via transported (invited)"*. J. Appl. Phys. **65**, 6714 (1994). (cited on p. 118)

[193] S. Takahashi and S. Maekawa. *"Spin current, spin accumulation and spin Hall effect"*. Science and Technology of Advanced Materials **9**, 014105 (2008). (cited on p. 118)

[194] M. Braun, J. Konig, and J. Martinek. *"Spin current through a tunnel junction"*. Superlattices and Microstructures **37**, 333 (2005). (cited on p. 118)

[195] T. N. van der Molen, S.J and van Wees B.J. *"Magneto-Coulomb effect in spin-valve devices"*. Phys Rev. B. **73**, 220406 (2006). (cited on p. 120)

[196] F. Zwanenburg, D. van der Mast, H. Heersche, E. Bakkers, and L. Kouwenhoven. *"Electric field control of magnetoresistance in InP nanowires with ferromagnetic contacts"*. Nano Lett. **9**, 2704 (2009). (cited on p. 120)

[197] L. Brey, C. Tejedor, and J. Fernández-Rossier. *"Tunnel magnetoresistance in GaMnAs: Going beyond Julliére formula"*. App. Phys. Lett. **85**, 1996 (2004). (cited on p. 120)

[198] J. M. D. Teresa, A. Barthélémy, A. Fert, J. P. Contour, F. Montaigne, and P. Seneor. *"Role of Metal-Oxide Interface in Determining the Spin Polarization of Magnetic Tunnel Junctions"*. Science **286**, 507 (1999). (cited on p. 120)

[199] W. E. Pickett and J. S. Moodera. *"Half Metallic Magnets"*. Physics Today **54**, 39 (2001). (cited on p. 137)

Universidad Autónoma de Madrid
Departamento de Física de la Materia Condensada

PROPIEDADES DE TRANSPORTE EN REDES DE NANOPARTÍCULAS

Tesis doctoral presentada por
Virginia Estévez Nuño

Programa de doctorado de Física de la Materia Condensada

Directora:
Elena Bascones

Madrid, Febrero de 2011

Resumen

Durante las dos últimas décadas ha habido una intensa investigación científica en nanociencia y nanotecnología, debido a la amplia variedad de aplicaciones en diferentes campos como la electrónica, el magnetismo, la biomedicina, la farmacéutica, el energético, o la ciencia de materiales. Los sistemas estudiados en nanociencia tienen un tamaño muy pequeño, que está comprendido entre 1nm y 100 nm. Una de las razones por la que los materiales a escala nanométrica son tan interesantes es porque debido a los efectos cuánticos y de confinamiento sus propiedades físicas son diferentes a las del material a escala macroscópica. Las propiedades físicas de las nanoestructuras dependen de su tamaño, forma y material. En esta tesis el estudio se ha centrado en las redes de nanopartículas. Hoy en día se pueden sintetizar redes de nanopartículas metálicas, semiconductoras y magnéticas en una, dos y tres dimensiones mediante diferentes técnicas como la litografía, la epitaxía molecular o las técnicas de autoensamblado. En dichos sistemas el coste de energía asociado a añadir un electrón a cada nanopartícula (energía de carga) es relevante y puede suprimir el transporte (bloqueo de Coulomb). Por otra parte, el comportamiento de estos sistemas se va a ver afectado por el desorden, ya sea de tipo estructural (vacantes), en los niveles de energía o potencial químico de las nanopartículas, o en la distancia entre partículas. La reproducibilidad de las propiedades frente al desorden será crucial para las aplicaciones. Además de sus posibles aplicaciones, estas redes constituyen un sistema excepcional para el estudio de la correlación electrónica y los factores que la modifican.

Aunque a lo largo de todos estos años se han realizado un gran número de trabajos experimentales y teóricos, las propiedades de transporte en redes de nanopartículas no se entendían completamente. En estos estudios previos todavia hay cuestiones sin resolver. En el caso de redes unidimensionales hay controversias entre las diferentes aproximaciones teóricas, mientras que en dos dimensiones en donde se ha realizado la mayoría del trabajo experimental, la comparación entre experimentos y teoría no está bien establecida.

El objetivo del trabajo presentado en esta tesis ha sido el estudio de las propiedades de transporte en redes de nanopartículas metálicas, y cómo se ven afectadas por diferentes factores como el desorden, los tipos de interacción entre las cargas o la dimensionalidad de la red. El transporte ha sido analizado desde el punto de vista teórico, utilizando principalmente simulaciones de Monte-Carlo dinámico o de no equilibrio. En algunos regímenes

también se han realizado aproximaciones analíticas.

El primer capítulo de la tesis es una introducción a los sistemas nanoestructurados y en concreto a las redes de nanopartículas, los tipos de redes y los diferentes tipos de desorden que aparecen en las redes sintetizadas experimentalmente. Se explica la física del bloqueo de Coulomb que controla el transporte en estos sistemas. Además se contextualiza sobre lo que ya se conocia en trabajos previos sobre el tranporte electrónico a través de las redes de nanopartículas. El resto de la tesis está dividida en dos partes, una dedicada a las propiedades de transporte en redes de nanopartículas cuando estan situadas entre electrodos metálicos no magnéticos y una segunda parte cuando los electrodos son ferromagnéticos.

Primera Parte: Electrodos no magnéticos

- En el Capítulo 2 se explica el modelo y la simulación numérica que se ha utilizado para estudiar el transporte en redes de nanopartículas metálicas cuando están situadas entre electrodos no-magnéticos. También se introducen los diferentes tipos de interacción que se han considerado en este trabajo.
- En el Capítulo 3 se analiza en detalle el caso de redes de nanopartículas unidimensionales cuando la interacción es de corto alcance. En este caso solo hay interacción entre las cargas dentro de un mismo conductor. He estudiado el voltaje umbral, V_T, por debajo del cual la corriente está bloqueada en el sistema. Para voltajes mayores que este voltaje umbral se han analizado las curvas $I-V$ características y la caída de potencial promedio a través de la red para diferentes regímenes de voltaje. Además he estudiado cómo se van a ver afectados V_T, las curvas $I-V$ y la caida de potencial por los diferentes tipos de desorden y la forma en la que se aplique el voltaje de polarización a la red.
- En el Capítulo 4 he realizado el estudio del efecto de las interacciones de largo alcance en redes de nanopartículas unidimensionales. En este caso las cargas en distintos conductores pueden interaccionar entre ellas. El apantallamiento que se produce por la proximidad entre conductores ha sido incluido en las interacciones. Al igual que en el caso de corto alcance estudiado en el capítulo anterior, se han analizado el voltaje umbral, las curvas $I-V$ y la caída de potencial atráves de la red, y cómo se ven afectados por el desorden y el voltaje de polarización aplicado.
- En el Capítulo 5 se han estudiado las propiedades de transporte en redes de nanopartículas bidimensionales, donde la mayoría de los trabajos previos experimentales han sido realizados. La interacción analizada es de corto alcance y me he centrado en el caso en donde el voltaje de polarización aplicado es del tipo $V_0 = V/2$ y $V_{N+1} = -V/2$. He

estudiado los cambios que se producen en el transporte al pasar de una a dos dimensiones, o en dos dimensiones las diferencias entre los distintos tipos de red, cuadrada y triangular. He analizado el V_T, las curvas $I-V$ y la caída de potencial para diferentes regímenes de voltajes, y cómo se van a ver afectados por el desorden. En este caso además del desorden de carga y en resistencias también se ha analizado el desorden de tipo estructural, que se produce cuando hay vacantes en la red.

Segunda Parte: Electrodos Ferromagnéticos

En la segunda parte he estudiado cómo se ven afectadas las propiedades de transporte por la interacción entre los efectos de carga de las nanopartículas y el ferromagnetismo de los electrodos.

- En el Capítulo 6 se introduce brevemente la interacción entre los efectos de carga y el ferromagnetismo. Se hace un repaso a los trabajos previos a esta tesis, que se habían centrado en el caso de una y dos islas situadas entre electrodos ferromagnéticos. Se explican el modelo y la simulación que me permite hacer este estudio. Además se introduce el caso de una sola nanopartícula no-magnética entre dos electrodos ferromagnéticos.

- En el Capítulo 7 he analizado la acumulación de espín y las propiedades de transporte en redes de nanopartículas metálicas situadas entre electrodos ferromagnéticos. Este estudio se ha realizado para interacción de corto alcance, en redes sin ningún tipo de desorden en una y dos dimensiones, para los casos en que los momentos magnéticos de los electrodos tienen orientación paralela y antiparalela. Se ha considerando que el tiempo de relajación del espín es infinito y que ambos electrodos tienen la misma polarización. He estudiado las curvas $I-V$ características, destacando las principales diferencias con respecto al caso de electrodos no-magnéticos estudiado en la primera parte de esta tesis. Las magnetorresistencias túnel también han sido analizadas.

- En el Capítulo 8 se han estudiado cómo los efectos originados de la interacción entre los efectos de carga y el ferromagnetismo se ven afectados por diferentes factores como distinta polarización en ambos electrodos, la temperatura, el desorden de carga o de resistencia y por las interacciones de largo alcance. Para el análisis del largo alcance se ha estudiado una interacción del tipo de caída exponencial. Todos los casos estudiados en este capítulo se ha realizado en redes unidimensionales.

Conclusiones

El trabajo presentado en esta tesis consiste en un estudio detallado de las propiedades de transporte en redes de nanopartículas y cómo se ven afectadas por diferentes factores como los diferentes tipos de desorden que apareren en las redes, el rango de interacción, la dimensionalidad de la red o el tipo de electrodos. Este estudio se ha hecho desde un punto de vista teórico, utilizando principalmente simulaciones de Monte Carlo de no equilibrio.

Hasta ahora la mayoría de los trabajos realizados en redes de nanopartículas entre electrodos no-magnéticos se centraban en la determinación del voltaje umbral y como era el comportamiento de la corriente para voltajes muy cercanos a este. En la primera parte de esta tesis se han resuelto las controversias que existían en el transporte en redes unidimensionales. Además se ha demostrado tanto numérica como analíticamente que la teoría que se había considerado válida en los últimos 17 años para el transporte electrónico a través de redes de nanopartículas bidimensionales para voltajes cercanos al voltaje umbral era incorrecta. La corriente depende linealmente del voltage como $(V - V_T)$. Esto se debe a que el transporte en esta región está controlado por una unión de contacto que actúa como cuello de botella, dando lugar a un régimen con comportamiento lineal en la corriente tanto en una como en dos dimensiones. Además esta dependencia lineal ocurre en todas las redes analizadas, con o sin desorden, con interacción de corto y de largo alcance, y en dos dimensiones para redes cuadradas y triangulares.

También se han estudiado las curvas $I - V$ en otros rangos de voltaje. La corriente muestra tres regímenes con diferente comportamiento, dos lineales y uno entre ambos que es conocido como la escalera de Coulomb. A altos voltajes aunque ya se conocía la existencia de este régimen, en esta tesis se ha resuelto analiticamente la predicción asintótica de la curva $I - V$ con su pendiente y su V_{offset}. También se ha estimado a que voltaje se va a alcanzar la linealidad.

En esta tesis se ha demostrado que el tranporte depende de cómo sea el voltaje de polarización aplicado a la red, es decir, si es simétrico ($V_1 = V/2$, $V_2 = -V/2$), totalmente asimétrico ($V_1 = V$, $V_2 = 0$) o intermedio. Hasta ahora esta dependencia apenas había sido discutida.

Otro aspecto original de este trabajo ha sido el estudio teórico de la caída de potencial a través de la red. En general la caída de potencial en una unión dada no es estrictamente proporcional a su resistencia. En particular, los resultados más interesantes aparecen en el rango de voltajes donde la curva $I - V$ muestra la escalera de Coulomb. En este régimen para una red sin desorden la caída de potencial en las uniones muestra oscilaciones casi periodicas que reflejan la correlación de las cargas.

En la segunda parte de esta tesis se ha estudiado el transporte en redes de nanopartículas en una y dos dimensiones cuando están situadas entre electrodos ferromagnéticos, hasta ahora los estudios previos se habían restringido a los casos de una y dos islas. Este estudio nos ha permitido entender cómo afecta al transporte la interacción entre el ferromagnetismo de los electrodos y los efectos de carga de las nanopartículas. Al contrario de lo que sucede en el caso de una sola nanopartícula, donde solo hay acumulación de espín cuando la orientación magnética de los electrodos es antiparalela, en una red de nanopartículas hay acumulación de espín en las dos configuraciones, paralela y antiparalela. Cuando la orientación es paralela la acumulación de espín influye fuertemente en las propiedades de transporte, apareciendo un régimen con conductancia negativa para unos voltajes donde en el caso de electrodos no-magnéticos la corriente está suprimida. Para este rango de voltajes en redes con $N \geq 3$ nanopartículas hay un gran aumento de la magnetorresistencia túnel (TMR), de más de dos ordenes de magnitud con respecto a los casos de una y dos nanopartículas.

En este trabajo también se han analizado cómo los efectos producidos por la interacción entre el ferromagnetismo y los efectos de carga se van a ver afectados por diferentes factores como la distinta polarización en los dos electrodos, la temperatura, el desorden de carga o de resistencia y la interacción de largo alcance. Para el caso en que los electrodos tienen diferente polarización el régimen con conductancia negativa aparece en ambas configuraciones magnéticas. En este caso los valores de la TMR son del mismo orden que en el caso en el que los dos electrodos tienen la misma polarización. El desorden en resistencias y la dimensionalidad apenas afectan a los valores de la TMR. Sin embargo, el desorden de carga destruye el régimen de picos, y como resultado la magnetorresistencia prácticamente desaparece. Por otro lado, las oscilaciones en la corriente y los valores de la TMR dependen de la temperatura, decreciendo cuando esta aumenta. Finalmente para el caso de interacción de largo alcance, la TMR puede ser suprimida si la interacción no está apantallada por la proximidad de los conductores.